ALMA MATER STUDIORUM
UNIVERSITÀ DI BOLOGNA

DOTTORATO DI RICERCA IN

INGEGNERIA CIVILE, CHIMICA, AMBIENTALE E DEI MATERIALI

Ciclo 36

Settore Concorsuale: 08/B2 - SCIENZA DELLE COSTRUZIONI

Settore Scientifico Disciplinare: ICAR/08 - SCIENZA DELLE COSTRUZIONI

BAMBOO AND ARUNDO DONAX FOR THE FUTURE OF EUROPEAN CONSTRUCTION: UNLOCKING THEIR STRUCTURAL POTENTIAL THROUGH A MULTISCALE INVESTIGATION

Presentata da: Silvia Greco

Coordinatore Dottorato

Enrico Sassoni

Supervisore

Luisa Molari

Co-supervisore

Alessandra Bonoli

Esame finale anno 2025

I dedicate this thesis to all dreamers,

to those who don't settle for what is easy,
but who can see the blue at the horizon
and choose to walk towards it,
despite the storm.

With the hope
that my contribution may make their path
a little less heavy, a little less alone.

ACKNOWLEDGEMENT

As I reach the end of this doctoral journey, I am filled with gratitude for the many people who supported me, guided me, and believed in this work, even when it was not easy to do so.

First and foremost, I would like to thank my supervisor, Prof. Luisa Molari. Her deep competence in her field is only surpassed by the humanity with which she approaches her students. I hold her in the highest esteem, not only for her knowledge and integrity, but also for her rare courage. In choosing to investigate and promote a topic that is still considered uncomfortable in many academic settings, such as natural materials in construction, she demonstrated uncommon bravery and determination that I deeply admire. Over time, the professional respect I felt for her has grown into sincere affection.

Since the topic was highly innovative, it challenged many of us to find unconventional, often complex solutions. I am especially grateful to the technical staff of the laboratory, whose dedication, creativity, and patience were crucial throughout the project. Their behind-the-scenes work was fundamental to bringing this research to life.

I am profoundly thankful to Prof. Jose Jaime Garcìa, Prof. Giovanni Valdrè, Margherita Bertoli, Matteo Mannini and the entire staff of CanyaViva, who welcomed me into their research environment, and generously shared their knowledge, guidance and practical help. Their support was both technically and personally meaningful, and I feel fortunate to have crossed paths with each of them.

There was also a significant personal chapter during this PhD, my maternity leave, which brought with it its own set of challenges. Balancing personal transformation with academic progress was far from simple, yet I was met with understanding and genuine support from every part of the academic community, from the department DICAM, to colleagues and staff across the university. For this, I am truly grateful.

I extend my warm thanks to the reviewers of this thesis for the time, care, and critical attention they will devote to reading and evaluating my work.

Finally, a special thanks goes to my sister, Ines, who not only stood by me with affection,

but also stepped in as an occasional reviewer. Her sharp eye and honest feedback were a real gift.

To all the people, animals and the living world around me, who make my life so reach and meaningful, thank you. The experiences I live with all of you give me the teaching and motivation to carry on with this work, which I truly and deeply believe in.

ABSTRACT

To address the growing demand for sustainable and high-performance construction materials, this thesis explores the structural potential of two natural resources: bamboo and Arundo donax. Though widely available and environmentally low-impact, bamboo and Arundo donax also exhibit promising mechanical properties. However, they remain underused, especially in Europe, due to insufficient scientific validation and persistent outdated perceptions.

Through a rigorous multiscale approach, this research aims to build a scientific basis for their integration into contemporary European construction. The study is structured across three interrelated scales.
At the microscale, six bamboo species cultivated in Italy, Phyllostachys edulis, bambusoides, viridiglaucescens, vivax, iridescens, and violacescens, were compared with Arundo donax through detailed anatomical analysis. Microscopy and image-based quantification revealed their differences, highlighting their influence on mechanical performance. Moreover, the results significantly contribute to the growing body of knowledge on European bamboo species.
At the mesoscale, the link between internal structure and mechanical behaviour was explored, leading to the development of predictive tools for estimating both longitudinal and transverse properties. Analytical and numerical FEM simulations were carried out. A fast and accessible flexural test was also developed and validated for small European bamboo. Its effectiveness has been demonstrated both as a material grading method, similar to those used for timber, and for assessing degradation, as shown by a UV ageing campaign on P. viridiglaucescens.
At the macroscale, the research translates material knowledge into practical structural systems. A multi-culm bamboo bundle beam and a full-span arch structure, based on the existing CanyaViva technique, were studied through experimental testing and numerical simulation. Bamboo offers greater load capacity, while Arundo donax exhibits higher ductility.

By bridging gaps in scientific knowledge and perception, this thesis encourages the incorporation of bamboo and Arundo donax into sustainable construction paradigms rooted in local and renewable resources, in Europe and beyond.

Index of Contents

List of Figures

INTRODUCTION

MICROSCALE

MESOSCALE

MACROSCALE

List of tables

INTRODUCTION

MICROSCALE

MESOSCALE

MACROSCALE

APPENDIX

INTRODUCTION

Motivation and Goal

The work presented in this thesis is the result of over three years of research and is grounded in the recognition of a fundamental need: to restore to human beings the right to a dignified and balanced way of living.

Contemporary society, as it has progressively developed, offers increasing material comforts, yet it is accompanied by a growing prevalence of physical and psychological illness. This condition reflects a deep imbalance, as the environments in which we live are rarely designed according to the true nature and needs of human beings — who, after all, are themselves part of the natural world. Many of the choices that have shaped our built environment have been guided by the assumption that human intervention can improve upon nature. As a result, nature has been systematically excluded from daily life and confined to marginal spaces such as parks or vacation destinations. This separation has contributed to a profound disconnection, with significant implications for both ecological stability and human well-being.

In this context, the only viable path toward truly sustainable human development lies in the restoration of a meaningful relationship with nature and in the pursuit of a collaborative dynamic with it. Sustainability must be understood as the ability of communities to endure over time while preserving the quality and integrity of the resources on which they depend. As articulated in the concept of permaculture, derived from “permanent culture”, the only possible future is one shaped by choices that foster integrated, adaptive, and self-sustaining systems, based exclusively on the use of renewable resources [1]. New solutions must therefore be evaluated from multiple perspectives of sustainability, ensuring that they meet the needs of the entire natural system, including those of human beings.

Sustainable design solutions also involve the way materials are employed. In many innovative proposals, natural materials undergo complex processing, which significantly reduces their overall sustainability. This study focuses on the raw material itself. In line with the concept of retro-innovation, contemporary challenges can be addressed through a critical and integrated re-evaluation of traditional cultural practices [2]. By integrating vernacular building traditions—often untouched by industrial processes—into contemporary architectural methods, it becomes possible to develop efficient, structurally reliable, and environmentally low-impact building solutions [2].

Bamboo and Arundo donax appear to meet these criteria, offering good mechanical performance combined with exceptional renewability, among other valuable characteristics. These materials can be considered true gifts of nature: even in their raw state, they are inherently suited to meet many human needs.

In various Indigenous cultures of Southeast Asia and South America, bamboo holds

a central, even sacred, role. It is often seen as the embodiment of divinity and the origin of humanity. For example, among the Piyuma tribe in Taiwan, it is believed that the first man and woman descended from separate internodes of the same bamboo culm. Since then, bamboo has provided them with shelter and protection [3]. Similarly, in the mythology of the Colombian Patangoro tribe, the sole survivor of a great flood wandered the earth in solitude until the “Heaven Master” descended and brought two pieces of bamboo—one became a woman, the other, a house [3].

Arundo donax is a native plant of the Mediterranean areas, similar to bamboo, recently rediscovered as a source of inexpensive, sustainable material for construction purposes. It has been studied by many academics because of a great interest in using it for several purposes, such as vibrating reed for woodwind instruments or a source of biomass, and recently there is a growing interest in this material in construction too.

There are countries in which bamboo or Arundo donax are currently used for a wide range of purposes, including construction. However, in other countries such as Europe, they are outside from the current construction chain. Bamboo mostly appears as an ornament which image refers to a meditative, peaceful or exotic sensation. Arundo donax is mainly connected to the memory of poverty and deterioration. That is why it is difficult to connect them to a meaning of safety and strength.

This introductory chapter is aimed and structured to establish a comprehensive framework for the study. It begins with an overview of the selected plants, focusing on their morphology, typologies, and geographical distribution. It then examines their historical and contemporary applications in construction, with attention to aspects such as durability and existing regulatory frameworks. Finally, it outlines the main motivations for their use -environmental, psychological, and economic- while also considering the factors currently limiting their broader adoption.

Building on this foundation, the chapter highlights a set of needs and potentially applicable strategies to support the increased use of plant-based materials. Within this broader context, the thesis identifies the areas in which scientific research can be most effectively positioned, and more specifically, defines the scope of the present work.

About the plants

Morphology

In the first monograph of bamboo of the history, Dai Kaizhi wrote that bamboo is “different from both trees and grasses. It is a strange plant” [4]. Indeed, bamboo's anatomical structure differs significantly from that of grasses and trees. It lacks secondary growth and a main trunk, among other characteristics that set it apart from typical woody plants.

The morphology of the plant is represented in Figure 1 and Figure 2. From a bud underground, the plant arises in a stem, the culm, characterized by hollow cylinders, the internodes, connected by membranes, the nodes.
In cooler and temperate regions, bamboo plants grow single-stemmed apart from each other, named leptomorph type, while in warm and tropical regions it grows in dense clumps, named pachymorph type [5].
The root system is made by intricate rhizomes. Thanks to that structure, it is capable to bind soils and raise the water table, becoming an important part of anti-desertification projects around the world [6].
The entire process from the birth of the shoots to the achievement of the final length takes few months and allows the plant to reach 30 m high and 30 cm diameters [5]. At 3 to 5 years old, culms are ready to be collected, due to the development of the inner microstructure, which gives them the strongest characteristics. After the achievement of the final length, the lignification process takes place and branches for the leaves start growing. The survival of the plant at the harvesting is guaranteed by the born of new shoots, which sprout each year from the rhizomes. The life of the plant can reach 40-80 years old, when it finishes after the flourishing, which generally happens simultaneously for an entire population across large regions [5].

The morphology of the Arundo donax is represented in Figure 3 and Figure 4. Its general structure is very similar to that of bamboo, although differences in dimension are significant. The height of the culm ranges from 3.0 to 8.2 meters, while its diameter varies from 1.5 to 3.3 cm at the base and from 0.35 to 2.45 cm at the top [7]. The rhizome is of the leptomorph type. At one-year old green canes have unbranched stems with the same diameter as the older one, and generally complete their life-cycle when they are 3-4 years old [8].

Figure 1 A culm and its cross section with relative nomenclature [9], roots [10]

Figure 2 From up to down: Bamboo flowering [11], Foliage [12] , Culms develoment (Ph. Lorenzo Bar) and Borning of a new shoot [13]

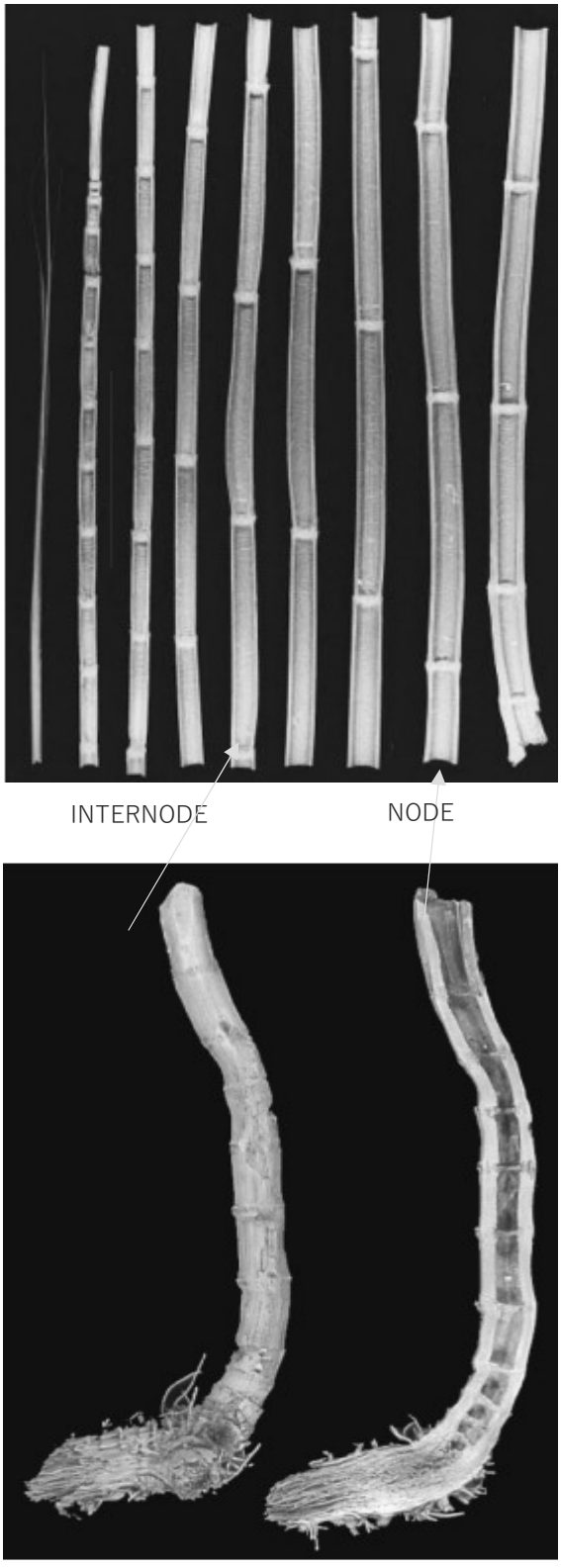

Figure 3 A culm and its cross section with relative nomenclature [14] rhizomes [15]

Figure 4 From up to down: Arundo donax flowering, leaves, culms development and birth of a new shoot. All the images come from [7]

Typologies

Bamboos belong to the subfamily of Bambusoideae, which comprise one of 12 subfamilies within the grass family of the Poaceae (or Graminaceae). According to International Network of Bamboo and Rattan, 1642 species are known at the present. This is due to their capacity to occupy a broad range of environments across the world, from tropical to temperate ecosystems [6].
Bamboos are grouped in three tribes. In molecular analyses, each of the three tribes is monophyletic, but their relationships to one another remain uncertain [16]. A description of each tribe is reported [17]:

- Arundinarieae: temperate woody bamboos, 546 species. They are primarily distributed into the forests of the northern temperate zone, but also in some high elevation tropical regions of both hemispheres. 12 different lineages are recognized and among these, Phyllostachys clade is the most plentiful, covering more the 70% of all the temperate bamboo species present. This clade is remarkable for contrasting high morphological diversity with low chloroplast DNA variation. These species are largely utilized both in construction and furniture or handicraft, due to their excellent mechanical properties.

- Bambuseae: tropical woody bamboos, 812 species. They comprise the Paleotropical and Neotropical woody bamboos. The formers include four subtribes: Bambusinae, Hickeliinae, Melocanninae, and Racemobambosinae, distributed throughout South-East Asia, northern Australia, India, Sri Lanka, Africa, and Madagascar. In particular, Bambusa subtribe is the most widespread genus of bamboo in tropical and subtropical Asia, where they can play an important role in local economies. That is due to the cultivation and the large use of many species of Bambusa, Dendrocalamus, and Gigantochloa, even in construction. The latter are diffused in Central and South America, and comprise the Arthrostylidiinae, Chusqueinae, and Guaduinae. In particular, this last one occupies an area of around 11 million hectares from Mexico to Argentina and it has great economic importance due to the usage G. angustifolia.

- Olyreae: herbaceous bamboos, 124 species. It is mainly native to tropical America.

Differently from bamboo, Arundo donax is the name of a unique species which belong to the family of Poacae and the genus Arundo [7].
Many names are commonly diffused for this plant, such as giant reed, bamboo reed, arundo, caña, canna comune among many others, but all of them refer to the same species. This is mainly due to the highly invasiveness of the plant which has caused the lack of differentiation of the plant all over the world.

Geographical distribution

Bamboo is native to various regions across Asia, Africa, and the Americas. It is predominantly found in tropical and subtropical regions, although it thrives in a wide range of climates, including temperate zones. It covers an area with a latitudinal distribution from 47° S to 50° 30'N, and an altitudinal distribution from sea level to 4300 m, as reported by Liese and Köhl[5]. In fact, the great diversity among species makes each one suitable for a particular climate.
An exhaustive overview of the bamboo distribution in the native countries, with occurrence and typology of the habitat, is reported in [4]. According to that study, bamboo has the richest diversity in Asia, accounting for about 75% of the total species in the world, and covering an area of about 25 million hm^2. In particular, it describes about 600 species in China over an area of 6.4 million hm^2, followed by India with 102 species across about nine million hm^2, and Japan (84 species). More than ten million hm^2 of bamboo forests can also be found in Myanmar, Indonesia, Malaysia, Vietnam, Laos, Cambodia, the Philippines, Thailand, Japan, Bangladesh, South Korea, Sri Lanka, Nepal, and other countries. In Africa, about 13 genera and 40 species have been identified, mainly distributed in East Africa, including Tanzania, Kenya, Zambia, Ghana, Ethiopia, Uganda, Mozambique, and Madagascar. However, the actual distribution of bamboo forests cannot be accurately established due to limited data, despite the abundance of the plant. In the Americas, 21 genera and 345 species are reported in the same study, mainly in Latin America, with only three species present in the southeastern part of the United States.
According to Ruiz-Sanchez et al. [16], Brazil has the greatest diversity in Latin America, with 168 species, followed by Colombia (78), Venezuela (71), Peru (58), Mexico (53), and Ecuador (48), among others. However, another overview of bamboo forest distribution shows that, except for China, very few studies are available, even in countries such as India, which has the largest bamboo-covered area, or in Japan, Brazil, and Ethiopia [18].

European bamboo distribution is not generally recognized in the worldwide mapping researches [18] [19], although it is becoming increasingly widespread. However, many years of experience with bamboo in Europe, both as ornamental garden plants and in agricultural settings, have shown that some temperate species, such as *Sasa*, *Fargesia*, and *Phyllostachys*, can thrive in this region [20]. The introduction of bamboo species to Europe dates back more than 150 years and has played an important role in ornamental horticulture, gardening, and landscaping[21]. Today, bamboo cultivation in Europe is expanding for a wide variety of uses, especially due to its huge potential for carbon sequestration. A collection of pilot bamboo plots in Europe [22] reports the presence of many *Phyllostachys* species in various countries. Notably: *P. vivax*, *P. aureosulcata 'Spectabilis'*, and *P. violascens* (syn. *P. praecox*) in Belgium, Germany, Spain, and Portugal; *P. edulis* and *P. viridiglaucescens* in Spain, Portugal, France, and Romania; *Phyllostachys humilis*, *P. mannii* (syn. *P. decora*), *P. bissetii*, and *P. aurea* in Ireland.
In Italy, several *Phyllostachys* species are also known to the author of the present study, such as *P. iridescens*, *P. bambusoides*, *P. violascens*, *P. vivax*, *P. edulis*, and *P. viridiglaucescens*. Although more species are likely present on the continent, few studies are currently available, possibly due to the relatively recent introduction of the plant. Moreover, the characteristics of the species are often based on data from Asian and South American varieties. In the author's opinion, further investigation and data collection are needed.

Arundo donax is widely distributed in many parts of the world. It mainly prefers subtemperate coastal continental areas without precipitation seasonality and with hot summers, as well as coastal mainland areas with an oceanic or Mediterranean climate featuring strong rainfall seasonality [8]. Due to the plant's widespread and ancient distribution, it is difficult to trace its exact geographical origin. Some sources suggest it is native to West and Central Asia and temperate East Asia, although it has been widely introduced into many other regions, including North and South America, Africa, Europe, Asia, and Australasia [7]. In any case, the presence of *Arundo donax* in the Mediterranean basin has been documented since ancient times, based on archaeological artifacts and written records[23].

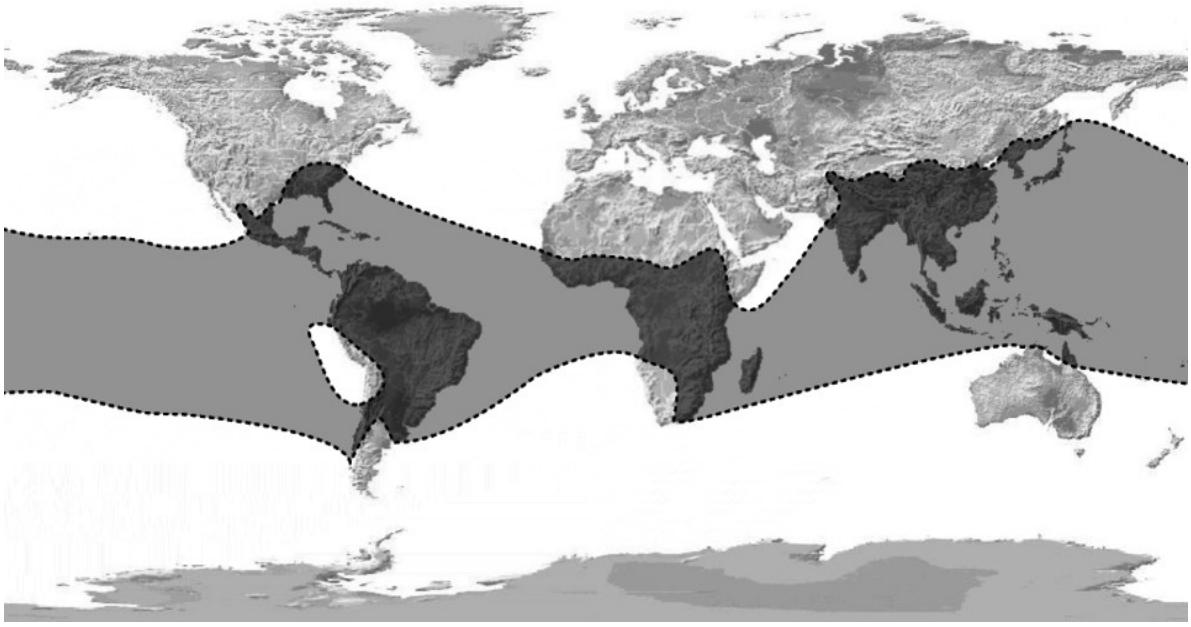

Figure 5 Distribution map of the Poaceae subfamily Bambusoideae [24]

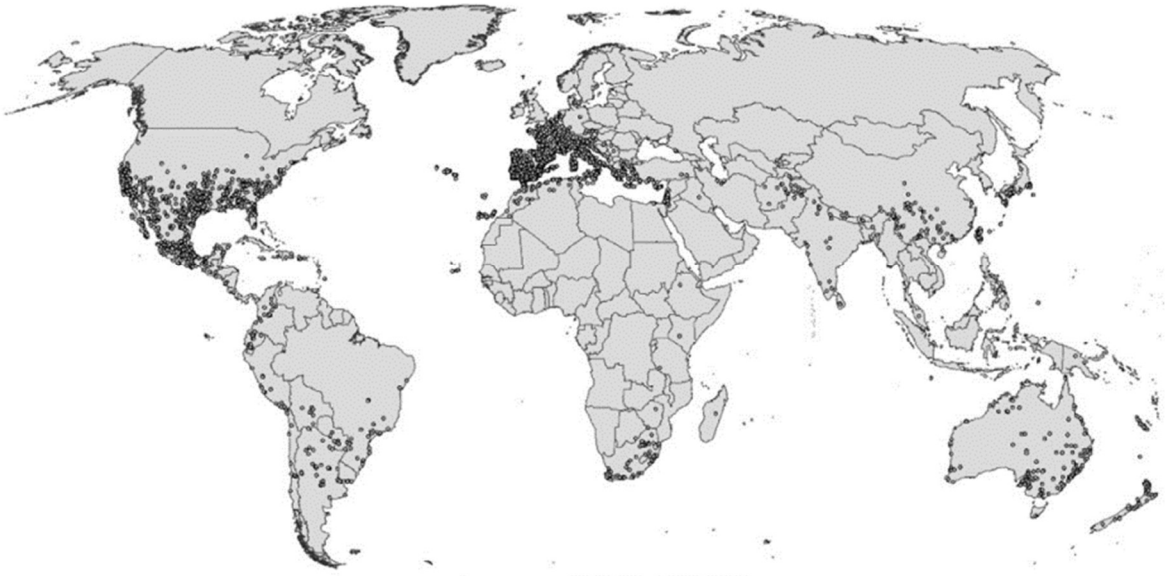

Figure 6 Distribution map of Arundo donax [8]

Application in Construction

Ancient uses

It is very probable that even in the prehistoric industry of our ancestors, bamboo was a fundamental resource. In fact, several clues suggest that, in Southeast Asia, complex implements were built modelling bamboo with simple stone elements needed just to cut it [25] [26]. From there, the man has developed very fine techniques to build entire structures. Actually, although they are only recently becoming part of sustainable concept of construction in the western culture, both bamboo and Arundo donax have been used in the traditional constructions all over the world.

Indian architecture has its beginning in the rudimentary bamboo houses of the Vedic Age, around the end of the second millennium B.C., when nomad populations such as the Aryans, settled down in the plains of India. Bamboo was mainly used for the construction of the roof, while the bearing structure was made of timber in a first period and bricks or stone in a second one. All the typical shape of the Indian roofs come from the bending capacity of bamboo. Initially, the circular form was predominant among the various shapes employed, giving rise to bamboo domes. Subsequently, in the evolution of the Vedic hut, this form was elongated into a rectangular shape, leading to the development of the barrel roof (see Figure 7a). It was the origin of vaults, as several types of arches combined. The lotus leaf shape, typical of the symbolism of the Indian culture, has been easily reproduced by bending bamboo ribs and forming lotus leaf arches before, and then bulbous dome, generated by the revolution of a lotus arch around its central axis (see Figure 7b). These construction schemes evolved into very famous buildings arrived to us, such as that of the Taj-Mahal [3].

Violet-Le Duc [27] reports a detailed description of an ancient Chinese bamboo house, which probably belonged to a rich family. Bamboo Vierendeel trusses have been used in the porch of the house and bamboo rigid frames as a support of the main room roof, which in turn consists of thick bamboo, bent and covered with reeds ingeniously disposed (see Figure 8). Later, bamboo structures were substituted with timber and bamboo was used as a reinforcement of adobe wall or mainly just for the roof [3].

Traces of bamboo structures in the Americas are even older and date back to 7500 B.C. The first bamboo structures had probably a diameter of around 2 m and were made of flexible sticks in a shallow trench fixed together in the shape of a beehive.

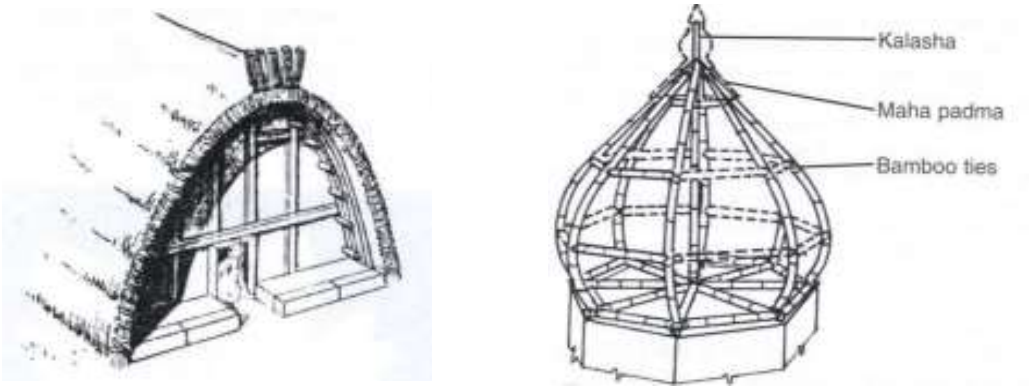

(a) (b)

Figure 7 Example of some Indian ancient bamboo construction: Bamboo barrel roof (a) Lotus leaf shape (b) [3]

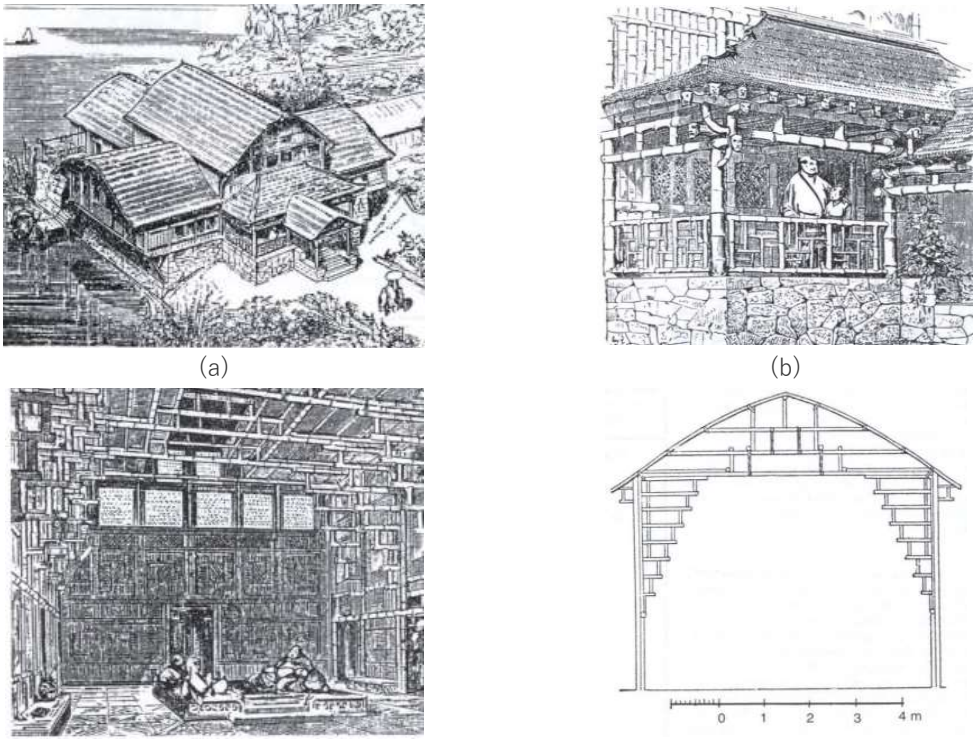

(a) (b)

(c) (d)

Figure 8 Ancient Chinese bamboo house. General overview (a), particular of the porch(b), interior (c) and detail of the structure supporting the roof (d) [27]

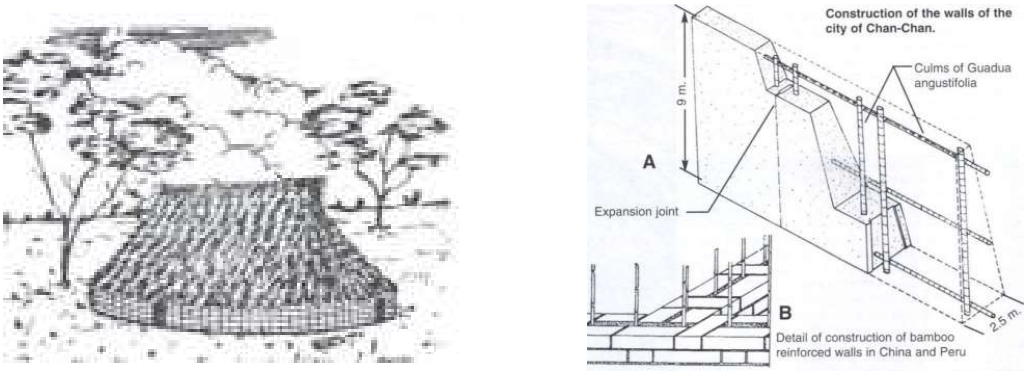

(a) (b)

Figure 9 Detail of the walls of the city of Chanchan [3]

The technique of using bamboo boards plastered with clay, known as bahareque, appears to have been used as early as 3,500 years ago [3]. The use of bamboo structures has evolved over the centuries in all South American countries where advanced construction techniques for houses and bridges existed. It was mainly developed in Guatemala and in the northwestern part of South America, between the Atlantic coast of Colombia and the Gulf of Guayaquil on the Pacific coast of Ecuador. An extraordinary example is the city of Chan Chan, in the coastal desert of northern Peru. Around 850 A.D., a 9-meter-high adobe wall of refined technology was built there, with interior reinforcement made of giant bamboo canes more than 12 centimeters in diameter, forming a grid of 4 meters in both directions. This structure served to "tie" the wall sections, which were divided longitudinally, allowing expansion during earthquakes [3].
Unfortunately, with the arrival of the Spanish conquerors in the Americas, a bloody persecution of the native peoples took place, exterminating the majority of the indigenous population—and with them, their bamboo-based culture.

Arundo donax also has a long constructive tradition. Written records attest to its presence since ancient times. Among others, Homer describes in the Iliad (Book 10, line 467) a field of donax beneath the walls of Troy, while Mesopotamian sculptures and bas-reliefs depict canes and reeds in pastoral, hunting, and warfare scenes [28]. Throughout history, Arundo donax has been used in many ways: in glyptic art and writing, for musical instruments, in medicine, shipbuilding, and construction—these are just a few of its many applications. A collection of literary references to the use of Arundo donax in construction is provided by [28]. One example describes Neolithic houses built of mud and straw bricks, with roofs and light ceilings made of reeds.
Moreover, some documents mention the purchase of thousands of reed bundles for the construction of temples, ziggurats, and palaces between 2700 and 2000 B.C. A specific technique involved layering crisscrossed reed bundles between raw bricks to consolidate buildings and prevent slippage and moisture infiltration. Evidence is also cited from Assyrian and Sumerian texts, as well as from Herodotus (written around 450 B.C.), who mentions houses and mats made of reeds, and from Vitruvius (written circa 30 B.C.), who describes ceilings and partitions in Roman architecture [28].
While in Southeast Asia and Oceania reed is predominantly used as a thatching material—with few exceptions—in Mesopotamia it served as a structural component, even in relatively large huts [29].
In Egyptian culture, the hieroglyph of the Upper Egyptian kingdom’s temple depicts a domed reed hut, while that of the Lower Egyptian kingdom’s sanctuary shows a vaulted rectangular house covered with reed mats [30] (see Figure 10).

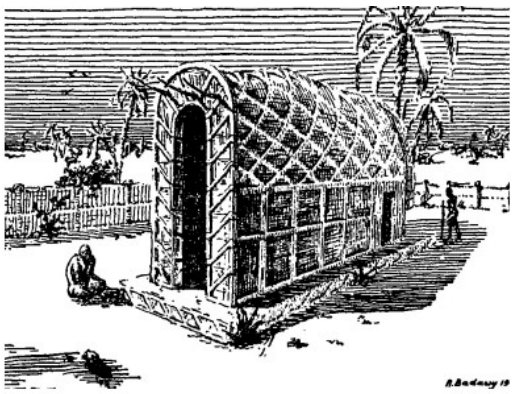

Figure 10 Reconstruction of an archaic Egyptian shrine. Image from [29] aftef Badawy (1954)

Figure 11 Typical mudhif of Marsh Arab [31]

Figure 12 House on the Lake Titicaca, Image from [29] Ph. E. Lehner

Figure 13 Reconstruction of a German house of the 3rd century [29]

Figure 14 Construction of a Baraccas [32]

Figure 15 Use of reed into the wall structure in Calabria [33]

The Sumerian mudhif is a paradigmatic example of designing with cane. The first examples were built in the marshes of what is now southern Iraq, over 5,000 years ago: huge parabolic arches made entirely of reeds, over which reed mats were tied to form walls that curved into roofs, while the flat end walls had reed lattice panels to admit daylight and air [34]. Mudhif represents the village hall in modern towns, and the idea among these people implies that it is open to everyone and that the hospitality offered is free [31]. Their use has continued to the present day.

Another example of reed buildings still in use can be found at Lake Titicaca in the Andes Mountains. Here, artificial islands constructed for defensive purposes, which float on the water surface, are made of reed. The houses consist of a wooden frame covered with reed mats (see Figure 12).

In European tradition, reed has been mainly used for the construction of roofs since the second or third century AD (see Figure 13) [29]. In the north, reed was used for shelter buildings such as huts for herdsmen, or U-shaped reed fences (vasaló) planted into the earth near the hut [29]. The local building tradition of West Sardinia is strongly connected to the use of Arundo donax. There, baraccas are the traditional fishermen's warehouses or resting places [32]. The main structure is made with wooden poles which support a reed lattice filled with a local grass. The ceilings are made in the same way. In southern Italy, the stems of this plant have been widely used to build fences, windbreaks, shading barriers, and temporary shelters. Its use in the building sector has been confined to the construction of false ceilings, supports for roof cladding, wall panelling for their thermal performance, or to the erection of internal and external earthquake-resistant walls [33].

Contemporary use

In the last decades, a revaluation process has been taking place for these materials. Bamboo and Arundo donax are shedding their identity as "poor" materials and becoming protagonists in stylish and luxurious sustainable designs. The process started in Colombia during the nineteenth century. Here, a group of people who emigrated from the State of Antioquia to the Andes went through bamboo forests together with Indigenous people and discovered its huge potential. They found and built the entire city of Manizales using this material, both for the poorest and the richest people. In this place, the new knowledge acquired over the years, and especially the influences from European architecture, mingled with Indigenous traditions, leading to the birth of an enhanced bamboo construction style.

Figure 16 Main applications of bamboo in the traditional construction: the entire culm, the splitted strips and the boards and some application. Images from [35]

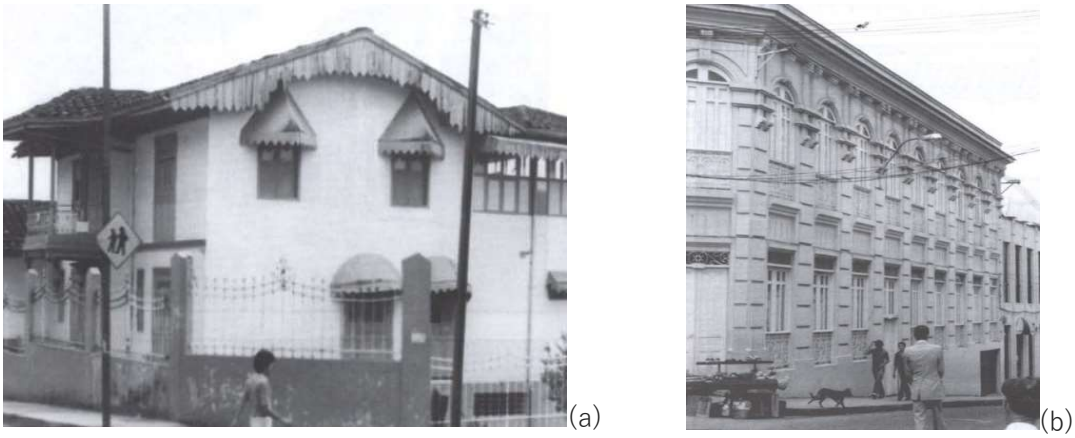

(a) (b)

Figure 17 Examples of beautiful buildings in Manizales built with bamboo: one counts more than a century and it is maybe the oldest one which is still presents in the city (a), and another enriched with details from French architecture (b) [3]

(a) (b)

Figure 18 Bamboo construction designed by Simòn Vèlez. The Zeri Pavillon for the Hannovero EXPO in 2000 (a), and a private Church (b) images from [36]

The bamboo species used were mainly Guadua angustifolia Kunth for structural purposes such as columns and beams, and Guadua cebolla for roofs, studs, and boards. The technology developed was similar to that of traditional wood framing, known as platform framing. The exterior of the houses was plastered in several coats of mortars made with different compositions and finally embellished with lime painting or decorative finishes. Some examples of these buildings are shown in Figure 17.

Generally, the most common traditional ways to use raw bamboo today consist of three methods: the entire culm, split strips, and boards (Figure 16). Despite several challenges due to its round shape, the first method is the most widely used because it is faster and easier to obtain. Applications are numerous, and it is mainly used for the load-bearing structure, either alone or as reinforcement for walls. The second method is widely used due to the almost rectangular section, which is easier to work with. Strips are obtained by cutting the entire culm along the radial direction. They can be used both as reinforcement and as the main structural component. The third method consists of opening and flattening the culm. In this way, larger pieces can be obtained, which are useful when covering large surfaces such as walls. Bamboo boards are generally used as cladding and can be combined with bamboo culms to contribute to the wall's load-bearing capacity.

Simón Vélez has been one of the major promoters of the redevelopment of bamboo for architectural works. He began designing large bamboo roofs in the 1980s in Colombia and continues to create modern examples of bamboo architecture around the world. His typical design process starts with the roof and then adds the necessary components. In this way, bamboo can be used to create structures with vast spaces and great height. Two examples are shown in Figure 18.

A very innovative bamboo structure is The Arc at Green School, designed by IBUKU (see Figure 19a). It consists of a series of intersecting bamboo arches, with a span and a height of 19 and 14 meters, respectively. Inspired by the functioning of the human ribcage, the structure is based on the collaboration between the arches, which work in compression, and tensioned anticlastic gridshells that hold them up. Although the gridshells appear to hang from the arches, they derive their strength from curving in two opposite directions. The result is a complex state of equilibrium that allows the creation of a very large volume without any visible trusses or the need for a significant amount of material. The outcome is a very interesting and beautiful design, in line with IBUKU's mission to promote innovative and sustainable bamboo architecture and design [37].

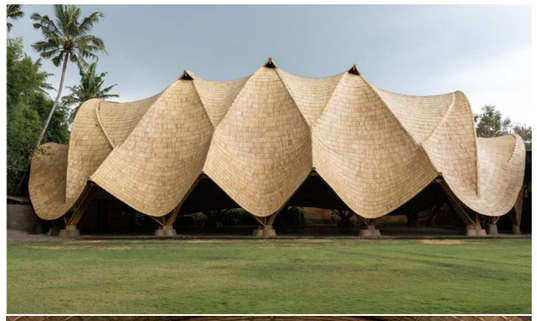
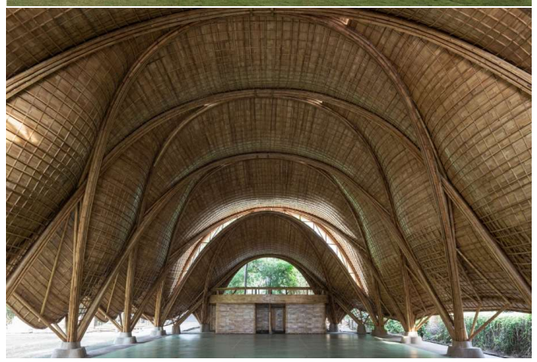

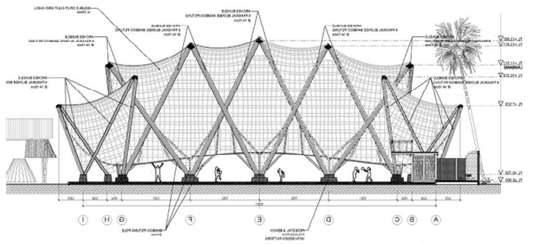

The Arc at Green School
IBUKU
Kecamatan Abiansemal, Indonesia
Ph. Tommaso Riva

(a)




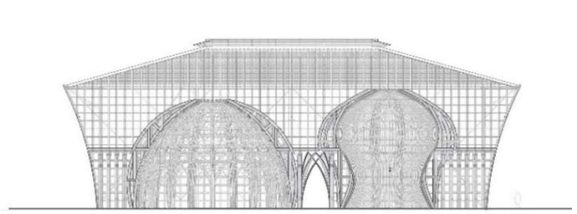

Welcome center of Grand World Phu Quoc Resort
Vo Trong Nghia Arquitects
Phu Quoc, Vietnam
Ph. Hiroyuki Oki [38]

(b)



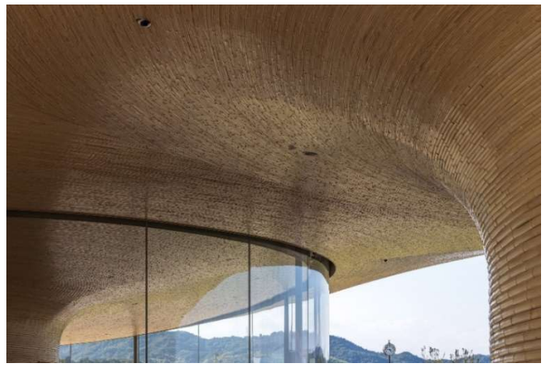


Bamboo Gate community
Kengo Kuma and Associates
Mabi, Japan
Image courtesy of Kengo Kuma and Associates [39]

(c)




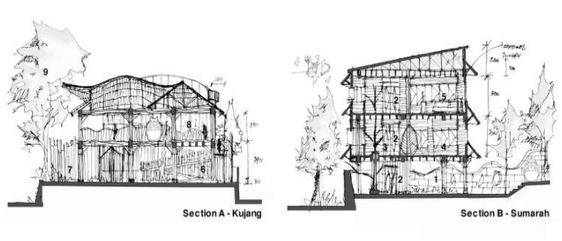

Piyandeling Artisan House
RAW Architecture
Mekarwangi, Indonesia
Ph. Eric Dinardi [40]

(d)

Figure 19 Modern bamboo architecture

An extraordinary example of the modern use of bamboo in construction is the building that welcomes visitors to Grand World Phu Quoc, designed by the Vietnamese studio Vo Trong Nghia Architects (see Figure 19b). Bamboo culms are combined into a series of arches, domes, and grids connected by ropes and pins, forming a structure that covers 1460 m^2. Inside, the play of light and natural ventilation makes the spaces within the internal void sculpted into the forms of a lotus and bronze drum truly amazing [38].

As a testament to the great capacity of bamboo as a resilient material, Kengo Kuma and Associates created the Bamboo Gate community centre to provide a disaster-resilient public space for the town of Mabi in Okayama Prefecture, damaged by flooding in 2018 (see Figure 19c). The building consists of two volumes separated by an opening. A sculptural roof curves out from a storage warehouse, which is clad almost entirely in bamboo, to form a column at the centre of the community centre, which has glass walls and will be used as an events space. The opening connects the city on one hand and the nature of the Oda River and the mountains where the structure is built on the other hand [39].

In West Java (Indonesia), the studio RAW Architecture created an impressive construction entirely built with bamboo (see Figure 19c). A bearing structure constituted by bamboo bundles supports the floor, ceiling finishes, balustrades, window frames, decorative carvings, and even door handles, all made with bamboo. Two main buildings were constructed: a three-storey cylindrical one, which contains the home, and an L-shaped open-air structure that can be used for meetings and gatherings. The shapes were chosen considering the direction of the winds and with the idea of recreating the silhouette of some local birds. As the goal was to give new value to this local, sustainable, and abundant material, the project was developed working with local people and using local material, which was engineered directly on site [40].

A very large number of surprising bamboo buildings can be found nowadays all over the world. Here, only a few examples have been illustrated to give an idea of the incredible possibilities that this material offers. Beyond the beauty of these artworks, bamboo is recognized to have incredible potential in satisfying the needs of a large number of people during emergencies. Some studies identify bamboo as a suitable solution for this purpose because of its characteristics that allow the construction of a lightweight, easy-to-mobilize and assemble, cheap, environmentally friendly, and resistant structure [41]. Moreover, bamboo allows the creation of solutions that consider the humanitarian, social, and psychological aspects of the situation [42].

In some countries of Latin America which are unfortunately affected by natural disasters such as earthquakes and hurricanes, bamboo has been embraced as a

viable solution to provide permanent housing for disaster survivors. The resilience demonstrated by bamboo houses, especially when compared to the collapse of concrete and brick structures, has prompted collaboration among academics, regional bamboo experts, and national governments to formalize the use of bamboo in construction in Colombia, Ecuador, and Peru [35]. As reported by [3], in 1978 Day observed that after the earthquake of 1970 in the Moche Valley, the modern adobe walls collapsed while nothing happened to the walls of the Chanchan ruins.

The development of the Ecuadorian building bamboo code in 2017 led the national housing ministry to carry out a large-scale housing project of 165 houses that can be built in only 15 days and which cost only 10,000 dollars (Figure 20a) [35]. Private associations also arose, such as CAEMBA (CAsas EMergentes de Bamboo), which developed low-cost, modular, and easy-to-build solutions (Figure 20b). The particularity of their solutions is that each building can be expanded over the years. In this way, in addition to providing a solution during emergencies, the owner becomes the protagonist of the process and can create their own home, reaching a sense of pride over their improved living situation [35].

A modern and elegant prototype of a shelter has been developed by the Vietnamese studio H&P Architects. The Floating Bamboo House (Figure 20c) is designed to offer a viable alternative for millions of low-income households, enabling them to construct stable and safe housing independently, while also enhancing their capacity to adapt to the most severe impacts of climate change. The shape is inspired by the vernacular Rông house, and it is built with a bearing structure of local bamboo tied with ropes. On the outside, it is covered by lightweight bamboo screens, woven bamboo sheets, leaves, and corrugated iron. It is able to float thanks to plastic drums attached to the underside. The large roof allows the collection of rainwater and solar energy [43].

A communal shelter for disadvantaged people has been designed by Esan Rahmani and Mukul Damle (see Figure 20d). It has been conceived entirely in bamboo, as it is an abundant local resource. A system of interconnected pipes channels rainwater into a central drum where it is filtered and stored for use. A large central living area connects the surrounding bedrooms and is illuminated by filtered light [44].

Contemporary architecture with Arundo donax is mainly related to the survival of traditional techniques in rural areas, as already discussed in the previous paragraph. An extraordinary example that reinterprets ancient techniques in a modern context is provided by the CanyaViva collective. As it will be deeply analysed in Chapter 4 of the present study, the reader is referred to that part of the book.

Duplex units with full services provided
Luis Rivera
La Chorrera, Pedernales Ecuador
Images from [35]

(**a**)

Evolutionary Home
CAEMBA
Esmeralda, Ecuador
Images from [35]

(**b**)

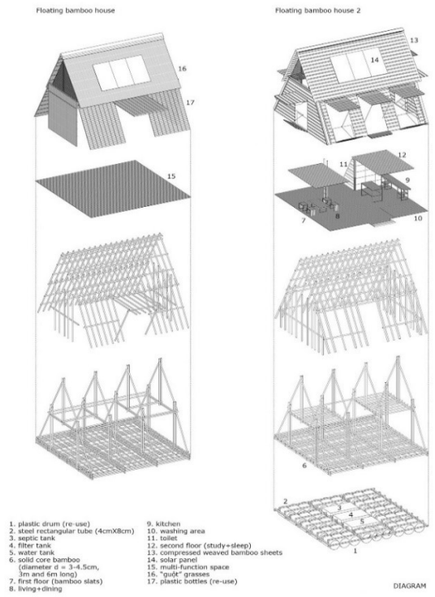

Floating Bamboo House
H&P Architects
Mekong Delta, Vietnam
Ph. Le Minh Hoang [43]

(**c**)

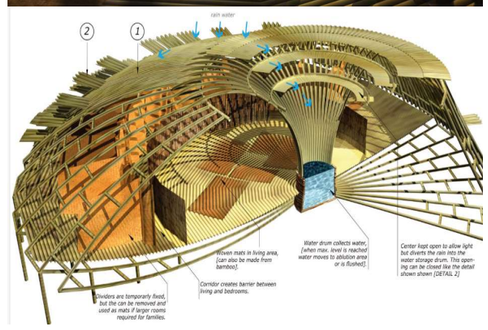

Bamboo Shelter
Esan Rahmani + Mukul Damle
cImage courtesy of Esan Rahmani + Mukul Damle [44]

(**d**)

Figure 20 Bamboo based shelter for emergencies

Durability

One of the most discussed topics about the suitability of bamboo and Arundo donax in construction is their durability. As they are natural materials, they are naturally susceptible to degradation. In particular, bamboo has a high content of starch, sugar and protein and a low content of tannin, wax and resin, which makes it particularly attractive for external degrading agents [45].
Moreover, as it has a very thin wall, a small amount of decay can have a significant percentage change in the capacity of the material [46].
Decay can be caused by biotic agents as beetles, termites and fungi [46]. Some studies have been done on the bamboo's susceptibility to fungal attack. It was found that soft-rot and white-rot induce a considerable deterioration in bamboo, which is more resistant to the brown-rot fungi, and that in any case, not all the species have the same response [47].
On the other hand, in non-tropical climate context as Europe, the main cause of the degradation of bamboo are cracks and splits due to its hydrophilicity and its structural heterogeneity. In fact, changes in moisture content together with the variable density of the fibres along the culm, can cause shrinking and swelling. More precise knowledge about the terminal layer could allow an understanding of moisture movement [48]. The increase in moisture content can cause a significantly reduction in compressive strength, in contrast to the light changes in the elastic modulus [49]. Also tensile strength is more affected than the elastic moduli by the change in moisture content, especially when fibre is older [50]. A study on the change of the modulus of elasticity of the fibre show that it is not significantly affected by moisture content, in contrast to that one at the macrolevel of the entire section, so moisture induced mismatch expansion [51]. Also thermal exposure seems to modify the modulus of elasticity of bamboo, which starts to decrease around 200° , while the modulus of rupture reduced significantly already when the material is exposed a temperature above 160 ° C [52].
The life span can change significantly according to the conditions in which it is used [46]. First of all, the "rule of hat and boots" is needed. In fact, design caution practices are fundamental in avoiding decay, as that one to protect the naked bamboo culm from the exposition to rain and UV light(hat), and prevent the direct contact with the soil (boots). Some suggestions for a good design are illustrated in Figure 21. Moreover, material needs to be perfectly dried to be closer to a moisture equilibrium condition when they are in use. It is important the storage in an aired and dried warehouse after collection.

The durability of bamboo depends on many factors, as age, species, climatic condition and nutrient content [53]. However, through the care, the age of the culms can sensibly increase before the need of its substitution. In Table 1 the suggested approximate life of bamboo in a warm aggressive climate is reported according to [46]. They say it change from 0.5 to more than 30 years. In particular in this table, the influence of treatment is evidenced.

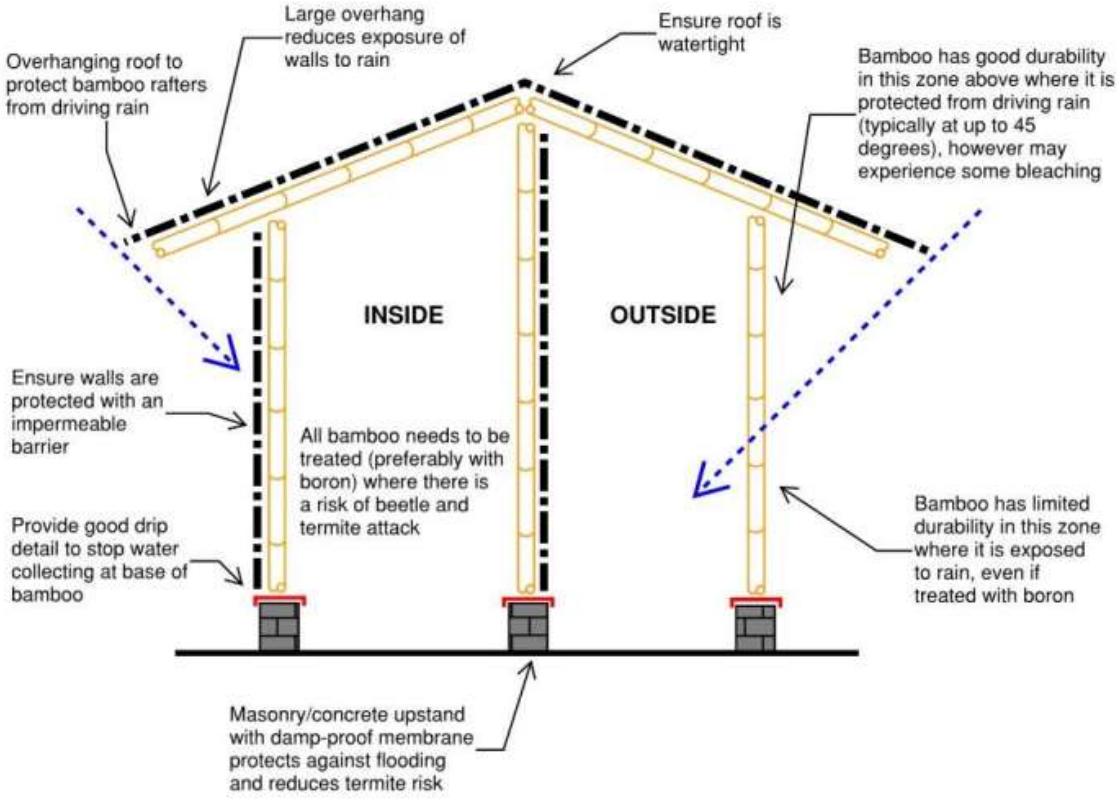

Figure 21 Recommendations for bamboo durability [46]

Table 1 Suggested approximate length of time before bamboo will need to be replaced in a warm aggressive climate, from [46]

	Untreated	Treated with boron	Treatment with fixed preservatives
Internal	2-6 years	30+ years	30+ years
External above ground	0.5-4 years	2-15 years	30+ years
External in ground contact	<0.5 years	<1 year	15+ years

Many treatments have been proposed for bamboo, and the right choice depends on various factors. On one hand, traditional techniques such as water soaking, curing, and smoking have been used for a long time and have proven effective without the need for chemical agents [53]. On the other hand, chemical treatments are widely applied in more aggressive environments. Common methods like soaking perforated culms and the more recent vertical diffusion process require the preservative to diffuse from the lacunae through the outer layer into the inner culm wall [48], since the external layer prevents the effective use of paint. Nowadays, innovative and sustainable solutions are being explored, with scientists and craftsmen around the world experimenting with many methods (see [54], [55] as examples).

Exposure to atmospheric agents results from the interaction of microorganisms with light, oxygen, humidity, and pollution. Since the Industrial Revolution, new anthropogenic factors have introduced air components that make material conservation more challenging [56]. Each of these factors can cause changes in the chemical, physical, optical, mechanical, and morphological properties of bamboo. This remains a critical research topic because, to the author's knowledge, there are only limited data available for a few bamboo species and potential solutions. More research is needed to promote the wider use of bamboo in construction

Regulations

Despite its advantages and its ancient tradition as construction material, the use of bamboo and Arundo donax in the modern era is quite limited. This is mainly due to a lack of knowledge which causes prejudice and insecurity when thinking to use it in the construction field. The standardization of the construction methods is very useful for both technical and social purposes [57]. In fact, on a hand, the provision of guidelines guarantees safety and effective constructions at those want to made it. On the other hand, the inclusion in the codes by the public institutions allow building companies and professionals to stop considering bamboo as a vernacular material in favour of a suitable alternative in their works. This is precisely what occurred in several Latin American countries, where, following natural disasters such as earthquakes and hurricanes, the superior performance of bamboo structures compared to concrete or brick buildings led to the legalization of bamboo construction. This, in turn, resulted in the development of national standards and practices aimed at promoting its use [35]. Today, Colombia, Ecuador, and Peru have

established their own standards and codes regulating bamboo construction, serving not merely as general guidelines, but as legally binding regulations (see Table 2).
In some region of Asia, standards and codes about bamboo exist too. In India, the first standard on bamboo construction with round poles has been introduced early in 1973 [57]. Several regulations and standard have followed this first one, as reported in Table 2.
China introduced its first regulation on bamboo construction in 1995, to characterize the physical and mechanical properties of the material. Nowadays it also has a code which discipline bamboo construction, especially regarding scaffolding which are extremely diffused in that country (see Table 2).
Bamboo enter into the international standard consideration when the standards on structural design and test methods have been published by the International Standard Organization ISO in 2004. This organization received also the impulse from the International Bamboo and Rattan Organization (INBAR) task force, guarantying the collaboration of bamboo and construction experts from all over the world [58]. The result is a complex framework of structural guidelines, which help to spread confidence with the use of this material.
However, in order to become effective and used, each country should adapt them into the national design code. The ISO standard are updated frequently, and the collection of the actual ones is reported in Table 2.
A standard on composite bamboo product is that one published by the American Society for Testing and Materials ASTM International, which included bamboo into the structural composite lumber portions of manufactured structural components.

In the case of Arundo donax, unfortunately, no regulation which discipline its use in construction exist at the knowledge of the author.

Table 2 Collection of existing standards and codes on bamboo structural use all over the world, at the knowledge of the author. The original draft is taken from [57] and some new codes have been added

Country	Year	Name
International	2018	ISO 19624:2018: Bamboo structures – Grading of bamboo culm – Basic principles and properties;
	2019	ISO 22157:2019: Bamboo structures – Determination of physical and mechanical properties of bamboo culms – Test methods;
	2021	ISO 22156: 2021: Bamboo structures — Bamboo culms — Structural design
	2022	ISO 23478: 2022: Bamboo structures — Engineered bamboo products — Test methods for determination of physical and mechanical properties
	2024	ASTM D5456-24 Standard Specification for Evaluation of Structural Composite Lumber Products
Colombia	2006	NTC 5407: Uniones de Estructuras con Guadua angustifolia Kunth
	2007	NTC 5525: Metodos de Ensayo para Determinar las Propiedades Fısicas y Mecanicas de la Guadua angustifolia Kunth
	2010	Reglamento Colombiano de Construcciòn Sismoresistente—chapter G.12 Estructuras de Guadua
Ecuador	1976	GPE INEN 42: 1976 - Bamboo Caña Guadua recomendaciones para el uso en la costrucciòn
	2011	Norma Ecuatoriana de la Construcciòn — chapter 17 - Utilizaciòn de la Guadua angustifolia Kunth en la Construcciòn
Peru	2012	Reglamento Nacional de Edificaciones, Section 3. Code E100 — Diseño y Construcciòn con Bamboo (ICG)
India	1976	IS 8242: Method of test for split bamboo
	1994	IS 13958: Bamboo mat board for general purposes: specification
	2005	The National Building Code of India — Section 3B: Bamboo
	2006	IS 9096: Preservation of bamboo for structural purposes – code of practice
	2008	IS 6874: Method of tests for bamboos (revised in 2024)
China	2007	JG/T 199-2007: Testing methods for physical and mechanical properties of bamboo used in building
	2011	JGJ 254: Technical code for the safety of bamboo scaffold in construction
	2014	JG/T 428: Composite ply bamboo form with steel frame

Purpose of the thesis

Why do we really need to use these materials

Environmental sustainability

Workers in the field of construction have a crucial role in our century, as it is known that the construction sector significantly contributes to global environmental impact. In 2022, buildings were responsible for 34 per cent of global energy demand and 37 per cent of energy and process-related carbon dioxide emissions [59]. The exigencies of the climate crisis and resource scarcity, together with the pace of rapid urbanization globally require creative and more sustainable models of intervention [2]. Conventional materials need to be substituted and wood cannot be considered a sustainable alternative, since the huge need of the market cannot be fulfilled by the current commercial timber forests. Bamboo can do it. In fact, apart from the abundance and the rapid renewability of the resource, its benefits support 8 of the 17 Sustainable Development Goals (see Figure 22). These include reducing poverty (1), promoting gender equality and women's empowerment (5), and generating affordable and clean energy (7). It also contributes to building sustainable cities and communities (11), enhancing efficient use of resources (12), combating the effects of climate change (13), and supporting biodiversity conservation and land restoration (15). Additionally, bamboo promotes South-South cooperation [6].
Both bamboo and Arundo donax grow locally in some of the poorest communities of undeveloped areas and can be used for countless products which are traditionally prepared by the local communities. Leveraging the skills developed in tradition and the simplicity of the manufacturing techniques, the involvement of possible stakeholders can significantly enhance the economy of these countries. In this view, many of this works are also capable of enhancing the integration of all the population, both male and female as happened in the tradition [60].

Apart from providing material useful for many purposes, spreading bamboo and Arundo donax cultivations has also a great potential as a contrasting strategy in stabilizing the carbon dioxide and of atmospheric greenhouse gases. Since CO_2in the atmosphere has been increasing constantly since 1958 leading to warming of the Earth's, strategies for such selection and development of species with a high fixing CO_2 capacity are fundamental [61]. Despite the decrease of the forest areas in many

Figure 22 Sustainable development goals reached by bamboo spreading [6]

countries of the world, bamboo forests have an increment at a rate of 3% annual, and is one of the favourable forest vegetation for carbon sequestration [61]. Song and its collaborators collected several literature references showing more ecological benefit of Chinese bamboo forest [62]. Firstly, an extensive rhizome system, a thick litter layer, and a dense canopy give bamboo forests a high capacity for erosion control, soil and water conservation and landslide prevention. On one hand, bamboo rhizomes act as powerful soil stabilizers; on the other, features such as canopy interception, the water-holding capacity of the litter layer, and the infiltration ability of woodland soils contribute to the bamboo forest's water conservation capacity, which is approximately 30–40% higher than that of a Chinese fir forest. Moreover, they suggest bamboo shelterbelt potential as windbreak, oxygen and noise bar due to the highly elastic culms and the dense canopy. Finally, they add the capacity of bamboo in maintaining wildlife biodiversity, providing food and habitat for numerous insect and other animal, and increasing number and variety of birds.

Some studies in countries in which the plant is not native, have been done as testified in a case study in central Italy [63]. There, the productivity for carbon trading and the eligibility qualities for a Greenhouse Gases (GHG) project are highlighted for a P. pubescens plantation.

Another important aspect of bamboo sustainability is that it is as a globally important biomass resource. Bamboo biomass can be used directly as fuelwood, converted into gas for thermal and electrical energy generation or modified into charcoal for cooking and heating [6]. During the growth of the culms, bamboo produces the highest amount of living biomass in the plant realm. Depending on type, location, and climate, the annual growth rate is about 5–12 metric tons of air-dried biomass per hectare

[5].

The author wants to point out the strictly need of considering bamboo as a local material. Only by the use of local climate-adaptive material can significantly reduce transportation costs and carbon footprint can be avoided, promoting sustainability and environmental well-being in construction projects.

Individual and Communitarian Psychological aspects

Urbanization and modern architectural practices have significantly altered the environments in which humans live. Most urban dwellings are made of synthetic, impervious materials that isolate inhabitants from natural elements, and it is known that the built environment has a significant impact on levels of psychological stress, depression, and reduced cognitive performance [64].

Therefore, apart from environmental sustainability, design and materials can play a crucial role in influencing psychological well-being. Environmental psychology addresses this topic. Biophilic design, promoting the integration of natural elements into architectural design, can effectively foster the connection between humans and nature, leading to well-being and satisfaction [65]. The restorative value of nature as a vehicle to improve cognitive functioning has also been shown in comparison to urban environments [66]. Attention Restoration Theory (ART) further supports this thesis, suggesting that environments rich in natural elements, such as bamboo, provide “soft fascinations” that effortlessly capture attention with mental bandwidth, allowing for mental rejuvenation [67]. Moreover, the shifts between externally oriented soft fascination and internally oriented mind wandering can happen during the experience with natural elements, providing mutually reinforcing pathways that improve attention control, while mind wandering might support additional benefits such as flexibility and new associations of ideas [68]. Buildings that incorporate natural elements like bamboo can simulate restorative environments. Some studies have focused specifically on the potential of the plant bamboo. In particular, the simple view of its natural aesthetics, including texture and colour, allows psychophysiological relaxation through brainwave variation and lower anxiety scores [69][70]. Moreover, reductions in blood pressure, slowing of heart rate, and maintenance of high levels of peripheral oxygen saturation have been measured in people experiencing bamboo forest therapy, indicating its potential in decreasing stress, relieving emotions, and increasing energy [71].

Beyond individual benefits, the use of bamboo or Arundo donax architecture can positively influence societal dynamics. Communities centred around natural material buildings often exhibit stronger social cohesion and collective well-being. In fact, the use of these plants can be done by anyone, as it doesn't require specialized tools or complex techniques. Since time immemorial, bamboo has been an integral part of cooperation and socialization rituals for entire communities in some places, such as the North Eastern region of India [60]. There, the traditional building of a house is undertaken with the help of family members, neighbours, and friends, who have differentiated tasks. Men help with tasks such as making doors, windows, pillars, and digging foundations, while the women perform tasks such as applying cow dung plaster to the walls or preparing the flooring. In fact, it has been shown that community involvement and multidisciplinary collaboration in architectural works result in a significant increase in social activities, restorative behaviours, inclusivity, and promote equitable use of public spaces through its potential for gender-sensitive design [72]. The emergence of spontaneous forms of solidarity and support among inhabitants, even in the absence of already established relationships, has been recorded also in [2] during the communal construction of bamboo buildings. Bamboo makes it possible for people to empower themselves in building their own dwellings, which is particularly important in post-disaster situations. Its availability, ease of access, affordability, versatility, and intuitive ease of use make it the choice of many people, as reported in [2]. In this study, it is also reported how the use of bamboo leads to well-being of people: on one hand, autonomy in design allows the building of a more intimate relationship with the home, and on the other hand, the self-building process is often a reason for pride. In the opinion of the author, this feeling could be echoed by each person who becomes able to build or eventually take care of their own home, not only in poor or post-disaster areas. A sensation of confidence and power through a place so long-lived can be generated by the knowledge of how it is made and how it functions, avoiding fear and estrangement in the case of repairs or modifications.

Moreover, the sustainable nature of these materials promotes environmental stewardship, instilling values of conservation and responsibility within communities, as also demonstrated in the literature [73]. A collective mindset based on this ethic can lead to broader societal changes towards sustainable living and mental health awareness.

Economical perspectives

Nowadays there are over 1000 described uses of bamboo and Arundo donax, among all food, renewable raw material, construction, scaffolding, handicraft products, furniture, and as material for products such as mats, boards, or flooring [5]. Several uses are presented in the graph of Figure 23 in the case of Ethiopian tradition related to bamboo [74]. Considering the few requirements it needs for cultivation, and the short time it needs before collection respect to other cultivations, it can be definitely considered an interesting resource and possible investment for the economy of many countries, among which also Europe [20]. Bamboo cost-effectiveness has been widely emphasized in many research works, and its potentiality in competing with building materials more commonly used in Western European countries has been also shown [75].

The cultivation of bamboo represents an opportunity for economic and social recovery in the areas which are undergoing an agricultural crisis, enhancing marginal and unproductive areas [22]. In fact, widespread bamboo utilization would also promote bamboo-related industries and significantly contribute to providing jobs and revenue to bamboo farmers, local communities, and the government [76]. At the present, although bamboo has provided enormous goods and services to rural communities, the management of bamboo forest resources rudimentary, impeding the sustainability of bamboo and, in turn, the daily lives of the local people that rely on the resource [74]. Therefore, an increase in employment for skilled labour and teachers, and in selling competitive products can be easily reached. Moreover, the acceptance of bamboo in construction would offer affordable housing options for low income earners, solving many housing problems [76]. Europe is the major importer of bamboo raw material, and the second exporter of bamboo products, as shown in the graph of Figure 24, in which the major exporters and importers of bamboo and rattan products in 2017 are reported according to INBAR. It means that bamboo has been already accepted and appreciated in the market of these countries, despite its huge transportation costs. Apart from the environmental damage, in the economical perspective it means a significant lowering of the convenience of the use of this material. However, although this cultivation is quite experimental at the present, bamboo cultivations are significantly boosting. This is primarily motivated by economic profit; however, in some cases, it results from a combination of economic and environmental factors, particularly those related to the production and sale of carbon credits [22]. The experience of two new plantations in Italy show that it was economically viable to use bamboo for an afforestation project, despite the planting cost. In Table 3, an analysis of strength, weaknesses, opportunities and threats (SWOT) has been reported [22] which clarify the convenience.

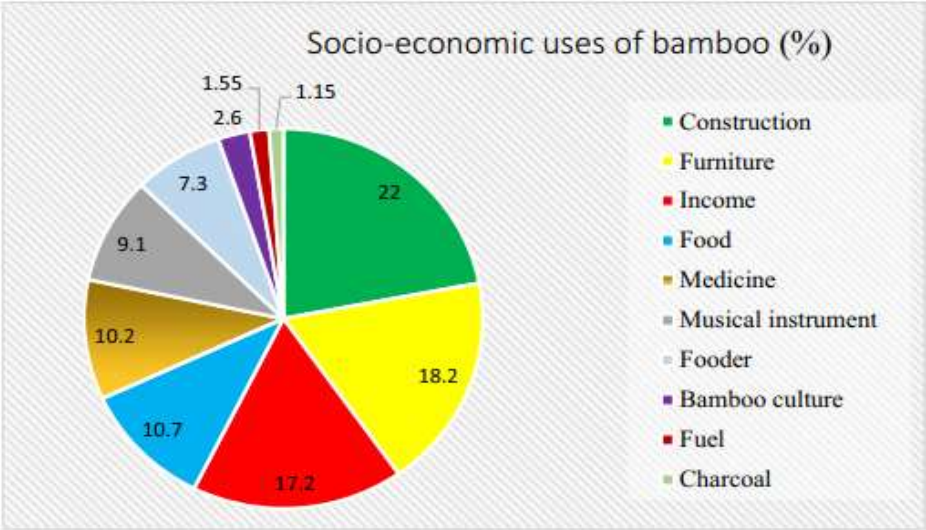

Figure 23 socio-economic use of bamboo in a region of Ethiopia [74]

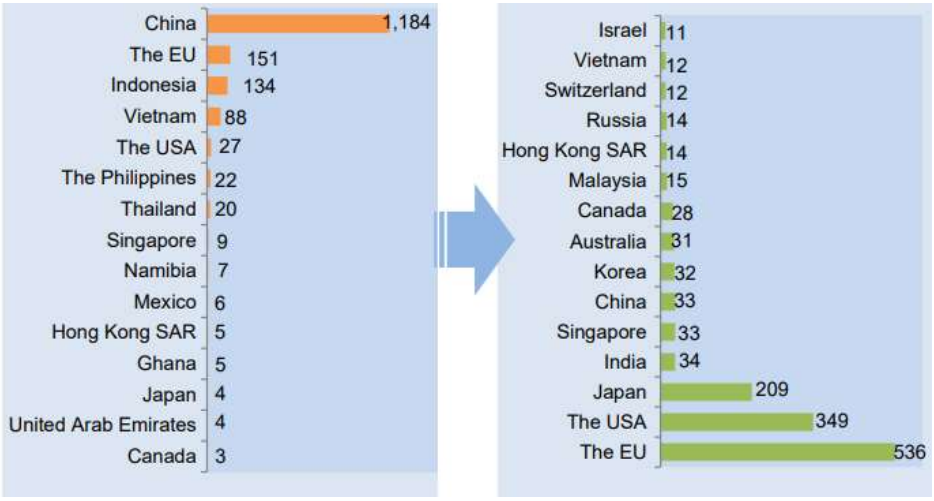

Figure 24 Major exporters and importers of bamboo and rattan products in 2017 (Unit: USD million) [77]

Table 3 SWOT analysis of the opportunity that bamboo cultivation can offer in the Italian context [22]

Strengths	Weaknesses	Opportunities	Threats
• Fast and easy growth • Sustainability of cultivation • High market prices for canes and sprouts • Agro-climatic conditions suitable for bamboo cultivations • Eligibility requirements for GHG projects • Suitability for carbon trading	• Intolerance to prolonged water-logging • Disinformation on bamboo cultivation practices among farmers • High investment costs for planting the crop, mainly due to the cost of the plants	• Several uses of bamboo in the bio-based economy • Increasing demand of bamboo products, both row and industrialized	• Possible invasiveness of bamboo • Water demand • Difficulties in the first years after planting • Need of a business network

Numerous strengths and increasing opportunities can be detected. The weaknesses and threats are also present, but evidently, the limits in the spreading of bamboo cultivations can be substantially solved with the help of targeted planning from the government, both with economic subsidies to help the start of cultivations and companies, and spreading detailed knowledge on how to proceed. This could significantly transform the value of these plants into a priceless treasure for the economy of all people.

Also, Arundo donax offers an economically sustainable market development opportunity. The interest in this crop is mainly due to its huge potential in lignocellulosic biomass production in Europe [78]. In fact, the direct production cost of Arundo donax is lower compared to woody plants or one-year energy crops, because of significantly less fertilizer, pesticide, and herbicide needs to produce high biomass yield [79].

Moreover, it can be cultivated on marginal or degraded lands which are not suitable for food crops, preventing competition with agriculture and allowing land rehabilitation. A case study in the marginal areas of the Sele River (Southern Italy) shows how Arundo donax represents a viable opportunity for local farmers to boost their incomes through woodchip production and, at the same time, produce energy/feed [80]. Anyway, the main costs of its production are related to harvesting, which may weigh heavily as a relative percentage on the overall balance, although some solutions are nowadays proposed [81].

Why we cannot use them at the present

The reasons why these amazing materials are not currently used are many. The first one is surely their degrading perception. Bamboo has been defined in modern times as the ‘Poor Man’s Timber’ [82]. In South America, for example, its huge value in native cultures made it a symbol of their identity, and thus of their misery. Therefore, it had to be hated and abandoned [3]. A study on a community in Colombia shows how the combined effect of cultural globalization and the standardization of construction practices has devalued natural local building materials in the opinion of inhabitants. A refusal of the local bamboo building tradition as an unsafe and temporary material guides their choices towards less sustainable contemporary building materials [2]. This opinion is also reinforced by the use of bamboo that has not reached its structural potential. Some intermediary harvesters sell canes without checking their age and without correctly treating and

storing them, resulting in poor performance and reinforcing a negative attitude towards bamboo, considered inferior to industrialized materials [35].

Moreover, the cultural perception of natural materials in construction within the Western world is ambivalent. On one hand, such materials are associated with ecological awareness and environmental responsibility, due to their natural origin and the low impact of their growth processes. On the other hand, they are often perceived as low-value when used in construction, primarily due to concerns regarding their functional performance and safety. Bamboo, in particular, has only recently begun to gain attention in the construction sector of Western countries. Consequently, the existing body of scientific knowledge predominantly focuses on species cultivated in Asia, Africa, and South America. However, since growth conditions can significantly influence culm structure, the absence of an understanding of the specific characteristics of each species strongly conditions its adoption. In addition, there is a general lack of familiarity in Western contexts with various stages of the development and production chain of non-native materials like bamboo, including plantation establishment and management, harvesting, processing, transportation, and marketing [22]. Potters and collaborators [20] point out that one of the main threats to spreading bamboo cultivation in Europe is that bamboos are exotic species on the continent, impacting the development of nearby ecosystems as happened in the past with Black Cherry (Prunus serotina) or Asian lady beetle (Harmonia axyridis). In fact, they continue, farmers have no tradition or practical knowledge about cultivating bamboo, although many solutions are proposed to address the possible invasiveness of the crop. Arundo donax itself has been considered a plant with a negative impact due to its invasiveness, as it competes with and displaces native plants, interferes with flood control, but especially because of its flammability, which increases the likelihood and intensity of fires [7]. That is why knowledge on its management is necessary.

In many cases, the knowledge we seek, whether in regions where bamboo is a traditional building material or not, already exists. However, much of this information remains confined to individuals who have dedicated their lives to this type of construction. Some are trained professionals, while others have inherited their expertise through generations of local practice. The challenge lies in bridging the gap between this relatively small, specialized community and the broader global audience seeking to harness the potential of bamboo as a sustainable building material.

Some architects and building contractors have started to increase interest in reintroducing natural materials. However, the lack of clear guidelines causes uncertainties regarding compliance with safety regulations, which can compromise safety measures and increase the risk of accidents or structural failures [76]. For

instance, in Ghana, both architects and building construction professionals agree on the many opportunities of bamboo, but also on its many threats, including the lack of knowledge and expertise in bamboo building, and especially the insufficient cooperation from the government to support bamboo in building construction [83]. Governments should have a huge role in the development of the potential of natural materials in construction, although strong resistance seems to be present. This may be due to the inability to see the economic opportunities in using natural materials since conventional construction industries contribute significantly to the economy of the country. In fact, the economic potential of bamboo is not well exploited in many areas of the world. In Ethiopia, for example, a study highlights that the potential of bamboo resources to rural livelihoods and the national economy is unrealized since bamboo product imports exceed exports, despite the huge resource base of the country, which counts around 7% of the total worldwide [84]. Moreover, this study comments that bamboo provides various subsistence benefits to households (such as construction material, furniture, farming tools, fodder, or fuelwood) that are, however, rudimentary and cannot be converted into monetary values. Some impetus needs to come from development policies which promote the use of natural building materials in construction, but in any case, these generally focus on technical performance while neglecting the prevailing impact of the cultural domain on housing preferences and behaviours [2].

How to reach our scope

The analysis of the factors limiting the use of bamboo clearly highlights the need for concrete actions aimed at promoting its adoption, along with that of other natural materials, among professionals, clients, and end users. From the perspective of the author of this thesis, three key concepts are fundamentally interconnected in any effort to advance this goal: trust, availability, and support.

Firstly, it is necessary to restore dignity to this “gift of the gods” [3]. On one hand, the existing knowledge should be made accessible to all people in order to allow them to trust these materials. Public installations, publicity campaigns and open conferences can help generate new openness in public opinion. The proposal of new architectural artworks must replace the image of the hut, and with it, its inconsistency and poverty. Moreover, students and professionals need to be properly trained through conferences, demonstrations, and certification programs which

could spread the knowledge on correct design, construction, and maintenance of bamboo structures. If professionals, or future ones, trust in bamboo structures, it is highly probable that a client can be convinced to invest in this choice. But apart from training practices, the real way to enable a professional to trust a material is the existence of a specific code. In fact, a guideline which has been written by experts and validated by the approval of the government gives significantly higher reliability to a material. The codes should cover many fields of its use, such as material specification, testing methods, grading, design, durability, transportation, safety measures, inspections, compliance and more. Regulation is an insurance for anyone: “if the government trusts it, I can do it too”.

Secondly, availability is a very important factor in enhancing bamboo construction. As already pointed out, it is necessary that natural materials are a local resource in order to be considered sustainable, avoiding the environmental costs associated with importing them from Asia and South America. Bamboo’s availability emerges as a key advantage, thanks both to the abundance of bamboo forests and its renewability. In parts of the world where it is already widespread, the lack of availability is caused by inefficiency. Here, interventions that streamline the production chain can significantly improve the viability of the material. In fact, specific bamboo propagation and stand management techniques should be developed mainly at the bottom stage of the chain, such as via farmer training [84]. In Europe, there are only a few cultivations, although the climatic conditions are suitable. In Southern Italy, some studies have shown that species like Phyllostachys edulis or pubescens are well-suited to the Mediterranean climate, offering products such as edible shoots or canes and serving as carbon sinks [22] [63]. Here, the spreading of this clade could be enhanced by information about the opportunities it can provide. In fact, awareness of the huge economic potential of investing in this sector can significantly reroute the economic condition of some struggling farmers towards a sustainable, innovative and profitable activity.

Finally, supporting the brave organizations, and in general every actor who starts developing this new activity, is a strict requirement to spread bamboo alternatives. It mainly starts with the support for the development of deep and detailed knowledge, which evolves to adapt to new needs and findings. Research and technological advancements can expand bamboo’s potential applications and fill the gap currently existing between potential and possibility. Research needs to be supported by economic aid, development plans and new sustainable policies which recognize the value of this investment. Collaborative research initiatives involving multidisciplinary teams can contribute significantly to advancing bamboo as a mainstream

construction material [76]. Moreover, private investors should be attracted. Carbon trading, for example, is a viable strategy, but the farms that invest in bamboo also need to be supported in the subsequent phases of cane marketing. Therefore, attention must be paid to the entire bamboo supply chain. This major task can only be handled by an entity capable of intervening effectively and simultaneously in several fields. It is therefore necessary that support starts from government entities, which have the capacity to direct intentions, efforts and financial resources toward this goal, causing a rapid change in many sectors. Collaboration among stakeholders, including educational institutions, industry professionals and government entities, is the only way to break down the barriers and allow society to take full advantage of the opportunities offered by nature through this material.

Organization of the thesis

This thesis aims to provide a significant scientific contribution to the integration of bamboo in European construction practices, where its adoption remains limited due to a lack of tradition and a strong reliance on standardized industrial materials. In this context, scientific research plays a pivotal role by acting as a bridge between innovative, natural materials and construction professionals accustomed to conventional solutions. Through the generation of technical knowledge and empirical data, research can foster trust, develop availability and support, reducing scepticism toward so-called "unconventional" materials.

The contribution of this work is structured across three interconnected scales—micro, meso, and macro—as illustrated in Figure 25.
Firstly, the thesis addresses a significant gap in the literature concerning the microstructural characteristics of bamboo species available in Europe. Six species of Phyllostachys—P. edulis, viridiglaucescens, iridescens, bambusoides, violacescens, and vivax—were systematically analysed and compared with Arundo donax. At the microscale level, a detailed morphological and anatomical dataset was compiled, including imagery and measurements of parenchyma, sclerenchyma, and vessel distribution. This foundational knowledge is presented in Chapter 2 and is critical for understanding the mechanical behaviour and performance potential of bamboo in structural applications.

Figure 25 Motivation and development of this research

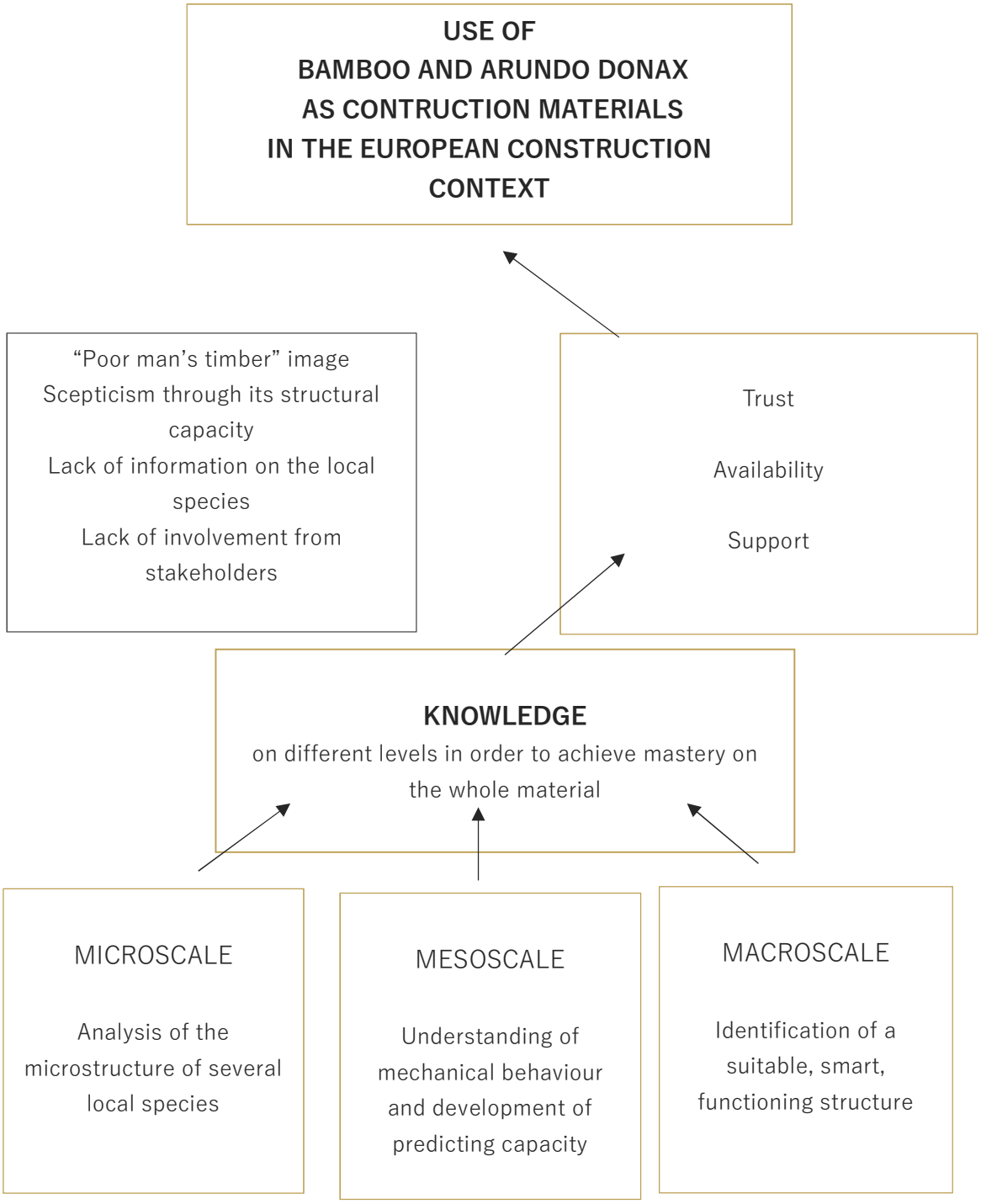

At the mesoscale, Chapter 3 explores how microstructural knowledge translates into practical understanding of mechanical behaviour and the development of predictive tools for construction use. Initially, correlations between specific microstructural features and mechanical performance are investigated. Building on this, an experimental testing procedure has been tested to provide a rapid yet informative overview of bamboo's mechanical properties. This method has also been applied to assess the effects of ultraviolet (UV) exposure on bamboo samples, offering insights into durability and performance over time. Lastly, a preliminary grading system for bamboo elements is proposed, aiming to support standardization efforts and enhance material reliability in construction contexts.

At the macroscale, the thesis investigates how bamboo-based materials can be integrated into building systems that are not merely imitations of those designed for steel or concrete. Rather than forcing bamboo into pre-existing structural models, this study explores a design approach that leverages the material's intrinsic properties. This is exemplified through the analysis of a case study structure, which serves as a prototype for material-smart design rather than material-substitution.

While this work does not claim to offer a comprehensive overview of bamboo's potential in European construction, its innovative, multi-scalar approach provides a robust framework for future research. It lays a scientific foundation for both academics interested in continuing the exploration of bamboo as a construction material and professionals seeking viable alternatives to conventional materials in response to the current ecological and industrial transition.

MICRO SCALE

Anatomic analysis of 6 Italian bamboo species and Arundo donax

In structural design, having precise knowledge of a material's characteristics is essential for predicting its behaviour and to ensuring its safe use throughout the building's entire lifespan. Designing with natural materials presents additional challenges as their standardization is strongly challenging due to their intrinsic variability, dependence on growth conditions, and limited technical data. Standardization requires robust classification systems, extensive empirical research, and tailored norms to manage variability rather than eliminate it. To enable the use of natural materials in construction, it is essential to develop tools that allow designers to place their trust in them. A first fundamental step is gaining detailed knowledge of their microstructure, as it is known to influence mechanical characteristics, as explored in numerous studies and deeply discussed in the next chapter. However, in many cases, obtaining reliable measurements of the microscopic characteristics requires specific equipment and added complexity. In view of the adoption of natural materials in construction, knowledge about them should be more accessible.

Bamboo is not a homogeneous material, since it consists of different components that serve different functions within the plant and are distributed in a not uniform way throughout its structure. Its microstructure has been studied for many years. Significantly contributions passed from [85] to [86], [87], [88] and many others. These studies have provided detailed insight into plant's anatomy, highlighting the differences between its parts and especially among the various species. Moreover, Arundo donax is composed of the same fundamental components as bamboo, but are arranged differently with its structure. Its microstructure has already been studied by researchers such as [14] [89] [90]

Although some detailed data on bamboo microstructure can be found in literature, it is fundamental to emphasize the importance of obtaining data specific to local species. Only by using locally available materials, can natural alternatives be truly considered sustainable substitutes for conventional construction materials. Therefore, the widespread use of bamboo in constructions depends on the understanding of the composition of the local material. In fact, a very important tool for designers is a thorough understanding of interspecies variations, enabling them to select the most suitable bamboo species for their specific project. Until now, studies have been focused on bamboo species grown in places such as Asia, South-America and Asia while a strong need is present in places such as Europe yet.

This chapter presents a microscopical analysis of six bamboo species cultivated in Italy, with the aim of initiating a systematic characterization of their anatomical and geometrical features. Using different levels of magnification, various observation and

analysis were performed. The analysis starts from the higher level of magnification, in order to present deeply each component of the material. Then, a zoom out will allow the better understanding of their disposition into the culm.

The main contribution of this work is addressing the current lack of data on European-grown bamboo, which hinders its integration into structural applications. By providing quantitative insights into tissue composition, cell distribution, and microstructural organization, the chapter contributes to the establishment of a reference database necessary for species comparison, selection, and potential grading. Identifying the most structurally suitable species will support informed material choice in engineering practice. Furthermore, by demonstrating the technical viability of locally grown bamboo, the study reinforces its role as a sustainable alternative to imported species, promoting local cultivation and use within construction systems.

Part of the content of this study has been published in:

Silvia Greco, Luisa Molari, Giovanni Valdrè & Jose Jaime Garcìa (2024). Multilevel analysis of six species of Phyllostachys bamboo and Arundo donax: preliminary survey on Italian grown stands. *Wood Science and Technology* (58), 1025-1049. https://dx.doi.org/10.1007/s00226-024-01547-0

Materials

The anatomical analysis presented in this thesis focuses on six different bamboo species and Arundo donax. All of the bamboo species analysed belong to Phyllostachys Genus, which easily grows in temperate climates such as Europe, as already discussed in the previous chapter. The name, location, age and appearance of each species are presented in Figure 26.

The culms used in this study were collected in the winter of 2018, except for those of P. viridiglaucescens species which were collected in the winter of 2017. After collection, the culms were stored without any treatments in a sheltered warehouse at the University of Bologna. To investigate structural differences along the culm length, two distinct sections from each culm of bamboo and Arundo donax were examined: the upper section (part A) taken from 2.5 to 3.5 m above the ground, and the lower section (part B) taken from 0.5 to 1.5 m above the ground. Table 4 collects the dimensional measurements of diameter, named as D, and wall thickness, named as t. In particular, three measurements were taken for each property from every sample [91].

Table 4 Geometrical data and number of the culms analysed in this study, reported for both part A and B of the culm of each species. D stands for the diameter while t stands for the thickness of the culm.

Name of the species		D [mm]		t [mm]		n. culms
		Mean	St. Dev	Mean	St. Dev	
P. edulis	A	62.42	3.88	5.81	0.59	6
	B	71.78	0.84	8.69	0.79	6
P. viridiglaucescens	A	59.45	3.44	5.28	0.34	6
	B	64.48	6.68	7.14	1.11	6
P. bambusoides	A	58.06	3.25	4.70	0.55	6
	B	58.67	2.96	5.95	0.41	6
P. vivax	A	77.67	8.88	5.49	0.81	6
	B	81.19	6.70	7.10	0.44	6
P. iridescens	A	62.07	2.30	5.74	0.31	6
	B	61.73	3.18	7.83	1.10	6
P. violacescens	A	46.18	4.15	3.94	0.19	6
	B	56.08	3.31	5.11	0.33	6
Arundo donax	A	10.3	0.04	1.50	0.11	9
	B	21,8	0,06	3.8	0.14	12

P. edulis

Pordenone

Between 3 and 4 years old

P. viridiglaucescens

Capezzano Pianore, Camaiore

Between 3 and 4 years old

P. bambusoides

La Morra, Cuneo

Between 3 and 4 years old

P. vivax

La Morra, Cuneo

Between 3 and 4 years old

P. iridescens

La Morra, Cuneo

Between 3 and 4 years old

P. violacescens

Bologna

Between 3 and 4 years old

Arundo donax

Cadriano, Bologna

1 year old

Figure 26 Presentation of the species used in this study. Each image is accompanied by a description of the name, provenience and age. Thanks to Lorenzo Bar for the pictures used.

To prepare the sample for the microscopic analysis, culms with averaged geometrical characteristics were selected. One sample from part A and one sample from part B for each species were prepared as shown in Figure 27.

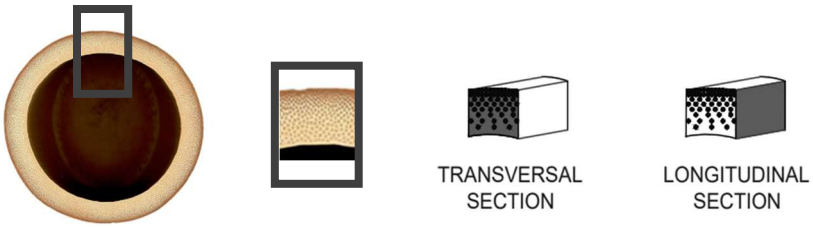

Figure 27 Provenience of the sample into the section of the culm

Morphology and dimensions

In this part of the work, the morphology of Phyllostachys species and Arundo donax is described and measured. First, a structural description of each tissue component is presented through the images obtained in this study. These images are commented on and interpreted with the support of relevant literature, in order to contextualize the observed features. Specific measurements of the tissue dimensions are also provided. Furthermore, a broader view is introduced to better understand the variation patterns along the culm cross-section.

Since no detailed morphological data are currently available in the literature for the specific species analysed in this study, the images and measurements presented here represent original documentation. Although the observed structures are consistent with the general anatomy of similar species, their description is supported by existing literature only as a comparative framework. This approach allows for a more comprehensive understanding of the anatomical characteristics and highlights any notable consistencies or deviations from what is generally known about related species.

Methods

Microscopic observations were conducted in both transversal and longitudinal directions. The decision to limit microscopic sample size was based on the intensive and time-consuming nature of the analysis and of the preparation of the specimens.

Microscopic observation required a very thin section (about 30 ± 1 μm). To achieve this dimension, the samples were embedded in resin under vacuum to provide a stable supporting layer. The resin used was Hardrock 554, an epoxy resin with a specific hardener, produced by REMET SAS (Casalecchio di Reno, Italy). After embedding, a flat surface (± 1 µm) was created using abrasives. A glass slide was then glued to this surface, and the specimens were thinned down to 30 µm through a combination of cutting, lapping and polishing (with 0.5 μm grit), over areas with several mm^2 in size. Microstructural observations were carried out using a Zeiss Photomicroscope III equipped with polarized light. Image acquisition was performed using an Edmund Optics CMOS-sensor colour camera. Observation were conducted at varying magnifications: 2.5X, 10X, 25X and 40X.

To further investigate the anatomical characteristics of the material, measurements were taken for some specific topics. Data presented correspond to the mean values of six measurements obtained by the observation of the microscopical images and the ruler corresponding to a level of magnification.

Analysis of the anatomical components

Figure 28 shows the main structural element of the anatomical morphology of both bamboo and Arundo donax, the vascular bundle. Here, the three anatomical components of those plants are clearly visible in both specimens, and are here reported for a clear explanation of the following text.

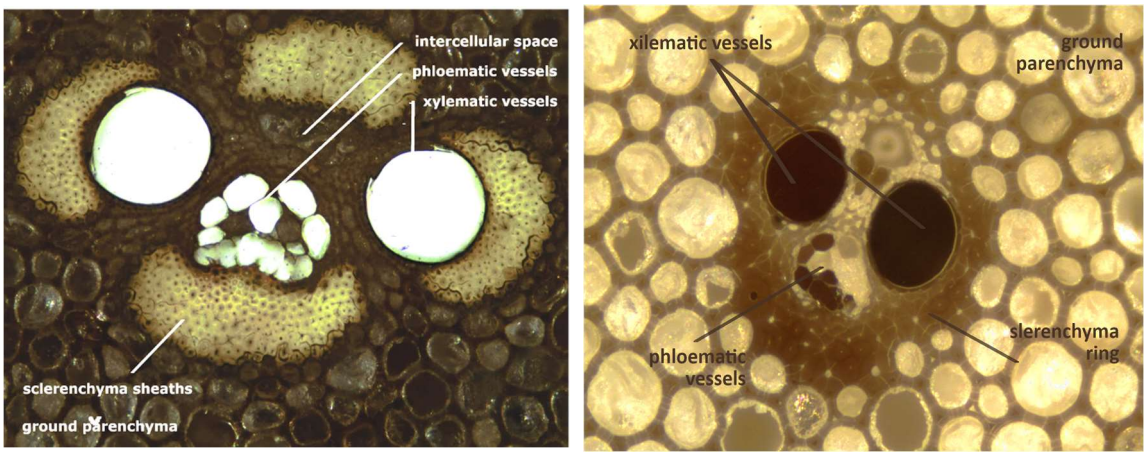

(a) (b)

Figure 28 Vascular bundle from the inner side of the wall from the part A of a P. viridiglaucescens (a) and from the middle part of the wall from the part B of Arundo donax (b). enlargement 10

Vascular tissues

The component of the plant which is responsible for distribution of water and nutrients is the vascular tissue. It is organized in two different types of vessels (see Figure 28): xylem and phloem, which correspond to the two big cavities or the group of smaller ones respectively. The xylem transports raw lymph from the roots to the leaves and it consists of longitudinally elongated dead cells which have undergone a lignification process that also provides mechanical support to the plant. Along the length they contain some holes to facilitate lateral movement of fluid from the vessels. In some cases, the images reveal intermediate spaces originating from the primary xylem or small protoxylem cavities, as shown in Figure 28a. Phloem is formed of sieve-tubes, transporting elaborated lymph from the photosynthesizing cells in leaves to use or storage as parenchyma. Unlike xylem, phloem cells remain alive during the life of the plant and do not lignify. They consist only of primary cell and do not contribute to plant's mechanical strength.
In this tissue starts the degradation process of the material when tylosis and degrading substances occupy the hollows of the vessels since it the culm is 8 years old [92]. Moreover, although this component occupies a relatively small volume compared to the other components, its role is crucial for several reasons. Firstly, it is important for the transpiration of the plant due to the high conductivity [93]. Secondly, it offers valuable opportunities for the application of preservatives. Finally, voids play an important role in structural behaviour, as will be discussed later.

Sclerenchyma

Sclerenchymatic tissue is composed of flexible and longitudinally elongated cells, known as fibres. In Figure 28, they are visible as the sheaths surrounding the vascular tissue vessels. In bamboo, each group of vessels is enclosed by an individual sheath, whereas in Arundo donax, a single ring-like sheath surrounds the entire vascular bundle area. Each group of vessels is surrounded by a sheath in the case of bamboo, while a unique sheath, as a ring, which surround all the vessels area is reported in the case of Arundo donax vascular bundle.
To provide the mechanical support to the plant, these fibres possess both a primary and a secondary cell wall that are strongly ad uniformly thickened, with a very high

percentage of cellulose into the microfibrils than that of the parenchymatic matrix. Microfibrils are composed of cellulose and embedded in a matrix of hemicellulose and lignin. Each fibre cell features a multilayer wall structure, which is described in Figure 29. It typically consists of eight lamellae [94], of different length, which are alternate forming a “criss-cross” pattern between thick and thin lamellae. That structure gives to the plant a very functional mechanical behaviour, since according to [95] the first type of lamellae allows expansion in the culm through the movement between fibrils, while the transversal one resist to the major internal stress of the plant.

Fibres undergo a lignification process that renders them impermeable and resistant to pathogenic microorganisms and are linked to strength and stiffness characteristics of the plant. The lignign content is not constant but generally increases with maturation of the plant. The lignification begins with the deposition of lignin into spaces between cellulose, hemicellulose and pectins, progressing from the secondary cell wall towards primary cell wall and median lamella. Macroscopically, it starts from the upper part of each internode to the lower one and from the external surface to the inner lacuna [93]. As bamboo grows, the fibre cell walls thicken progressively. This increase in wall thickness, primarily due to lignification, is a key factor for the bamboo suitability for structural applications. It is generally accepted that bamboo reaches sufficient mechanical maturity sufficient for construction from around three years of age. Li et al. [96] studied the chemical composition of bamboo culms at different age, reported for a three years old bamboo a concentration of lignin around the 23%, while Fiore et al. [89], which compared the chemical composition of different natural fibres, reported a value of 17% for Arundo donax. Regarding lignin distribution, Parameswaran and Liese [94] observed that the narrow lamellae have a higher lignin concentration than the broad ones.

Data on fibre length are available from the literature and show considerable variation between species. Liese & Grosser [97] reported values ranging from 1.04 to 2.88 mm. In particular, four species of Phyllostachys were studied in that work—P. edulis, P. bambusoides, P. nigra, and P. reticulata—with fibre lengths of 1.56 mm, 2.15 mm, 1.04 mm, and 1.56 mm, respectively. It is reasonable to assume that fibre length of our Phyllostachys species is in a similar range. Wahab and his collaborators [98] studied changes in fibre length according to the part of the culm. In particular, they found it decreases towards the node and along the cross section, in which they found values of 1.6, 2 e 1.8 mm respectively for the external, middle and inner section of the thickness of the culm of a Gigantochloa Scortechinii.

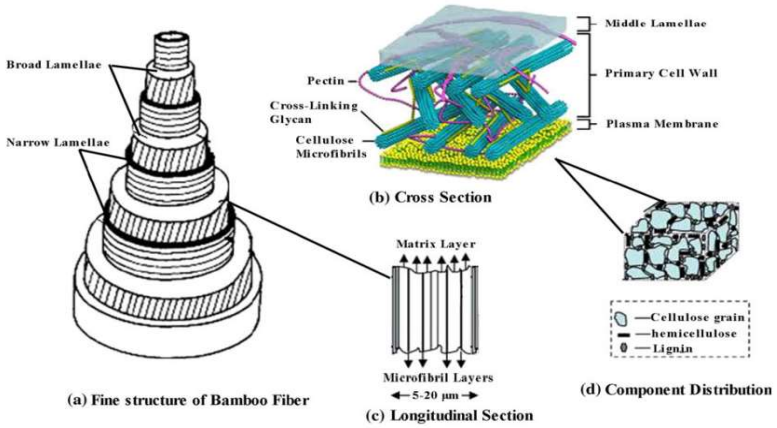

Figure 29 Model of the polylamellate structure of a thick-walled bamboo fibre. From [94]and [99]

The cross-section of sclerenchymatic tissue is shown in Figure 30 at a magnification of 25X for each species. All images were taken from the same area of the culm cross-section. Even at this level of zoom, structure and channels between layers are clearly visible. At first glance, no significant differences can be observed in the fibre structure, while differences in dimensions are already noticeable.

The multilayer structure of the fibres has been clearly encountered in this investigation. In Figure 31, the entire structure of the cell of a P. edulis is shown through a magnification of 40X: a central hole which name is lumen and around it a series of layers which correspond to the cell walls.
Moreover, several channels have been found between the cell walls, which respond to the need of exchanging substances. The same result has been obtained for the other six species.

Dimension of the fibres are reported in Table 5. The average fibre diameter ranges from 12 to 20 μm in the inner part and from 15 to 22 μm in the outer part. The average lumen diameter ranges from 2 to 6 μm and from 2 to 7 μm in the inner and outer parts, respectively**.** Cell wall thickness varies from 4.5 to 7 μm internally, and from 6 to 9 μm externally. While the lumen appears to remain relatively constant, the fibre diameter shows a slight increase toward the outer part of the cross-section. Cell wall thickness is more strongly influenced by position within the culm, following the same increasing trend as the diameter. Despite these variations, the ratio between fibre diameter and wall thickness remains consistent.
Furthermore, in all six Phyllostachys species, fibres from the upper part of the culm (part A) are larger than those from the lower part (part B).

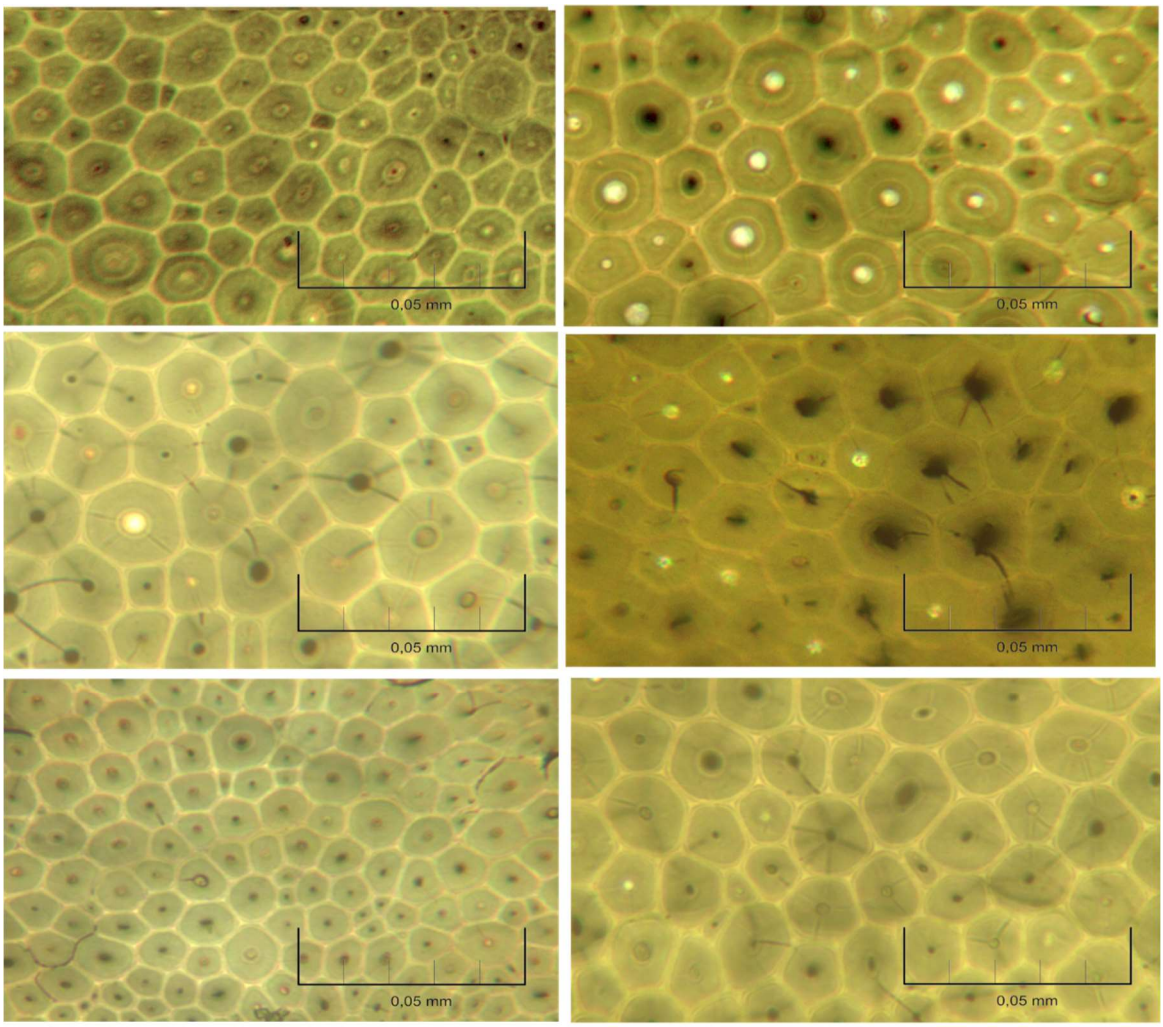

Figure 30 Sclerenchymatic tissue from the external side of the culm wall of P. a) edulis, b) bambusoides, c) viridiglaucescens, d) vivax, e) violacescens, f) iridescens. Transmission optical microscope, 25X enlargement.

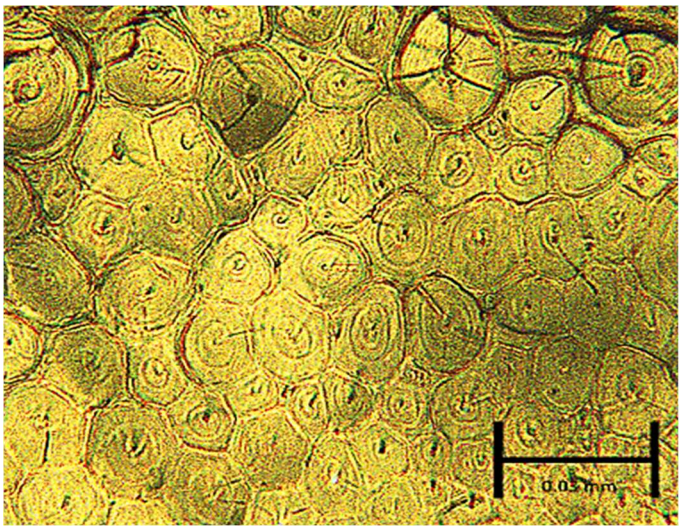

Figure 31
Structure of fibres in a P. edulis. The structure of the cell is evident: a central lumen, the multilayer structure of cell walls and channels between them. Transmission optical microscope, enlargement 40X.

Table 5 Fibre morphology. Fibre diameters, lumen diameters, and wall thicknesses are here reported for parts A and B of all the six bamboo species. The data refer to the average fibre were taken from both the inner and outer parts of each sample's cross-section. Each fibre was approximated as having a circular cross-section.

		INNER			OUTER		
Name of the species	Part of the culm	Fibre diameter (µm)	Lumen diameter (µm)	Wall thickness (µm)	Fibre diameter (µm)	Lumen diameter (µm)	Wall thickness (µm)
P. edulis	A	14	2	6	17	3.5	6.75
	B	14	3	5.5	15	2	6.5
P. viridiglaucescens	A	15	3	6	21	4	8.5
	B	14	4	5	19	4	7.5
P. bambusoides	A	18	4	7	20	4	8
	B	16	2.8	6.6	22	7	7.5
P. vivax	A	20	6	7	19	2	8.5
	B	13	2	5.5	21	5.8	7.6
P. iridescens	A	16	2	7	21	3	9
	B	18	6	6	17	2.5	7.25
P. violacescens	A	12	3	4.5	17	3.8	6.6
	B	13	4	4.5	15	3	6
Arundo donax	A	14	2	6	16	1.5	6.5
	B	18	1	8.5	20	3	8.5

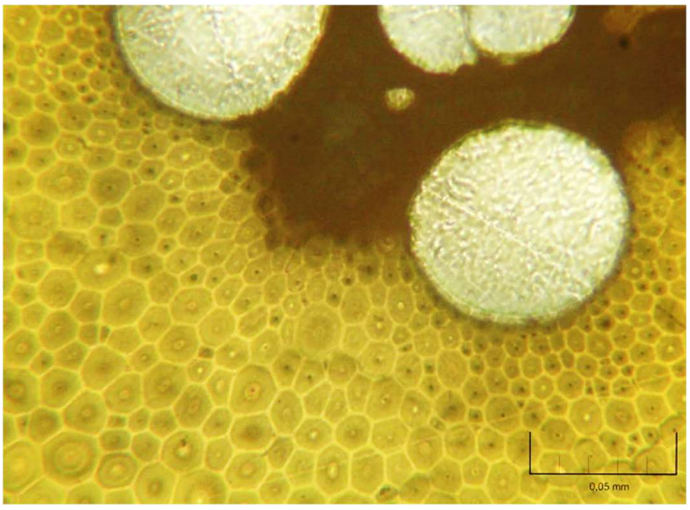

Figure 32
Progressive increase of fibre dimension from the vessel's edge to the parenchymatic matrix. An image of a P. edulis from the upper part of the culm. Transmission optical microscope, enlargement 25X.

Dimensional variations have also been observed within the sclerenchymatic islands. Specifically, a general trend of increasing fibre size is seen toward the boundary near the parenchyma, and a decrease is observed near the vessels, as though they exert compressive forces on each other. This phenomenon is illustrated in Figure 32.
Along the culm length, fibre width tends to increase with height, while along the cross-section fibre thickness tends to increase towards the outer surface. This observation is consistent with findings in the literature [100].

Parenchyma

The matrix in which fibres and vessels are embedded is the parenchymatic tissue, made by elongated polyhedral cells. In Figure 28, parenchymatic tissue is visible as several pads between fibres and vessels. In particular, the biggest ones surround the group of sclerenchyma and vessels, while the smallest ones fill the interstices between them.
These cells have a very simple structure which consist of middle lamella, primary wall and cytoplasm structure. The primary cell wall is very thin made by a rigid lattice of microfibrils embedded in a matrix made of water and pectins which form the major percentage of the total volume of the cell wall. Adjacent cells are connected by some channels that allows the transmission of thin strands of cytoplasm and endoplasmic reticulum, as these cells remain alive during the life of the plant. For this reason, parenchymatic tissue does not undergo lignification except during the germination. Parenchyma serves as a major storage of substances for the plant, which are located into vacuoles and plastids through starch granules.
In Arundo donax, parenchymatic cells have significantly lignified cell walls, in contrast to bamboo parenchymatous cells.

In this study, no significant differences were found in the parenchymatic tissue among all six species of bamboo and Arundo donax, as can be noticed by the comparative images in Table 6, while cell dimension is highly variable. Dimension of parenchyma cells are extremely variable at every height of the section, but generally they tend to decrease near sclerenchyma cells and towards the external surface of the culm. Morphology is almost the same but towards the inner side cells tend to exhibit an almost circular shape in Arundo donax while they tend to get longer in bamboo culm.
The particular morphology of these cells made them difficult to observe using the optical transmission microscope. Due to their short and “cube-like” shape [92] the light struggles to pass through the section resulting in dark images result dark.

Name of the species	INNER		MIDDLE		OUTER	
	A	B	A	B	A	B
P. edulis	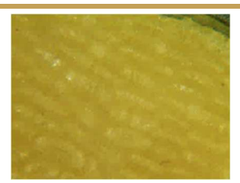	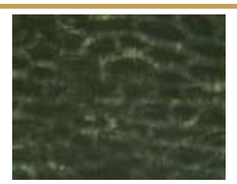	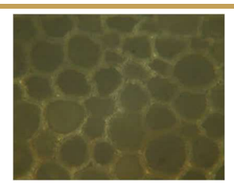		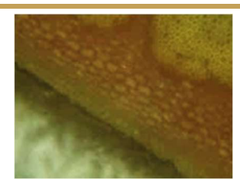	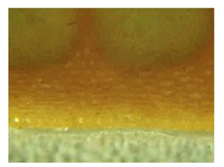
P. viridiglaucescens	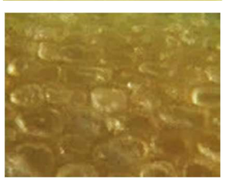	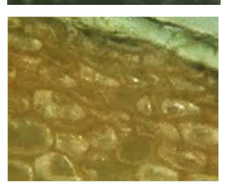	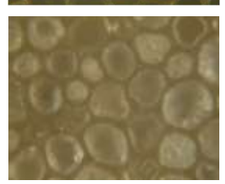	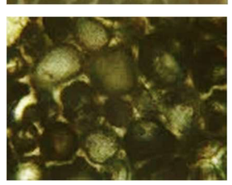	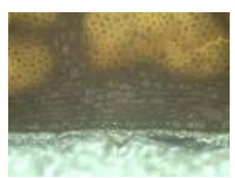	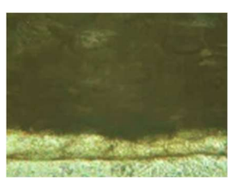
P. bambusoides		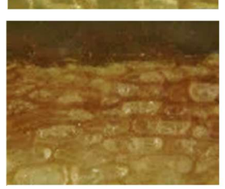	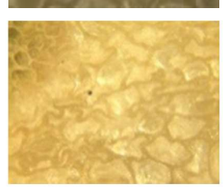	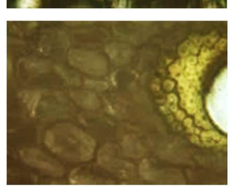	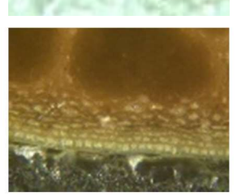	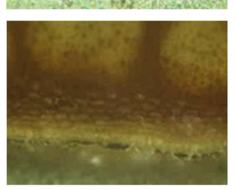
P. vivax			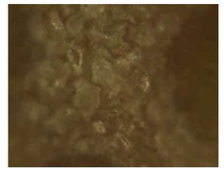	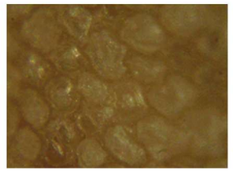	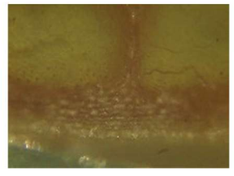	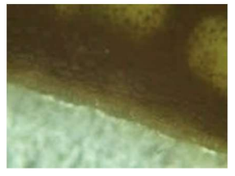
P. iridescens		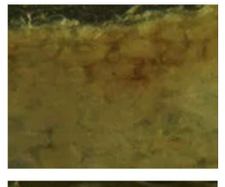	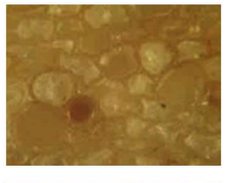	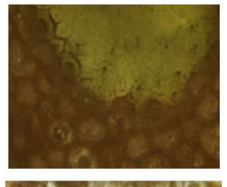	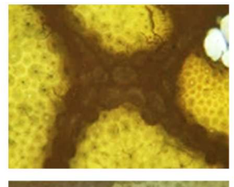	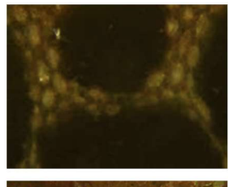
P. violacescens			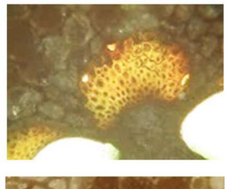	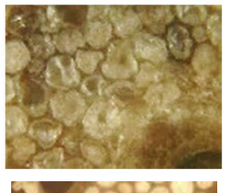	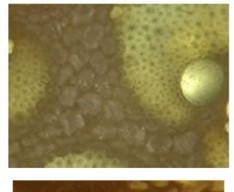	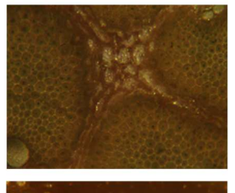
Arundo donax		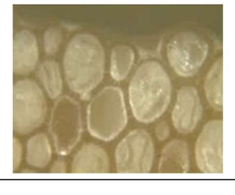	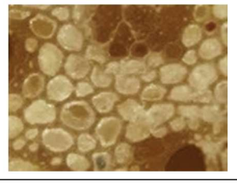	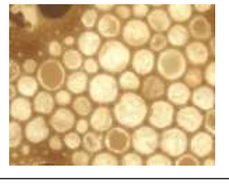		

Table 6 A small portion of parenchyma taken from the inner, middle and outer part of the cross section of each species, considering both part A and part B of each culm. Transmission optical microscope, enlargement 25

However, in this study, clear visualization was achieved using optical reflection microscopy or in some cases with a mixed technique to enlighten sclerenchymatic tissue too. The inner part of the cell is generally visible as a white circle, due to the presence of resin that filled the empty parenchyma cell during the preparation of the sample.

Vascular bundles

In Figure 33, a collection of the vascular bundles from the inner, middle and outer part of the culm wall cross-section of each species is reported. P. edulis, P. bambusoides, P. iridescens, P. violacescens, P. vivax and P. viridiglaucescens all exhibit a single type of vascular bundle across the culm wall thickness, which consists of a single central vascular strand and the island is concentrated only in sheaths around vessels. This is typical for all the bamboo species with leptomorph rhizomes [92].

The shape of the sheaths varies along the thickness. In the inner side, the sheaths appear as four little islands around the vessels and the intercellular space. Towards the external side, they extend becoming two big fibres islands surrounding the vessels: a bigger one for the two xilematic vessels and a smaller one for the phloematic ones. The intercellular spaces seem to disappear. Finally, near the external surface, vessels became very small and rare, while fibres islands remain.

Dimensions of an average vascular bundle are reported in Table 7. Generally, it can be observed that the inner vascular bundle has a greater width and a smaller height, while the outer vascular bundle has a greater height and a smaller width; moreover, the ones from the top part of the culm look smaller than those from the bottom part, both in width and height. The increase of the dimension of the average vascular bundle will be clearer in the next paragraph. Different species present similar dimensions of the vascular bundles, except for P. violacescens species, which has lower vascular bundle dimensions, both in height and width. In the case of Arundo donax, a ring of sclerenchymatic tissue surrounds the vessels, without any subdivision in island. No difference in the shape of the vascular bundles was found along the thickness, while dimensions decrease appreciably near the external part of the culm wall, as a result from the observation of Table 7 and Figure 33.
Regarding differences along the length of the culm. has been observed that vascular bundles from the upper part of the culm (part A) are smaller than those of the lower part (part B).

SPECIES	INNER		MIDDLE		OUTER	
	A	B	A	B	A	B
P. edulis	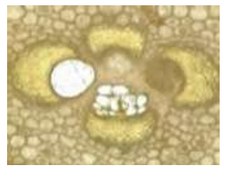	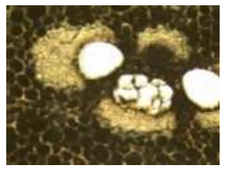	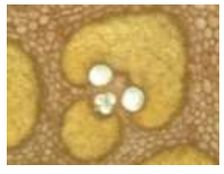		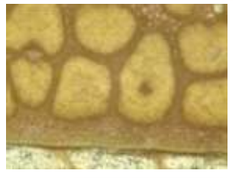	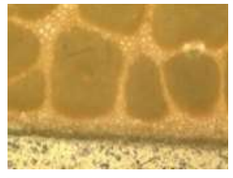
P. viridiglaucescens		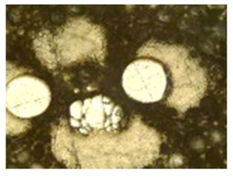			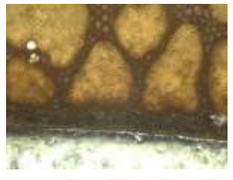	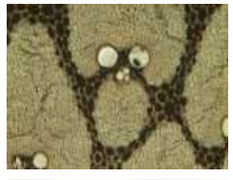
P. bambusoides					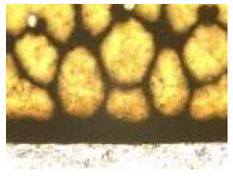	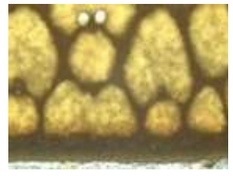
P. vivax		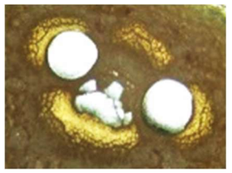	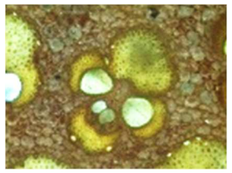	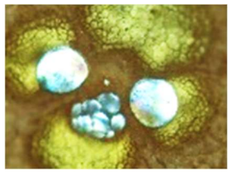	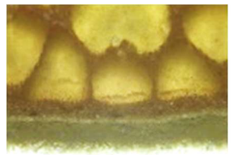	
P. iridescens		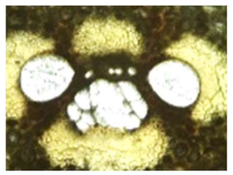	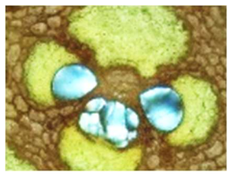		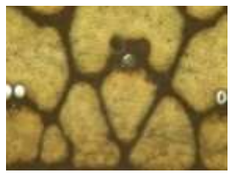	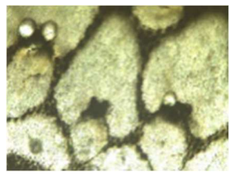
P. violacescens				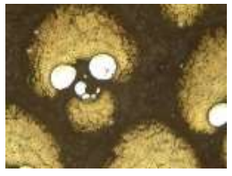		
Arundo donax	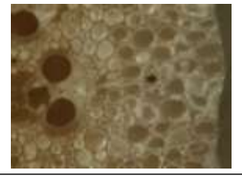	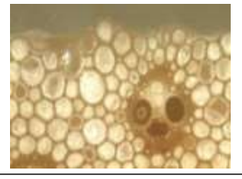	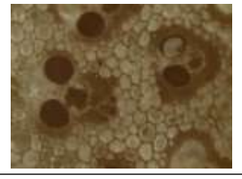	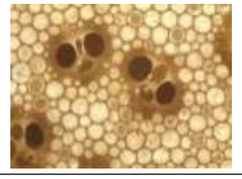		

Figure 33 A vascular bundle taken from the inner, middle and outer positions along the culm wall, for part A and B of each culm. Transmission optical microscope, enlargement 10x

Table 7 Dimensions of an average vascular bundle from the inner, middle, and outer parts of the culm wall considering three typical bundles in each portion. W_{max} stands for the maximum width (measured along the circumferential direction), while H_{max} for the maximum height (measured along the radial direction)

Name of the species		INNER			MIDDLE			OUTER		
		W_{max} [mm]	H_{max} [mm]	$\frac{W}{H}$	W_{max} [mm]	H_{max} [mm]	$\frac{W}{H}$	W_{max} [mm]	H_{max} [mm]	$\frac{W}{H}$
P. edulis	A	0.66	0.40	1.69	0.49	0.47	1.06	0.31	0.51	0.61
	B	0.72	0.45	1.60	0.59	0.57	1.03	0.35	0.49	0.71
P. viridiglaucescens	A	0.76	0.50	1.52	0.58	0.61	0.95	0.34	0.60	0.57
	B	0.76	0.53	1.43	0.51	0.69	0.74	0.30	0.57	0.53
P. bambusoides	A	0.68	0.41	1.33	0.46	0.63	0.73	0.25	0.42	0.60
	B	0.72	0.48	1.76	0.49	0.58	0.86	0.25	0.49	0.51
P. vivax	A	0.70	0.40	1.78	0.54	0.59	1.04	0.36	0.56	0.64
	B	0.75	0.44	1.57	0.60	0.72	0.77	0.34	0.49	0.69
P. iridescens	A	0.42	0.36	1.25	0.37	0.41	0.90	0.24	0.40	0.60
	B	0.45	0.37	1.22	0.41	0.45	0.91	0.28	0.40	0.68
P. violacescens	A	0.66	0.47	1.40	0.56	0.56	1.05	0.32	0.59	0.54
	B	0.75	0.51	1.47	0.58	0.65	0.86	0.40	0.66	0.61
Arundo donax	A	0.27	0.30	0.90	0.24	0.19	1.26	0.19	0.15	1.27
	B	0.20	0.33	0.61	0.21	0.21	0.98	0.18	0.18	1.00

A zoom-out on the cross-section

In order to better understand the changes along the length of the culm cross section described by the measurement previously reported, a zoom out has been done. A subdivision of the whole cross section in three main zones has been reported. The representative case of P. viridiglaucescens is reported in Figure 34a, while the images from the three zones of the other species are provided in Appendix A. A magnification of 10X has been chosen, in order to allow a good display of the components. From the lower part of the picture, can be identified three main zones:

- The external layer,

  which protects the culm from the environment and reduces water loss. In the figure, two types of parenchymatic cells are clearly distinguishable in this section. The almost circular ones around the vessels, and the elongated ones near the external surface. The fibre bundles occupy the biggest part of the surface, since they are big and very closer to the others. Vessels are disappearing, and only a small xylematic and a little group of phloematic ones can be detected in that picture. That means that fibres are grouped together without the function of supporting vessels, in two or even a unique island. Finally, near the end, changes in colour indicate a change in composition. This is the epidermis, which, according to Liese [87], contains axially elongated cells, shorter cork and silica cells, and the stomata. High amount of silica strengthens the epidermal layer. The epidermal cells are often covered on the outside by a cutinized layer of cellulose and pectin with tangential lamellated structure, finally sealed by a wax coating.

- The central layer,

  in which the entire area of the picture is occupied by a unique vascular bundle. It means that, with respect to the previous layer, dimensions of the vascular bundle have significantly increased. In fact, vessels increase a lot towards the inner lacuna, and fibre sheaths consequently expand. It results in a sequence of vascular bundles, distributed into the space even more largely towards the internal layer. The increase of dimension of parenchyma cells previously described is here evidently shown, since they occupy even more spaces between fibre sheaths.

- The internal layer

  is that one which surrounds the lacuna, and consists mainly of parenchyma cells. In the representative picture of Figure 34a, most of the space is occupied by parenchyma cells in fact. Just a small end of the sclerenchymatic tissue of a vascular bundle is present. The change in shape of parenchyma is clearly shown in the picture, when they stretched tangentially and shortened in radial and longitudinal directions, in the “transition layer” which precedes the skin of the lacuna. According to Liese and Schmitt [101], the composition of the skin

consists of 2-6 rows of parenchyma thin—walled collapsed cells, which number can vary according to the species. The great importance of this layer is strictly connected to its diffusion capacity, which might have a distinct influence on the treatment efficiency.

The same subdivision is here presented also for Arundo donax. For comparison, it is divided into three zones, although the literature [14] suggests that two may be sufficient. By the observation of Figure 34b is it possible to distinguish from the bottom to the top:

- The external layer

  characterized by a darker zone, which is a sclerenchymatic ring. It includes some small vascular bundles and divide this layer into two zones. On one side of this ring there are epidermis and cortical cells organized in small cells [102], on the other side the ground parenchyma of the middle layer. It means that, differently from bamboo, Arundo donax has a sort of defensive wall before the epidermis, which intensively strengthens this part.

- The central layer presents a structure similar to that one of bamboo, with vascular bundles surrounded by sclerenchymatic tissue embedded in the ground parenchyma. However, fibres bundles seem to be significantly thinner with respect to those observed in bamboo and with a circular crown shape around the vessels. Vascular bundles look smaller and more recurring near the external layer, while they seem to become bigger and sparser near the terminal surface of the cross-section. The same trend is observable for parenchyma cells.

- In the internal layer, the reduction of vascular bundles continues until the cavity, leaving the place at a parenchyma band. Unlike bamboo, no significant differences in shapes and dimensions of parenchyma cells are observed in this case.

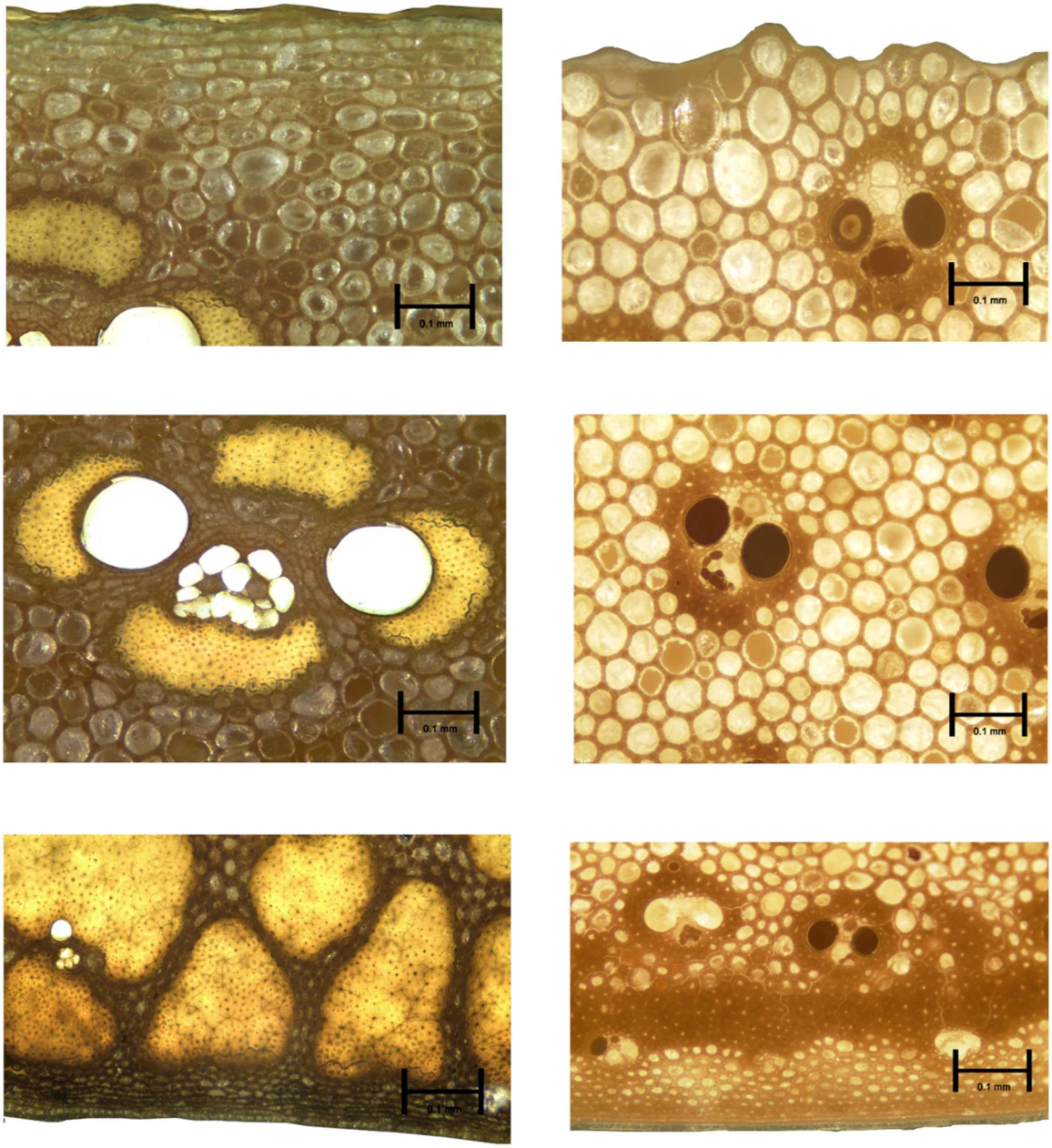

(a) (b)

P. viridiglaucescens **Arundo donax**

Figure 34 From the bottom to the top: a piece from the external, central and internal part of the section of a P. viridiglaucescens on the left, and Arundo donax on the right. Enlargement 10x

Finally, the complete cross-sectional views of the bamboo species and Arundo donax are presented in Figure 35. In the case of bamboo, due to the size of the specimens and the need to preserve image detail, the full cross-sections were obtained by stitching together multiple adjacent images. Conversely, the smaller size of Arundo donax allowed to capture the entire cross-section in a single image of the same enlargement.
The first evidence is the spreading out of the vascular bundles, from the external part of the culm wall to the inner one. They intensifying their number and decreasing their thickness. This particular distribution of the components is functional to bamboo mechanical behaviour as it can be considered a natural functionally graded material. This is true for both bamboo and Arundo donax, despite in the part A of this species it is less evident.

Some differences between the species can be also distinguished by the observation of these pictures. Firstly, the distance from the inner lacuna to the last vascular bundle, can notably changes. For instance, in the case of P. edulis, a thick transitional layer completely made by parenchyma cells is evident. On the contrary, in the case of P. vivax, the last vascular bundle seems to want to get out. Differences in dimensions of the vascular bundles are also evident at a glance, confirming the results reported in the measurement of Table 7.
Differences in colours are mainly due to the modification in light which allowed a better understanding of the morphology.

No meaningful images were found from the longitudinal sections; therefore, they are not included in this thesis.

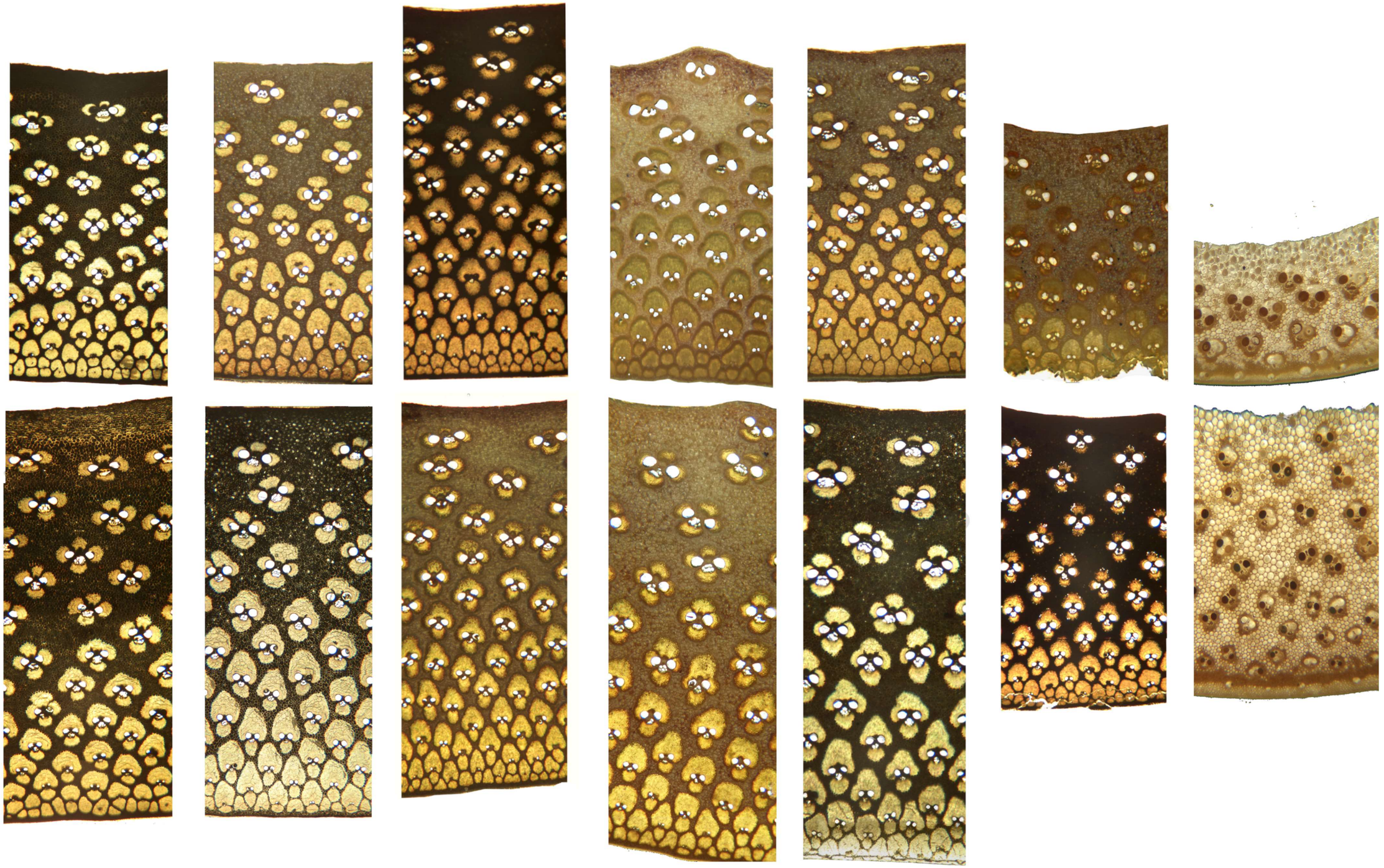

Figure 35 Slices from the cross section of bamboo plants and Arundo donax. Sample from A part in the upper figures and sample from B in the lower part of the figur

Amount and distribution

Since the presence of each component influences the mechanical behaviour of the material, the next phase of this study focused on quantifying their relative amount and distribution. Both bamboo and Arundo donax are not homogeneous materials, therefore a detailed understanding of the amount and distribution of their internal structure component is fundamental.
In literature, some studies have been conducted on other bamboo species. Dai and co-workers [103] investigated the morphological characteristics of Dendrocalamus sinicus vascular bundles along the radial direction and discovered that the distribution of length, width, length to width ratio, and area of vascular bundles can be described by quadratic functions. Li and co-workers [96] observed in a five-year old bamboo a vascular bundle concentration of 298 to 458 bundles/cm^2, for the bottom and top parts respectively, in the external part of the culm, and a difference of 458 to 148 bundles/cm^2 for the outer and inner parts of the culm wall.
The present study focuses on the surface area occupied by each component in respect to the overall surface and then, on the analysis of their location along the radial and tangential direction. The attention was placed primary on fibres, which are largely connected to mechanical strength and stiffness, and vessels, which act as voids within the structure and can significantly affect the mechanical performances of the culm.

Area percentage

Methods

The process to obtain the image for the calculation of the area percentage occupied by each component is described in Figure 36. For each species analysed, a representative cross-sectional image has been selected and redrawn with splines using CAD software (Autocad 2023, from Autodesk). Subsequently, the presence of each component has been highlighted by applying black and white contrast filters using the opensource images manipulation software GIMP 2.10.24. The analysis focused on two primary components: fibres and vessels. Vessels have been identified as voids, since the area of the walls of vessels can be overlooked as it is very small,

and can be included in fibres for its big amount of lignin. Moreover, the importance of the study of this component is mainly connected to the role that voids can be in mechanical behaviour. The percentage of parenchyma has been obtained by the difference between the total area and the ones of the other two components. The mean area percentage of each component is reported in Table 8 for both bamboo and Arundo donax.

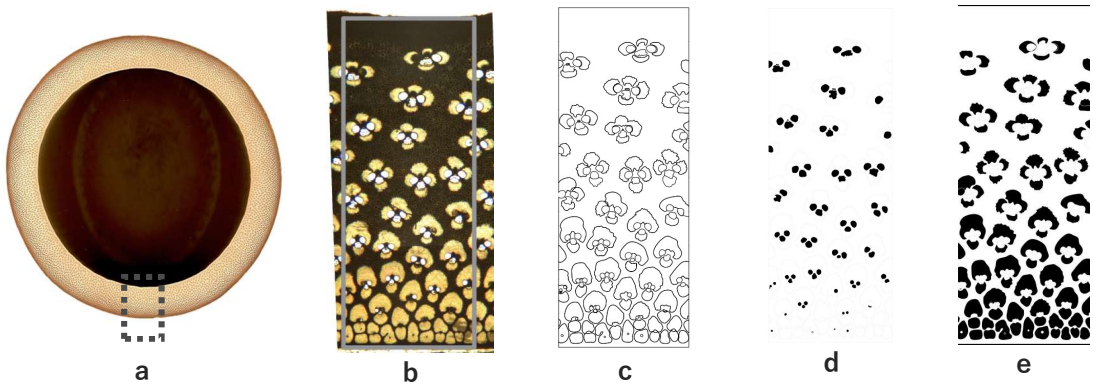

Figure 36 Image processing for P. edulis from the part A of the culm: the portion was selected from the culm section (a) and then an image was obtained with transmission microscope (b). A vectoral image (c) was then obtained with Autocad and divided into vessels(d) and fibres (e)

Results

Bamboo has a fibre content between 26 and 39%. Some species turn out to have a higher content than others, as P. bambusoides, P. viridiglaucescens, P. vivax, and P. iridescens. Arundo donax has a fibre area percentage under 20%, significantly less than bamboo. Generally, part A showed a fibre percentage ranging from 0.78% to 20.5% higher than part B, for all the species analysed, except P. viridiglaucescens, in which the fibre percentage is higher in the part B. Results are similar to those reported in the literature for other species. Studies on other Phyllostachys species reported fibre percentages of 32.2% for a Phyllostachys glauca [104], and a range of 36 to 44% for a Phyllostachys aurea [105]. Studies on other well-known species document a percentage of fibre of 37.66% for a Dendrocalamus giganteus [88] or 40% for Guadua angustifolia [106].

The percentage of area occupied by vessels, ranged from 4 to 7% in bamboo samples. No significant trend was found to define a difference between part A and part B or between bamboo species. Arundo donax displays a higher percentage of area occupied

by vessels, which is about 160% of that in bamboo. Results for P. species in this study are slightly lower than those reported in the literature for other Phyllostachys species, such as 8.7% for P. glauca [104], a range between 9 and 13% for P. aurea [105]. The same result concern also other bamboo species, as Dendrocalamus giganteus in which the voids percentage is 9.2% [88] and Guadua angustifolia for which 9% is reported [106].

The content of parenchyma is the biggest amount between the components, ranging from 55% in P. vivax from the part A to 69% in P. edulis from the part B. Generally, a biggest content of parenchyma is observed for the part B of each bamboo species, except for P. viridiglaucescens in which is the opposite. Species which shows a bigger amount of fibres have a lower amount of parenchyma, as the content of vessels is almost the same for all the species. In particular, P. edulis and P. violacescens have a major amount of parenchyma. Arundo donax has a parenchyma area percentage around 75%, significantly more than bamboo one.

Table 8 Percentage of area occupied by each component for part A and B of each species analysed

Name of the species		Fibre (%)	Vessels (%)	Parenchyma (%)
P. edulis	A	29.4	5.0	65.7
	B	27.0	3.9	69.1
P. viridiglaucescens	A	33.3	4.6	62.1
	B	38.1	4.9	57.0
P. bambusoides	A	38.8	4.5	56.7
	B	38.5	4.7	56.8
P. vivax	A	38.8	6.1	55.1
	B	33.3	4.7	62.0
P. iridescens	A	37.6	6.9	55.5
	B	31.2	5.0	63.8
P. violacescens	A	27.9	5.8	66.2
	B	26.3	6.5	67.2
Arundo donax	A	17.0	8.7	74.3
	B	15.6	6.0	78.5

Methods

The distribution of fibres and voids has been studied both along the radial and circumferential directions of the culm cross section. Part A and B have been considered for each Phyllostachys species and Arundo donax. Graphs and functions have been obtained for each distribution, employing the Labfit software [107]. Various types of three-parameter functions were tested, such as exponential, hyperbolic, and linear.

Results

Along the radial direction, specific trends have been observed for the distribution of fibres. Arundo donax presents an almost constant fibre distribution until the approach to the external extremity in which there is a peak, just in correspondence of the sclerenchyma ring, that is clearly visible in Figure 37. Bamboo shows an increase of the content of fibre from the inner to the outer part of the section. The best fit in this case was obtained using exponential and hyperbolic functions, as visible in Figure 38, in which curves for a P. bambusoides from part A are shown. However, it is shown that a linear curve could be a good approximation too. All the bamboo species shown a similar behaviour, so only one is here presented. Functions describing the trend for all the others species can be consulted in Appendix B. Regarding voids distribution along the radial direction, the best fit has been founded using the parabolic functions, for both bamboo species and Arundo donax. Figure 39 and Figure 40 report the results for a P. bambusoides from the part A and Arundo donax from part A respectively.

No significative trend was found along the circumferential direction, as the distribution is almost constant for both bamboo species and Arundo donax, as visible in Figure 42 for a P. bambusoides from the part A.

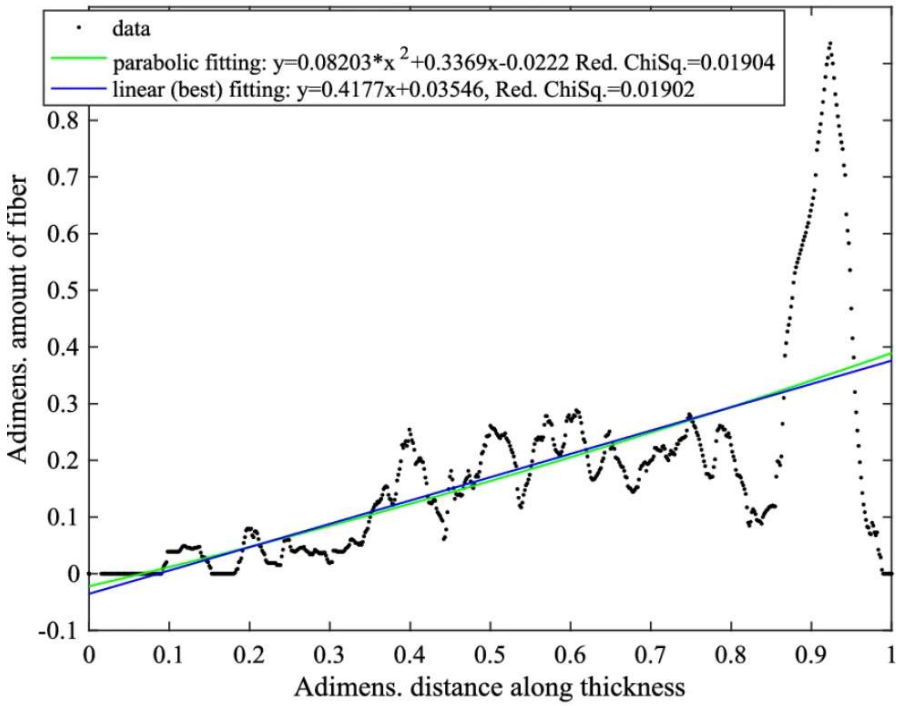

Figure 37 Distribution of the fibres along the radial direction, named as thickness, and fitting curves for Arundo donax, from part A of the culm

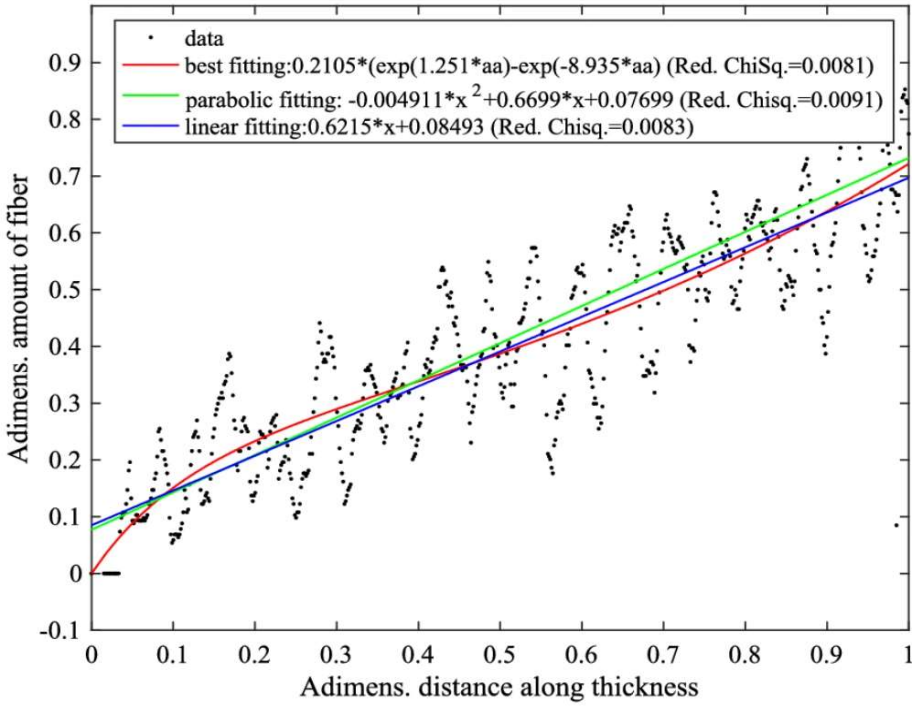

Figure 38 Distribution of fibres along the radial direction, named as thickness, and fitting curves for P. bambusoides, from the part A of the culm

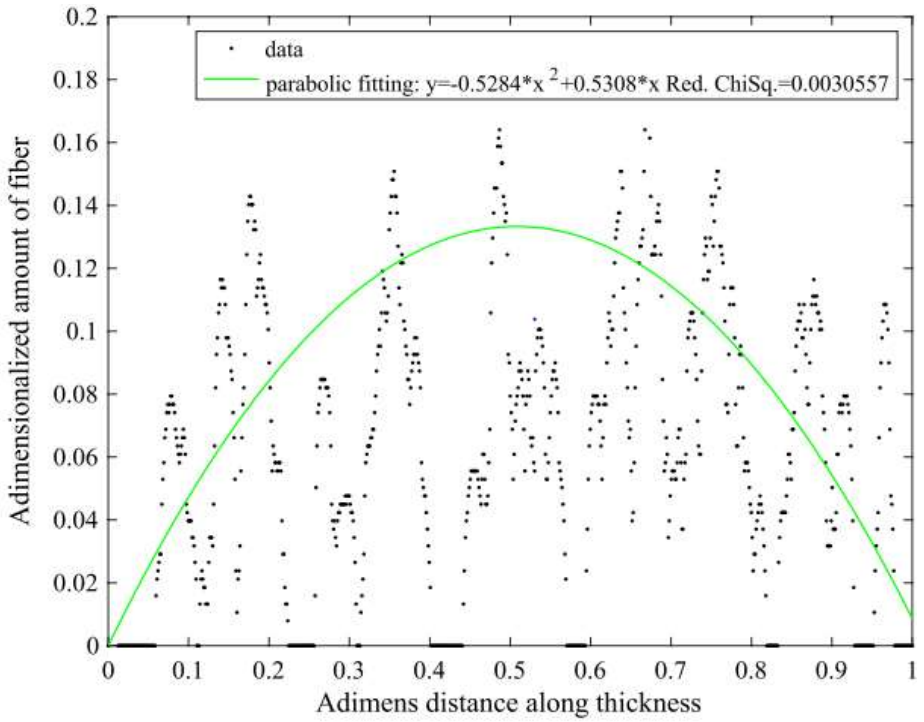

Figure 39 Distribution of the voids along the radial direction, named as thickness, and fitting curves for Arundo donax, from part A of the culm

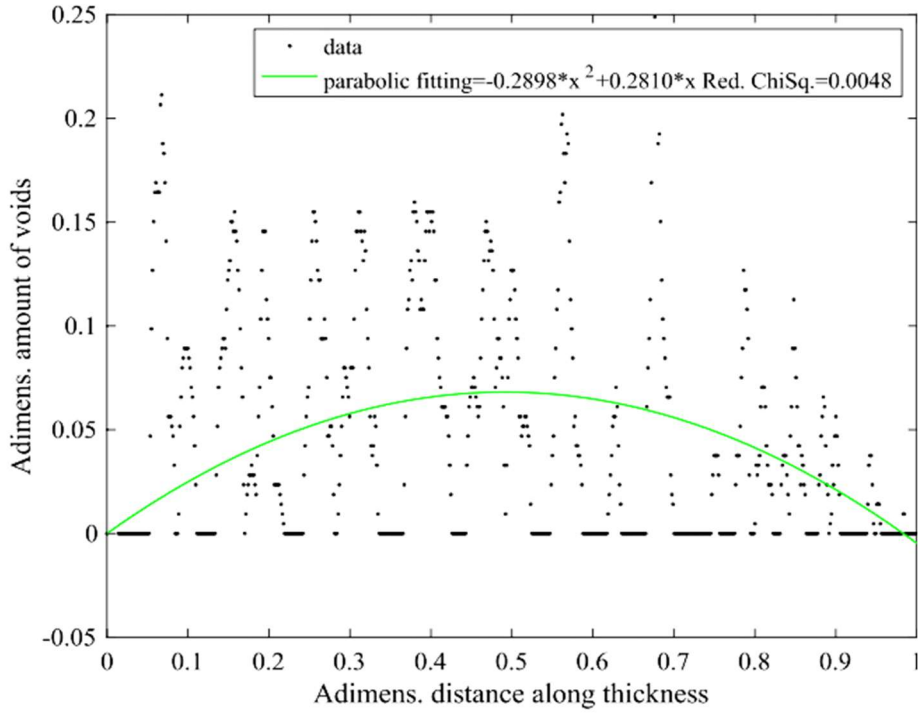

Figure 40 Distribution of voids along the radial direction, named as thickness, and fitting curves for P. bambusoides, from the part A of the culm

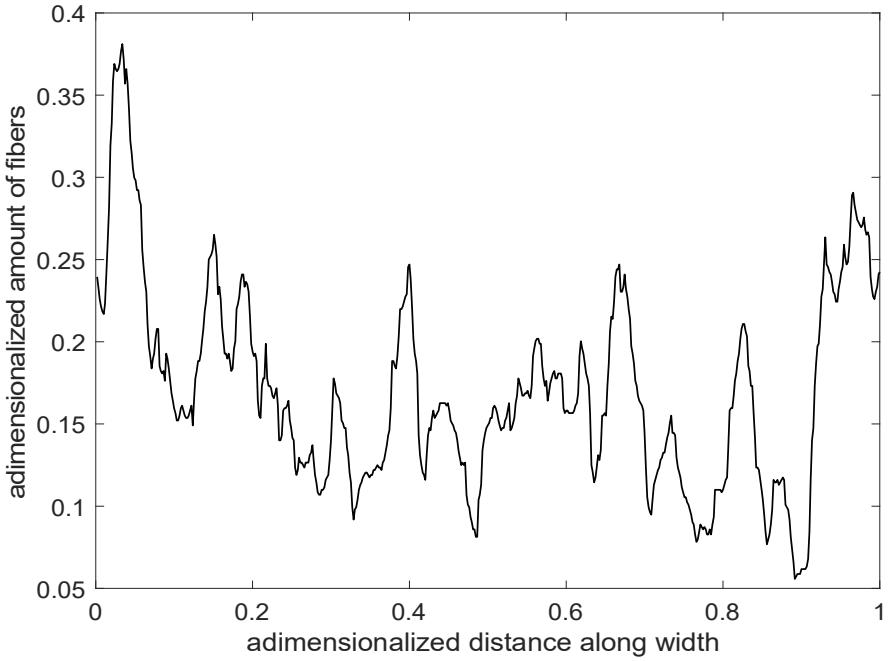

Figure 41 Distribution of the fibres along the circumferential direction, named as width, for Arundo donax, from part A of the culm

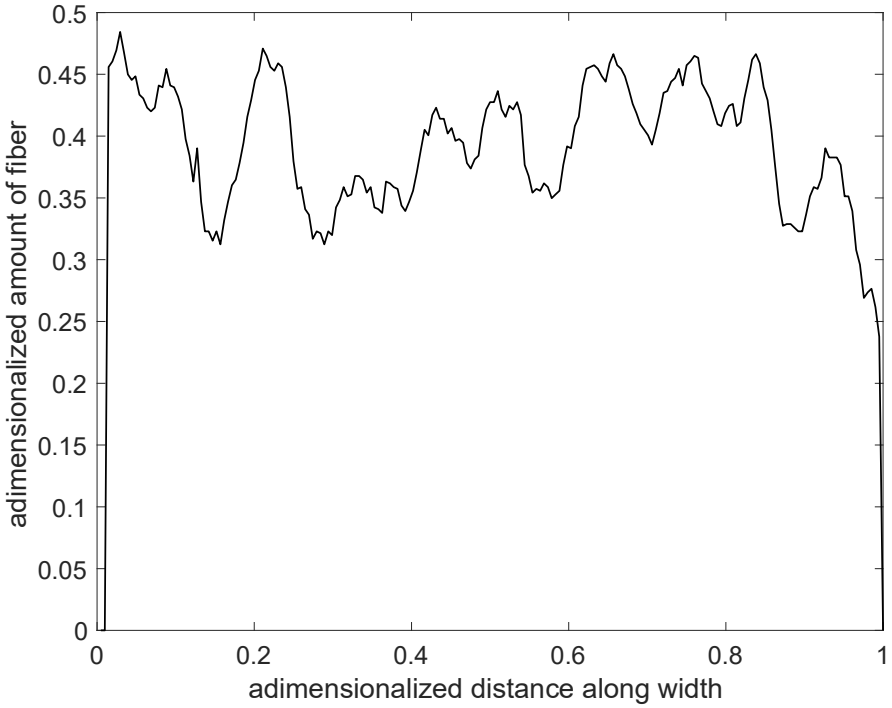

Figure 42 Distribution of the fibres along the circumferential direction, named as width, for P. bambusoides, from part A of the culm

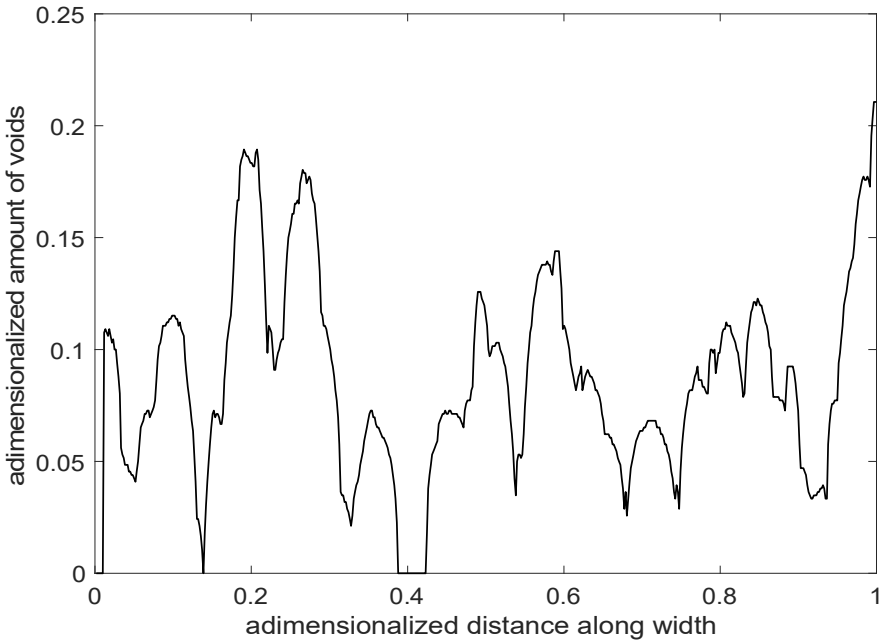

Figure 43 Distribution of the voids along the circumferential direction, named as width, for Arundo donax, from part A of the culm

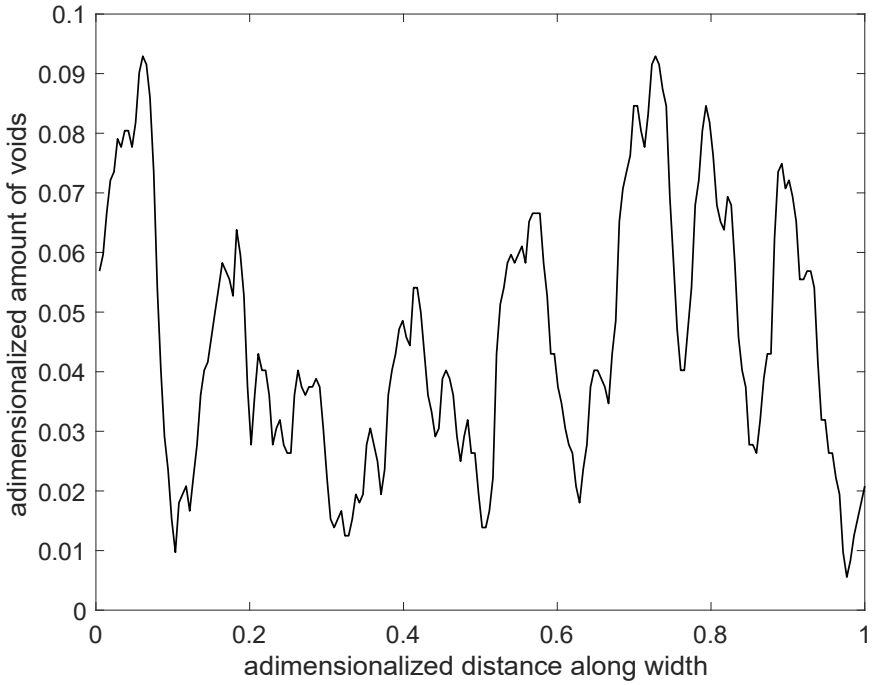

Figure 44 Distribution of the voids along the circumferential direction, named as width, for P. bambusoides, from part A of the culm

MESO SCALE

Bridging microscopic features with mechanical behaviour

In the third chapter, a broader perspective is adopted to explore how the microstructure influences the mechanical behaviour of the material.

The role of the microstructural components of bamboo in macroscopical behaviour has been largely discussed in literature. The relatively small (2° –10°) angle of microfibrils in fibre cell wall is a significant factor which contribute to the extremely high tensile strength, flexural strength, and rigidity of the fibre poly-lamellate wall structure [99]. The modulus of elasticity in longitudinal direction is connected to the stiffness of fibre, in particular from the stiffness of the single crystal cellulose and the characteristic microfibril angle [108]. Wang et al. [109]observed that the almost axially oriented cellulose fibrils in the fibre walls maximize the longitudinal elastic modulus of the fibres and their lignification increases the transverse rigidity [107]. Wahab and co-workers correlated shear and tensile strengths with vascular bundles and fibres dimensions [98]. They found that shear and tensile strengths have a positive relationship with the number of vascular bundles, while a decrease is observed for tensile and shear strengths when vascular bundle size increases. Regarding fibre morphology, only the fibre wall thickness has been deemed to have a significant positive correlation with shear strength, but a clear correlation with tensile strength cannot be observed. Krause et al. observed that fibre bundles consist of an exclusively tension-resistant geometry, but when associated with the matrix along their length, they also provide reinforcement in compression due to the stiffer and stronger crystalline cellulosic composition, as compared to the lignified amorphous nature of the parenchyma [88]. Dixon and Gibson highlighted that the compressive strength of bamboo in the axial direction increases linearly with density, while the radial and tangential compressive strengths are almost constant with density [110].

Generally, the structure of bamboo is the one of a functionally graded composite material thanks to the cooperation between its strong fibres and the soft matrix in which they are embedded, as it has been recognized by Amada et al. [86]. But it means a significant anisotropy, which makes the tensile and compressive strength along the longitudinal direction relatively high when compared to transverse and shear strengths. This explain why detailed studies on the correlation between microstructure and mechanical performance are necessary and are explored in this thesis.

In the first section, a direct correlation between data obtained from the observation of the microstructure and those obtained from experimental tests will be presented. In the second section, the prediction of the longitudinal properties of bamboo will be explored through analytical solutions. In the third section, a numerical solution will explore the transversal properties of the material. In the fourth section, a method for

the bending test of bamboo will be analysed, providing information on both components of the material through a simple and effective procedure. The application of that test on the ageing of the material due to UV light will be also presented. Finally, the use of this procedure as possible grading method will be exposed in the last fifth section.

Parts of this chapter have been published in:

Silvia Greco and Luisa Molari, «Flexural Behaviour of Five Species of Italian Bamboo» (2022) *Construction Technologies and Architecture. Trans Tech Publications Ltd*, vol. 1, pp. 723-729, https://doi.org/10.4028/www.scientific.net/cta.1.723

Silvia Greco, Luisa Molari, Giovanni Valdrè and Jose Jaime Garcia (2022, July 8) «Finite element analysis for the prediction of the circumferential bamboo strength» 18th International Conference on Non-conventional Materials and Technologies (NOCMAT 2022). https://doi.org/10.5281/zenodo.6811560

Silvia Greco, Mirko Maraldi and Luisa Molari «Grading bamboo through four-point bending tests. A report on six species of Italian bamboo» *Construction and Building Materials,* November 2023; 404, 133168 https://doi.org/10.1016/j.conbuildmat.2023.133168

Silvia Greco, Stefania Manzi, Luisa Molari, Andrea Saccani, Gianfranco Ulian, Giovanni Valdrè «Photodegradation of Bamboo: A Study on Changes in Mechanical Performances» *Materials* 2023; 16(1):285 https://doi.org/10.3390/ma16010285

Silvia Greco, Luisa Molari, Giovanni Valdrè and Jose Jaime Garcìa, « Multilevel analysis of six species of Phyllostachys bamboo and Arundo donax: preliminary survey on Italian grown stands» (2024) *Wood Science and Technology*, no. 58, pp. 1025-1049, https://dx.doi.org/10.1007/s00226-024-01547-0

A. Sghedoni “Analisi microscopica del comportamento meccanico e igro-meccanico di diverse specie di bambù italiano” (2024) Master Thesis, Università degli Studi di Bologna, 2024.

Correlation of microstructure with mechanical properties

A correlation between the mechanical characteristics and the data on microstructure of the studied material has been done. Mechanical characteristics of the six Phyllostachys species and Arundo donax were collected from literature, in particular from the results of experimental tests conducted in other studies by the author of this thesis and others researchers. Data used are collected in Here, maximum strength and modulus of elasticity are reported for: axial tension and its modulus, respectively $\sigma_{t,axial,max}$ and E_t ; axial compression and its modulus, respectively $\sigma_{c,max}$ and E_c; circumferential tension and its modulus, respectively $\sigma_{t,circumferential,max}$ and $E_{t,circumferential}$, which are calculated for both the inner and outer part of the culm wall; bending, for which are reported the bending strength $\sigma_{b,max}$ and a Young modulus E_h calculated approximating bamboo as a homogeneous material. The complete version of data and methods of those work can be found in the relative publications [111] [91] [112] [113] [114]. .

Differences between species can be read in light of what explored in the previous chapter and the reading of the mechanical characteristics.
P. bambusoides and P. iridescens species have a large percentage of fibre area and a large average fibre diameter and thickness. Both species exhibit a higher tensile and compressive strength and moduli of elasticity, respectively $\sigma_{t,axial,max}$ and E_t and $\sigma_{c,max}$ and E_t . On the contrary they have a relatively smaller circumferential inner strength and a medium bending strength in both configurations.
P. edulis has a lower percentage of fibre area compared to the others, while the average diameter of its fibres is smaller. It shows a good axial tensile $\sigma_{t,axial,max}$ and compressive strength $\sigma_{c,max}$ and a high circumferential inner strength. Compared to other bamboo species, P. edulis' s modulus of elasticity is lower in tension, compression, and bending, while it is twice that of the others in the circumferential tensile direction.
P. violacescens has the lowest values of fibre and vascular bundle dimensions and percentage fibre area. It results in a substantially lower tensile strength $\sigma_{t,axial,max}$ and a slightly lower compressive strength $\sigma_{c,max}$compared to the other species. It also shows a higher circumferential inner strength. In bending, it has the lowest strength in both configurations.
P. viridiglaucescens has a higher percentage of fibre area in part B of the culm, while

a medium value in part A. The average fibre size is higher near the external side of the culm wall, while it has medium values near the inner side of the culm wall. It results in medium tensile and compressive strength but shows the highest bending strength in both configurations.

P. vivax has a slightly lower tensile $\sigma_{t,axial,max}$ and compressive strength $\sigma_{c,max}$but a higher circumferential inner strength, similar to P. violacescens and P. edulis. It also shows good behaviour in bending tests, especially under fibre tension. This species has a high percentage of fibre area, especially in the upper part of the culm, and a thicker wall in both parts of the culm.

Arundo donax has, generally, strengths between 45 and 75% of those of bamboo, depending on the species considered. Compression strength $\sigma_{c,ma}$ ranges from 70 to 100% of the strength of the bamboo species considered. The modulus of elasticity is slightly lower compared to almost all the bamboo species. No differences between species regarding the circumferential outer strength were found.

Moreover, correlation between fibre area percentage and tensile strength was studied. Results show a linear correlation, as depicted by the graphs presented in Figure 45. The average value of the tension is represented by dots. The value of R^2 is higher than 0.7

Table 9 (in the next page) Values from experimental tests executed on al the six Phyllostachys species and Arundo donax. Maximum strength and modulus of elasticity are here collected. They are obtained from axial tension, respectively $\sigma_{t,axial,max}$ and E_t ; axial compression, respectively $\sigma_{c,axial,max}$ and E_c; circumferential tension, respectively $\sigma_{t,circumferential,max}$ and E_c, which are calculated for both the inner and outer part of the culm wall; and bending strength, respectively $\sigma_{b,max}$ and E_h. Moreover, the percentage of area occupied by fibre across the culm wall, the diameter and thickness of the average fibre are indicated

Species		Axial Tension [91] [111] [112]		Axial Compression [91] [111] [112]		Circumferential Tension [113]				Bending [114]		Fibre Area	Diameter of the Avg. Fibre	Thickness of the Avg. Fibre
		$\sigma_{t,axial,max}$ [MPa]	$E_{t,axial}$ [GPa]	$\sigma_{c,axial,max}$ [MPa]	E_c [GPa]	$\sigma_{t,circumferential,max}$ [MPa]		$E_{t,circumferential}$ [GPa]		$\sigma_{b,max}$ [MPa]	E_h [GPa]	[%]	[µm]	[µm]
						inner	outer	inner	outer					
P. edulis	A	210.3	17	75.6	27.0	36.4	26.3	3.9	2.8	143.7	15.9	29.4	15.5	6.375
	B	188.4	14.2	61.8	33.3	35.2	24.4	3.5	2.5			27.0	14.5	6
P. viridiglau-cescens	A	216.5	18.8	71.3	18.1	-	-	-	-	155.9	17.8	33.3	18	7.25
	B											38.1	16.5	6.25
P. bambusoides	A	234	21	82	38.8	13.3	30.6	1.3	3.5	147.5	20.25	38.8	19	7.5
	B	204	17	79	38.5	18.6	43	1.4	4.8			38.5	19	7.05
P. vivax	A	193.8	16.6	65.2	38.8	28.2	31.7	1.1	1.7	159.6	17.8	38.8	19.5	7.75
	B	176.3	15.3	64.5	33.3	12.1	40.3	0.7	2.1			33.3	17	6.55
P. iridescens	A	240.5	19.8	83.6	37.6	19.4	32.9	1.6	3.0	151	16.6	37.6	18.5	8
	B	220.7	16.2	76.6	31.2	16.9	31.8	1.4	3.6			31.2	17.5	6.625
P. violacescens	A	151	17.4	62.1	27.9	27.5	32.3	0.9	2.4	98.2	12.2	27.9	14.5	5.55
	B	138.2	19.1	56.8	26.3	16.3	23.8	1.2	1.7			26.3	14	5.25
Arundo Donax	A	111.7	15.2	57.0	13.4	-	-	-	-	74.4	10	17.0	15	6.25
	B											15.6	19	8.5

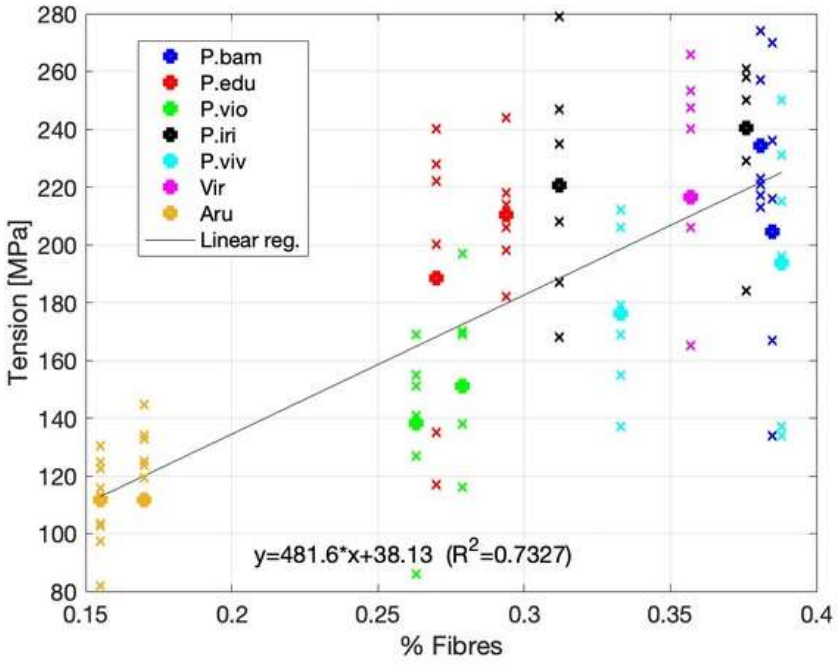

Figure 45
Tension strength in the longitudinal directions versus fibres area percentage

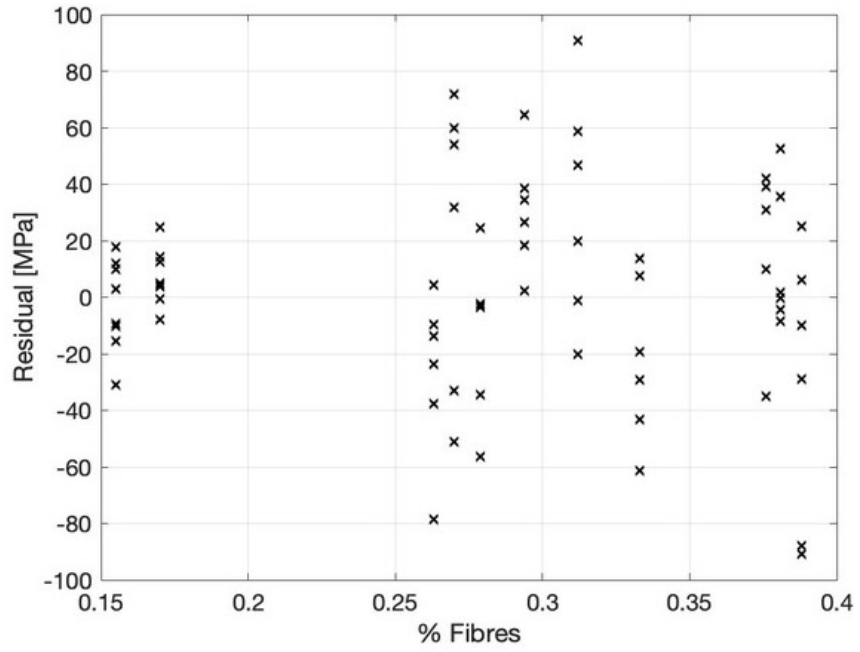

Figure 46
Residuals of the data for the linear regression

Prediction of the longitudinal modulus of elasticity and tensile strength

The relationship between the microscopical features and the macroscopical characteristics of the material is here studied by estimating two representative properties: the longitudinal modulus of elasticity and the tensile strength. These properties of bamboo have been studied until now [86] [115] [116], with both experimental and numerical models and that have led to very different results. Akinbade and Harries [117] collected existing literature on the fibre longitudinal modulus of elasticity for a P. edulis, ranging from 5.9 to 55 GPa, and on the matrix longitudinal modulus of elasticity, ranging from 0.2 to 5.8 GPa.
In their study, the Rule of Mixtures (RoM) has been used for this purpose, since it is an analytical model capable to predict the properties of a fibre-reinforced composite material [117]. The model, displayed in Figure 47, assumes that the composite material has an intermediate behaviour between the one of the fibres, represented by the blue line, and the one of the matrix, represented by the red line. Until the failure of the fibre, which happens firstly because of its smaller ultimate strain. Beyond this point the load is entirely transferred to the matrix.

An analysis to predict the failure has been carried out for each species. The initial zone, in which both matrix and fibres are in the elastic range, has been considered.

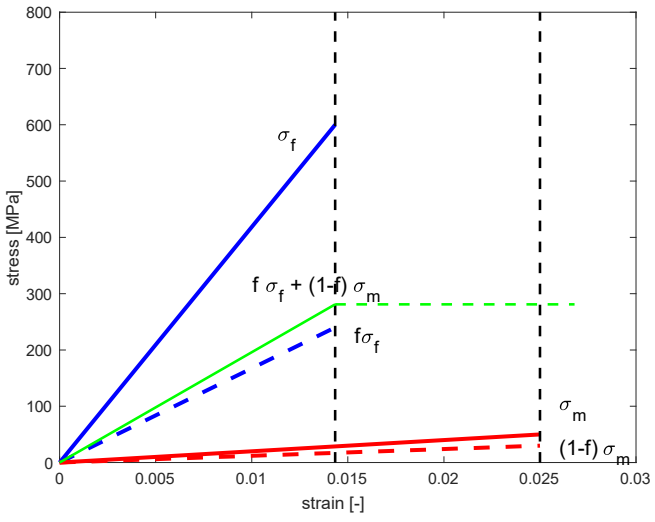

Figure 47
Behaviour of a fibre reinforced composite material undergoing a longitudinal stress, according to the Rule of Mixture. The blue line represents the behaviour of fibres, the red line represents the behaviour of matrix and the green line represent the behaviour of the composite

Each constituent contributes to supporting the external load according to its stiffness that is equal to the product of the modulus of elasticity times the area A over the length L for the axial case. Thus, the total force F in the composite can be calculated as the product of the sum of the stiffnesses of both fibres and matrix for the elongation of the specimen Δ:

$$F = \left(\frac{E_f A_f}{L} + \frac{E_m A_m}{L}\right) \Delta \tag{1}$$

where E_f and E_m are the longitudinal modulus of elasticity for the fibres and matrix respectively, while A_f and A_m are the area occupied by fibres and matrix. By dividing F over the area of the whole composite A_t, the effective stress σ can be obtained as:

$$\sigma = \frac{F}{A_t} = \left(E_f \frac{A_f}{A_t}\frac{\Delta}{L} + E_m \frac{A_m}{A_t}\frac{\Delta}{L}\right) \tag{2}$$

At this point, considering V_f and V_m as the percentage of area occupied by fibres and matrix respectively, which are defined by

$$V_f = \frac{A_f}{A_t} \qquad V_m = \frac{A_m}{A_t} \tag{3}$$

the following equations of the stress σ can be obtained

$$\sigma = \left[E_f V_f + E_m V_m\right] \varepsilon \tag{4}$$

where ε is the strain. Considering that the composite fails when fibres reaches its limit, the strain ε can be obtained from the value of the maximum fibre stress σ_f, since $\sigma_f = E_f \varepsilon$. Therefore, substituting the expression

$$\varepsilon = \frac{\sigma_f}{E_f} \tag{5}$$

in the equation (4), the following value of σ_1 can be obtained:

$$\sigma_{eq6} = V_f \sigma_f \ + \ E_m \, V_m \frac{\sigma_f}{E_f}$$

(6)

Values of E_f and $E_m$have been assumed from two different studied: [110] and [118]. In particular, 40 GPa and 55 GPa have been considered for the longitudinal modulus of elasticity for the fibres, while 1.9 GPa and 2 GPa have been assumed for the matrix. A value of 610 MPa [86] has been used for σ_f. Values related to fibre area percentage and matrix area percentage correspond to those measured in this study and reported in the previous chapter.

Moreover, observing Figure 47, it can be deduced that the behaviour of the composite material, the green line, is quite similar to those of blue dashed line, since the matrix has a lower modulus and fibres are the main responsible for the stiffness. So, an approximation of the value of failure stress in tension can be calculated considering only fibres, as

$$\sigma_{eq} \ = \ f \sigma_f$$

(7)

Results of the calculation of the tensile strength considering both σ_1, expressed by eq. (6), and σ_2, expressed by equation (7) are compared with those obtained in the experimental tests of axial stress from literature. already reported in Table 9, Figure 48 and Figure 49. Results of the tensile strength prediction show a good agreement, especially in the case of P. edulis and P. iridescens species.

The effective Young's modulus E of the culm has been calculated by the equation (4), with the formula

$$E = f E_f \ + \ m \, E_m$$

(8)

Results are presented in Table 10. Estimated Young's modulus is similar with those from experimental tests, especially for P. viridiglaucescens, P. iridescens and P. edulis species, while some differences can be observed for P. bambusoides, P. violacescens, and P. vivax species.

Generally, results well correspond the experimental value, and in both cases of E and σ, RoM can be considered an affordable method to have valid predictions. Both methods used to calculate the values of the strength give similar results. Not all the

species have the same correspondence with experimental result, ranging from 0.17% to 26.2%. No significative trend can be observed to define a possible explication for the differences, which may be attributed to many factors. Variations in the mechanical parameters with respect to the values assumed in this study or the low number of samples on which bamboo component have been calculated, can be possible explications.

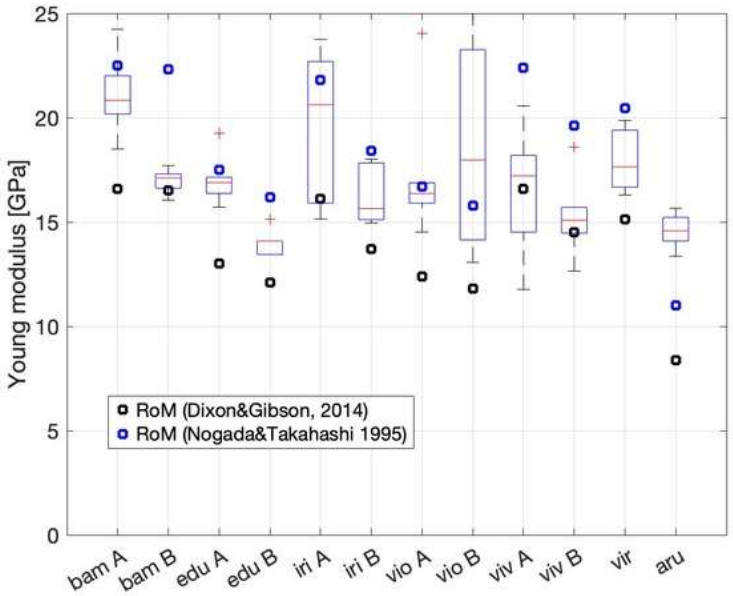

Figure 48 Comparison between the experimental modulus of elasticity in the longitudinal direction and that one obtained with RoM prediction. Results for P. viridiglaucescens (vir) and Arundo donax (aru) refer to the average value of samples from part A and B of the culm.

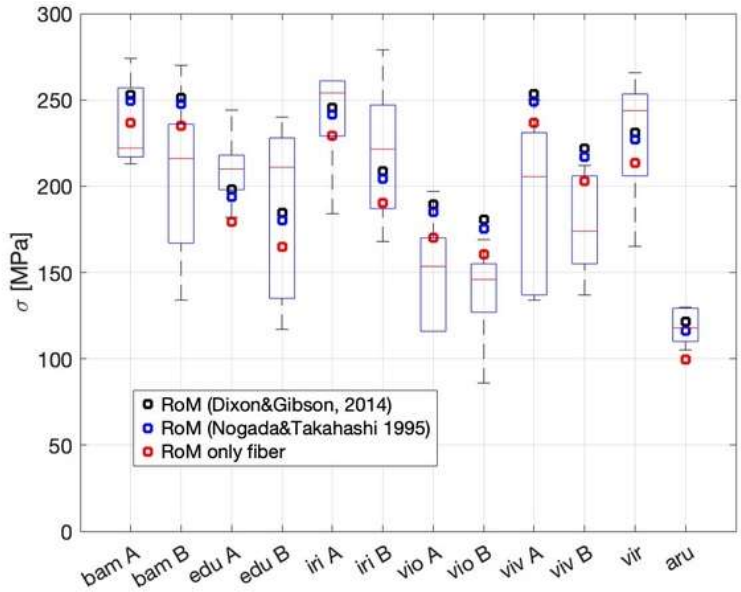

Figure 49 Comparison between the experimental longitudinal tensile strength with those obtained with prediction through the equation (3) based on the RoM. Results for P. viridiglaucescens (vir) and Arundo donax (aru) refer to the average value of samples from part A and B of the culm.

Table 10 Comparison between results obtained from experimental results and estimated values of the modulus of elasticity in the longitudinal direction E and the longitudinal tensile strength σ. CoV is the ratio of the standard deviation over the mean. *P. viridiglaucescens and Arundo donax experimental data do not consider the position along the culm.

Species	Culm part	Fibres %	E [GPa]			σ [MPa]			
			Estimated value		Experimental average value (CoV)	Estimated value			Experimental average value (CoV)
						(6)		(7)	
			Dixon and Gibson (2014)	Nogata and Takahashi (1995)		Dixon and Gibson (2014)	Nogata and Takahashi (1995)		
P. edulis	A	29.4	13.01	17.48	17.04 (0.07)	198.35	193.89	179.34	210 (0.10)
	B	27.0	12.11	16.23	14.21 (0.06)	184.72	180.03	164.70	188 (0.31)
P. viridiglau-cescens	A	33.3	14.50	19.56	18.82 (0.15)*	221.12	216.90	203.13	214 (0.12)*
	B	38.1	16.32	22.10		248.92	245.05	232.41	
P. bam-busoides	A	38.8	16.60	22.47	21.09 (0.11)	253.01	249.25	236.68	234 (0.11)
	B	38.5	16.48	22.31	16.91 (0.04)	251.31	247.45	234.85	205 (0.26)
P. vivax	A	38.8	16.57	22.44	16.58 (0.19)	252.64	248.90	236.68	194 (0.25)
	B	33.3	14.50	19.56	15.35 (0.16)	221.09	216.88	203.13	176 (0.16)
P. iridescens	A	37.6	16.09	21.79	19.79 (0.19)	245.44	241.67	229.36	241 (0.12)
	B	31.2	13.69	18.44	16.19 (0.09)	208.80	204.47	190.32	221 (0.18)
P. vio-lacescens	A	27.9	12.42	16.67	17.34 (0.19)	189.40	184.89	170.19	151 (0.22)
	B	26.3	11.80	15.81	19.16 (0.31)	179.90	175.34	160.43	138 (0.21)
Arundo Donax	A	17	8.21	10.84	15.29(0.01)*	125.228	120.18	103.70	111.70(0.12)*
	B	15.6	7.73	10.15		117.88	112.55	95.16	

Prediction of the transversal modulus of elasticity and circumferential strength: a FEM model

The behaviour of these natural composite materials results very different according to the direction of the stress. In particular, the transversal strength is considerably lower with respect to the longitudinal one, as has been pointed out in the previous paragraph. In fact, transversal stress is mainly faced by the weak matrix which embeds the fibres bundle and the thin external layer. Knowledge about the transversal modulus of elasticity and the circumferential strength of bamboo and Arundo donax is fundamental for designing with these materials, since they play frequently and important role in the behaviour of the structure, such as in connections between elements. Therefore, a method to predict them is necessary.

Unfortunately, as noted by Akinbade and Harries [117], the Rule of Mixtures (RoM) used for predicting the along-the-grain properties fails to accurately capture the actual behaviour of the composite bamboo material, even when incorporating the Halpin–Tsai correction.
Al-Rukaibawi and his collaborators [119] highlighted how analytical homogenisation models overlook the anisotropic structure of bamboo. Therefore, they studied the elastic properties of a finite element analysis software based on an RVE (representative volume element) model based on microscopical images of vascular bundles, and showed good results along the longitudinal direction compared to experimental ones. Silva et al. [120] employed computational techniques, including the Finite Element Method (FEM), to study the mechanical behaviour of bamboo. Additionally, its functionally graded structure was investigated using a multiscale method based on homogenization.
Finally, finite element method (FEM) analysis could be a useful alternative to understand and predict specific features of natural materials, such as bamboo and Arundo donax, whose biological composition makes often very difficult to apply successfully analytical models. The complex trend of voids cannot be described with simplified models such as the rule of mixtures, but requires a more complex model that considers the real distribution of voids and fibres. To find the stress peak that causes the failure, a finite element model is therefore necessary, which however demonstrates

how the maximum stress peak occurs in the central area of the thickness.

In this thesis, a FEM analysis has been proposed to predict bamboo behaviour along the weak circumferential direction, focusing on the transversal modulus of elasticity and the circumferential strength.

To validate the proposed model, the results will be compared with those reported by Akinbade et al. [121], who investigated the bending behaviour of flat ring specimens with varying thickness reductions at different radial positions. This experimental setup enabled the evaluation of circumferential strength across the radial direction. In their study, the modulus of rupture was determined for different segments at various heights of the culm wall. Full cross-section specimens—each approximately 0.2 times the culm diameter in length—were clipped so that the portion subjected to circumferential loading represented about 20% of the total cross-section. This configuration allowed the results to be linked to a specific region of the specimen, as illustrated in Figure 50. The findings revealed a clear parabolic trend in circumferential strength, with the minimum resistance occurring at the mid-thickness of the ring.

Figure 50 Flat ring flexure specimen (a and b) and test (c) in the reference experimental study [121]

Some of the results appearing in this section, are already published in:

Silvia Greco, Luisa Molari, Giovanni Valdrè and Jose Jaime Garcia (2022, July 8) «Finite element analysis for the prediction of the circumferential bamboo strength» *18th International Conference on Non-conventional Materials and Technologies (NOCMAT 2022).* https://doi.org/10.5281/zenodo.6811560

A. Sghedoni “Analisi microscopica del comportamento meccanico e igro-meccanico di diverse specie di bambù italiano” (2024) Master Thesis, Università degli Studi di Bologna, 2024.

The FEM analysis has been based on the real geometries of the material. The entire process is illustrated in Figure 51 for the P. bambusoides species. The vectoral image of the cross section of each species, as described in the previous chapter, has been used (see Figure 51a). Each cross-sectional area has been divided radially into 10 portions (Figure 51c). and each one of these has been used to create the geometry of one model, representing the microstructure of the material at 10 different radial positions (Figure 51d).

The name, distance from the outer surface and the calculated area occupied by each component are listed in Table 11. Detailed specifications of each model of each species are provided in Appendix C.

Figure 51 Creation of the geometry of each model: from the slice of the cross section (a), a vectoral image has been obtained with Autocad 2023 (Autodesk) (b) and then divided into 10 portions (c), that have been finally converted into 10 FEM models (d)

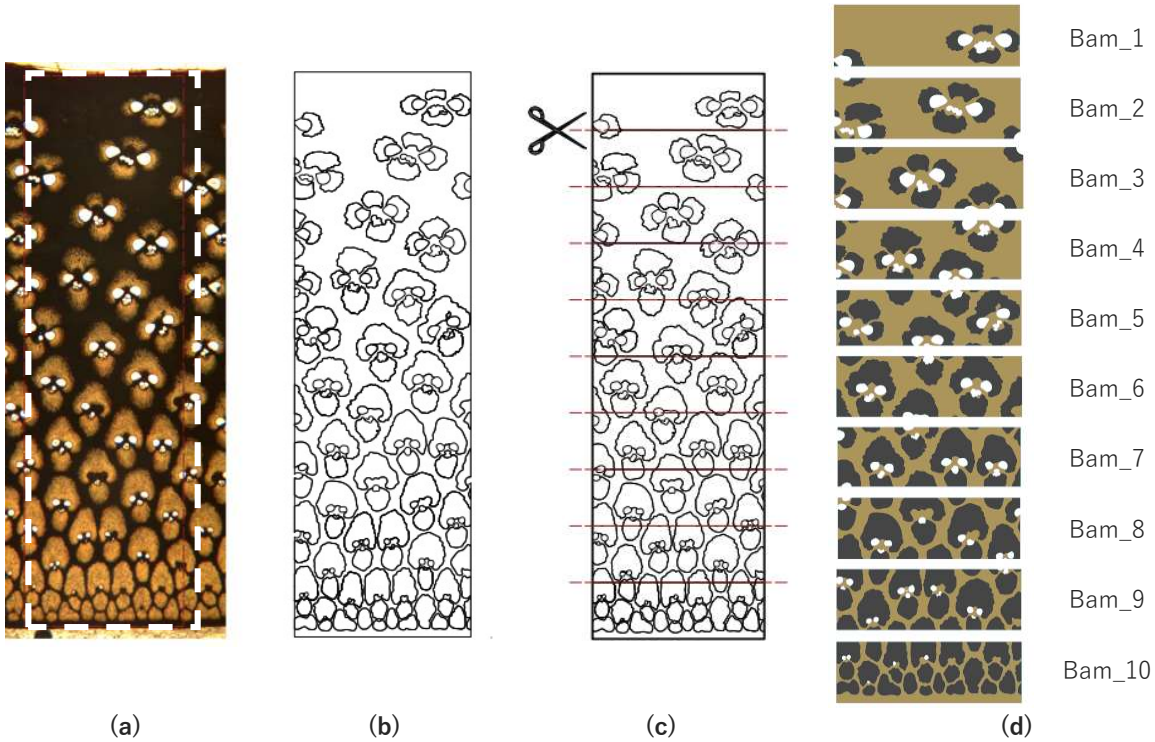

Table 11 Description of the geometries of each model for the P. bambusoides species

Name	Normalized distance from the inner surface (mm)	Area %		
		Fibre	Matrix	Voids
Bam_1	0-0.1	10,50	83,92	5,58
Bam_2	0.1-0.2	23,87	69,25	6,88
Bam_3	0.2-0.3	28,39	65,63	5,98
Bam_4	0.3-0.4	31,71	59,45	8,84
Bam_5	0.4-0.5	45,00	47,36	7,64
Bam_6	0.5-0.6	49,07	45,05	5,88
Bam_7	0.6-0.7	53,79	40,13	6,08
Bam_8	0.7-0.8	60,15	36,03	3,82
Bam_9	0.8-0.9	63,92	32,56	3,52
Bam_10	0.9-1	67,54	31,91	0,55

Stress Analysis

Methods

The anatomy-based models have been analysed using Ansys Mechanical software. To allow the assignment of different properties for each component, geometries have been divided into 2D elements, named as regions, which can have independent properties.

A mesh with quadrangular elements of a 0.02 mm base dimension has been defined for each model, using the “capture curvature” option to ensure accurate bonding between surfaces.

In order to test the validity of the model, two border conditions will be studied in parallel, and are illustrated in Figure 52.
The first model, referred to as *configuration EXP*, aims to replicate the conditions of the experimental study conducted by Akinbade et al. [121]. To reproduce the same boundary conditions of that test, displacements are constrained only along the left

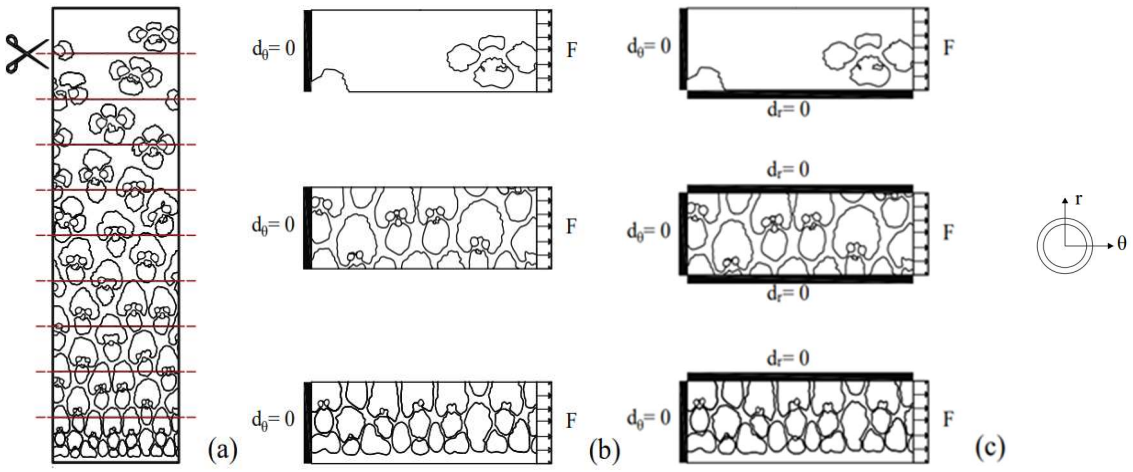

Figure 52 Explanation of the two different border condition: Initial geometry of a P. bambusoides (a), configuration EXP(b) and configuration REAL(c) for the three case in the cross section: the upper extremity, one from the middle part, and the lower extremity, respectively named Bam_1, Bam_9, and Bam_10.

edge of each model, with $d_\vartheta = 0$, allowing the model to remain otherwise free to move. A uniformly distributed circumferential force F is applied on the right edge. These boundary conditions are illustrated in Figure 52b.

The second type of boundary conditions, referred to as *configuration REAL*, aims to simulate the actual behaviour of the portion of the material within a complete cross section where each strip is surrounded by other material on its borders. The main difference with the previous case is that here the radial displacements are constrained on the upper and lower boundaries, $d_r = 0$, while also in this case the circumferential displacements have been constrained on the left boundary $d_\vartheta = 0$. A uniformly distributed circumferential force is applied on the right boundary. The conditions are clarified in Figure 52c.

The force magnitude was selected to ensure that the test remained within the linear elastic range, in accordance with experimental results reported in the literature by Molari and Garcia [113], who conducted circumferential tension tests on the same bamboo species. The value of 5 N was chosen for each model.

Under the assumption that the material works in the linear-elastic field, constants for both fibres and matrix, which are considered as isotropic, have been chosen from the literature and are summarized in Table 12. A plane stress model is used, with no tension along the axis of the culm. In this study, the analysis remains within the elastic

range, and failure is not considered. However, the Rankine-Navier criterion is included for potential future analyses, where the maximum principal stress would define the onset of failure beyond the elastic limit.

The objective of the strength analyses was to evaluate the variation in circumferential stress along the radial direction in order to assess the relative strength at different radial positions. For this purpose, it was assumed that the mechanical properties of the fibres and matrix remained constant across the radial direction. The maximum principal stress was calculated for each model at the i-th radial position, denoted as $S_{i,max}$. The stress distribution was then plotted in graphs, with stress values normalized against the overall maximum stress observed across all strips in the cross-section models, denoted as S_{max}. Given that the ultimate stress S_u is unknown, the relative strength at each location was approximated by substituting $S_u$the with the highest stress S_{max} observed in the 10 models.

Furthermore, the entire strip of the cross section of a P. edulis has been modelled. It has been subjected to the sum of the solicitations applied to each model on the right boundary, while displacement is forbidden on the left boundary. The load is applied on the left boundary, and it is equal to the sum of the solicitations previously applied to the 10 model of the strips, that is 50 N. In Figure 53 the configuration used for modelling is shown.

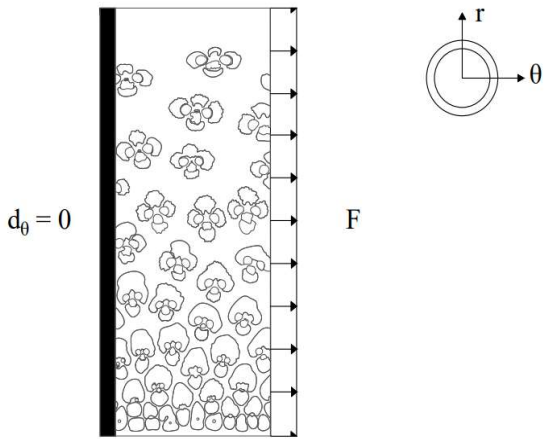

Figure 53 Boundary conditions for the FEM model of the whole cross section of a P. edulis

Table 12 Elastic properties for fibre and matrix used in FEM analysis

Component	E Young modulus (GPa)		ν Poisson ratio
Fibre	40	[110]	0.3
Matrix	1.9	[110]	0.3

At this point, the R index has been introduced to estimate the relative strength at a specific radial position within the cross-section of the model. The formula used is:

$$R = \frac{S_{max} + |S_{i,max} - S_{max}|}{S_{cross\ section}} \tag{9}$$

where $S_{cross\ section}$ is the maximum value of the stress of the entire cross section, while $S_{i,max}$ and S_{max} have been previously defined. The index R combines stress values from two modeling approaches. The term $|S_{i,max} - S_{max}|$ quantifies the deviation of the stress at each position from the global maximum. This difference is added to S_{max} , capturing the effect of local variations relative to the global maximum. The result is then normalized by $S_{cross\ section}$, enabling a standardized comparison of stress distribution across the section. Thus, R provides a comprehensive measure of stress distribution, highlighting regions where local stresses significantly differ from the global maximum and offering insights into the overall stress behaviour.

Results

The distribution map of the maximum principal stress S_{max} is presented in Table 13 for three models, corresponding to the outer, inner, and central regions of the culm wall of Phyllostachys bambusoides. The highest stress values are concentrated in the central stripes. For the same representative case, the maximum stress values in the matrix ($S_{m,max}$) and in the fibres ($S_{f,max}$,) are summarized in Table 14 for each stripe under both boundary conditions. As expected, tensile stress is higher in the fibres, which constitute the stiffer component of the material. Stress peaks are observed near the holes. Additional data for other species is provided in Appendix D.

The trend of the distribution of the adimensionalised maximum principal stress along the thickness is shown in the graphs of Figure 54 and Figure 55 related to or both configurations. It can be described by a parabolic curve under both the cases of boundary conditions, even if the parabolic trend in the case of the configuration REAL results weaker, as displayed by the lower R^2 value presented.

Table 13 Maximum principal stress map, for both the configuration EXP and REAL, of the models named as Bam_1 (near the inner surface), Bam_6 (in the middle) and Bam_10 (near the external surface) of a P. bambusoides

Model	EXPERIMENTAL CONDITIONS	REAL CONDITIONS
Bam_1	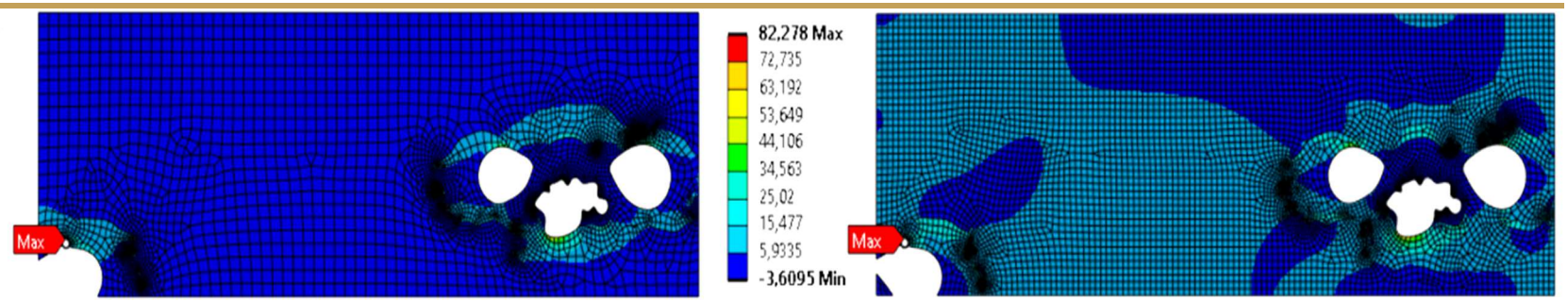	
Bam_5	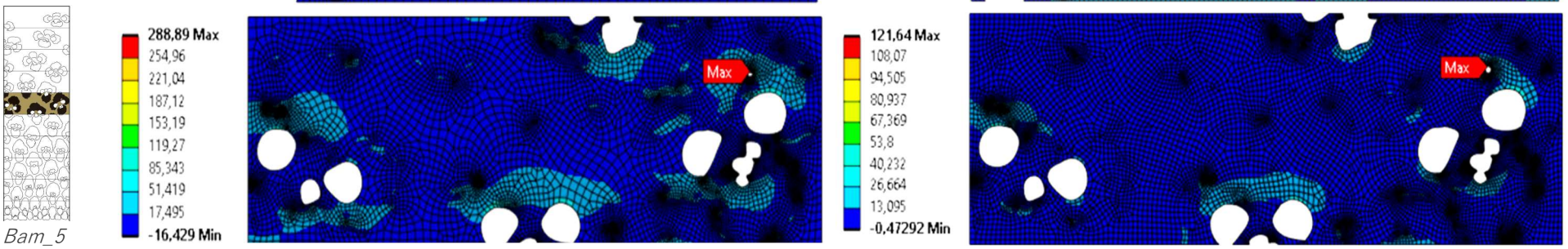	
Bam_10	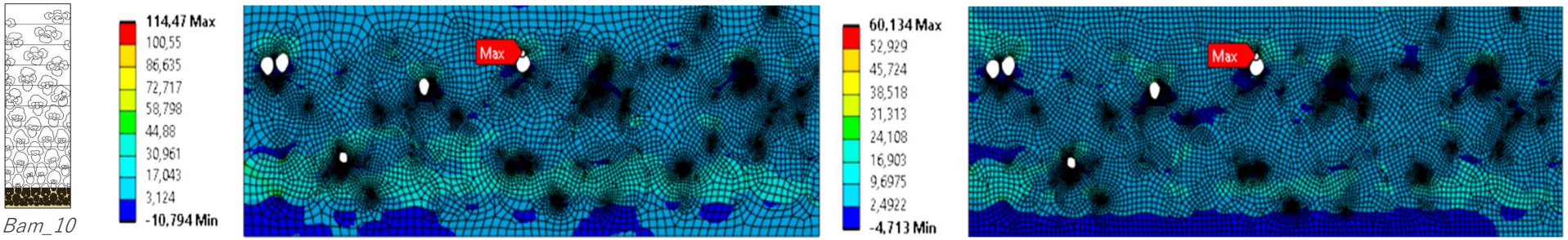	

Table 14 Results for both the experimental and real boundary conditions of the maximum stress of fibre $S_{f,max}$ and matrix $S_{m,max}$ for every model of a P. bambusoides

Name	Adimensionalised radial distance from the inner surface	Configuration EXP		Configuration REAL	
		$S_{f,max}$ (MPa)	$S_{m,max}$ (MPa)	$S_{f,max}$ (MPa)	$S_{m,max}$ (MPa)
Bam_1	0-0.1	137.71	173,70	68.00	82,28
Bam_2	0.1-0.2	125,92	77,90	64,88	41,06
Bam_3	0.2-0.3	208,41	123,70	73,82	45,95
Bam_4	0.3-0.4	249,13	55,70	69,47	23,64
Bam_5	0.4-0.5	288,9	60,60	121,60	27,84
Bam_6	0.5-0.6	152,4	27,43	55,17	15,24
Bam_7	0.6-0.7	143,6	27,61	66,35	16,4
Bam_8	0.7-0.8	128	53,57	49,46	26,93
Bam_9	0.8-0.9	132,6	27,48	59,59	15,75
Bam_10	0.9-1	114,5	35,29	60,13	17,44

The trend of the distribution of the R index along the radial direction can be described by a parabolic curve too. Moreover, a good agreement between the numerical results and those obtained in literature from experimental tests [121] is clearly illustrated in the graph of Figure 56. Here, a comparison between the normalized modulus of rupture, determined from each segment against that one of the whole cross section, and the R index has been reported. The trend of the two values is very similar, as also shown by the value of R^2 which is of 0.86 in numerical model case while 0.81 in the experimental one. Therefore, the FEM model here proposed can be considered a reliable solution for the prediction of the transversal properties of the material, since it is very close to experimental results.

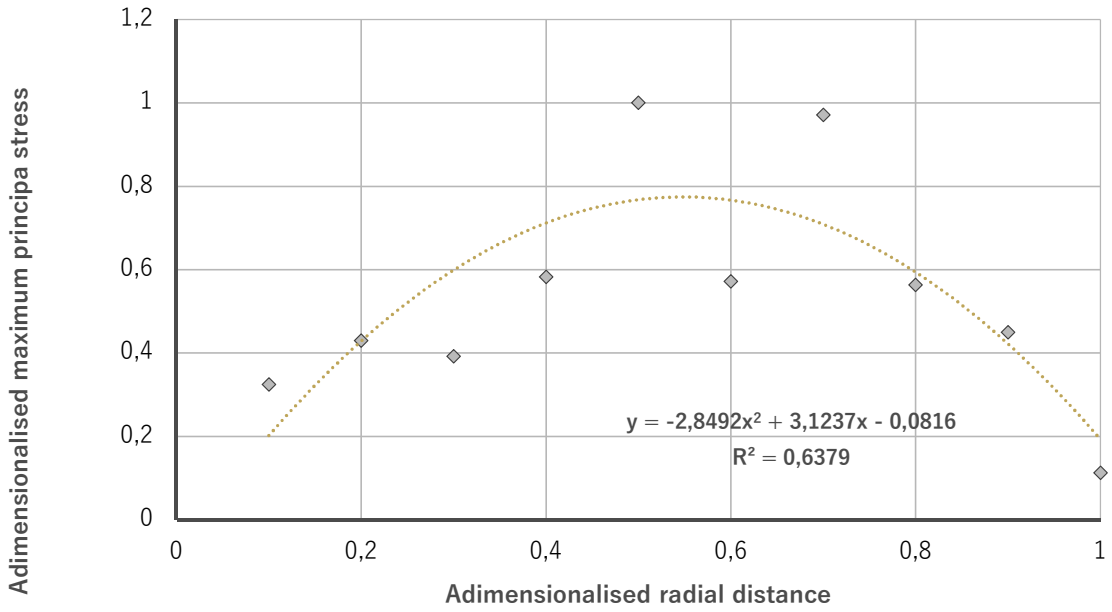

Figure 54 Distribution of the maximum principal stress along the thickness of a P. edulis, according to the boundary conditions of the configuration REAL

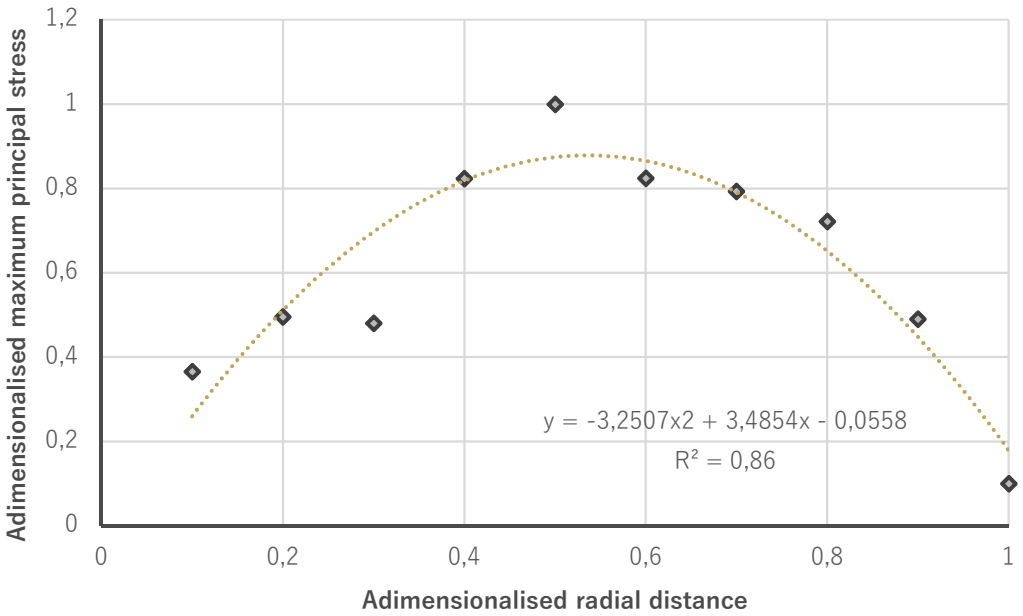

Figure 55 Distribution of the maximum principal stress along the thickness of a P. edulis, according to the boundary conditions of the configuration EXP

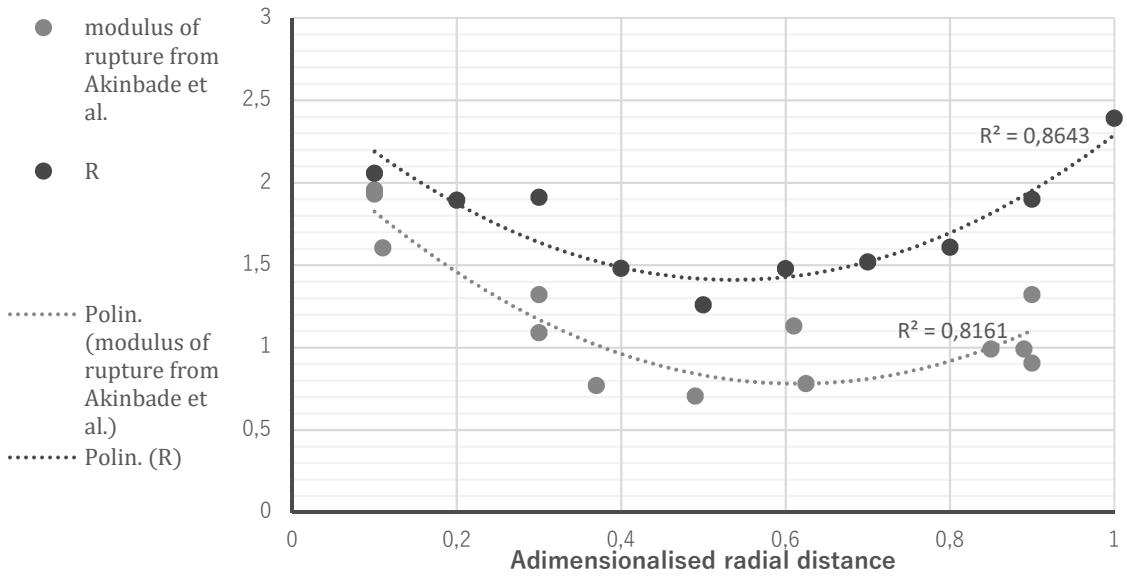

Figure 56 Comparison between the results of the experimental study of Akinbade [121] (in grey) and those of the FEM model of the present study (in black)

Stress concentration analysis

Considering the results of the finite element analysis, the maximum stress peaks are always localized in the central part of the thickness. Observing the anatomic analysis, the central part of the thickness is the weakest part of the culm wall where the major concentration of voids has turned up.

The increase in stress cannot be explained solely by the reduction of material. Stress localization around the holes plays a crucial role, as well as the presence of two components with significantly different stiffnesses leads to a non-uniform stress distribution. This could explain the variation of the circumferential strength along the thickness obtained in experimental tests [121], in which the distribution of the stress is described by a parabolic shape with its smallest values in the inner part. For this reason, particular attention to voids has been paid into this study.

Methods

Firstly, two parameters have been observed: the area and the diameter of the average vessel, respectively named as $A_{v,avg}$ and $D_{v,avg}$, calculated as following:

$$A_{v,avg} = \frac{A_{vessels}}{N_{hol}} \qquad D_{v,avg} = \sqrt{4\,\frac{A_{vessels}}{N_{holes}}}{\pi} \tag{10}$$

where $A_{vessels}$ is the total area occupied by vessels and N_{holes} is the number of holes into each geometry.

A measure of the influence of the voids into the results of the stress state can be provided by the Stress Concentration Factor (SCF), which has been defined as:

$$SCF = \frac{S_{max}}{S_{mean}} \tag{11}$$

where S_{max} is the maximum value of the stress while S_{mean} is the value of the stress of the same geometry considered without voids, that can be calculated as

$$S_{mean} = \frac{F}{A} \tag{12}$$

where F is the force applied and A is the total area of the model. Moreover, to isolate the effects of material heterogeneity from those of the voids, a comparison was made with a model of Phyllostachys edulis assuming a homogeneous composition, subjected to the same applied force and boundary conditions.

Results

In the graphs of Figure 57, the trend of the number of holes N_{holes} and the area of the average vessel $A_{v,avg}$ along the thickness of the culm wall are shown. The first one exhibits a linear decreasing trend towards the external surface, while the latter linearly increases from the inner to the external one. The result of these two linear opposite trends is the parabolic distribution of the area occupied by voids. In the anatomic analysis, the parabolic distribution of voids has been already discussed, but these finding reveals that presence of voids affects the reduction of the strength not only because of the reduction of the section, but also in terms of shape of voids.
Moreover, the influence of voids on the stress distribution trend is clearly highlighted by the results presented in Table 15. In this table, both the maximum principal stress

S_{max} and the stress concentration factor SCF are reported for the FEM model and for the equivalent model with homogeneous material properties. Although the peak stress values are lower in the homogeneous model—due to the absence of material heterogeneity—their locations remain consistent with those observed in the original, non-homogeneous models. This confirms that while the overall magnitude of the stress is affected by the material structure, the voids play a significant role in amplifying stress locally, without significantly altering the general distribution pattern.

Table 15 Analysis of void influence for each model of the slice of the cross section of a P. edulis. Firstly, amount, number, and geometry of the voids are presented. Then, maximum stress value S_{max} and SCF are presented for the equivalent homogeneous material model, and the reference one.

Name	Adimens. radial distance from the inner side	Voids fraction (%)	N_{holes}	Average vessel		Homogeneous model		Non-homoge-neous model	
				$A_{v,avg}$ (10^{-4} mm^2)	$D_{v,avg}$ (10^{-2} mm)	S_{max} (MPa)	SCF	S_{max} (MPa)	SCF
Edu_1	0-0.1	0	0	-	-	-	-	79.4	7.94
Edu_2	0.1-0.2	6.35	5	121.7	12.4	49.1	4.9	107.6	10.8
Edu_3	0.2-0.3	6.46	5	123.9	12.5	63.1	6.3	104.3	10.4
Edu_4	0.3-0.4	7.32	7	100.3	11.3	61.6	6.1	178.8	17.9
Edu_5	0.4-0.5	9.11	9	97.0	11.1	116.5	11.6	217.0	21.7
Edu_6	0.5-0.6	7.14	12	57.0	8.5	65.0	6.5	179.0	17.9
Edu_7	0.6-0.7	8.43	14	57.7	8.5	64.5	6.4	172.1	17.2
Edu_8	0.7-0.8	3.59	14	24.6	5.5	54.3	5.4	156.6	15.7
Edu_9	0.8-0.9	4.31	19	21.7	5.2	71.3	7.1	106.4	10.7
Edu_10	0.9-1	0.74	7	10.2	3.6	28.5	2.8	21.8	2.2

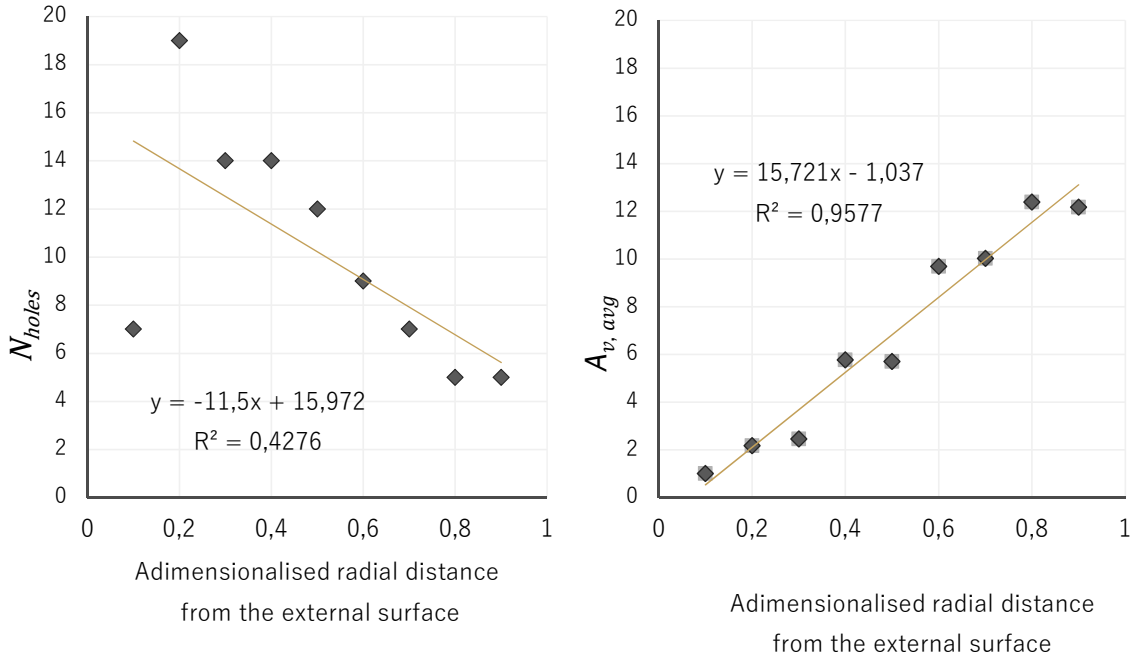

Figure 57 Number of the voids N_{holes} (on the left) and average area of the voids $A_{v,avg}$ (on the right) along the thickness of the culm wall for each model the Phyllostachys edulis species

Bending test and flexural behaviour of each component: an experimental procedure

Bamboo is optimized to resist to flexural actions with its peculiar microstructure along the thickness, in which the amount of fibres intensifies towards the outer layer and the inner part is composed mostly of parenchyma. The microstructural components play a different role in its mechanical behaviour: the flexural strength depends on the amount of fibres, whereas the flexural ductility is correlated to the parenchyma content, as depicted by [123]. They found a clear relation between the macroscopic strain of bamboo and the microscopic deformations of bamboo cells: fibres bear load but limit the deformation of the nearest cells, while matrix provides lateral confinement for fibers.

Current European standard [124] proposes a bending test on the whole culm, as

illustrated by Figure 58, which requires complex instrumentation and is strongly influenced by the shape of the culm. Alternatives have been studied by many academics, as [125], [126], [127].

In this section, the flexural properties of bamboo will be studied considering its microstructure. In particular, the flexural strength in external and internal surfaces of the bamboo culm and the elastic modulus in both the internal and external surfaces have been assessed. The aim of this work is to identify a procedure which can provide reliable information on the properties of the material components, in a fast and simple way.

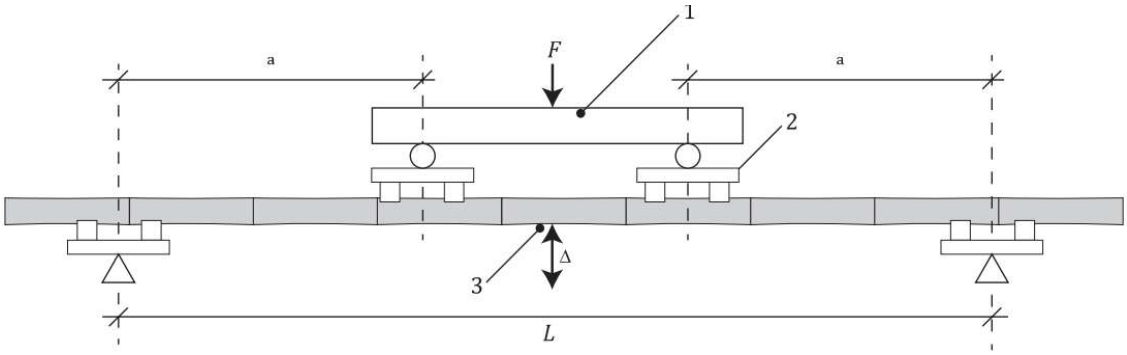

Figure 58 Bending test procedure according to European standard ISO 22157:2019

Parts of this chapter has been already published in:

S. Greco and L. Molari, “Flexural Behaviour of Five Species of Italian Bamboo,” *Construction Technologies and Architecture. Trans Tech Publications Ltd*, vol. 1, pp. 723-729, January 2022 https://doi.org/10.4028/www.scientific.net/cta.1.723

S. Greco, M. Maraldi and L. Molari, “Grading bamboo through four-point bending tests. A report on six species of Italian bamboo,” *Construction and Building Materials,* vol. 404, no. 133168, 2023. https://doi.org/10.1016/j.conbuildmat.2023.133168

Silvia Greco, Stefania Manzi, Luisa Molari, Andrea Saccani, Gianfranco Ulian, Giovanni Valdrè «Photodegradation of Bamboo: A Study on Changes in Mechanical Performances» *Materials* 2023; 16(1):285 https://doi.org/10.3390/ma16010285

Methods

Bending test has been performed on twelve specimens for each species of bamboo as those already described in the previous chapter. Characteristic of each species can be consulted in Table 4 of the second chapter. The part of the culm from 1.5 to 2.5 m from the ground, named as A, has been used for the preparation of the specimens. Executing test on Arundo donax has presented more complexities, because of its very thin section which maybe requires a different typology of this test. A reductive campaign of three samples has been done to test this material, in order to have a qualitative idea of the difference in comparison to bamboo.

Three culms per species have been selected and, from each one of them, straight and defect-free internodes of minimum 220 mm length have been chosen. The cylindrical shape of the culm has been cut using a circular saw. Then, four sticks have been obtained by the use of a cutter and the help of a screwdriver, to open the cylinder trying to respect the fibre path. The dimensions of the specimens have been decided considering dimension of the thickness of the culms: the width has to balance the requirement of the application of a strain gauges and the requirement of a rectangular cross section. Unfortunately, because of the small dimension of European bamboo, a relatively small width means a big curvature, so finally a width of 8 mm was chosen and then the specimen was cut to have a rectangular cross section in order to avoid effects due to the curvature of the culm. The process is graphically described in Figure 59.

The strain has been measured by the use of two types of instrumentation, in order to avoid possible influences on results due to the small dimensions of the specimens. On a hand, two electrical strain gauges of 3 mm (FLAB-3-11, Tokyo Measuring Instruments Lab.) have been used (Figure 60a). They were applied in the middle part on the upper and lower surfaces of the specimen (Figure 61 a and b respectively). On the other hand, the strain gauge was applied only in the upper part, while the deformometer (Inductive strain gauge D1-5, HBM) was applied in the lower one, as shown in Figure 60b. For Arundo donax, only test with strain gauges have been performed, due to its very thin section.

The bending test has been executed on a test machine (Amsler Otto Volpert- Werke GMBH D-6700), with a displacement rate of 7 mm/min in order to ensure a duration of the tests between 3 and 7 minutes, as required by ISO 22157:2019 standard [124]. A four-point bending test has been carried out in two different loading configurations in order to test the functionally graded structure of the material, as illustrated in Figure 59. In U configuration, the specimen surface from the external side of the culm wall, has been positioned “Up”, where the load has been applied, while in D configuration, it has been positioned “Down”, on the opposite side.

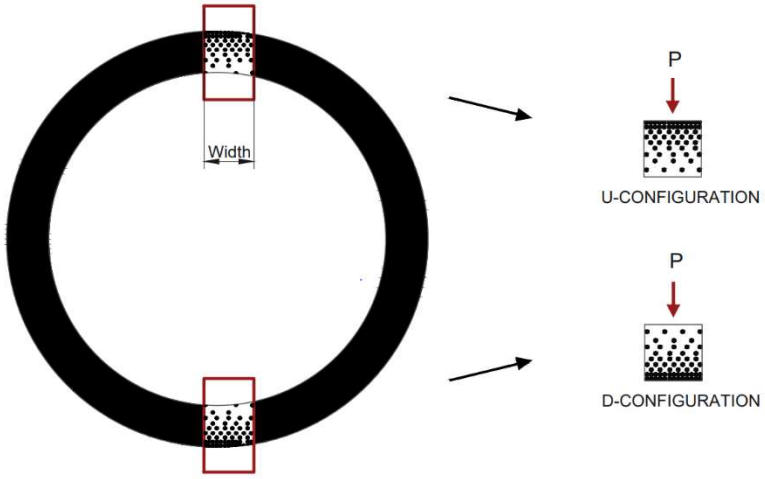

Figure 59 (on the left) Section of the specimen of U and D configurations, extracted from the whole culm

(a)

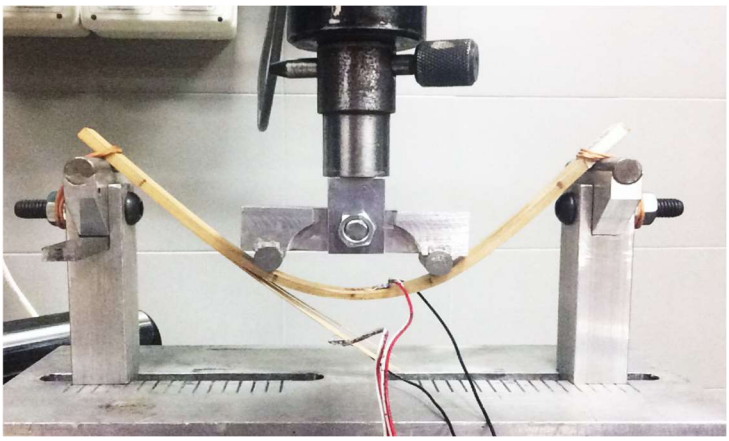

(b)

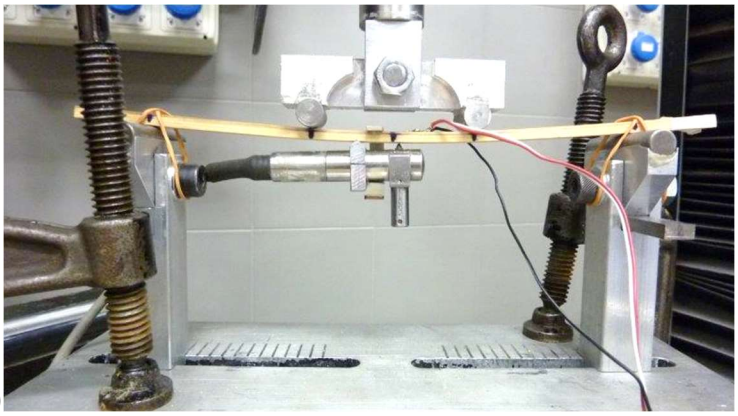

Figure 60
(on the left) Two types of instrumentation have been used for the measurement of the strain: two strain gauge (a) and a strain gauge and a deformometer (b)

(a)

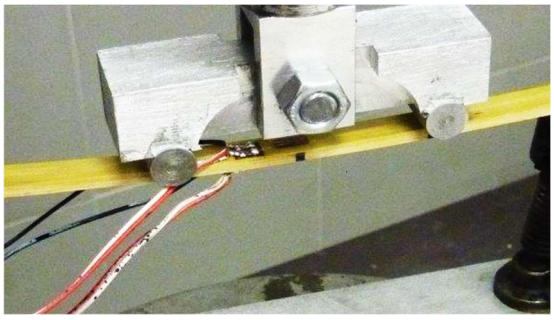

(b)

Figure 61
(below) Position of the strain gauges in the upper (a) and lower (b) side of the specimen during the bending test

Considering A span length of 60 mm was chosen to allow a span-to-depth ratio of 15. Finally, humidity has been measured for each specimen according to ISO 22157:2019 [124].

Results

In Table 16 and Figure 62, the behaviour of the specimens during testing is illustrated through a data collection and load-strain graphs. The overall trend is similar across all the species analysed. As expected, specimens oriented such that the side with a higher concentration of fibres is subjected to tension exhibit lower deformation compared to those where the matrix-rich side is in tension. This behaviour is attributed to the greater stiffness of the fibrous tissue. However, despite the lower deformation, a more pronounced elastic recovery is observed in the fibre-dominant configurations, reflecting their higher capacity for elastic energy storage and release.

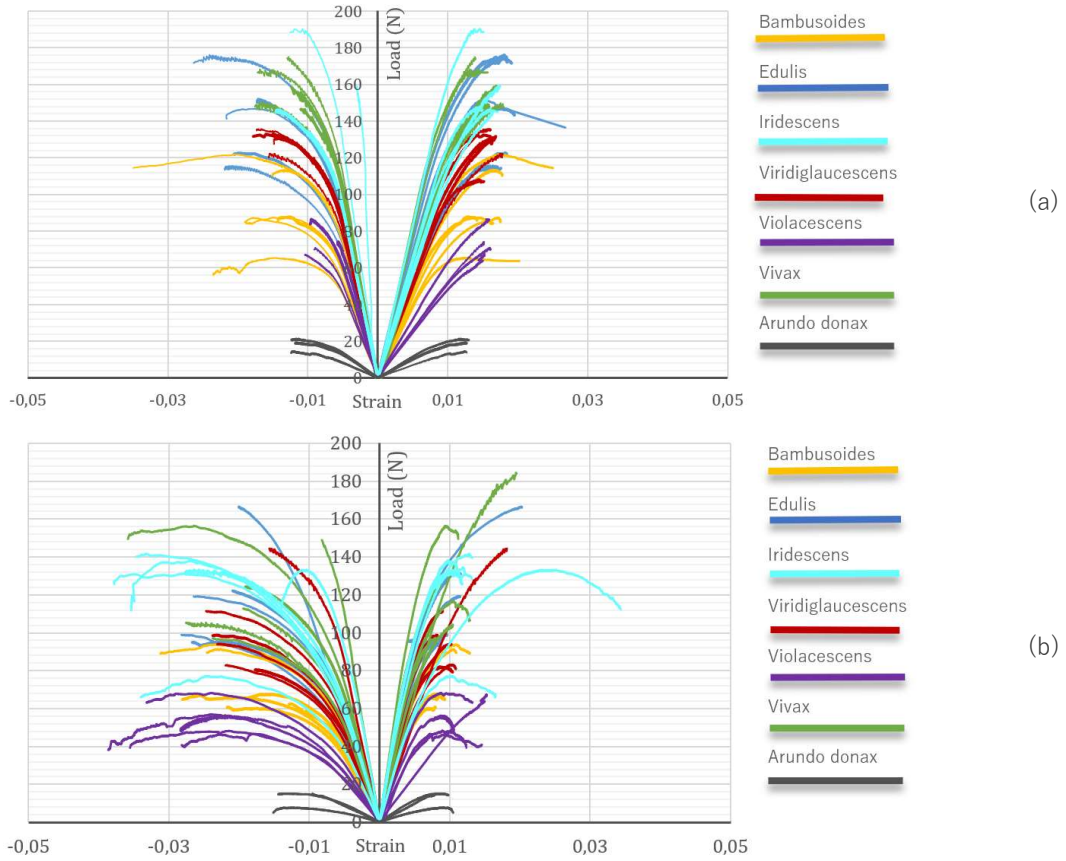

Figure 62 Load-strain graph for all the samples used in this study, U- configuration up (a), D-configuration down (b)

Table 16 Average values, and standard deviation in bracket, for the tests of both for U and D configuration: h and b stand respectively for the thickness and width of the section of the specimens, while P_{ult} stands for the maximum load and Δ_{ult} for its relative displacement

Species	U-configuration				D-configuration			
	h (mm)	b (mm)	P_{ult} (N)	Δ_{ult} (mm)	h (mm)	b (mm)	P_{ult} (N)	Δ_{ult} (mm)
P. edulis	4,26	9,04	152,47	29,31	4,17	8,76	122,93	29,65
	(0,32)	(0,46)	(28,18)	(2,61)	(0,22)	(0,58)	(25,73)	(3,24)
P. viridi-glaucescens	3,77	8,19	126,87	26,37	3,83	8,01	102,84	28,33
	(0,22)	(0,51)	(10,19)	(3,07)	(0,21)	(0,33)	(23,74)	(4,44)
P. bam-busoides	3.31	8.44	93.80	30.71	3.25	8.48	73.79	31.77
	(0,29)	(0,30)	(20,50)	(1,07)	(0,28)	(0,58)	(14,74)	(4,07)
P. vivax	4,25	9,03	157,88	23,03	4,04	8,96	131,12	31,00
	(0,20)	(0,72)	(11,50)	(2,91)	(0,39)	(0,72)	(33,16)	(7,88)
P. iridescens	4,23	8,79	153,83	21,37	4,08	8,91	125,81	31,72
	(0,28)	(0,36)	(19,37)	(3,11)	(0,34)	(0,71)	(24,12)	(4,26)
P. vio-lacescens	3,55	7,80	74,88	21,88	3,54	8,03	55,09	31,92
	(0,05)	(0,24)	(10,16)	(0,96)	(0,16)	(0,35)	(8,77)	(2,58)
Arundo Donax	1.65	7.24	18.18	30.94	1.46	7.32	12.24	21.12
	(0.29)	(0.49)	(3.39)	(14.8)	(0.17)	(0.49)	(3.96)	(3.08)

Generally, values measured with deformometer describe a more rigid behaviour, showing that it is not capable to catch the real behaviour of this material. Moreover, in the case of P. violacescens, data from deformometer has been not evaluated as it has fallen during the test, while in the case of Arundo donax it has been not even applicated because of the very small size of the sample. Therefore, the use of strain gauge has been defined as the right way to measure the strain in this test.

Failure occurs in the lower part of the specimen, in both configurations, and are shown in Figure 63. In U-configuration, failure occurred at the matrix a, while, for specimens in D-configuration, the failure occurs through a fibre's delamination. In some cases, specimens do not break until the end of the race, but show a great permanent deformation.

(a) (b) (c)

Figure 63 Failure mode occurred for matrix breakage (a), fibre's delamination (b), and only a great deformation (c)

Homogeneous material model

Bending strength

Bending strength has been calculated considering a homogeneous material model, as illustrated in Figure 64. The hypothesis of the conservation of the planarity of the cross-section under bending is assumed. The deformation is supposed to be linear along the specimen thickness, while normal stresses are linear along the specimen thickness in the elastic region.

The maximum bending strength $\sigma_{b,ult}$ is equal to the maximum tensile stress which happens at the lowermost fibre, for a given load P, and can be calculated as:

$$\sigma_{b,ult} = \frac{M_{ult}\, y}{J} \tag{13}$$

being M_{ult} the bending moment for P_{ult}, while y the distance of the extreme fibre from the neutral axis and J the moment of inertia of the cross-section. Considering

$$M_{ult} = \frac{P_{ult}\, L}{2} \qquad y = \frac{h}{2} \qquad J = \frac{bh^3}{12} \tag{14}$$

in which h defines the height of the specimen while b defines its width, can be obtained the final formula for the ultimate bending strength, that is :

$$\sigma_{b,ult} = \frac{3PL}{bh^2} \tag{15}$$

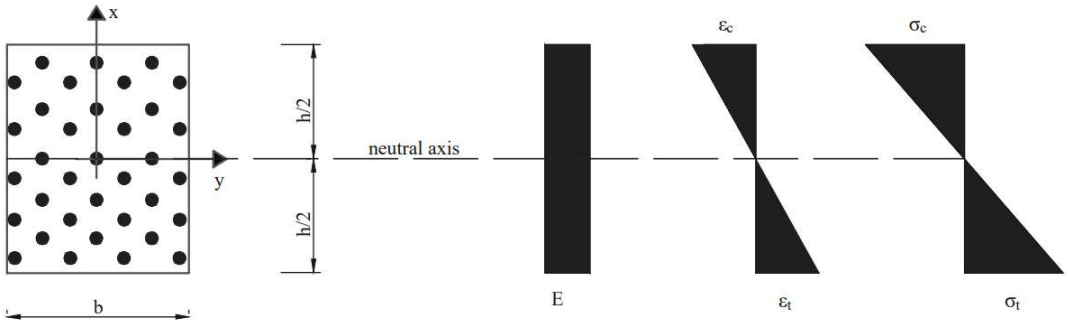

Figure 64 Homogeneous material model: cross-section, Young modulus E, compressive ε_c and tensile ε_t strain and compressive σ_c and tensile σ_t stress into the section

that has been used to calculate the strength of each samples as reported in Table 17.

For U-configuration, the main value of $\sigma_{b,ult}$ varies from 196.26 MPa for P. viridiglaucescens species to 131.96 MPa for P. violacescens species. For D-configuration the main value of $\sigma_{b,ult}$ varies from 159.66 MPa for P. vivax species to 98.19 MPa for P. violacescens species. P. violacescens species presents a significative lower bending stress with respect to all the others in both configurations. Arundo donax results in both cases to have a weaker bending strength respect to those obtained for all the bamboo species, being 113.61 MPa and 74.47 MPa respectively in U and D-configuration.
In contrast to what expected from the anatomy of the bamboo stick, the value of $\sigma_{b,ult}$ is lower in D-configuration where the side with the major amount of fibres is responsible for the tensile stress. This behaviour is attributed to delamination between fibres and matrix.

Young's modulus

Remaining in the same assumptions of the previous case in which the homogeneous model has been considered, the bending Young's modulus can be calculated as

$$E_{hom} = \frac{M_{40} - M_{20}}{(J/r)_{40} - (J/r)_{20}} \tag{16}$$

where M_{40} and M_{20} are the bending moment respectively at 40% and 20% of the maximum applied load, and r the radius of curvature

$$r = \frac{h}{2\,\varepsilon_t} \tag{17}$$

being h the thickness of the specimen and ε_t the strain. Since ε is equal for tension and compression in the homogeneous model, values of ε_t has been used in these calculations. Considering the equations (14) and (17), the equation (16) can be written as:

$$E_{hom} = \frac{h\,L}{4\,J}\frac{P_{40} - P_{20}}{\varepsilon_{t,40} - \varepsilon_{t,20}} \tag{18}$$

Results are reported in Table 17. The average value in U-configuration ranges from 18.16 GPa for the P. bambusoides species to 9.57 GPa for the P. violacescens, while from 25.5 GPa for P. bambusoides to 17.98 GPa for P. violacescens for specimen tested in D-configuration. As predictable, values of E_{hom} are higher in D-configuration, since the side with the major amount of fibres is the one which undergoes to the tensile stress. Arundo donax has a E_{hom} correspondent to 10.75 MPa and 14.12 MPa for U and D-configuration respectively and do not present a marked difference with respect to bamboo species as in the case of the bending strength.

Table 17 Results bending strength $\sigma_{b,ult}$ and Young's modulus E_{hom} considering the homogeneous model for both U and D configurations.

Species	$\sigma_{b,ult}$ (MPa)		E_{hom} (GPa)	
	U-configuration	D-configuration	U-configuration	D-configuration
P. edulis	164,43	143,67	14.50	22.30
	(19,86)	(15,79)	(1.68)	(2.99)
P. viridiglau-cescens	196,25	155,95	18.15	24.1
	(3,62)	(18,67)	(1.99)	(5.55)
P. bambusoides	179,82	147,55	18.16	25.5
	(7,33)	(16,12)	(2.19)	(1.75)
P. vivax	175,24	159,66	15.46	23.80
	(17,55)	(17,55)	(1.92)	(5.48)
P. iridescens	177,99	151,05	14.87	22.20
	(29,80)	(5,88)	(2.90)	(5.20)
P. violacescens	131,96	98,19	9.57	17.98
	(23,99)	(9,21)	(1.94)	(1.24)
Arundo Donax	113,61	74.47	10.75	14.12
	(28.28)	(16.73)	(0.13)	(4.92)

Non-homogeneous material model

Moreover, as the material is not homogeneous and its components have different mechanical properties, the Young's modulus has been calculated considering a non-homogeneous material model, as those presented in Figure 65 and Figure 66. In the previous chapter, distribution of fibres has been analysed and an almost linear trend has been recognized. So, it is reasonable to hypothesize that the Young's modulus varies linearly along the section. The deformation is supposed to be linear along the stiffness, conserving the hypothesis of cross section's planarity, and it is different at each position, so also the maximum compressive strain ε_c is different, in absolute value, from the maximum tensile strain ε_t. The neutral axis is consequently shifted with respect to the centroidal axis of the quantity d, defined as:

$$d = \frac{h}{2}\frac{\varepsilon_t + \varepsilon_c}{\varepsilon_c - \varepsilon_t} \tag{19}$$

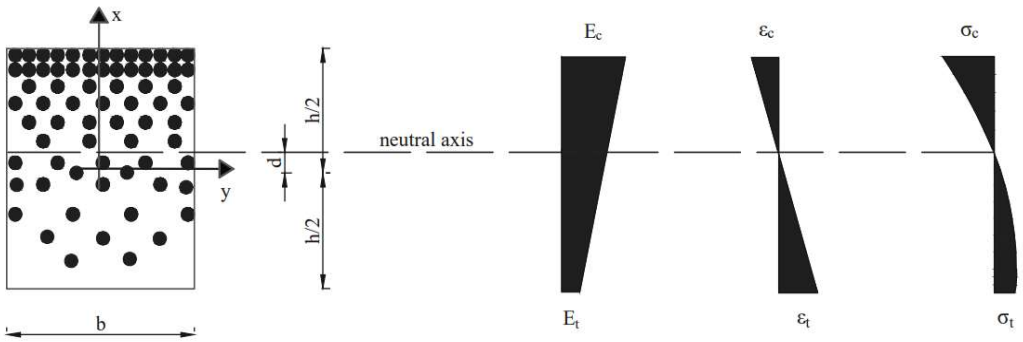

Figure 65 Non-homogeneous material model: cross-section, Young modulus E, compressive ε_c and tensile ε_t strain and compressive σ_c and tensile σ_t stress into the section for the U-configuration

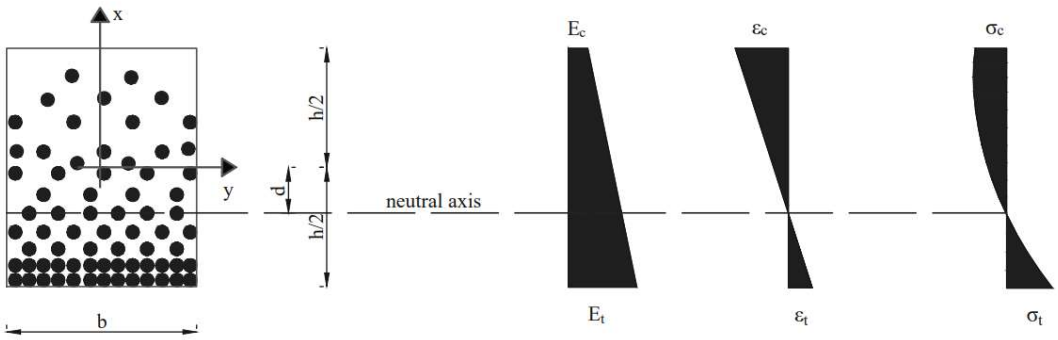

Figure 66 Non-homogeneous material model: cross-section, Young modulus E, compressive ε_c and tensile ε_t strain and compressive σ_c and tensile σ_t stress into the section for the D-configuration

The strain $\varepsilon_{(x)}$ at the generic coordinate of the x axis along the thickness of the specimen can be calculated as

$$\varepsilon_{(x)} = \frac{x}{h}(\varepsilon_c - \varepsilon_t) + \frac{1}{2}(\varepsilon_c + \varepsilon_t) \tag{20}$$

Assuming that each fibre behaves in the linear elastic region, the strength at the generic coordinate of the x axis along the thickness of the specimen can be calculated according to the Hooke's Law:

$$\sigma_{(x)} = E_{(x)}\varepsilon_{(x)} \tag{21}$$

The extreme values of $E_{(x)}$ correspond to the E_{inner} and E_{outer}, which can be obtained by integrating the two equations

$$\int_{-\frac{h}{2}}^{\frac{h}{2}} E(x)\varepsilon(x)dx = 0 \tag{22}$$

$$\int_{-\frac{h}{2}}^{\frac{h}{2}} E(x)\varepsilon(x)xb\,dx = -M \tag{23}$$

In U-configuration, the outer culm wall is placed the upper surface of the specimen, as specified in Figure 59. The maximum value of the Young's modulus can be found at the uppermost fibre, and varies according to

$$E_{(x)} = \frac{x}{h}(E_{outer} - E_{inner}) + \frac{1}{2}(E_{outer} + E_{inner}) \tag{24}$$

Substituting equations (20) and (24) into the system of the equations (22) and (23), can be obtained:

$$E_{inner} = \frac{2M}{W}\frac{\varepsilon_t + 2\varepsilon_c}{\varepsilon_t^2 + \varepsilon_c^2 + 4\,\varepsilon_t\,\varepsilon_c} \qquad E_{outer} = -\frac{2M}{W}\frac{\varepsilon_c + 2\varepsilon_t}{\varepsilon_t^2 + \varepsilon_c^2 + 4\,\varepsilon_t\,\varepsilon_c} \tag{25}$$

In D-configuration, the outer culm wall is placed on the lower surface of the specimen, as specified in Figure 59. The maximum value of the Young's modulus can be found at the lowermost fibre, and varies according to

$$E_{(x)} = -\frac{x}{h}(E_{outer} - E_{inner}) + \frac{1}{2}(E_{outer} + E_{inner}) \tag{26}$$

Substituting equations (20) and (26) into the system of the equations (22) and (23),

can be obtained:

$$E_{inner} = -\frac{2M}{W}\frac{\varepsilon_c + 2\varepsilon_t}{\varepsilon_t^2 + \varepsilon_c^2 + 4\,\varepsilon_t\,\varepsilon_c} \qquad E_{outer} = \frac{2M}{W}\frac{\varepsilon_t + 2\varepsilon_c}{\varepsilon_t^2 + \varepsilon_c^2 + 4\,\varepsilon_t\,\varepsilon_c} \tag{27}$$

which are calculated as the average of the values determined at 20% and 40% of the ultimate bending load, considering both configurations. Each configuration describes the behaviour of the inner or outer part of the culm wall subjected to tension or compression.

Results are reported in Table 18 for all the species analysed. Data obtained using the two different instrumentation, as previously described, are distinguished in order to compare them.

Values of E_{inner} result slightly generally higher in tension than in compression. Data obtained from the tests in which the deformometer has been used for the measurement of the strain of the lower part, result higher in tension while lower in compression. In every case P. violacescens has the lowest result, that is around 1 GPa both in tension and compression. P. bambusoides has the higher result, that is 9.95 GPa and 8.85 GPa respectively in tension and compression. However, no significative differences have been detected for all the bamboo species. Arundo donax exhibits an opposite trend: it has a significant higher value when it is subjected to compression, which exceed also those of bamboo, as 8.2 GPa and 12.4 GPa in tension and compression respectively.

In the case of E_{outer}, there is not a big difference between results obtained in compression and those obtained in tension, according to data from those tests in which only two strain gauge have been used. When deformometer has been used, values of E_{outer} in tension are clearly higher than those in compression. It could be due to the dimensions of the instrumentation, which could not be able to catch little values of defomations.

In the first case, results range from 29 GPa to 37 GPa in tension, while from 30 GPa to 38 GPa in compression. In the second case, results range from 41 GPa to 47 GPa in tension, while from 24 GPa to 36 GPa in compression. In both cases, the lowest value is always represented by P. edulis, while the higher one is attributed to P. iridescens or P. viridiglaucescens. Arundo donax has lower results respect to bamboo species, that are 16 GPa in compression while 20 GPa in tension.

Generally, E_{inner} and E_{outer} can be considered as the approximation of the Young's modulus of the matrix and fibres respectively, as in those part of the cross section, the

Table 18 Values of E_{inner} and E_{outer}, related to matrix and fibres, resulting from the analytical modelling of data obtained from the bending test. For each one, results in tension and compression are shown. A comparison between results obtained from two types of instrumentation has been done.

Species	E_{inner} (MPa)				E_{outer} (MPa)			
	TENSION		COMPRESSION		TENSION		COMPRESSION	
	Strain gauge + Strain gauge	Strain gauge + Deformometer	Strain gauge + Strain gauge	Strain gauge + Deformometer	Strain gauge + Strain gauge	Strain gauge + Deformometer	Strain gauge + Strain gauge	Strain gauge + Deformometer
P. edulis	8.15 (1.76)	11.473 (1.382)	6.719 (1.924)	2.974 (2.511)	29.448 (0.754)	41.104 (5.243)	30.671 (2.652)	24.433 (2.852)
P. viridiglaucescens	7.80 (1.03)	13.602 (1.486)	6.043 (0.665)	3.576 (1.573)	34.877 (1.365)	47.097 (5.745)	37.969 (0.335)	32.496 (1.377)
P. bambusoides	9.95 (3.102)	13.996 (2.043)	8.855 (0.726)	3.460 (1.212)	35.066 (1.405)	46.043 (3.050)	32.500 (5.127)	30.358 (1.002)
P. vivax	5.762 (1.251)	11.029 (1.271)	5.250 (0.557)	4.061 (1.678)	34.953 (2.642)	45.460 (5.231)	33.855 (1.501)	30.466 (5.194)
P. iridescens	7.701 (2.587)	8.883 (0.998)	2.543 (0.711)	2.436 (0.172)	37.738 (2.789)	44.416 (3.752)	34.955 (3.493)	35.964 (5.194)
P. violacescens	1.085 (0.405)	-	1.313 (0.481)	-	31.384 (1.814)	-	32.657 (6.821)	-
Arundo Donax	8.197 (1.153)		12.416 (0.354)		20.066 (3.746)		16.114 (3.447)	

percentage of area attributed to that component is very high. It can be noticed that results are very similar to those obtained in literature with experimental procedures, as those considered in the previous section of this thesis in [110] and [118], testifying the reliability of the analytical procedure here described. Therefore, the values just obtained have been used to calculate the modulus of elasticity in axial loading of the whole section by the use of the iso-strain analytical model of the rule of mixture, that has been previously well described. Applying equation (8), results have been calculated for all the species and are presented in Table 19. Here they are compared with those obtained from in longitudinal tensile tests, and are very close to experimental one.

Table 19 Values of the Young's modulus are compared with those obtained considering a non-homogeneous model through E_{ROM}, and with those obtained from the experimental tensile test E_{exp}

Species	E_{hom} (GPa)		E_{ROM} (GPa)	E_{exp} (GPa)
	U-configuration	D-configuration		
P. edulis	14.50	22.30	16.75	17.04
	(1.68)	(2.99)		
P. viridiglaucescens	18.15	24.1	20.29	18.82
	(1.99)	(5.55)		
P. bambusoides	18.16	25.5	22.52	21.09
	(2.19)	(1.75)		
P. vivax	15.46	23.80	20.23	16.58
	(1.92)	(5.48)		
P. iridescens	14.87	22.20	20.05	19.79
	(2.90)	(5.20)		
P. violacescens	9.57	17.98	9.40	17.34
	(1.94)	(1.24)		
Arundo Donax	10.75	14.12	9.50	15.29
	(0.13)	(4.92)		

Application of the procedure: UV degradation and heat degradation

The proposed experimental bending test can provide information on the material through a fast and simple procedure. Obtaining reliable information in this way can be extremely helpful when it is necessary to understand the convenience in using the material for any situation. For instance, it can be applied for examining the effects of ageing caused by UV exposure and thermal degradation.

Many studies have been conducted on reactions occurring in wood caused by UV light. The main cause of its degradation is the modification in lignin, which is responsible of the bearing ability of the material. Strength and stiffness of bamboo are strongly dependent from the presence of lignin which amount varies with the age and the position of the culm. Li et al. [96] found that the outer layer of the culm had the highest holocellulose, a-cellulose and Klason lignin contents, while no significant differences in Klason lignin were detected from the base to the top of the culm. Moreover, in the study conducted by Maulana et al. [128], an analysis of variance showed that bamboo species has significant influence on lignin content. Regarding Arundo donax, its content of lignin is about the 19.66% [129], and it seems to vary along the culm, decreasing from the bottom to the top [130].
Wang et al. [131] analysed the effect of UV irradiation on a Phyllostachys bamboo species. In this case, the formation of new carbonyl groups and a decrease in the intensities of the characteristic aromatic lignin peak was noticed. Moreover, relevant damage in the fibre wall was observed by a SEM micrography, as intense cracks that causes the separation of the secondary cell wall, while slight distortion of the cell wall and cracks on the inside of the cell wall were observed in parenchyma cells.
Yu et al. [132] analysed the changes in lignin content according to the time of exposure. They observed an abrupt change in lignin content in the first five days and then a soft decrease until the stabilization in the following fourteen days. Another study [133] compared bamboo photodegradation with that of wood and a significative lower carbonyl formation and lignin degradation was observed in the bamboo case: a colour change was noticed in the first twenty hours and then it remains constant.
Generally, studies on degradation caused by UV exposure are mainly related to changes in the colour of the surface, while alterations in its mechanical properties remain less well understood. An investigation on this topic it is required in the view to use this material in construction and therefore, an experimental study is here presented in order to assess the eventually modification on a Phyllostachys viridis bamboo, due to the exposure on UV light. A reduced version the previously exposed bending test has been proposed, in order to evaluate the simplest version of this

procedure. In fact, since the non-homogenous model is suitable for the applications in which is important to know the changes in the mechanical properties along the thickness, the homogeneous model is simpler and can be used when the aim is to understand the mean mechanical properties.

Materials and methods

Three years old bamboo culms were collected in February 2021 in Macerata, then washed with a pressure washer and then stored vertically in a protected storage room, according to requirement of regulation [124]. The part of the culm between 0.5 to 1.5 m from the ground (which has been defined as Part B in the previous chapters) has been considered for this campaign. Eleven samples have been obtained from the same portion of each culm, according to the procedure previously exposed for the bending tests. The number of the specimens has been chosen to evaluate the effect of UV light. In particular:

- Seven samples have been tested to different times of exposure to UV rays, in order to evaluate the changes along 6, 12, 24, 48, 96 e 192, and 360 hours
- Three samples have been exposed to only temperature, to evaluate how the degree caused by temperature has affected results. The temperature has been chosen at 40° , as the one registered into the box with UV lamps. In this case, the time of exposure has been 96, 192 and 360 hours
- One sample has been tested without any treatment, to compare the effect of the exposures to a virgin one

UV radiation has been reproduced in a box with reflecting walls and UV lamps (Osram Dulux S 9 Watt 78 BLUE UV-A), shown in Figure 67. To reproduce the environmental condition, the external side of the culm has been exposed to the radiation. During the test, temperature and relative humidity were measured. The temperature oscillated between 35 and 40° C during the same day while the humidity was constant around 28 ± 2%.

Bending test were performed in the laboratories of the LISG at the University of Bologna, following the procedure explained in the previous paragraph. In this case, strain was measured using a strain gauge along the lower surface, in which fibres have

been subjected to tension as in D configuration. This has been done in order to test as simplified version of the bending procedure. Bending strength has been evaluated, according to the homogeneous model, as expressed by equation (15).

(a) (b)

Figure 67 Instrumentation used for the UV ageing, before (a) and during the ageing (b)

To investigate how the UV light exposure affects the microstructure of the bamboo, microscopical observations have been done. Environmental scanning electron microscopy (ESEM) imaging and optical microscope have been used.

The external part of the specimens was subjected to attenuated total reflection ATR FTIR analysis. It has been performed using a Perkin Elmer Spectrum 3 instrument, fitted with a diamond prism with a resolution of 4 cm^{-1}, while 64 scans have been applied in the measurements.
For ESEM analysis, samples have been embedded in epoxy resin, cut and polished with abrasive pastes in order to obtain thin sections of 100 µm thickness. The analyses have been carried out with a Thermo Fisher Quattro S environmental scanning electron microscope, operating with a 12 kV beam acceleration voltage and in low vacuum conditions (170 Pa).
Low vacuum (LVD) and angular backscatter (ABS) detectors have been employed to collect secondary and backscattered electrons, respectively. The ESEM operation conditions were selected according to Monte Carlo simulations of the electron beam/specimen interaction.

Results

In Table 20, the average values (and standard deviation) of the bending strength $\sigma_{b,ult}$, and deformation of the external surface ε, are reported for the samples subjected to different hours of exposures to UV light and the temperature of 40° . Moreover, in Figure 68, the trend of the changes in bending strength is visible. UV exposure does not seem to affect the mechanical performances. After 48 hours of irradiation, a slight increment of strength is already visible. After 96 hours, the increment reaches a value of the 31% higher than the initial one. At 192 hours of exposure, the increment starts decreasing, going to the 21% of the initial one. Then, strength goes down but remains higher than the initial one. A slight increase of deformation shows that modifications have occurred, but in any case, there are no significant changes at different times of exposure.

A statistical analysis of bending strength at each time of exposure has been performed with anova1 in Matlab R 2021b. Data are statistically indistinguishable, as it is shown in the box plot of the data obtained in Figure 69. A trend in the average values is recognizable, even if the groups are not distinguishable considering threshold values for the p-value of 0.05 presented in Figure 69.

.

Table 20 Average values (and standard deviation) of the bending strength $\sigma_{b,ult}$ and deformation of the external surface ε of the samples results of the mechanical test for the sample exposed to different hours of exposures to UV light and the temperature of 40°

Hours of exposure	UV light		Heat (40° C)	
	$\sigma_{b,ult}$ [MPa]	ε [%]	$\sigma_{b,ult}$ [MPa]	ε [%]
0	113.26 (18.94)	0.98 (0.16)		
6	125.12 (11.44)	1.27 (0.02)		
12	119.45 (15.14)	1.23 (0.1)	-	
24	119.75 (14.09)	1.36 (0.04)		
48	125.30 (10.46)	1.3 (0.05)		
96	149.72 (12.55)	1.2 (0.17)	123.25 (9.03)	1.39 (0.09)
192	137.69 (17.33)	1.51 (0.13)	120.62 (20.30)	1.44 (0.12)
360	122.20 (26.70)	1.39 (0.04)	132.10 (6.16)	1.36 (0.07)

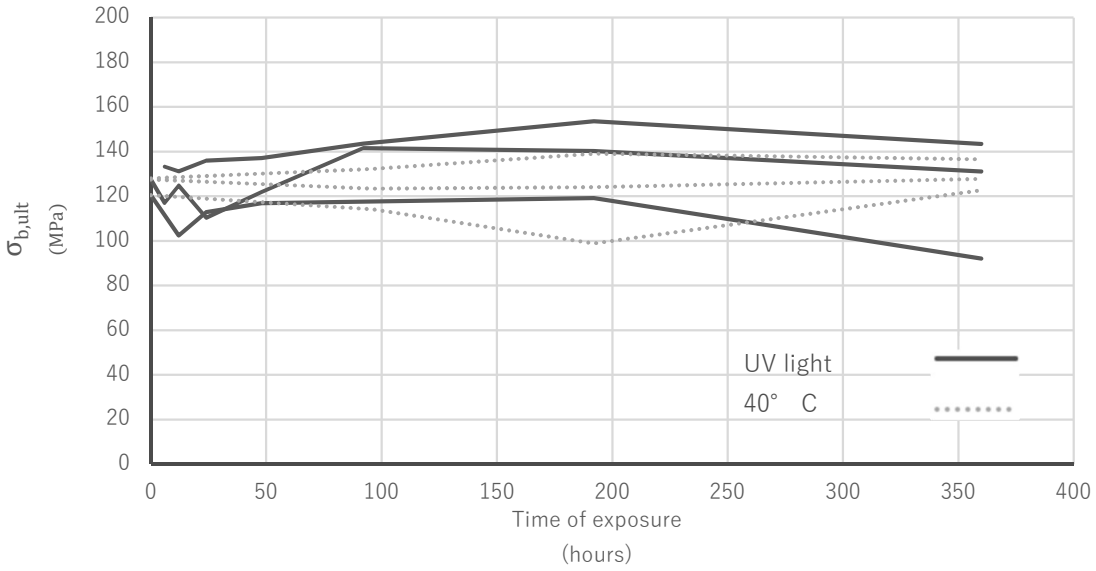

Figure 68

Comparison of the trend of the bending strength along the time of exposure between the samples exposed to UV light and those exposed to only the temperature of 40°

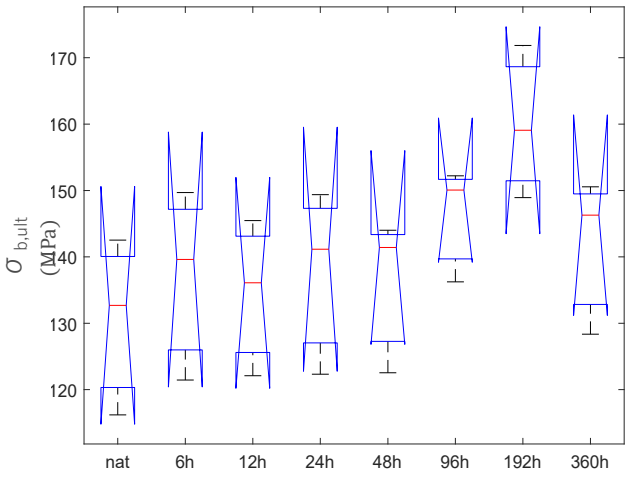

	6h	12h	24h	48h	96h	192h	360h
0h	0.997	0.999	0.995	0.999	0.759	0.125	0.941
6h	-	1.000	1.000	1.000	0.978	0.346	0.999
12h		-	1.000	1.000	0.931	0.245	0.995
24h			-	1.000	0.986	0.381	0.999
48h				0.964	0.304	0.998	
96h					0.853	0.999	
192h						0.614	

Figure 69 Box plot and p-values for the specimen with different hours of exposure to UV light

The microscopical investigation demonstrates modification in the material after UV exposure. By the ATR-FTIR spectroscopy, lignin results as the most affected component. The reduction of two bands on account of the UV stress, the ones at 1512 and 1654 cm^{-1} in Figure 70, clearly shows the result. Moreover, the broad band at 1046 cm^{-1} decreases. This peak is also related to the lignin phase and confirms the degrading reactions affecting this phase.

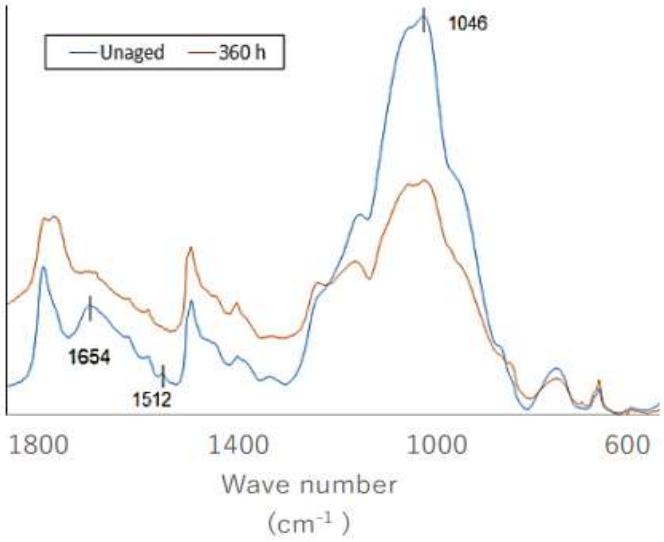

Figure 70
ATR FTIR spectra of unaged and UV (360h) aged samples

Moreover, a backscattered electron image in Figure 71 compares a fibre from a sample subjected to 192 hours of exposure to UV rays and a fibre from a virgin sample. The aged one result significantly affected by UV rays, since it presents a visible separation of the layers constituting the fibre wall and some cracks into the same layer. In the virgin one, only small fissures have been detected between vascular bundles and ground parenchyma or in some cases between fibres into the same vascular bundle. Another comparison has been done between fibres from the external and inner part of a vascular bundles. The former was more affected by deterioration than the latter, as visible in Figure 72. No differences have been found regarding a different position of the fibres in the culm wall. Samples have been analysed also along the longitudinal direction of the culm, in order to detect modification along the fibres development but no changes have been found, as depicted by Figure 73. This result could explain why aged samples exhibit an almost unaffected mechanical behaviour in bending tests.

Optical microscope observations reveal the appearing of parenchyma zones into the fibres island of the vascular bundles into the aged samples, as shown in Figure 74 where the comparison with the virgin sample is presented. In the latter case it is not present, so it is probably a consequence of the UV exposure. In conclusion, it can be assumed that UV exposure up to 360 hours causes a decrease of the content of lignin and a change in the surface, but do not compromise the structure of fibres along their longitudinal development. This is an important result which could allow the use of bamboo along the culm axis which is actually the main way for whom this material is used.

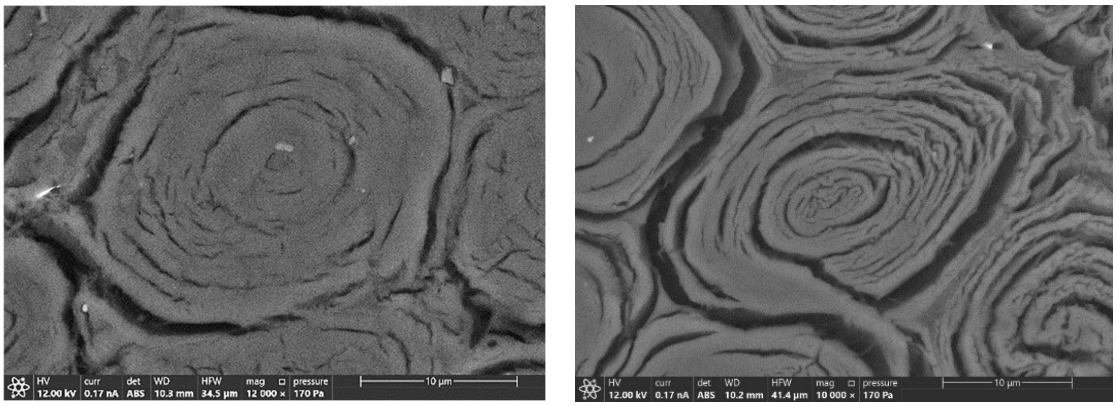

(a) (b)

Figure 71 Backscattered electrons ESEM micrograph of a fibre of unaged sample (a) and UV (192 h) aged specimen (b), both taken from the external part of a vascular bundle of the central part of the culm wall

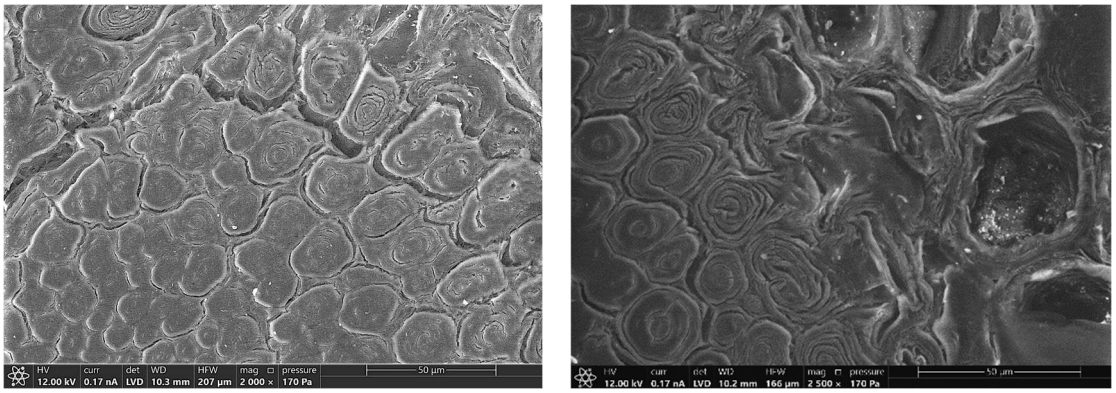

(a) (b)

Figure 72 Secondary electrons ESEM images of the border between fibres and ground parenchyma of unaged (a) and UV (192 h) aged (b) samples, both collected from a vascular bundle of the central part of the culm wall

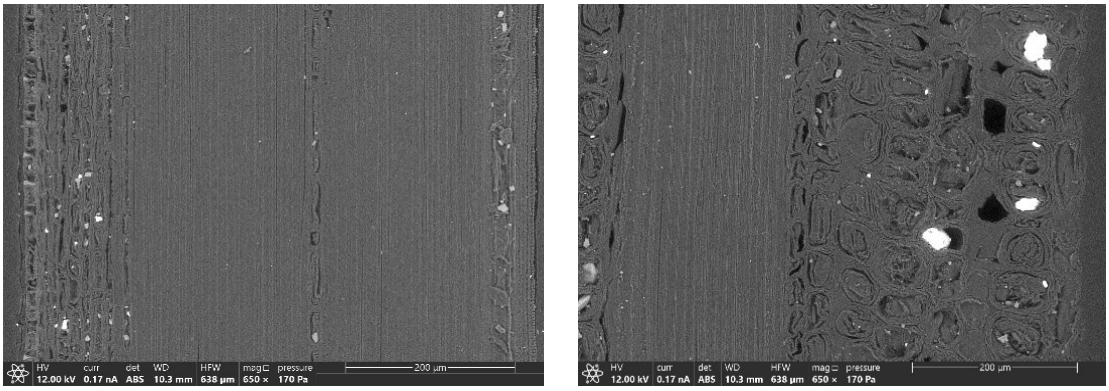

(a) (b)

Figure 73 Backscattered electrons ESEM micrograph of the longitudinal section of an aged sample (192 h), taken from the external surface on the left to the inner surface on the right, of the culm wall

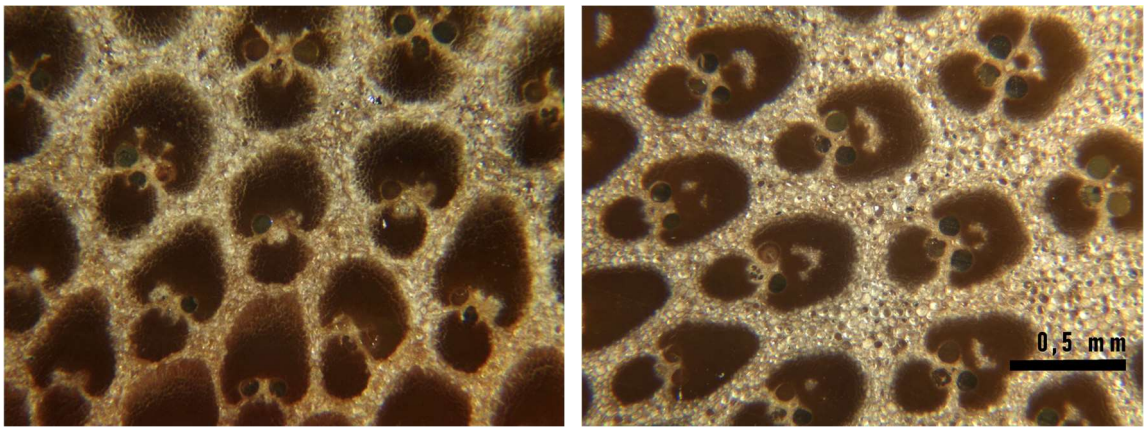

(a) (b)

Figure 74 Optical microscopy images showing holes in the fibre island of the vascular bundles of the middle part of the culm wall for an unaged (on the left) and aged (on the right) samples after 192 hours of exposure to UV irradiation.

Grading

One of the main lacks in the regulation regarding bamboo as a construction material, is the absence of an effective grading method. The considerable difference in the mechanical properties between species and within the same species as well, need to be adequately handled avoiding the limitation in its use. In fact, the existence of an affordable grading protocol and a system made by strength classes which guarantee general material properties, could fill a very important gap in terms of knowledge and make bamboo a reliable solution for all the designers.

Some of the content of this paragraph has been already published in:

Silvia Greco, Mirko Maraldi, Luisa Molari «Grading bamboo through four-point bending tests. A report on six species of Italian bamboo» *Construction and Building Materials,* November 2023; 404, 133168 https://doi.org/10.1016/j.conbuildmat.2023.133168

Current procedure

The actual grading procedure for bamboo is collected into ISO Standard 19624 [134]. The process consists of two methods: a visual grading based on observable characteristics of the piece and a machine grading process based on non-destructive measurement.

The visual grading consists in the observation of the characteristics known to affect the mechanical or structural properties of the culm. A first observation concerns the condition properties, such as the observation of state of the material in terms of insect and/or fungal damage, and defects such as fissures and longitudinal indentation. A second observation concerns the geometrical properties, such as diameter, wall thickness, internode length, length, external and internal taper, bow, ovality. Some of these are shown in Figure 76.

The machine grading process comprises one or more devices capable to measure with repeatability some physical or mechanical properties of bamboo culm as stiffness, flexibility, linear mass, wall thickness or diameter. In any case, each culm is tested allowing its subsequently use.

An example of a possible grading procedure within a hybrid approach is illustrated in Figure 75. Some studies in literature have applied this grading method to various bamboo species [135] [136], demonstrating that the grading process cannot rely solely on geometric or physical properties. Furthermore, the Standard does not define general classification categories for the material. Rather, it appears to adopt a selective approach, aimed at identifying, from a large number of culms, only those that meet the specific requirements for the design of a given structure.

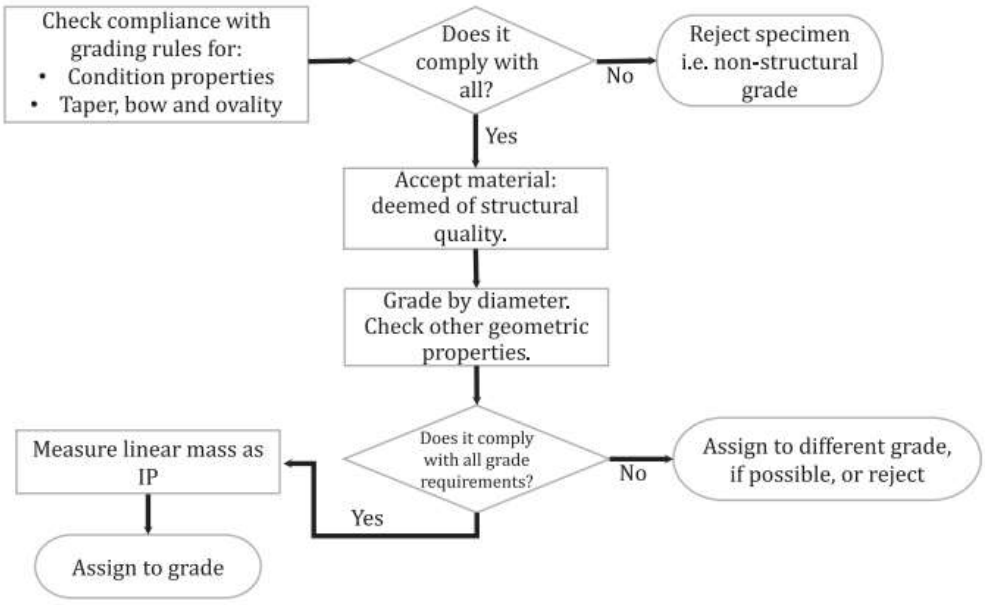

Figure 75 Flowchart of a diameter-based visual grading combined a machine graded process [134]

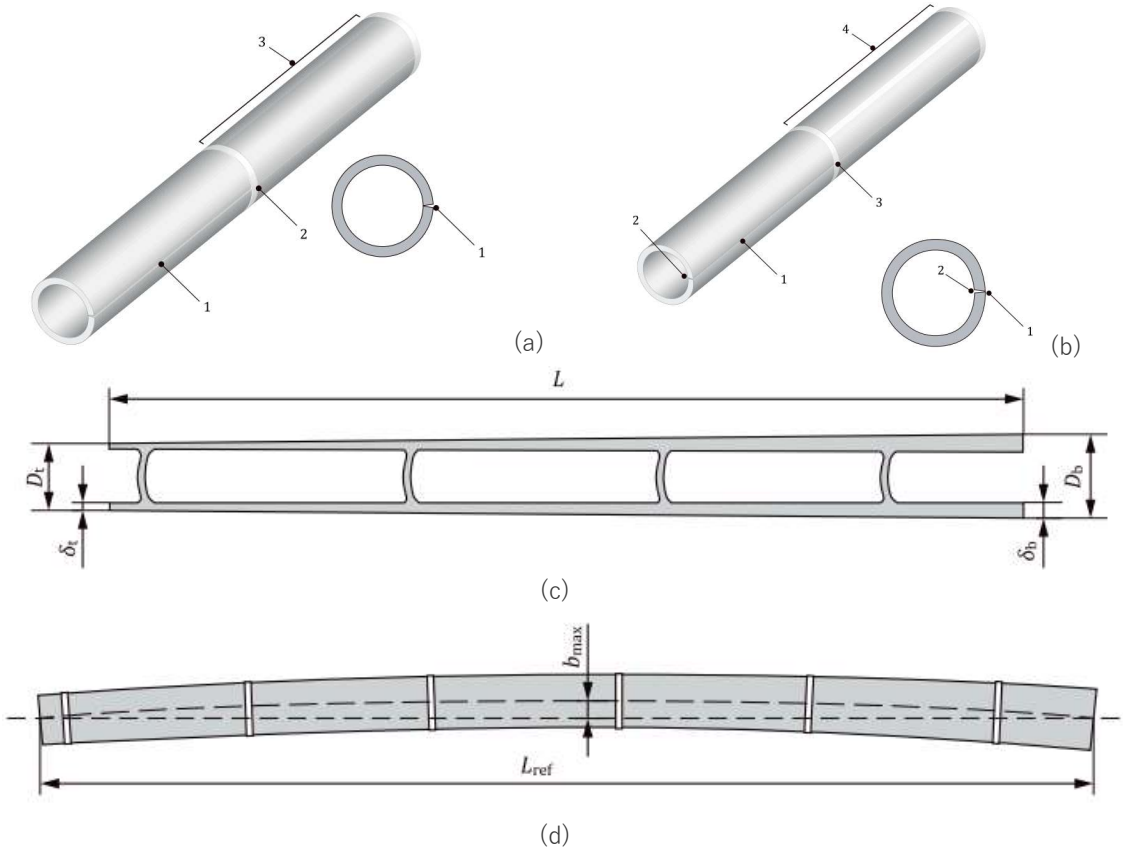

Figure 76 Visual criteria for grading bamboo, fissures in the external (a) and inner (b) surface, inner and external taper (c) and bow (d), from [134]

The proposal

This proposal presents a simplified grading approach, inspired by the timber grading system. According to EN 14081, timber grading evaluates three fundamental properties: bending strength, bending stiffness, and density. Following this evaluation, timber is assigned to a specific strength class, which is identified by numerical values corresponding to these properties. These values can then be directly applied in design calculations. For softwoods, common strength classes range from C16 to C24, while hardwoods fall within the range of D18 to D70, with the numbers referring to bending strength.

A similar strength classification system could be developed for bamboo, based on its own mechanical properties. These properties can be assessed through bending tests, and thus, a strength-based grading system using a four-point bending test emerges as an effective solution. The method outlined in the previous section provides a fast,

efficient, and practical way to collect essential data. It allows for the assessment of how material properties change along the thickness of the bamboo culm wall, thus providing valuable information in a time-efficient manner. Ultimately, the goal of this proposal is to supplement the grading guidelines outlined in ISO 19624.

To test this solution, a grading procedure has been conducted on the species used in this thesis. Experimental results from the bending test adopted in the previous section have been processed through the analysis of variance test, reported in Figure 77a-f. The box is bordered by the values of the 25th and 75th percentiles at the bottom and top edges respectively, the central red mark indicates the median value and the extreme data are indicated by the tips of the boxes, while outlier values are plotted as'+' red marker symbol. Moreover, in Table 21, the p-values of the analysis of variance are shown regarding the σ_b. In this case, values <0.05 mean that distinguishable groups can be found while greater values mean that the groups analysed are not statistically distinguishable.
In the homogeneous material model, P. violacescens is the only statistically distinguishable species between all. In the non-homogeneous material model, P. violacescens is the only statistically distinguishable species for E_{inner} while no statistically distinguishable species were detected for E_{outer}. This result suggests that bamboo grading based on the species does not have big significance from the point of view of its mechanical properties.
Statistical groups can be defined, based on the values of the mechanical properties rather than on the bamboo species, hence supporting the appropriateness of strength classes.

An example of bamboo classification based on strength grades is shown in Table 22 where σ_b has been used as the grading property. In order to account for results variability from specimen to specimen, the critical strength value was calculated at the 5th percentile. Four different strength grades were established:

- B80 (having 80 MPa ≤ σ_b< 100 MPa) in which P. violacescens falls
- B100 (having 100 MPa ≤ σ_b < 120 MPa) in which no one of the species analysed in this study falls
- B120 (having 120 MPa ≤ σ_b < 140 MPa) in which P. edulis, P. bambusoides and P. viridiglaucescens fall
- B140 (having 140 MPa ≤ σ_b < 160 MPa) in which P. iridescens and P. vivax fall

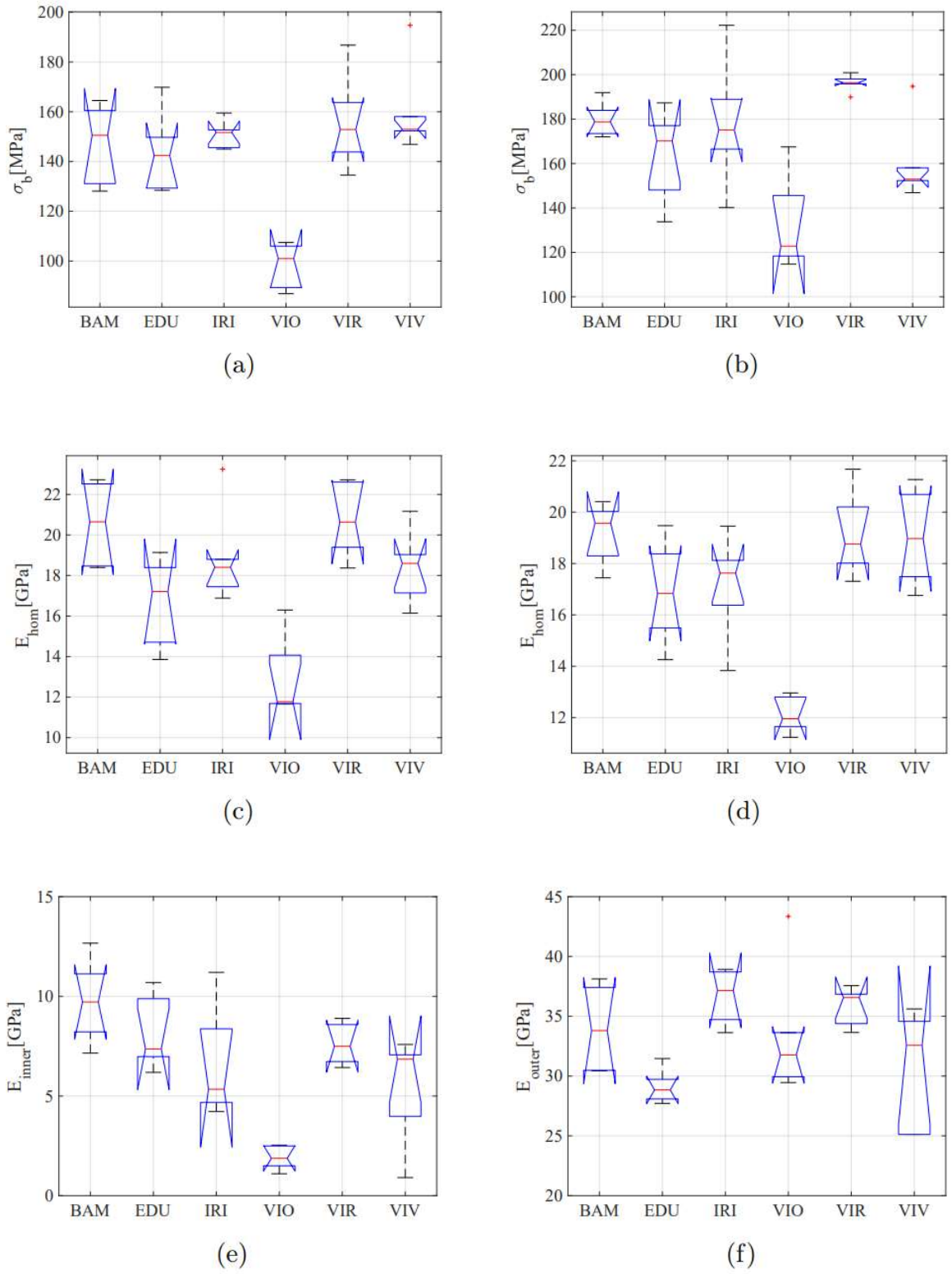

Figure 77 Box plots of the mechanical properties for all the tested species. (a) σ_b for specimens tested in U-configuration; (b) σ_b for specimens tested in D-configuration; (c) E_{hom} for specimens tested in U-configuration; (d) E_{hom} for specimens tested in D-configuration; (e) E_{inner} for both U-configuration and D-configuration; and (f) E_{outer} for both U-configuration and D-configuration.

Table 21 P- values for σ_b

	P. edulis		P. iridescens		P. violacescens		P. viridiglaucescens		P. vivax	
	E_{inner}	E_{outer}	E_{inner}	E_{outer}	E_{inner}	E_{outer}	E_{inner}	E_{outer}	E_{inner}	E_{outer}
P. bambusoides	0.997	0.688	0.998	1.000	**0.000**	**0.004**	0.922	0.627	0.706	0.412
P. edulis			0.951	0.787	**0.000**	0.094	0.708	0.053	0.426	0.997
P. iridescens					**0.000**	**0.006**	0.993	0.519	0.906	0.515
P. violacescens							**0.000**	**0.000**	**0.000**	0.205
P. viridiglaucescens									0.997	**0.018**

Table 22 Strength-based grading of the species used in this study

Species	σ_b average value	σ_b standard deviation	Numbers of specimens	critical value (5^{th} percentile)	Strength grades
P. violacescens	113.2	24.0	9	86.9	**B 80**
P. edulis	154.1	20.2	12	128.5	**B 120**
P. bambusoides	164	20.4	12	128.4	**B 120**
P. viridiglaucescens	176	24.7	12	135.4	**B 120**
P. iridescens	165.6	23.3	12	140.7	**B 140**
P. vivax	167.4	17.5	12	146.9	**B 140**

It must be noticed that identifying strength classes to classify bamboo batch in strength grades for construction purposes, request a number of tested specimens which must necessarily be extended. However, results obtained in this paper are illustrative of the effectiveness of the procedure presented and depict a good solution for this very important topic.

MACRO SCALE

Translating Material Knowledge into Structural Innovation towards a Smart Building Design

Designing buildings with natural materials poses considerable challenges, largely because conventional construction paradigms are often incompatible with the inherent properties of these materials. However, the study of traditional architecture reveals an impressive capacity to employ local materials in effective and intelligent ways. The fundamental distinction lies in whether the design process seeks to force a material into a predetermined form or, conversely, leverages the material's intrinsic properties to inform and shape the design itself.

This issue becomes particularly evident when discussing bamboo structures. Bamboo culms present themselves as ready-to-use cylindrical beams. In many cases, builders have attempted to replace conventional materials with bamboo poles in standard structural schemes. This often results in numerous difficulties in making reliable connections between the culms. Bamboo culms lack strong transverse resistance, as they are hollow and their microstructure is optimized to withstand primarily axial loads. This can lead to the formation of fissures and subsequent cracking in the culm. Furthermore, the smooth, rigid surface and circular cross-section of the elements introduce additional complexities to an already challenging task. This topic has been widely explored (see for instance [137] [138] [139] [140] [141] [142]) and several attempts have been made to find a solution to this topic.
On a hand, low-tech solutions are currently diffused in bamboo construction, such as the traditional tying with ropes, as in Figure 78, or using screws and bolts after the mortar filling of the culms, as shown in Figure 79. These techniques have the advantage of being easy to implement; however, they come with several drawbacks. For example, they are difficult to standardize, and in the case of mortar filling, they result in a significant increase in the overall weight of the structure. More critically, both approaches tend to weaken the structural performance.
On the other hand, high-tech solutions -such as 3D-printed custom connectors or complex-shaped steel elements, as shown in Figure 80- have been proposed to address connection inefficiencies. While these methods can improve joint performance, they rely on highly complex design and industrial processes, significantly increasing construction costs. Despite numerous efforts, issues still persist, and a truly ‘perfect solution’ has yet to be found.

The design approach can shift from problem-solving toward the enhancement of material performance. This change in perspective, centered on the material's structural potential rather than its limitations, leads to more rational and efficient solutions. Bamboo and Arundo donax are characterized by high longitudinal tensile strength and notable flexibility, coupled with relatively low transverse strength. These mechanical properties make them particularly suitable for structural systems in

which loads are primarily directed along the axis of the elements. One such system is the arch, which transfers compressive forces along a curved geometry down to its supports. This configuration minimizes transverse stresses and allows the material to perform near its optimal structural capacity. Additionally, the natural morphology of these plants often exhibits curved forms under environmental loading, such as wind, making the arch a structurally coherent and biomimetic solution.

One of the main challenges in adopting bamboo as a construction material in Europe relates to the limited culm diameter of the species available in temperate climates. While tropical bamboos can reach large cross-sectional dimensions, and consequently high capacity, these species are restricted to specific geographic zones. Relying on them would require intensive cultivation and long-distance transportation, thereby compromising the material's sustainability. A more viable and context-sensitive approach involves the use of common local species, regardless of their individual size.
To overcome dimensional limitations, structural capacity can be achieved through the assembly of multiple culms. The adoption of multi-culm members enables the use of a broader range of species, including Arundo donax, while also offering potential improvements in mechanical performance. Although multi-culm configurations are already employed in practice (Figure 81), their structural behaviour remains partially understood. In particular, the mechanical interaction between individual culms within a composite element has shown limited reliability [143], indicating a need for further investigation.
This chapter explores the development of an efficient structural typology based on multi-culm bamboo arches. The study begins with the characterization of a multi-culm beam element, the simplest structural element. An experimental bending test and a finite element numerical are performed, in order to gain a better understanding of the factors that most affect the behaviour of the moment of inertia during load application. Subsequently, the role of the beam within the overall arch configuration is examined through an experimental test on an arch. The research follows a structured sequence: experimental testing, numerical simulations, and comparative analysis with Arundo donax elements.

Some of the results discussed in this chapter have been already presented in:

Kiara Perolli, *Comportamento meccanico di bambù in fasci al variare della geometria della sezione: un'analisi sperimentale e numerica* - Master Thesis, Università degli studi di Bologna, 2024.

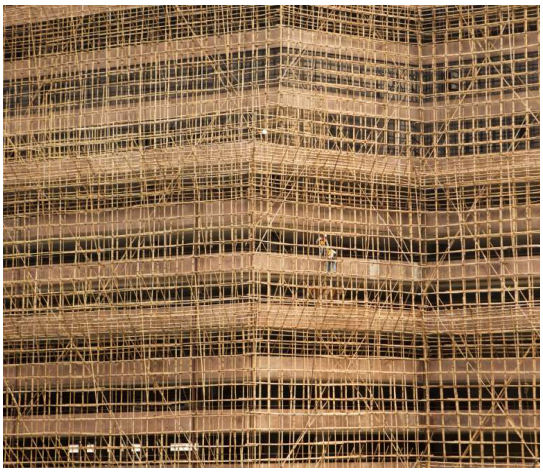

Figure 78
Tying with ropes is the largest used type of connection in bamboo scaffolding in Hong Kong.
Ph. Matt Ragen [144]

Figure 79
Bolted bamboo connections
Bamboo Shelter at Galapagos, Scarcity and Creativity Studio [145]

Figure 80
High tech connection between culms
Energy Efficient Bamboo House – Studio Cardenas Conscious Design. Ph. Copyright Longquan International Bamboo Commune [146]

Figure 81
Multi-culm bamboo structure - Vo Trong Nghia Architect, Naman Retreat Conference Hall, Ngu Hanh Son District, Danang, Vietnam – Ph. Hiroyuki Oki [147]

Multi-culm bundle structure: the examples of CanyaViva

In order to study the feasibility of a multi-culm bundle structure, an existing method has been analysed. CanyaViva is an architectural technique developed by the architect Jonathan Cory-Wright in 2006, based on the use of Arundo donax as the main construction material. The structure consists of multiple arches, each formed by joining two multi-culm columns. This construction technique is of particular interest as it satisfies several critical criteria identified by the author for the efficient use of bamboo and Arundo donax. Firstly, it responds to structural requirements by exploiting the longitudinal tensile strength of the culms, making it possible to utilize a broad range of diameters, including the small dimensions typical of Arundo donax. Secondly, the method is both highly sustainable and low-tech, relying exclusively on natural materials and manual assembly processes. It requires minimal transformation of the raw material, which can be used with limited processing directly after harvesting. Furthermore, the construction timeline is notably short, with the entire process —from material collection to the completion of the structure— achievable within a few months. Finally, the technique yields architecturally expressive forms characterized by organic geometries and fluid spatial configurations, which establish a coherent relationship with both human sensory perception and the surrounding natural context. As stated on CanyaViva website "*Our work philosophy is inspired by a sustainable lifestyle. To do this, we build spaces of high aesthetic value with natural, local, and abundant materials. Working hand in hand with the beauty of natural materials we give value back to where we come from and inherently give value back to ourselves*" [148].

CanyaViva builds structures both permanent, as pergolas, porches, and domes, and ephemeral as stages and shades for festivals and events, all over the world. Some examples are collected in the pictures of Figure 82. Although it was designed using Arundo donax, over the years bamboo has been integrated into the CanyaViva methods, especially thanks to the experimentations made in Italy by Margherita Bertoli (Arundo Art) and Matteo Mannini (Bamboo Lab), which used to work together in CanyaViva Italia. A collaboration with CanyaViva Italia was established and they prepared the material which has been subjected to the experimental tests of this thesis.

Casa de Layla, exterior, Malaga - 2013 [148]
Courtesy of Canyaviva

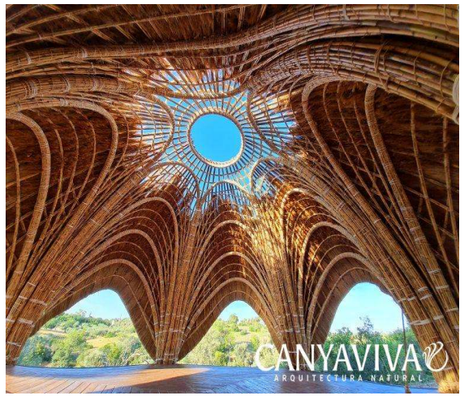

Alcantarilha - 2022 [148]
Courtesy of Canyaviva

Bosco di Rovo (PT) -2022
Courtesy of Arundo costruzioni organiche

Labirinto della Masone, Parma - 2022
Courtesy of Arundo Costruzioni Organiche

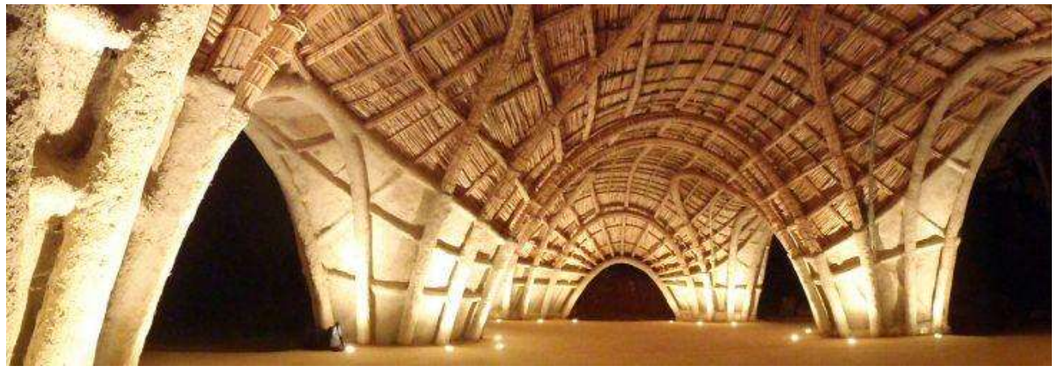

Casa de Layla, interior, Malaga - 2013 [148] – Courtesy of Canyaviva

WAO festival 2017 – Courtesy of Arundo costruzioni organiche

Tavira 2019 [148]
Courtesy of Canyaviva

Expo Saragoza - 2008 [148]
Courtesy of Canyaviva

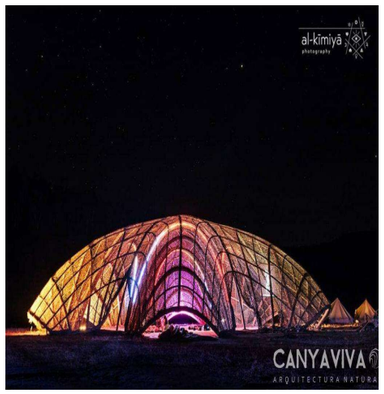

Lost Theory, Las Hurdes & Sierra De Francia - 2018 [148] – Courtesy of Canyaviva

Primavera Sound, Barcelona [148]
Courtesy of Canyaviva

Figure 82 Examples of structure made by CanyaViva in Arundo Donax and bamboo, both permanent and ephimeral

Structures in bamboo require a few differences from the original technique, but generally, both materials can be widely adopted. In this work, a bamboo structure will be analysed, and consequently, specifics of the technique needed to make this structure will be discussed below. The entire process starts with the harvesting of the cane and finishes with the completion of the structure, mainly articulated in 5 steps. A brief summary is here reported in order to lead to a better understanding of the following analysis, but the methodology is highly more complex and specifications can be found in the manuals which deeply explain the technique (see [149] and [150]).

Canes aged between one and two years are harvested between January and February, ideally during the waning moon phase, in order to minimize the sugar and sap content within the culms. Harvesting is typically conducted in pairs, as illustrated in Figure 83.

Figure 83 Harvesting of the canes and creation of the modulus. Images courtesy of Arundo Costruzioni Organiche

A variety of diameters are selected to allow for the formation of arches of different dimensions, which will later be combined in the structural composition. Once collected, the canes are bundled and transported to a storage area that must be shaded, well-ventilated, and dry. Bundles are stored vertically to facilitate the release of moisture.
Each culm is then thoroughly cleaned along its entire surface, removing leaves, node outgrowths, and branches to ensure straightness and maximize the contact surface within the bundle. After cleaning, the canes are sorted according to their physical characteristics —diameter at specific lengths, total length, and natural bending direction (clockwise or counter-clockwise, see Figure 84 a). Several categories are created through this selection process. This step is essential to the final outcome of the structure and requires meticulous execution.

The base of each arch consists of a multi-culm bundle, or “column,” typically constructed from a basic module of seven canes. The module is assembled by placing the straightest cane in the centre, flanked on the lower side by canes of larger diameter to form a cradle, and completed on the upper side by smaller-diameter canes, which will form the intrados of the arch (as in Figure 84 b and c).
The original technique using Arundo donax considers the natural tapering of the canes, which is corrected by adding new culms along the length, starting from 1 meter above the base and then every 50 cm in the case of Arundo donax, or every 1 meter for bamboo. The connection of the culms within the bundle is achieved in two main phases. First, a clove hitch is tied 10 cm above the base and repeated every 50 cm as additional culms are added along the bundle. Second, a thinner rope is spiraled around the bundle to compress it and stabilize it (Figure 85).
In CanyaViva Italia’s adaptation, a 4 mm polyester nautical rope is used for both operations. Unlike the original method, CanyaViva Italia does not add culms along the length of the column, having observed that this modification increases preparation time and it does not significantly affect the performance of the final structure.
Specifications regarding the typology of columns mainly used in bamboo construction by CanyaViva Italia, and which are object of the study in this thesis, are reported in Figure 86.

The next step is the making of the arches. They are formed by pairing a clockwise-curved bundle with a counter-clockwise one. Special attention is given to the “V point,” where all the canes have a diameter of approximately 18 mm.

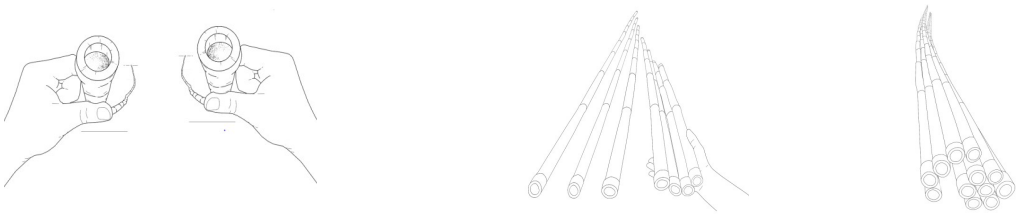

(a) (b) (c)

Figure 84 Assembly of the multi-culm beam. Evaluations of the twisting (a), positioning of the culms into the end (a) to make the whole modulus (b), at which more canes can be added (c)

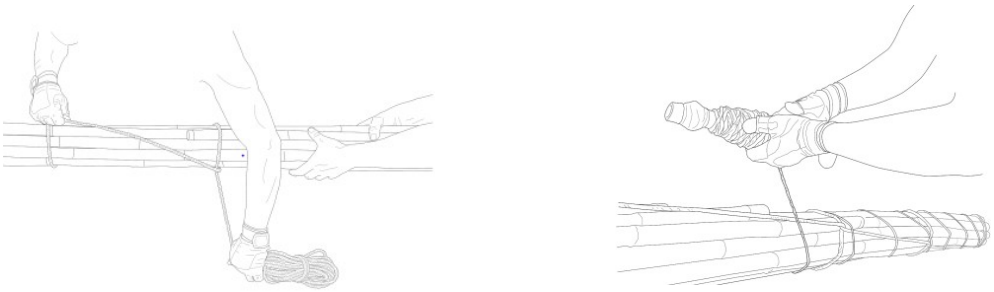

(a) (b)

Figure 85 Tying of the beam: the first phase, with the thicker rope, which block the canes (a) and the second one with the thinner rope, to compact the bundle (b). Images from [149]

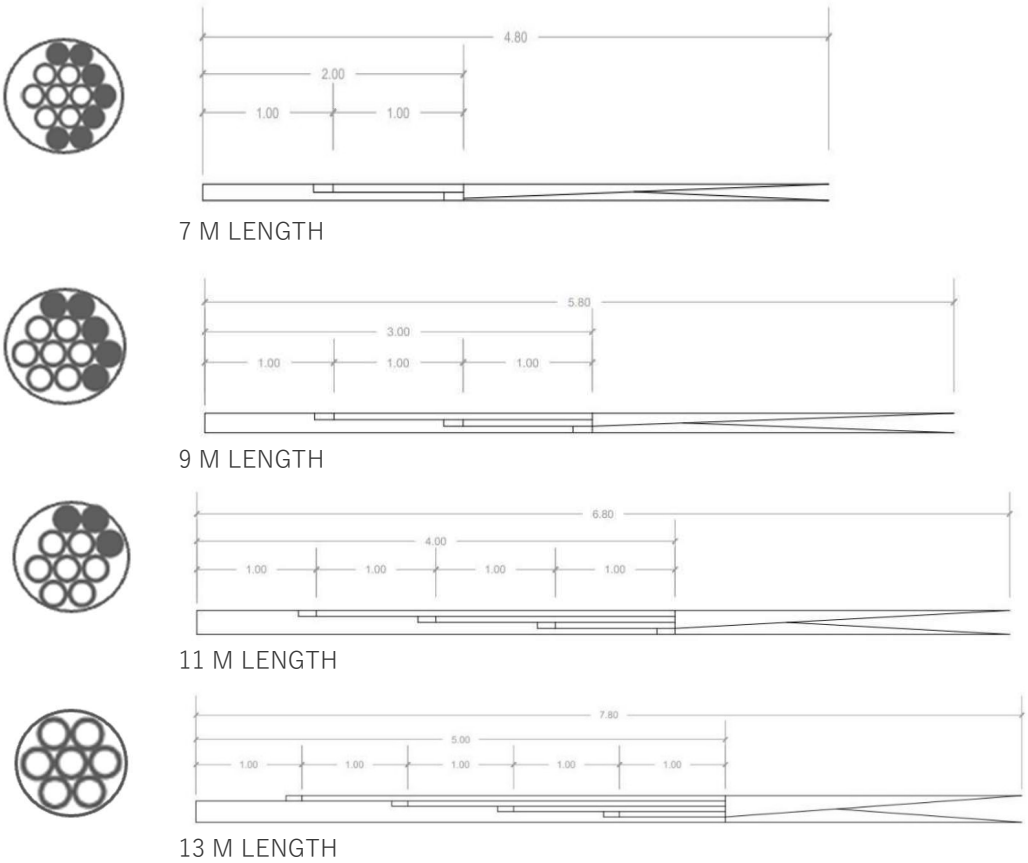

Figure 86 Typology of columns used in bamboo construction by CanyaViva Italia, used in this thesis to study the beams. Images from [150]

At this point, the column is divided into two fingers of equal size: one horizontal for the clockwise bundle and one vertical for the counter-clockwise. This is where the columns are connected, by interlocking the fingers. The connection, spanning 3 meters, is secured in both directions with a spiral of rope fastened using a clove hitch. The arches are formed by applying force to the bundle on the ground until the desired curvature is obtained, then held in place using tensioned ropes (Figure 88).

The arches are then raised and positioned (Figure 89), a process that requires at least three people due to the significant size and weight of the elements. Once the arch is lifted, its final shape is defined through the application of tension forces, transmitted via ropes anchored to the ground. Arches of different dimensions are assembled together to create the structural framework, onto which transverse ribs are installed to ensure the monolithic behaviour of the entire system (Figure 90).

The foundation is usually composed of successive layers of stones of varying sizes, sometimes completed with a concrete wall if required by the structure. The final step involves finishing the building to make it usable. The covering can vary according to the specific project and may include other canes, either sewn or braided, or alternative materials such as gypsum, flexible paints, or clay. Additionally, decorative elements can be created using split bamboo, tied into small and highly flexible beams, allowing for the design of visually refined and expressive structures.

A campaign conducted on several CanyaViva beams and arches made with Arundo donax by Andùjar et al. [151] reports a stiffness value (EJ) between 0.99 and 1.20 $\times$ 10^{10} N·mm^2 for the analysed arch. Variations along the arch were also investigated: a stiffness (EJ) ranging from 8.93 to 13.79 $\times$ 10^8 N·mm^2 was recorded at the bases, while values between 4.32 and 5.85 $\times$ 10^8 N·mm^2 were observed at the centre of the arch.

Since the investigation was originally based on the use of Arundo donax, no data are currently available for the version employing bamboo. In light of the technical modifications introduced to accommodate bamboo, and considering the differences in the mechanical behaviour of the two materials—as discussed in the previous chapters—such knowledge appears to be essential for a comprehensive understanding of the system

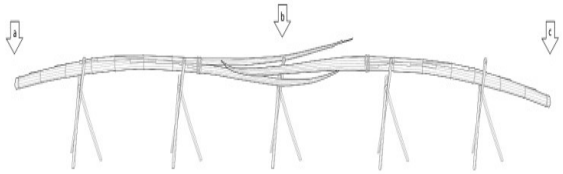

Figure 87 Union of a clockwise bundle with an anticlockwise bundle to form the arch. Image from [149]

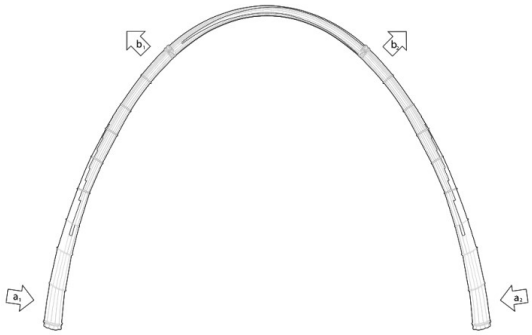

Figure 88 Forces applied to the bundle to obtain the arch. Image from [149]

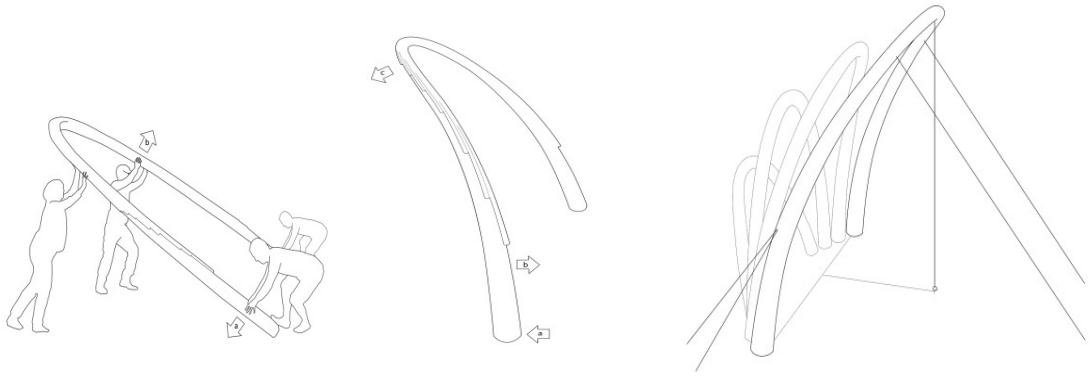

(a) (b) (c)

Figure 89 Placement of the arch. Once its shape has defined, it needs to be raised by three or more people (a). Once it is raised, directions of tensions are individuated (b) and tensors are applied (c). Images from [149]

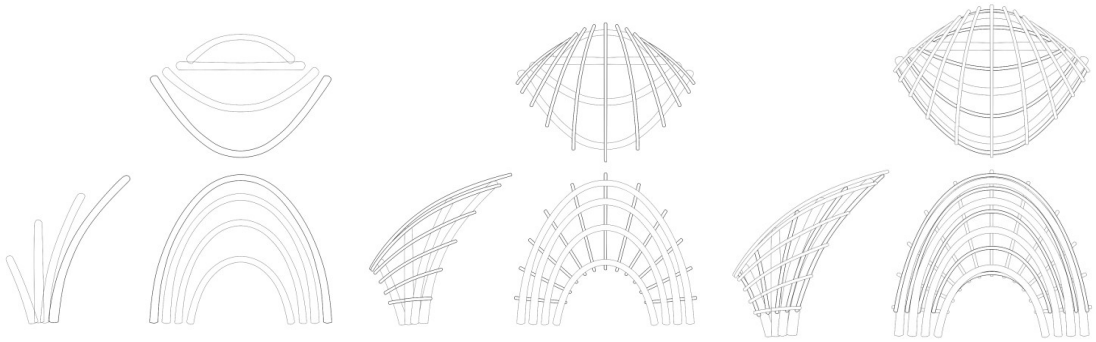

(a) (b) (c)

Figure 90 Composition of the structure: multiple arches (a), unified by linear beams(b)in two directions (c). Images from [149]

The beam

The objective of this chapter is to analyse the mechanical performance of the multi-culm beam, specifically in terms of strength and stiffness—parameters that are central to the discourse on structural applications of bamboo.

The stiffness of a multi-culm beam is not easy to calculate as the beam works as a whole very difficultly. For this reason, ISO 22156 suggests considering the sum of the stiffnesses of the individual culms [152]. García et al. [153] studied the stiffness of a two-culm bamboo beam, and found that the moment of inertia is the sum of the inertia of the two culms even in presence of connectors. Some attempts have been made to find effective connectors. As an example, Zhou et al. [154] studied the effect of nailing in connecting different culms of a beam through its flexural properties and found that the bending capacity of the two-culm beams increased more significantly than the single one when it is nailed. Generally, dowel connections with steel bolts are used to join multiple-culm beams. However, due to the orthotropic nature of bamboo, there is the risk of cracks forming near the holes, which can lead to a reduction in the beam's performance [153] [155]. The Colombian code [156] prescribes the minimum number and type of connectors that should be used to consider the beam as a built-up section. However, it remains the engineer's responsibility to demonstrate that the beam performs as a unified structural element.

The behaviour of this type of beams requires a very deep level of knowledge. For instance, the impact of the number and dimension of culms within the bundle on its mechanical properties can significantly change the design and has not been explored yet. In this chapter, the behaviour of various bamboo culm bundles with around the same diameter but different composition will be studied through an experimental bending test and a numerical analysis.

Experimental tests on various typologies of beam

Material

The tested beams have been prepared by CanyaViva Italia in the winter of 2023, according to their procedures, which are described in the previous chapter. The culms were not subjected to any treatment after harvesting and were stored in a dry place for 6 months. Culms of Phyllostachys edulis bamboo species, grown in the province

of Lucca, have been used for the preparation of the beams. The part between 1 to 8 meters from the ground has been used, since they select the culm according to the diameter more than the height from ground. The rope used to tie the culms is a 4 mm diameter polyester nautical rope.

Four typologies of bundles have been tested, as the different types used by the CanyaViva Italia, and are reported as A, B, C and D in Table 23. Three samples for each typology of the beam have been tested, referred to as 1,2,3.
Each typology refers to a different arch, which have a span of 13 m, 11 m, 9 m, and 7 m of span respectively for the beam A, B, C and D. The idea is to have similar overall diameters at the extremities, but a different number of culms. Type A is characterized by the base core of 7 culms. In all the other types, the base core is supplemented with additional culms. Specifically, type B consists of the base core enhanced with 3 additional culms. Type C consists of the base core plus 5 additional culms, while the final type, D, is made up of the base core plus 7 additional culms. A marked difference between the schematic beam and the real one is evidenced in Table 23.

Methods

A geometrical characterization of each beam has been performed. Measures have been done at both extremities of each bundle. Firstly, the external diameters of the bundle, indicated as $D_{ext,avg}$ have been measured at 10 cm from both extremities of the beam, considering the average of the two equivalent diameters calculated as circumference length, that is from the length of a rope encircling the bundle. Moreover, the inner and external diameters of the individual culms at both ends of the bundle, indicated as $d_{ext,avg}$ and $d_{int,avg}$ have been measured. The presented values are considered as the average between three measures for each culm, which has been approximated as a circular ring. The values of the thickness t_{avg} is also calculated as the difference between $d_{ext,avg}$ and $d_{int,avg}$.
The area of the section has been considered as the sum of the areas of the section of each culm i of the total number of culms n, according to the formula:

$$A = \sum_{i=1}^{n} \frac{\pi}{4} \left(d_{ext}^2 - d_{int}^2\right) \tag{28}$$

In order to estimate the amount of area in relation to the change in number of culms, the percentage of solid material has been calculated as the differences from the equivalent area considering a full section of diameter as the external one $D_{ext,avg}$, less the area A obtained by the eq. (28).

Table 23 Description of the four typologies of beam analysed in this study. The composition of the section is illustrated as the schematic and the real ones. In the former, additions that modify the base modulus in the typologies B, C and D are evidenced in black. Images are not in scale. Each one of the extremities, named as L (left) and R (right) are presented. Characteristics of the arches for which each beam is used are also illustrated.

Typology	n_{culm}	Schematic section	Number of the sample						Corresponding Arch			
			1		2		3		Distance from the bases [m]	Total Length [m]	Height of the arch [m]	Height of the column [m]
			Extremity L	Extremity R	Extremity L	Extremity R	Extremity L	Extremity R				
A	7		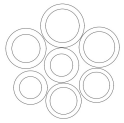		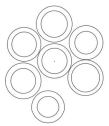			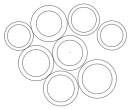	5.2	13	5.6	7.8
B	7+3								4.8	11	4.6	6.8
C	7+5		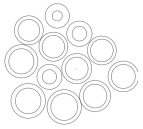						4	9	3.7	5.8
D	7+7								3.4	7	2.8	4.8

Each beam has been subjected to a three-point bending test in order to study its mechanical behaviour. The set-up of the test is shown in Figure 91 and Figure 92. The span of the beam between the supports has been fixed at 1 meter, compatibly with the length of the beam. Cylindrical saddle supports with circular cross-section with a diameter of 140 mm and 40 mm wide, have been used both for the supports and under the load application to distribute the load as much as possible to the surface of the beam (Figure 92a). The deflection in the middle point has been measured with a displacement transducer attached with a strap to the underside of the beam. For the tests on samples of types A and B, a second displacement transducer system was also used to measure the displacement at the highest point of the section to be able to verify the crushing (Figure 92b).

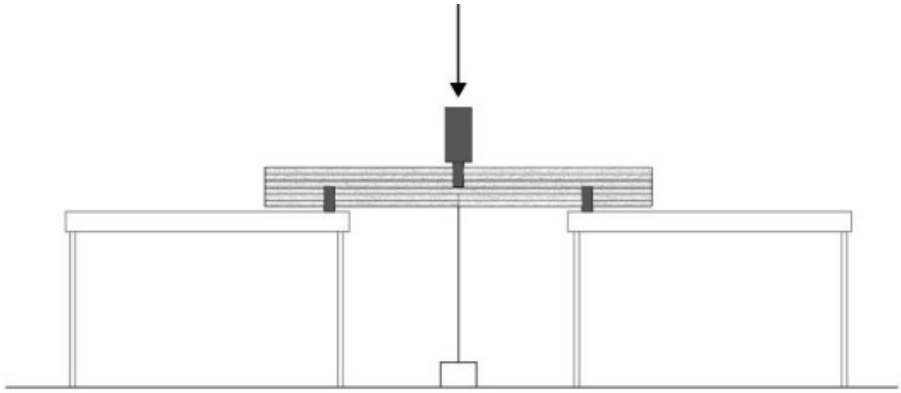

Figure 91 Schematic of the experimental set-up for bending test of the beam [157]

Figure 92 Details of the set-up and the beam during the execution of the test. On the left, the instrumentation to measure the displacement and the transmission of the load is shown. On the right, detail of the support of the beam,

In order to compare the results with those of a previous study on CanyaViva beams made with Arundo donax [151], a load has been applied in 5 cycles with an increment of 200 N:

- from 0 to 200 N, then unloading
- from 0 to 400 N, then unloading
- from 0 to 600 N, then unloading
- from 0 to 800 N, then unloading
- from 0 to failure

The test was conducted with displacement control at a speed of 1 mm/s.

After the test, results are processed as following. The stiffness EJ of the beams can be determined as:

$$\mathrm{EJ} = \frac{\frac{P\,L^3}{48\,\delta}}{1 - (\frac{\Omega PL}{4AG\delta})} \tag{29}$$

where P is the concentrated load applied at midspan, L is the span, δ is the deflection experimentally determined from the tests, Ω is a parameter which considers the non-uniform distribution of shear stress across the section, A is the area of the cross section and G is the circumferential–longitudinal shear modulus. This formula considers also the effects of shear deformations, as reported by García-Aladín et al. [153]. The values of Ω and G have been chosen from literature, and are respectively 2 [153]. and 143 [158] MPa.
The stiffness is calculated between the 20 and the 40% of the maximum load, based on the observation of the results ensuring that calculation remains into the elastic range.

Particular attention has been paid to the moments of inertia of the section and a comparison between different moments of inertia has been done. In the first case, culms are considered as not cooperating. In particular J_1 has been calculated as sum of all the moments of inertia at the ends of the section of all the individual culms i approximated as circular rings, that is:

$$J_1 = \sum_i \frac{\pi}{64}(d_{ext}^4 - d_{int}^4) \tag{30}$$

In the second case, J_2 is calculated as the average of the moments of inertia at the ends of the section, considering all the cooperating culms, through the formula:

$$J_2 = \sum_i \frac{\pi}{64}\left(d_{ext,i}^4 - d_{int,i}^4\right) + A_i\, l_i^2 \tag{31}$$

where A_i is the area of the section of the i culm and l_i is the distance from the barycentre of the culm to that one of the bundle.

In order to compare the analytical solution with an experimental one, a J_3 was back-calculated from experimental results, employing the stiffness obtained by the application of the eq. (29), at the 40% of the maximum load. The modulus of elasticity of the material has been chosen from previous studies, as 14,5 GPa [159]. A correction has applied according to [160] consider possible variations due to different grades of humidity. A possible range between E_{min}=11,30 GPa and E_{max}= 17,90 GPa has been identified.

Results

The results of the geometrical characterization are reported in Table 24. The external diameter $D_{ext,av}$ is similar for the beams of the typologies A, B and C, while the beams of the typology D result significantly smaller. Values of $d_{ext,avg}$, $d_{int,avg}$ and t_{avg} decrease progressively from the typology A to the D one. It can generally be observed that as the number of culms increases, smaller dimensions are adopted. However, the culms in the beams of Type D appear to be more widely spaced compared to the others.

Values of the area A are similar for the cases of the typologies A, B and C, while the difference is higher in the case of the typology D. However, the latter has a higher percentage of solid area, that is around 40% respect to the around 35% in the others case. It looks that building a beam with smaller culms allows a better filling of the area and reduce the waste generate by voids between culm, despite the smaller dimension of the thickness.

Table 24 Geometrical characterization of the average beam tested in this study. The average values and relatively standard deviation in brackets are presented for the external diameter of the beam $D_{ext,av}$, the inner and outer diameter and the thickness of the average culm, named as $d_{int,av}$, $d_{ext,av}$, and t_{av} respectively, the area of the entire beam and its percentage of solid

Name	n_{culm}	Schematic section	$D_{ext,av}$ [mm]	$d_{ext,avg}$ [mm]	$d_{int,avg}$ [mm]	t_{avg} [mm]	A [mm^2]	Solid %
A	7		123.72	39.41	29.23	5.13	4186.3	34.78
			(1.93)	(0.65)	(0.97)	(0.51)	(200.2)	(1.05)
B	7+3		124.31	33.02	23.62	4.70	4251.7	35.01
			(2.36)	(0.75)	(0.04)	(0.60)	(405.4)	(2.35)
C	7+5		121.42	30.47	22.71	3.90	4283.7	36.76
			(4.74)	(1.30)	(1.39)	(0.30)	(651.4)	(3.49)
D	7+7		94.01	21.03	13.52	3.77	2963.0	42.15
			(4.42)	(0.21)	(0.75)	(0.40)	(331.3)	(3.43)

Values resulting from the test for the maximum load P_{max} and displacement δ_{max}, and the stiffness EJ are reported in Table 25 for all the typologies. Beam A and Beam B behave very similarly in term of maximum load, stiffness and displacements. Beam C shows slightly lower load, higher stiffness but with greater variability. Beam D underperforms in both load capacity and stiffness.

The behaviour of the beams performed during the test is clearly reflected in the graphs shown in Figure 93 and Figure 94, where sudden drops in the load correspond to the crushing of the culms that were sustaining the load and consequential readjustments. It can generally be observed that the beams exhibit a "sequential load-bearing" behaviour, where individual culms act independently in resisting the applied load. When the load is applied, the culm directly in contact with the press initially absorbs the stress. Once it fails or it is crushed, the load is then transferred to the underlying culms. This sequential failure mechanism is more evident in configurations with fewer, larger culms, as the case reported in the load-displacement graph of the beam A in Figure 93. In this case, a strong difference in stiffness shown in the curve is present. This is due to the fact that in the first part of the test, the response of the beam was mainly performed by the first culm, and only after the readjustment around 300 and 400 N of the load, more culms start collaborating and stiffness grows.

Table 25 Values resulting from bending test for all the four typologies considered in this study. The values reported are obtained as the average between the results of the tests of each beam, and the standard deviation is reported in brackets.

Typology	P_{max} [N]	δ_{max} [mm]		EJ [10^8 Nmm^2]		
		lower	upper	P_{20}	P_{40}	P_{60}
A	8469	62	79	48.08	54.46	56.26
	(214)	(3)	(13)	(5.29)	(11.6)	(10.22)
B	8686	63	79	41.89	41.26	39.09
	(1028)	(8)	(1)	(12.34)	(2.36)	(4.34)
C	7683	47	-	34.88	38.04	43.48
	(1259)	(4)	-	-	-	-
D	3971	77	-	17.45	21.39	22.22
	(441)	(11)	-	(6.97)	(3.25)	(1.97)

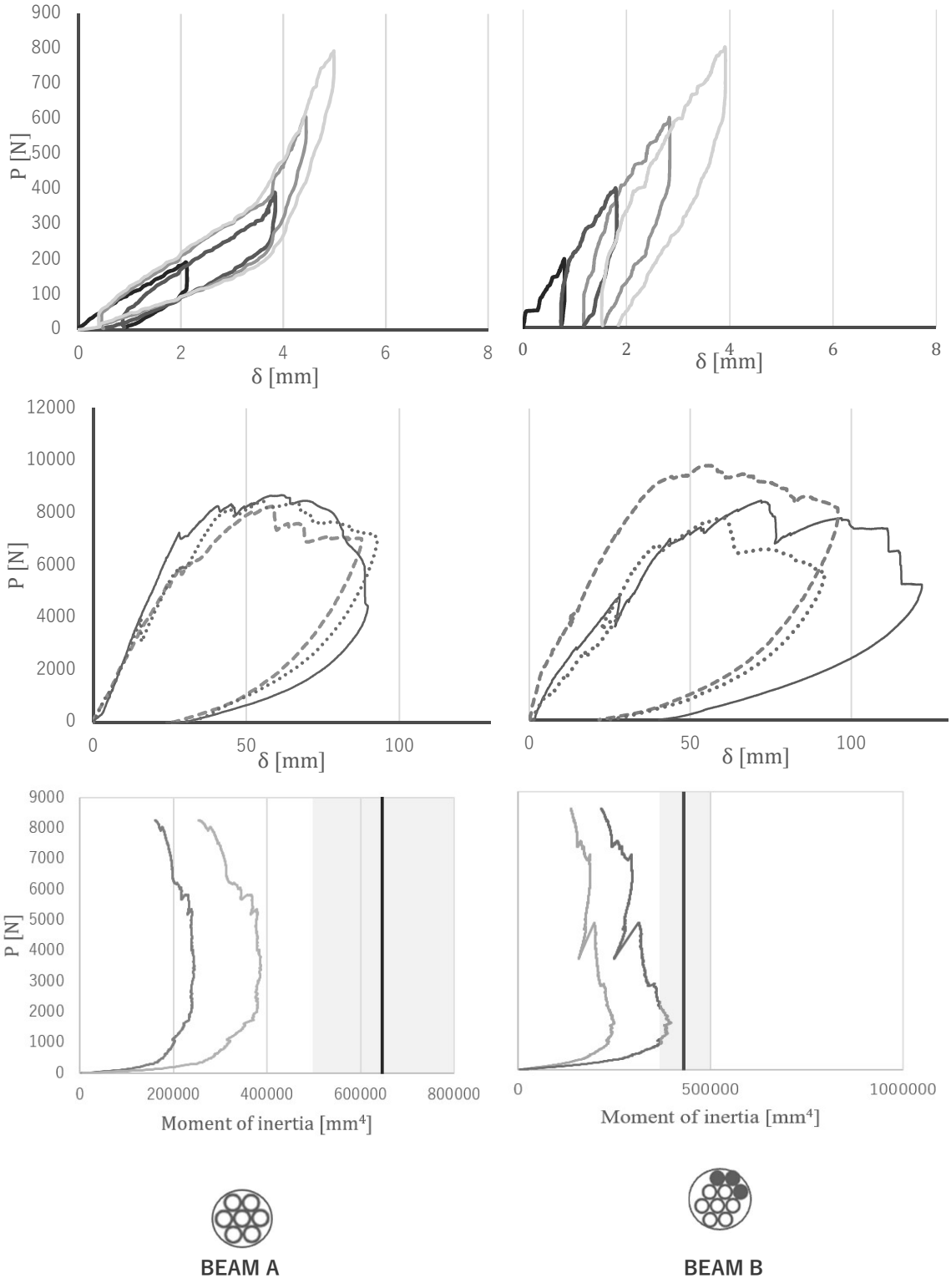

Figure 93 The first graph shows the load-displacement relation during the four cycle from 0 to 800 N (in the elastic field) for the beam A2 and B2 respectively. The second one represents the final cycle to rupture for all the beams of each typology. The bottom graph shows a comparison between the minimum and maximum values of J3 (represented by curves) and J1, which is illustrated as a grey band. This band spans the range of J1 values calculated at the two ends of the beam, with the central dark vertical line indicating the average value.

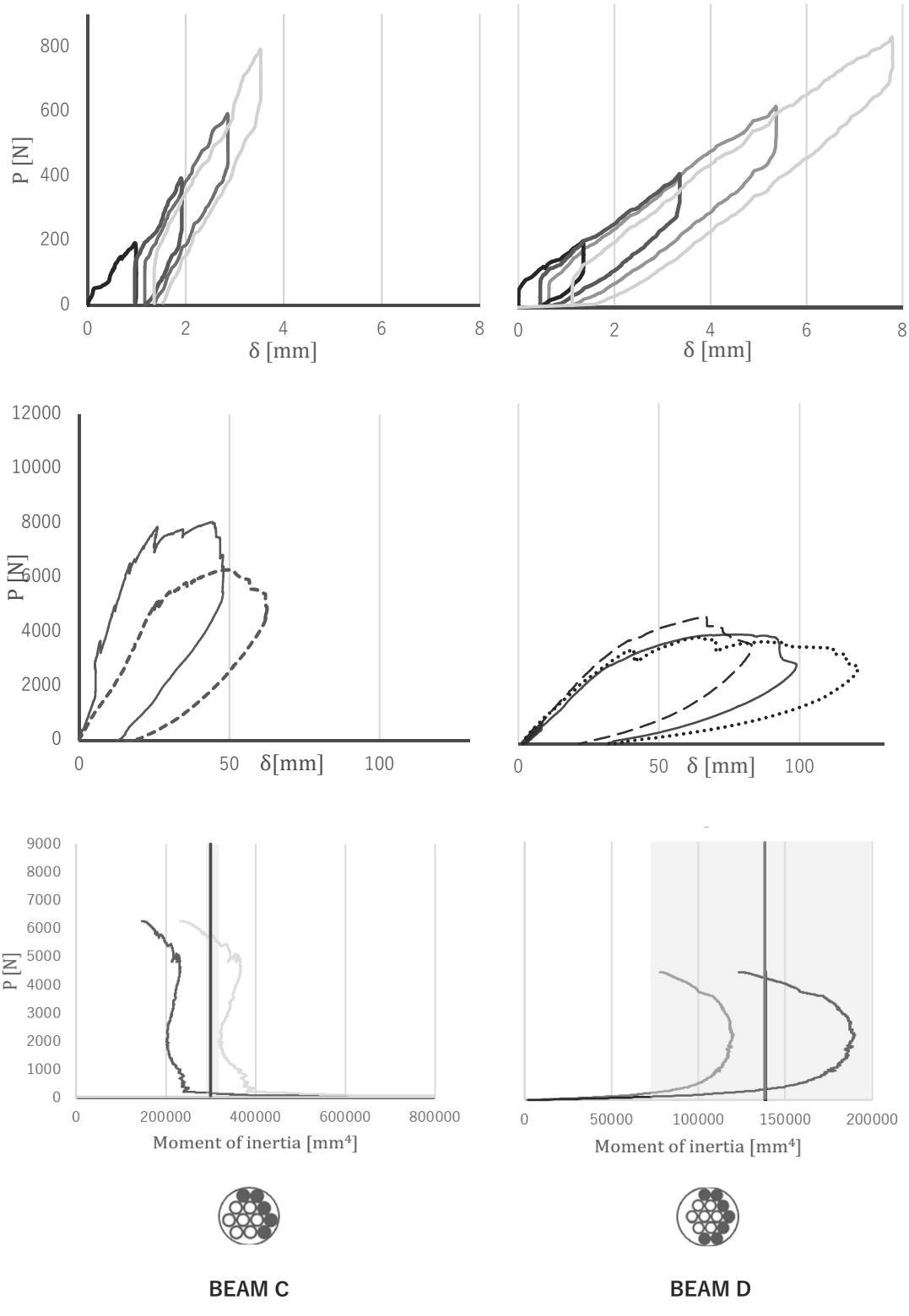

Figure 94 The first graph shows the load-displacement relation during the four cycle from 0 to 800 N (in the elastic field) for the beam C2 and D2 respectively. The second one represents the final cycle to rupture for all the beams of each typology. The bottom graph shows a comparison between the minimum and maximum values of J3 (represented by curves) and J1, which is illustrated as a grey band. This band spans the range of J1 values calculated at the two ends of the beam, with the central dark vertical line indicating the average value.

Calculation of the moment of inertia are reported in Table 26. As expected, the second moment of inertia J_2 is an order of magnitude higher than the sum of the individual moments of inertia J_1. Furthermore, in the case of J_2 all the moments of inertia are fairly similar, with little variation even between beams with very different average areas and diameters. In contrast, for J_1, these differences are more pronounced, as the reduction in diameter can no longer be compensated by the distance from the central axis of inertia. Moreover, values of J_1 are little higher than those indicated in the range of the values of J_3, while the values of J_2 are very fare from the experimental ones. In the case of the beams of the typologies A, B and C, J_1 is similar to the highest value of J_3, but still outside of that range, while in the beams of the typologies D, J_1 lies perfectly in the range between the two values of J_3. This is even more evident by the observation of the last graph in the Figure 93 and Figure 94. This implies that the more the beam is composed of a greater number of smaller culms, the more accurately its overall moment of inertia can be approximated by the sum of the individual moments of inertia of the culms.

The comparison between the three methods for calculating the moment of inertia shows that the experimental value is close to the simple sum of the individual culms' moments of inertia. This indicates that the beam does not behave as a cohesive element: the culms do not contribute collectively to the global stiffness of the section. Therefore, the interaction between the culms appears to be negligible, and the beam can be modelled as a set of independent elements.

Table 26 Comparison between three different calculation of the moment of inertia. The values reported are obtained as the average between the three samples of each typology. Standard deviation is reported in brackets. The moment of inertia J_1 and J_2 are calculated according to eq. (30) and eq.(31) respectively, while J_3 has been obtained by the eq. (29) and the use of two values of the modulus of elasticity.

Typology	J_1 [10^4mm^4]	J_2 [10^4 mm^4]	J_3 [10^4 mm^4]	
			E_{min}	E_{max}
A	64.92	128.10	48.19	30.42
	(3.83)	(4.84)	(10.26)	(6.48)
B	44.32	158.20	36.52	23.05
	(3.94)	(10.65)	(2.09)	(1.32)
C	39.14	138.82	33.66	21.25
	(7.90)	(21.18)	-	-
D	14.15	114.55	18.93	11.95
	(1.51)	(28.91)	(2.87)	(1.81)

Methods

The experimental bending test has been reproduced in a finite element numerical simulation to gain a better understanding of the factors that most affect the behaviour of the moment of inertia during load application. The Abaqus software has been used and a beam of the typology A has been chosen, as it is the basic modulus of each beam.

In the geometric model, the 7 culms have been considered as perfectly cylindrical, tangent to each other, with an overall cross-section similar to the average of the experimentally measured end sections, that is 40 mm for the external diameter and 28 mm for the internal one. Supports and the load press have been modelled as those used during the experimental tests, with the same shape and size. Taking advantage of symmetry properties, only half of the beam was represented to simplify the modelling. The geometrical model is presented in Figure 95 while the boundary conditions are illustrated in Figure 96. Symmetrical boundary conditions have been enhanced: null displacements in the direction of the bundle axis at the midpoint section, null displacement at the base of the support saddle. The culms were, in turn, constrained to the saddles using "tie" constraints: at a single point for the support and along the tangent line between the upper culm and the semi-circular section of the load application. Moreover, to simulate the action of the string, a general mechanical contact interaction has been considered between all the elements in the tangential direction (in Abaqus, "Hard" contact with a friction coefficient of 0.3).

Loading conditions have been reproduced as those used in the experimental test: a vertical load has been applied at the midspan, as described in Figure 95. The value of the load has been chosen according to the results obtained in the experimental test, at 10%, 20%, 30%, 40%, 50% and 60% of the maximum load, in order to study changes into the beam.

A quadrangular mesh of 6 mm has been defined for the culms of the beam, while a 10 mm one has been used for the saddles, and are shown in Figure 97.
The material has been considered elastic, homogeneous, and orthotropic. Its properties have been assigned based on literature data [158] and are summarized in Table 27. The simulation has been conducted in linear-elastic regime.

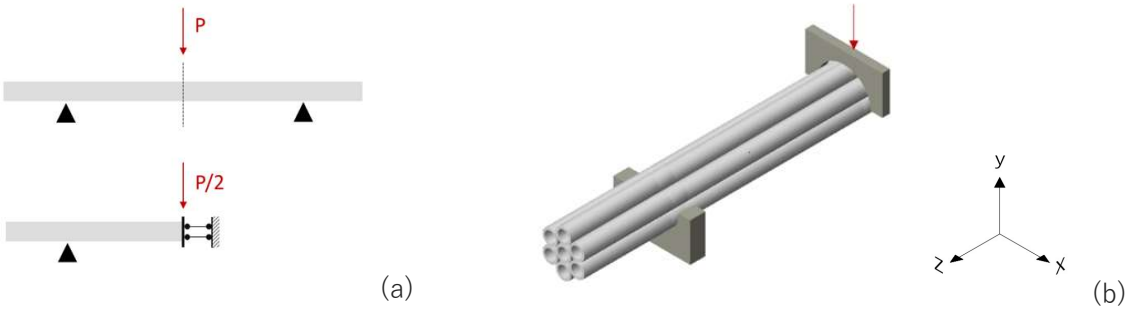

Figure 95 Loading conditions (a) and geometry of the model (b) of the beam

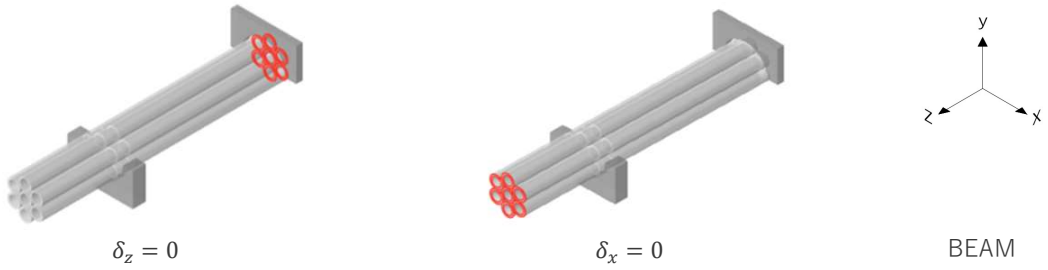

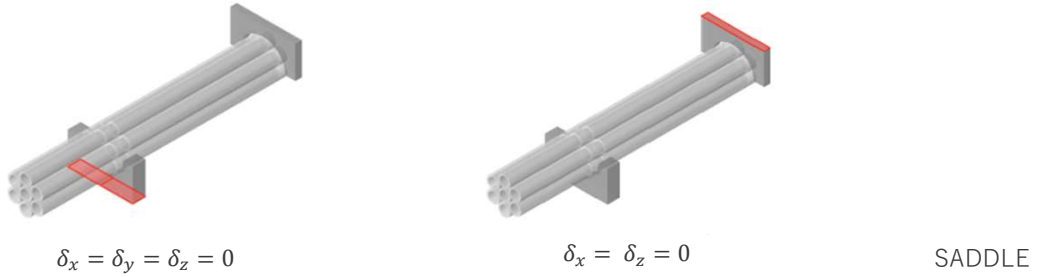

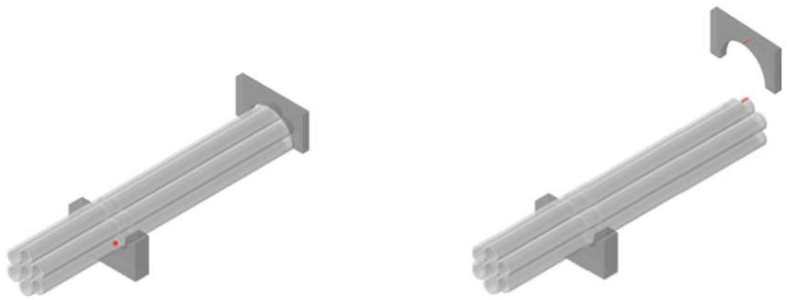

Tie constraint between the saddles and the beam

Figure 96 Boundary conditions defined for the model

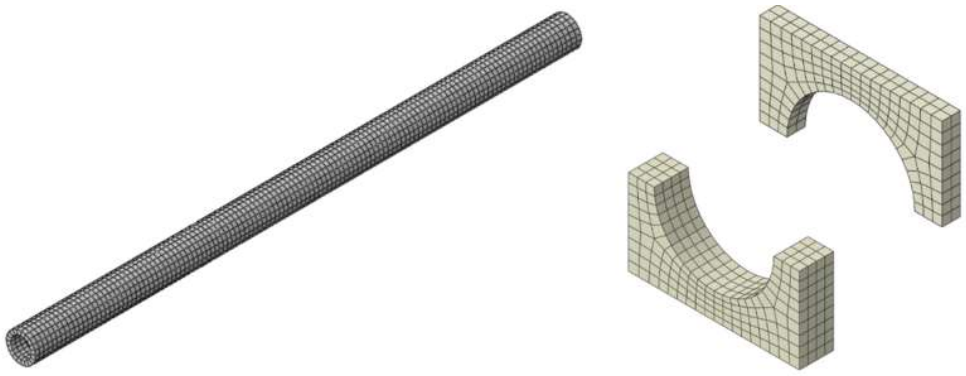

Figure 97 Mesh defined for the geometry

Table 27 Material properties assigned in the FEM model of the beam. Data from literature [158]

	E_z (GPa)	$E_x = E_y$ (GPa)	$\nu_{xy} = \nu_{yz} = \nu_{xz}$	$G_{xy} = G_{yz} = G_{xz}$ (GPa)
Beam	14.27	0.413	0.34	0.143
Saddles	210	210	0.3	-

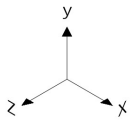

Results

Change in stress at the progressively increasing load has been studied. It can be described by Figure 98. At 10% of the maximum load, the load saddle has not touched the lateral stems yet, so the load is primarily resisted by the upper stem and, to a lesser extent, by those directly beneath it. At 20% of the load, the saddle also touches the lateral stems, which begin to react together with the underlying stems, though still much less than the central ones. At 40%, all the stems are engaged, but the upper stem still shows a higher stress, partly due to compression. From 50–60% of the load, the stems' sections begin to collaborate more equally, but by this point, the section has already undergone deformations due to the applied load.

The maximum stress under the load along the axis of the bundle is shown in Figure 99. The stress along the axis of the beam, the z-axis, is clearly higher than the others. Moreover, it can be observed that each stem is both tensioned and compressed, clearly demonstrating how each beam works separately from the others.

A comparison between the load-deflection curve obtained experimentally and numerically is presented in the graph of Figure 100. The line which describes the behaviour of the beam depict a stiffer behaviour respect to the experimental one. The two lines are similar until 800 N, and after that, the slope start changing. This is probably due to the differences between the geometrical model adopted, in which culms perfectly touch each other, and the real geometry of the beam, which considers the differences of the section along the length of the beam and the presence of nodes. Moreover, in the experimental case, during the application of the load, fissures, ruptures and movements between culm modify the geometry of the beam while the numerical model is limited by the lack of modification. However, graphs are not so distant, and the model can be considered reliable to study the behaviour of the beam.

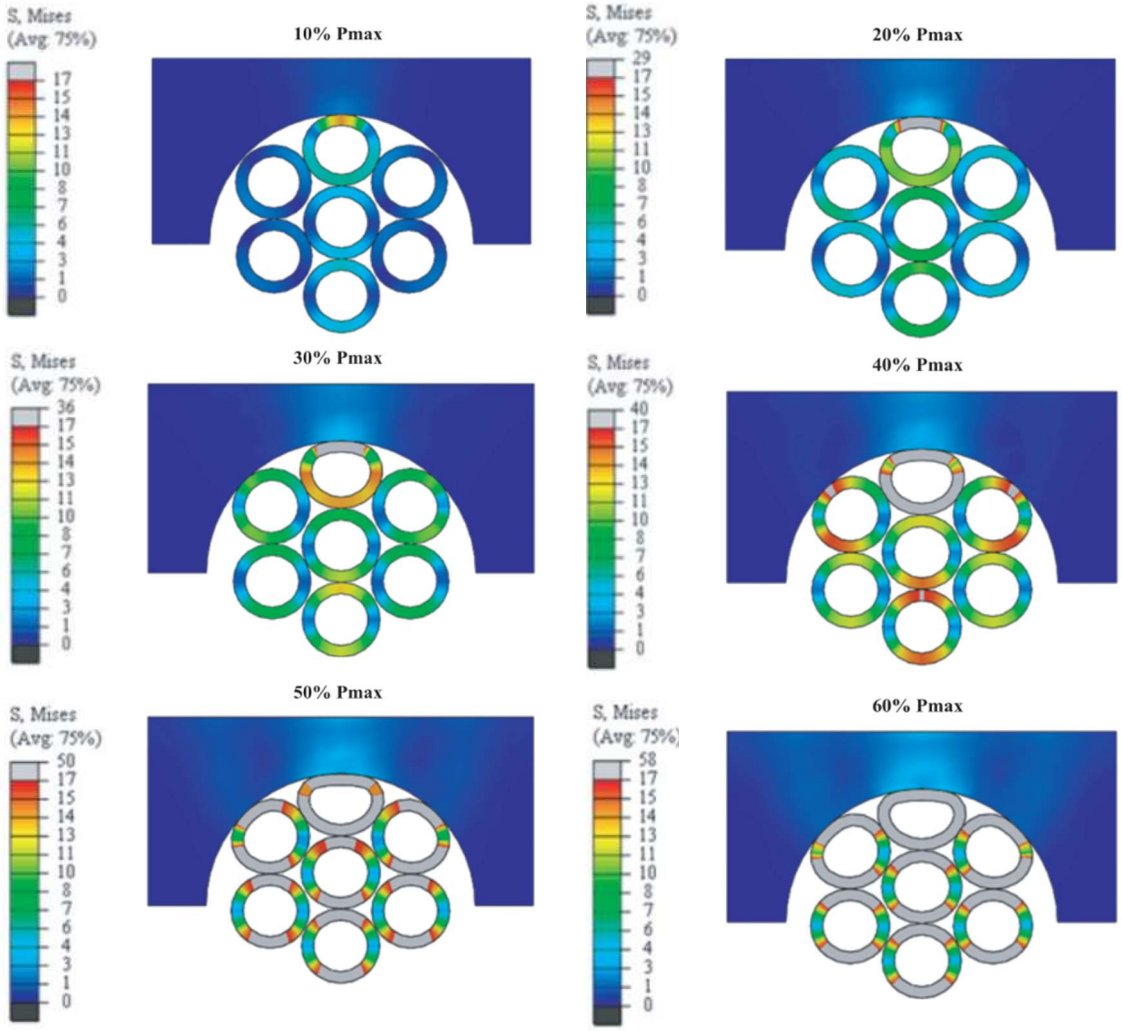

Figure 98 Von Mises at 10%, 20%, 30%, 40%, 50%, 60% the maximum load into the beam

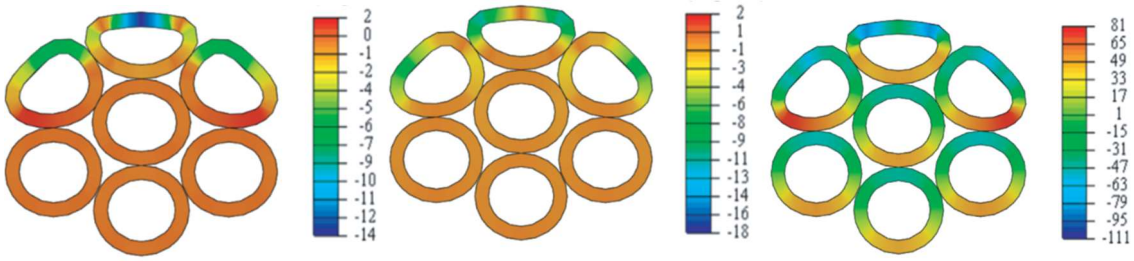

X - ax Y - ax Z - ax

Figure 99 Distribution of the maximum stress along all the axis

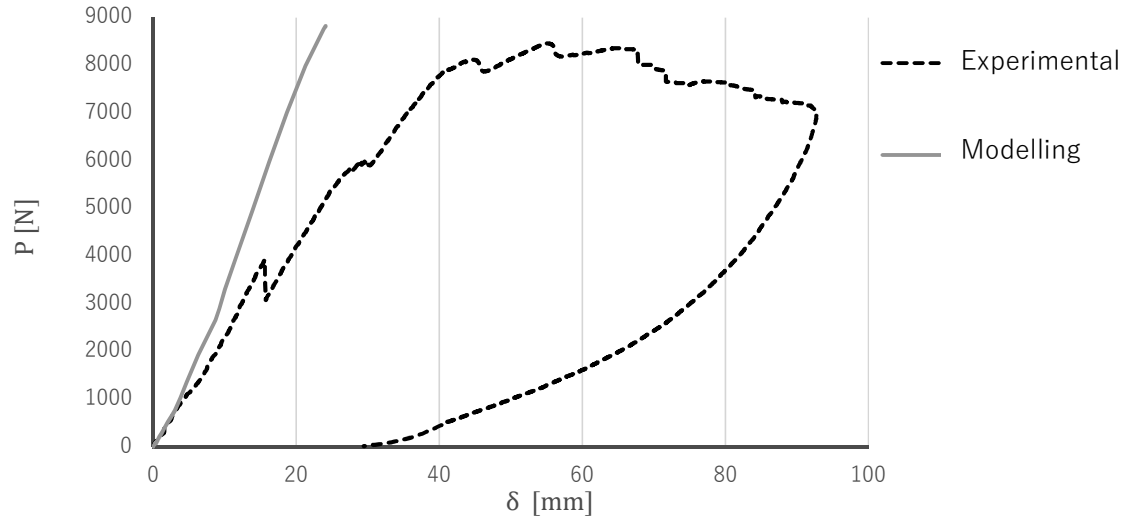

Figure 100 Comparison between the experimental graph of the load-deflection (indicated by the dotted line) and that one obtained from the modelling (indicated by the continuous line)

The moment of inertia has been studied by the comparison between the value obtained from the model as a function of the load and that one obtained from experimental data with an E value equal to that one used in the modelling, as reported in Figure 101. Moreover, in the graph are indicated through grey bends in ascending order, the moments of inertia as the sum of a different number of culms: the first lighter band corresponds to the simply moment of inertia of one culm, while the last darkest one corresponds to the moment of inertia of all the seven culms. It can be observed that in the case of this beam, the inertia falls within the range given by the sum of the inertias of 3 / 4 culms. In fact, as observed in Figure 99, in the initial phase, the stress is transmitted only to the few culms directly beneath the loading saddle. Inertia increases when the load is distributed across all the culms into the section but at that point, the culms have also changed the shape of their cross-section due to compression, which results in the inertia being lower than the sum of the inertias of the culms as they have been initially considered. Moreover, as observed by [153] differences between modelling and reality can be attributed to the capacity of the shear connectors to provide a composite action between the culms.

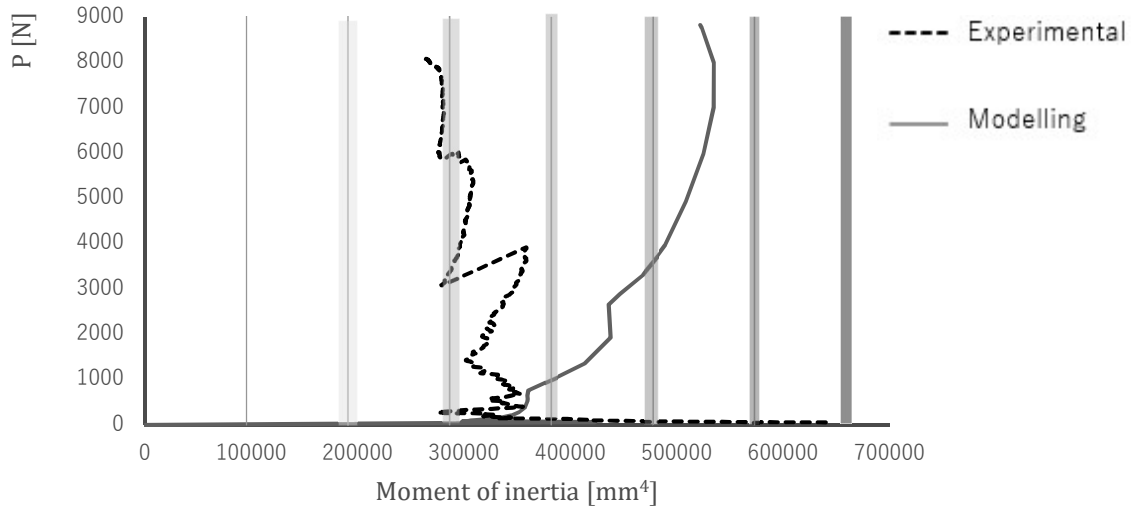

Figure 101 Comparison between the experimental moment of inertia (depicted from the dotted line) and that one obtained from the modelling (depicted from the continuous line). Each grey bend represents the moment of inertia related to a different number of culms: the first lighter one corresponds to the simply moment of inertia of one culm (100000 mm^4); while the last darkest band corresponds to the moment of inertia of all the seven culms (700000mm^4).

The arch

Experimental test on arch

This second part of the analysis of the beam focuses on its behaviour as part of the arch. Therefore, an experimental test has been conducted firstly on two whole bamboo arches made with CanyaViva technique. Secondly, a three-point bending test on the beam extracted from the arch at different length has been carried out.

Materials and methods

The arches have been prepared by CanyaViva Italia in the winter 2022, according to their procedures, which are described in the previous section of this chapter. The culms were not subjected to any treatment after harvesting and were stored in a dry place for 6 months. Culms of Phyllostachys edulis bamboo species, grown in the province of Lucca, have been used for the preparation of the beams. The part between 1 to 8 meters from the ground has been used, since they select the culm according to the diameter more than the height from ground. The rope used to tie the culms is a 4 mm

diameter polyester nautical rope.
The smallest typology of arch has been chosen for the tests, in order to allow the use of the testing machine into the laboratory. The arch has a clear span of almost 3 m and the distance from the keystone to the floor of 1,90 m. Geometrical features of the bundle which constitutes the arches are specified in Table 28. Two samples have been tested, referred to as Arch 1 and Arch 2 in the following text.

The arches have been subjected to a compression test using a Galdabini PMA10 Ultimate Testing Machine (UTM, Galdabini Cesare S.p.a., Cardano al Campo, Italy).
The set-up can be described by the scheme reported in Figure 102. The load has been applied on the keystone through a saddle applied to a rotating cell. The arch has been bounded at the two bases as detailed in Figure 103. Horizontal and vertical translations have been forbidden, while the rotation has been allowed.

Table 28 Geometrical features for the arches 1 and 2, average values and relatively standard deviation. Data are presented for the external diameter of the beam $D_{ext,avg}$, the inner and outer diameter, named as $d_{int,avg}$ and $d_{ext,avg}$, and the thickness t_{avg} of the average culm, the total area A and the percentage of solid. Image from the sections are not in scale.

Arch	Part of the arch	Section	$D_{ext,avg}$ [mm]	$d_{ext,avg}$ [mm]	$d_{int,avg}$ [mm]	t_{avg} [mm]	A [mm^2]
1	KEYSTONE		79,43	15,60	10,70	2,50	2584,00
2			84,81	13,70	9,10	2,30	2310,00
Average (St.Dev.)			82,12 (3,80)	14,65 (1,34)	9,90 (1,13)	2,40 (0,14)	2447,00 (193,75)
1	BASE		118,09	16,00	11,10	2,50	2413,00
2			106,33	18,80	13,10	2,90	3188,00
Average (St.Dev.)			112,21 (8,31)	17,40 (1,98)	12,10 (1,41)	2,70 (0,28)	2800,50 (548,01)

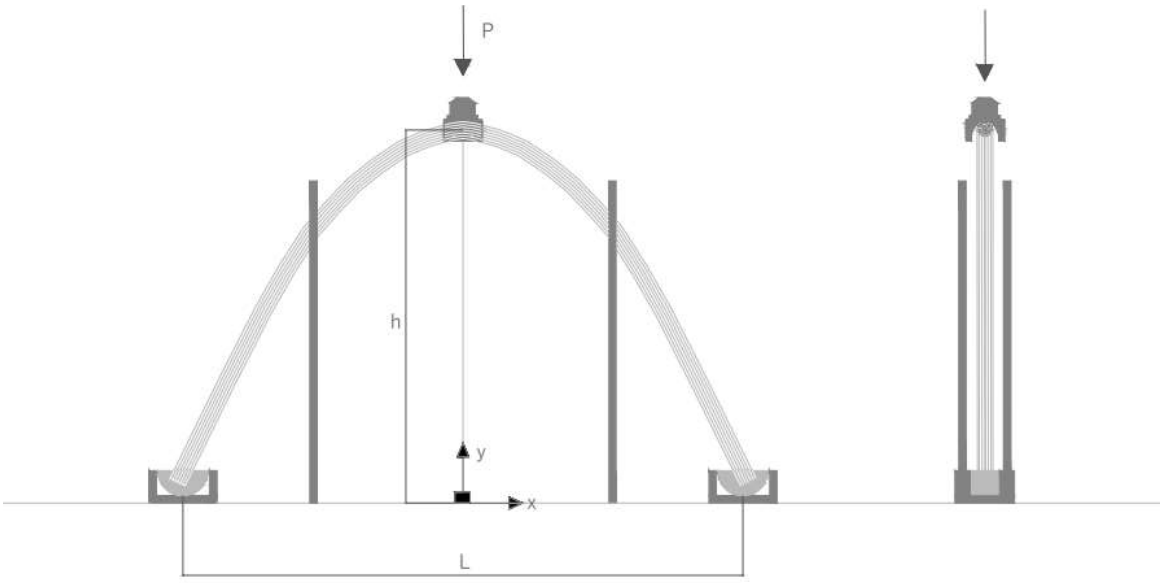

Figure 102 Set-up for the compression test executed on the arches

(a) (b) (c)

Figure 103 Ad-hoc made cradle for the supports of the arch before the filling of mortar(a), iron boxes fixed at the floor to avoid displacements of the bases (b) and verticaing support to avoid movements outside the plane of the arch (c)

(a) (b)

Figure 104 Arches under the loading machines (a) and detail during the execution of the test (b)

Results of the tests have been processed under the assumption that the arch is parabolic, and the stiffness is constant along the entire length of the arch. The stiffness of the arch has been determined as:

$$\mathrm{EJ} = \frac{83}{6144}\frac{Pl^3}{\delta} \tag{32}$$

where P is the concentrated load applied at midspan, l is the span of the arch, b is the while δ is the deflection experimentally determined from the tests. The formula has been analytically developed considering the equation of a generic parabolic arch which has the vertex in $V\,(0;h)$ and passes from the points $A\,(-l/2;0)$ and $B\,(l/2;0)$, as depicted in Figure 102, that is:

$$y = h\,(1 - \frac{4hx^2}{l^2}) \tag{33}$$

Moreover, stiffness has been calculated employing a formula which has been used by Andùjar et al. [151] in previous studies on CanyaViva Arundo donax structures, that is:

$$\mathrm{EJ} = \frac{5}{48}\frac{P\,h\,b^2}{\delta} \tag{34}$$

where P is the concentrated load applied at midspan, h the high of the arch, b is the half of the clear span, while δ is the deflection experimentally determined from the tests.

The test on the arch has been conducted avoiding any rupture of the canes. This has allowed the extraction of four beam: two samples from the bases and two samples from the keystone. Names and specifics of those samples are reported in Table 28. The bending test on those beams has been performed according to the same conditions used for the tests of the beams in the previous section dedicated to the test on beams.

Results

By the observation of data reported in Table 31, relevant differences can be highlighted, already in the geometrical characterization, considering the central part of the arch and the base one. The value of the external diameter of the beam $D_{ext.avg}$ has a

difference of around 30%, calculated on the average values, between the part of the base and that one of the keystone.
As expected, the average dimension of the diameters of the cane which form the bundle $d_{ext,avg}$, are slightly lower because of the tapering effect. Although differences in dimension of the external diameter is higher, that one of the total area of the section A is slightly lower, around 15%. Little differences have been found between the geometrical characteristics of the two arches, due to the nature of the material.

The behaviour of the arch during the test is illustrated in the graph of Figure 105. Results of the compression tests executed on the arches are reported in Table 29. The average value of the maximum load P_{max} obtained is 4805 N while that one of the maximum displacement d_{max} is 162.81 mm. The arches don't reach the breaking point, as the loading phase has been stopped because of the slipping from the press, leading to a lateral thrust of the arch. Thus, values of displacement δ are also calculated at 800, 1500 and 2000 N in order to allow comparison. The difference in deformation between arch 1 and arch 2 decreases as much the load increases.
By the observation of the graph reported in Figure 105, a change in the slope can be noticed around 3000 N. Data obtained from the analysis of the beams in the previous paragraph, suggest that very higher values can be reached.
No signs of rupture have been detected at the end of the test, as reported in Figure 106. The difference between before and after impressing the load is 2 cm, so deformation after unloading is very small.
Stiffness of the arch has an average value equal to $318.77 \cdot 10^8$ Nmm^2. The value is comparable with that one obtained employing the formula already used by Andùjar et al. [151], that has an average value of $379.93 \cdot 10^8$ Nmm^2.

Table 29 Results of the test. P_{max} stands for the maximum recorded value of the load, while δ_{max} for the deflection of the top of the arch, EJ for the stiffness calculated at the 40% of the maximum load according to eq. (32), and EJ * for the stiffness of the arch calculated according to eq. (34)

	P_{max} [N]	δ [mm]				EJ [10^8 Nmm^2]	EJ* [151] [10^8 Nmm^2]
		$P = P_{max}$	$P = 800N$	$P = 1500\ N$	$P = 2000\ N$		
Arch - 1	4329	126.02	8.16	18.73	28.34	272.94	333.23
Arch - 2	5281	199.74	4.54	12.86	22.07	364.58	426.63
Avg. (St. Dev.)	4805 (673.16)	162.81 (5.21)	6.35 (2.56)	15.80 (4.15)	25.21 (4.43)	318.77 (64.80)	379.93 (66.04)

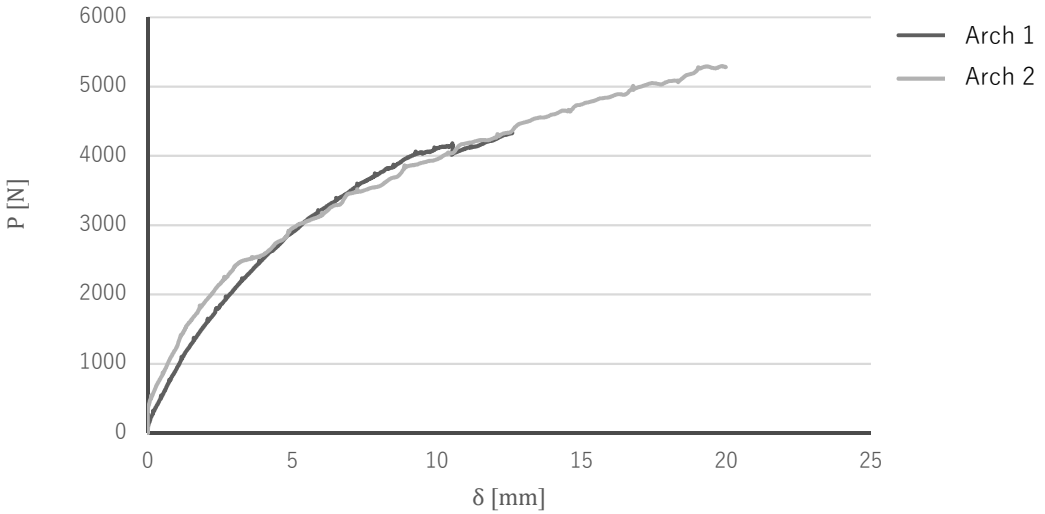

Figure 105 Load-displacement graph for both Arch 1 and Arch 2 during the test

Figure 106 keystone point after the execution of the test. No visible signs of damage are visible

Figure 107 Lateral thrust of the loading cell which causes the interruption of the test

The behaviour of the two beams extracted from keystone and from the base of the arch are different, as reported in Table 30 and Figure 108. In particular, the average value of the P_{max} at the keystone beams is 35% lower than those of the base, while deflection is 20% higher. At the keystone the arch results weaker and more flexible respect to the bases. The different behaviours are mainly due to geometrical reasons, as confirmed by the calculation of the moment of inertia, which has been executed by the use of equations (30) and (31). In fact, the moment of inertia calculated from the sections at the keystone of the arch is almost 40% of that calculated from the sections at the base. In contrast, the modulus of elasticity is enough similar in both cases.

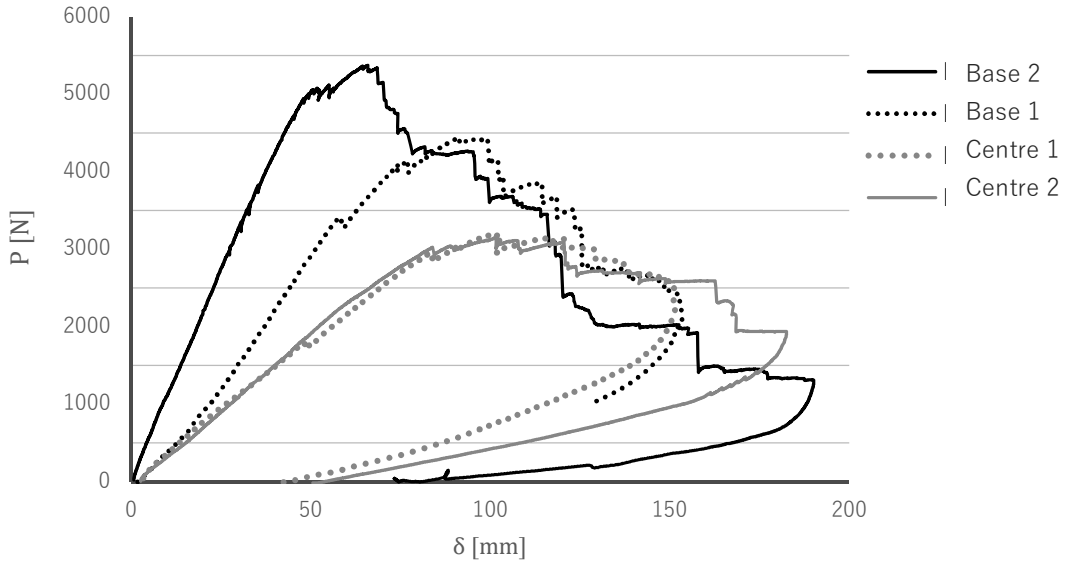

Figure 108 Load-displacement graph for the beams extracted from the base (the darker ones) and the centre (the lighter ones) of both Arch 1 and Arch 2

The stiffness of the beam results significantly lower respect to that one of the arches. The main value is of $7.67 \cdot 10^8$ Nmm^2 for those ones extracted from the keystone of the arches, and $19.19 \cdot 10^8$ Nmm^2 for those ones extracted from the bases of the arches. The observed difference in stiffness between the arch and the corresponding beam likely arises from the presence of concrete at the base of the arches, which ensures a stable connection with the supports. The concrete enables the arch to function more like a monolithic element, rather than as a collection of independent culms acting separately, as is the case with the beams analysed in this study. This highlights a key limitation in the current beam configurations: the lack of effective interaction between individual culms compromises the overall structural stiffness, as the beam behaves more like a loose assembly of discrete elements than as an integrated structural unit. These findings suggest that substantial improvements in stiffness could be achieved by enhancing the connections at the ends and fostering a more unified response among the culms in multi-culm beam systems. Future research should therefore focus on developing design strategies that allow the beam to operate as a single, cohesive element. In this regard, the use of a beam configured as an arch represents a significant improvement in structural performance, offering a more efficient solution for the design of advanced and reliable structural systems.

Table 30 Bending test results for the beam obtained from the arches. P_{max} stands for the maximum recorded value of the load, while δ_{max} for the corresponding deflection, J_1 and J_3 are the moments of inertia calculated as described in the paragraph of the beams; EJ stands for the stiffness calculated at the 40% of the maximum load.

Beam		P_{max} [N]	δ_{max} [mm]	J_1 [10^3mm^4]	J_3 [10^3 mm^4]		EJ [10^8 Nmm^2]
					E_{min}	E_{max}	
KEY-STONE	Arch – 1	3210	102	58.28	7.28	4.59	8.22
	Arch - 2	3150	102	46.30	6.29	3.97	7.11
	Avg.	3180	102	52.30	6.78	4.28	7.67
	St. Dev.	(43)	(1)	(8.47)	(0.70)	(0.44)	(0.79)
BASE	Arch – 1	5374	65	94.13	10.93	6.90	12.35
	Arch – 2	4430	97	161.78	23.03	6.29	26.03
	Avg.	4902	81	127.96	16.98	6.60	19.19
	St. Dev.	(668)	(23)	(47.84)	(8.56)	(0.43)	(9.67)

Comparison with Arundo donax

Since this construction technique originated with the use of Arundo donax, it has already been examined in previous studies [151] [161]. To enable a direct comparison between the mechanical behaviour of bamboo and Arundo donax, the experimental tests in this study were carried out using a similar methodology. Specifically, arches with spans ranging from 3.25 to 3.7 meters and heights between 1.4 and 1.8 meters, with a base diameter of approximately 13 cm, were tested. The load was applied at the central upper point of the arch using a dynamometer and a belt, as shown in Figure 109.

Additionally, beams were extracted from both the base and the central part of the arches. These beams, with a diameter of around 20 cm, were subjected to three-point bending tests, with the load applied at midspan between two supports, also illustrated in Figure 109. Further details regarding materials, methodologies, and results are available in the referenced publications [151] [161].

The outcomes of these tests are shown in the graphs of Figure 110.The comparison between the arches made of Arundo donax and those made of bamboo, as tested in this study, reveals significant differences in stiffness. Although the geometrical dimensions of the arches are comparable, the bamboo arches exhibited a much higher maximum load P_{max}. However, since the tests were interrupted before structural failure occurred, a direct comparison of their ultimate strength is not possible.

In terms of deformation, Arundo donax showed considerably larger displacements than bamboo. At a load of 800 N, Arundo donax arches deformed between 32 and 46 mm, while bamboo arches only deformed between 4 and 8 mm.

This trend is also evident in the beam tests. Arundo donax beams exhibited lower stiffness, with values ranging between 9 and 13 N/mm² at the base and 4 to 6 N/mm² at the centre. In contrast, bamboo beams showed higher stiffness, with average values around 19 N/mm² at the base and approximately 8 N/mm² at the centre. Moreover, values reported for the beams which are not extracted from the arches are also higher.

In conclusion, while both materials share similar structural geometries, bamboo demonstrates significantly superior mechanical performance, particularly in terms of stiffness. This suggests its greater suitability for structural applications where rigidity and reduced deformation under load are required.

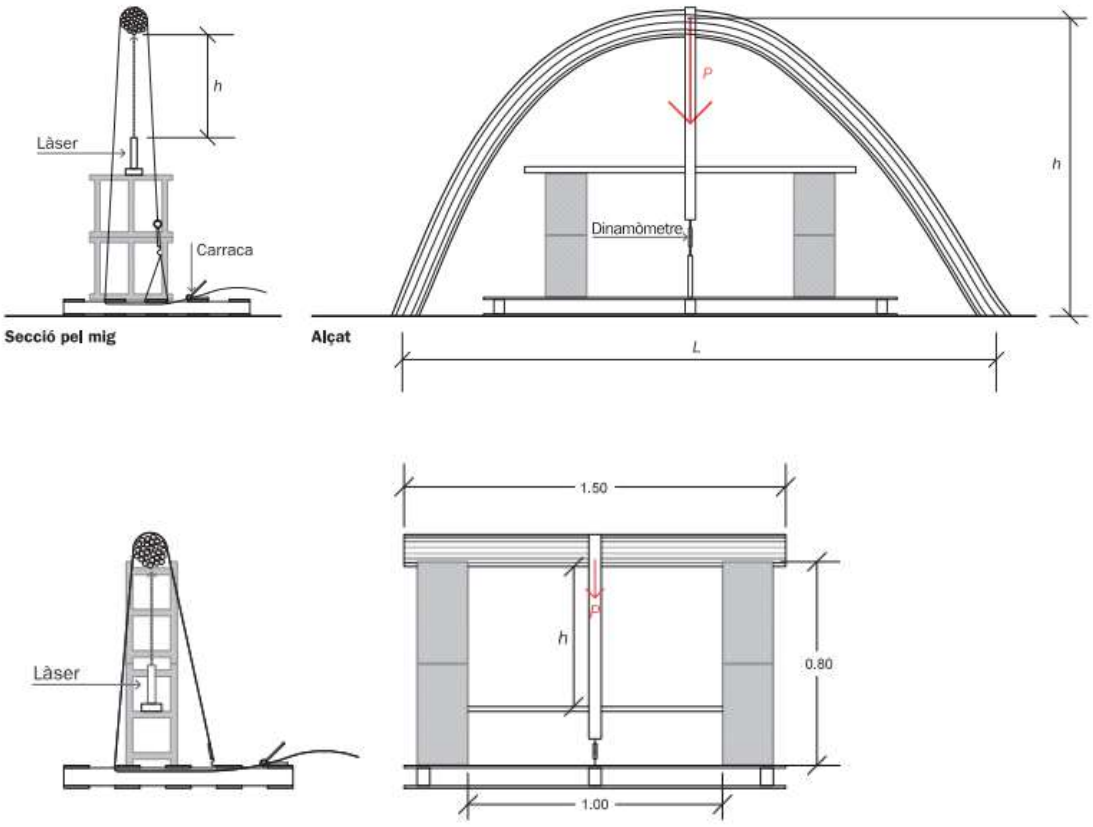

Figure 109 Scheme of the test executed by Andùjar et al. on Canyaviva arches and beam made with Arundo donax [151]

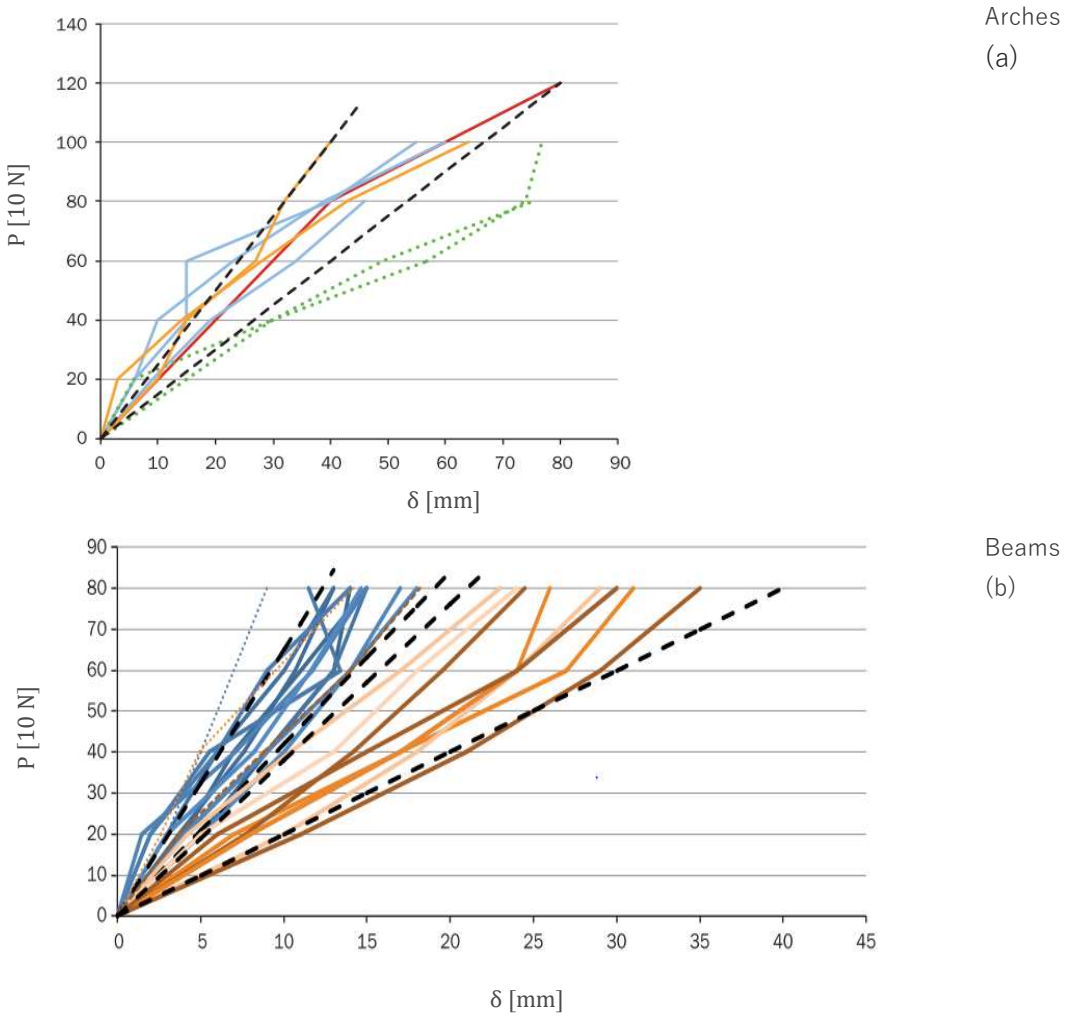

Figure 110 Behaviour of the arches and the beams of Arundo Donax structure, as reported in the study conducted by Andùjar et al. [151]. In the graph relative to arches (a) each color indicates a different arch. In that one of beams (b), the blue lines represent samples from the bases of the arches, while orange lines describe the behaviour of the keystone beam.

CONCLUSION

A groundwork for a new chapter in construction

This thesis seeks to establish the groundwork for a new chapter in the field of construction, focusing on two promising natural materials: bamboo and Arundo donax.

In the current global context, there is an urgent need for rapid, effective, and sustainable solutions to address a wide range of interconnected challenges. Our society faces multiple crises, including a growing disconnection from nature and from ourselves, widespread poverty in many regions where natural resources remain underutilized, and increasingly frequent and severe climate-related emergencies. These signals highlight the critical need for smart and immediate responses. Expanding knowledge and research on bamboo and Arundo donax is essential, as these materials hold significant—yet largely untapped—potential to contribute to addressing these issues.

In countries where these resources are already present, they are often undervalued: perceived as low-cost or primitive options, and used in limited, non-innovative ways. Conversely, in regions such as Europe, where conventional construction materials dominate, there is a strong scepticism regarding the structural capabilities of these alternatives, alongside a general lack of information about local species. This lack of recognition and understanding, in both contexts, greatly hinders the involvement of stakeholders who could otherwise play a crucial role in promoting the responsible and innovative use of these natural materials. The fundamental keys to go beyond these limits are trust, availability and support. And at the base of those, there is the need of a detailed knowledge which provide a scientific foundation for their integration into modern construction practices within the European context.

Recognizing the intrinsic connection between microstructural configuration and macroscale behaviour, this thesis undertakes a rigorous multiscale investigation into the structural potential of bamboo and Arundo donax. It integrates anatomical, mechanical and structural analysis considering the interplay between structure and function across biological and engineered dimensions. The study focuses on six Phyllostachys species cultivated in Italy, P. edulis, P. bambusoides, P. viridiglaucescens, P. vivax, P. iridescens, and P. violacescens, together with Arundo donax.

At the microscale, a comparative anatomical examination has been conducted to understand the morphological and dimensional characteristics of sclerenchyma, parenchyma, and vascular tissue in each species. Culm samples have been obtained from two different heights and examined at four levels of magnifications. Fibre dimensions exhibit a clear dependence on culm height: both mean fibre diameter and wall thickness increase radially toward the outer cortex. In the fibre sheath, inner

diameters range from 12 µm in P. violacescens to 20 µm in P. vivax, while outer diameters span 15 µm (P. violacescens) to 22 µm (P. bambusoides). Wall thickness varies from 4.5 µm (P. violacescens) to 7 µm (P. bambusoides) in the inner zone, rising to 6–9 µm at the exterior. Arundo donax displays analogous dimensions. In contrast, parenchyma cells show pronounced dimensional variability at any height, yet generally diminish in size adjacent to sclerenchyma and towards the cortex. Morphologically, Arundo donax parenchyma tends toward circularity on the inner side, whereas bamboo cells elongate tangentially. Vascular bundle dimensions are broadly comparable across species, save for P. violacescens, which exhibits smaller bundles in both height and width. Arundo donax bundles are morphologically distinct, being encased by a continuous sclerenchymatic ring without subdivision into vascular islands. Representative micrographs at both component level and whole-section scale were compiled for all taxa.

Subsequent quantitative image analysis yielded the area fractions of vessels, sclerenchyma, and parenchyma across the culm wall. Bamboo fibres account for 26–39 % of cross-sectional area, whereas A. donax fibres remain below 20 %. Within bamboo, P. bambusoides, P. viridiglaucescens, P. vivax, and P. iridescens exhibit the highest fibre contents; fibre volume in the upper wall exceeds that of the lower by 0.78–20.5 %. Vessel area occupies 4–7 % in bamboo but rises to roughly 160 % of this value in A. donax, with no marked axial trend.

Radial and circumferential distributions of constituents were then modelled. For Arundo donax, fibre content remains nearly uniform before peaking near the cortex. Bamboo displays a monotonic increase from pith to cortex best captured by exponential or hyperbolic functions, which may be linearly approximated for design. Void (vessel) distribution conforms to parabolic fits in both materials. Circumferentially, component percentages are statistically uniform in all species.

At the mesoscale, links between microstructure and macro-mechanical response were probed via two representative properties: longitudinal modulus of elasticity E and tensile strength σ. These have been estimated using the Rule of Mixtures, based on microstructural data and the mechanical properties of fibres and matrix reported in two independent studies. Prediction obtained showed excellent agreement with experimental measurement, demonstrating that a micromechanics-based approach is a robust predictor of macroscopic longitudinal behaviour.

In order to address the inherently anisotropic and heterogeneous nature of bamboo, especially in the weaker circumferential direction, a finite element model (FEM) grounded in actual anatomical geometries was developed. Simulations have been conducted at ten discrete positions across the culm wall thickness and benchmarked against experimental data, achieving strong agreement. This approach revealed a

parabolic stress distribution analogous to that found in the radial void arrangement, highlighting the strong correlation between internal morphology and stress localization. A detailed stress concentration analysis uncovered that the parabolic voids distribution results from two opposite linear trends: the number of voids increases while the average area of each void decreases. This dual mechanism underscores the nuanced role of voids, not merely as geometric discontinuities reducing net section, but as entities whose morphology directly influences local stress intensities and, consequently, failure modes.

Furthering the mesoscale framework, the thesis presents the development and validation of a laboratory test, designed to be both easy and highly informative. It enables a reliable information of flexural strength and Young's modulus while offering insight into the mechanical contribution of matrix and fibre. Its validity was demonstrated by an ultraviolet ageing campaign on P. viridis (irradiation 6–360 h) followed by four-point bending. Up to 360 h, the bending test that UV exposure does not compromise longitudinal integrity. Interestingly, bending strength increased after 48 h, declined slightly after 96 h, but never fell below the initial value. Moreover, strain capacity remained unchanged. FTIR confirmed progressive lignin degradation, while ESEM and optical microscopy revealed fibre-wall microcracking.

Crucially, this new test procedure was also deployed as a grading method across all bamboo species, offering practical route to standardisation in structural application. Its ability to sensitively detect material performance and degradation further elevates its utility.

At the macroscale, the transition from material knowledge to structural design has been achieved by characterising a multi-culm bundle beam. It is part of a multi-culm arches system, which intend to exploit the structural logic of these materials. Bundle beams were assembled from parallel culms of uniform length, axially aligned and laterally restrained with periodic ties.

A three-point bending test and a subsequently FEM analysis showed that individual culms behave largely as independent units. They carry load sequentially: the culm directly under the indenter sustains load until crushing, after which load is transferred to subjacent culms and producing a stepped softening curve rather than abrupt collapse. It means that load redistribution and interface mechanics, rather than intrinsic culm strength alone, governs ultimate capacity. Bundles assembled from numerous small culms show a smoother stiffness decay and greater post-peak ductility than bundles of fewer large culms, indicating that culm count is a critical design variable. Moreover, strategies to improve the collaboration between culms should be implemented.

Finite-element replication of the bending test further elucidate and confirmed stress transmission and deformation patterns. While global inertia rises if load is artificially distributed across all culms, concomitant cross-sectional deformation under compression reduces the potential of the inertia as the sum of the culm falling within the range defined by the sum of three to four culms. The model therefore serves as a practical design tool for optimising tie density and culm selection.
The modulus of inertia of the whole section can be approximated by summing individual culm inertias. Sectional moments of inertia behave additively. overall stiffness approximating the sum of individual moments of inertia. Thus, beams comprising numerous small culms exhibit a global inertia closely approximating the sum of individual inertias.
A series of full-span arches fabricated from identical bundle beams were subjected to vertical loading. Extracted beam segments showed that culms located near the keystone experienced cumulative damage and measurable stiffness loss. Across all trials, keystone segments retained lower bending strength and higher deformability than bases. This gradient underscores the importance of region-specific safety factors in design, particularly for long-span arches.
Literature benchmarks on similar Arundo donax structures indicate a strength–ductility trade-off between the two species: bamboo achieves higher ultimate loads, while Arundo accommodates larger displacements before failure.

Yet the relevance of this research extends beyond technical innovation. By challenging entrenched perceptions that continue to marginalize bio-based materials as informal or structurally unreliable, exploring materials that are renewable, locally available, and often culturally undervalued, this thesis intersects with broader questions of environmental justice, economic inclusion, and individual empowerment. The adoption of bio-based construction resources like bamboo and Arundo donax offers opportunities for creating decentralized, circular economies that reduce dependency on extractive supply chains and promote self-sufficiency—particularly in regions rich in natural resources but lacking access to industrial infrastructure. In alignment with the UN Sustainable Development Goals, this work contributes to several objectives. Moreover, by challenging the dominance of conventional materials and systems, it opens space for alternative knowledge systems and practices rooted in ecological intelligence and social resilience. This work challenges entrenched perceptions that continue to marginalize bio-based materials as informal or structurally unreliable. It repositions bamboo and Arundo donax as viable, adaptable, and high-performance solutions, capable of contributing meaningfully to the transformation of the built environment.

Rather than offering a conclusion, this thesis offers a beginning: a solid foundation from which future research, innovation, and application can grow. It invites designers, engineers, and policymakers to move beyond conventional approaches and to reimagine construction through the lens of natural intelligence, local availability, and long-term resilience. Thus, construction becomes not a means of consumption, but a path toward regeneration - of ecosystems, of knowledge, and of individual empowerment.

BIBLIOGRAPHY

[1] B. Mollison, Permaculture: a designer's manual, Sisters Creek, Tasmania, Australia. : Tagari Publications, 1988.

[2] B. Galmarini, P. Costa e L. Chiesi, «Natural Building Materials and Social Representations in Informal Settlements: How Perceptions of Bamboo Interfere with Sustainable, Affordable, and Quality Housing,» *Sustainability,* vol. 14, n. 19, 2022. https://doi.org/10.3390/su141912252

[3] O. H. Lòpez, *Bamboo: The Gift of the Gods,* University of Minnesota, 2003.

[4] Z. Ahmad, A. Upadhyay, Y. Ding, A. Emamverdian e A. Shahzad, «Bamboo: Origin, Habitat, Distributions and Global Prospective,» in *Biotechnological Advances in Bamboo*, Springer Nature Singapore, 2021. https://doi.org/10.1007/978-981-16-1310-4_1

[5] W. Liese e M. Köhl, Bamboo - The Plant and its Uses, Hamburg: Walter Liese and Michael Köhl, 2015.

[6] INBAR, «Why bamboo and rattan,» 2025. [Online]. Available: https://www.inbar.int/why-bamboo-and-rattan/.

[7] C. Ngernsaengsaruay, B. Puangsin, N. Leksungnoen, S. Khantayanuwong, P. Chanton, T. Thaepthup, P. Wessapak, R. Meeboonya, P. Yimlamai, K. Wanitpinyo, K. Chitbanyong, T. Andriyas e N. Banja, «Morphology, Taxonomy, Culm Internode and Leaf Anatomy,and Palynology of the Giant Reed (Arundo donax L.), Poaceae,Growing in Thailand,» *Plants,* vol. 12, n. 1850, 2023. https://doi.org/10.3390/plants12091850

[8] J. A. Goolsby, P. J. Moran, M. M. Jiménez, C. Yang, K. Canavan, Q. Paynter, N. Ota e D. J. Kriticos, «Biology of Invasive Plants 4. Arundo donax L.,» *Invasive Plant Science and Management,* 2023. doi:10.1017/inp.2023.17

[9] T. Gangwara e D. Schillinger, «Microimaging-informed continuum micromechanics accurately predicts macroscopic stiffness and strength properties of hierarchical plant culm materials,» *Mechanics of Materials,* 2019. doi:10.1016/j.mechmat.2019.01.009

[10] B. Botanicals, «Containing and Removing Bamboo,» [Online]. Available: https://extension.umd.edu/resource/containing-and-removing-bamboo/.

[11] 先従隗始, «File:The flower of bamboo(Phyllostachys bambusoides) 20230429 01.jpg,» 2023. [Online]. Available: https://commons.wikimedia.org/wiki/File:The_flower_of_bamboo(Phyllostachys_bambusoides)_20230429_01.jpg.

[12] Mashkawat.ahsan, «Wikimedia Commons,» 2019. [Online]. Available: https://commons.wikimedia.org/wiki/File:Bamboo_forest_in_Bangladesh.jpg.

[13] ひでわく, «File:Bamboescheut bij de rivier Izumi in Yokohama, -30 Apr. 2011 a.jpg,» 2011. [Online]. Available: https://commons.wikimedia.org/wiki/File:Bamboescheut_bij_de_rivier_Izumi_in_Yokohama,_-30_Apr._2011_a.jpg.

[14] H.-C. Spatz, H. Beismann, F. Bruchert, A. Emanns e T. Speck, «Biomechanics of the giant reed Arundo donax,» *Philosophical Transactions of the Royal Society of London,* vol. 357, pp. 1-10, 1997. doi: 10.1098/rstb.1997.0001

[15] O. Speck e H.-C. Spatz, «Mechanical Properties of the Rhizome of Arundo donax L.,» *Plant Biology,* vol. 5, n. 6, pp. 661-669, 2003. https://doi.org/10.1055/s-2003-44714

[16] E. Ruiz-Sanchez, C. D. Tyrrell, X. Londoño, R. P. Oliveira e L. G. Clark, «Diversity, distribution, and classification of Neotropical woody bamboos (Poaceae: Bambusoideae) in the 21st Century,» *Botanical Science,* pp. 198-228, 2021. doi:10.17129/botsci.2722

[17] L. Clark, X. Londoño e E. Ruiz-Sanchez, «Bamboo Taxonomy and Habitat,» in *Bamboo, the Plant and Its Uses*, Walter Liese and Michael Köhl, 2015. doi:10.1007/978-3-319-14133-6

[18] M. Tamang, S. Nandy, R. Srinet, A. K. Das e H. Padalia, «Bamboo Mapping Using Earth Observation Data: A Systematic Review,» *Journal of the Indian Society of Remote Sensing,* p. 2055–2072, 2022. https://doi.org/10.1007/s12524-022-01600-0

[19] H. Du, F. Mao, X. Li, G. Zhou, X. Xu, N. Han, S. Sun, G.Gao, L.Cui, Y. Li, D. Zhu, Y. Liu, L. Chen, W. Fan, P. Li, Y. Shi e Y. Zhu, «Mapping Global Bamboo Forest Distribution Using Multisource Remote Sensing Data,» *IEEE Journal of Selected Topics in Applied Earth Observations and Remote Sensing,* vol. 11, pp. 1458-1471, 2018. doi:10.1109/JSTARS.2018.2800127

[20] G. Potters, F. Schutte, D. V. Goethem, S. D. Nollin, R. Samson e J. Gielis, «Bamboo as a Crop in Western Europe – a SWOT Analysis,» *Acta Horticulturae,* 2013. doi:10.17660/ActaHortic.2013.1003.11

[21] J. Gielis, «Future possibilities for bamboo in European agriculture». Retrieved from

https://www.researchgate.net/publication/228719908_Future_possibilities_for_bamboo_in_European_agriculture

[22] E. Lombardo, «An overview of bamboo cultivation in Southern Italy,» *Advances in Bamboo Science,* vol. 1, 2022. https://doi.org/10.1016/j.bamboo.2022.100002

[23] A. Bucci, F. C. Badone e R. Pilu, La canna comune (Arundo Donax L.). Aspetti storici, scientifici e tecnologici, Aracne Editrice, 2012.

[24] Pixeltoo, «File:Bambusoideae World map.png,» [Online]. Available: https://en.wikipedia.org/wiki/File:Bambusoideae_World_map.png.

[25] G. Pope, «Bamboo and Human Evolution,» *Natural History,* vol. 98, n. 10, pp. 48-57, 1989.

[26] H. Xhauflair, A. Pawlik, C. Gaillard, H. Forestier, T. J. Vitales, J. R. Callado, D. Tandang, N. Amano, D. Manipon e E. Dizon, «Characterisation of the use-wear resulting from bamboo working and its importance to address the hypothesis of the existence of a bamboo industry in prehistoric Southeast Asia,» *Quaternary International,* vol. 416, pp. 95-125, 2016. https://www.jstor.org/stable/10.2307/envirevi.19.418

[27] E. Viollet-le-Duc, Histoire de l'habitation humaine : depuis les temps préhistoriques jusqu'a nos jours, Paris: Bibliothèque d'éducation et de récréation, 1875.

[28] R. Verlaque, M. Verlaque, G. Renoux, L. Hardion e B. Vila, «Arundo/Phragmites: Identification and Uses of Essential Plants in Mediterranean Civilizations,» *Human Ecology,* vol. 52, pp. 273-288, 2024. :https://doi.org/10.1007/s10745-024-00501-9

[29] F. Zámolyi e U. Herbig, «Reed as building material – renaissance of vernacular techniques,» in *International Symposium on advanced methods of monitoring reed habitats*, Rhombos Verlag Berlin, 2011, pp. 83-108.

[30] A. Badawy, A history of Egyptian architecture, Berkeley : University of California, 1954.

[31] D. Al-Jumeily, K. Hashim, R. Alkaddar, M. Al-Tufaily e J. Lunn, «Sustainable and Environmental Friendly Ancient Reed Houses (Inspired by the past to motivate the future),» in *11th International Conference on Developments in eSystems Engineering (DeSE)*, 2018. doi:10.1109/DeSE.2018.00032

[32] B. Brunetti, «Baraccas: esempi antichi di architettura in canna palustre,» 7 Gennaio 2015. [Online]. Available: https://www.architetturaecosostenibile.it/architettura/progetti/baraccas-esempi-canna-187.

[33] F. Barreca, «Use of giant reed Arundo Donax L. in rural constructions,» *Agric Eng Int: CIGR Journal,* vol. 14, n. 3, pp. 46-52, 2012.

[34] G. Broadbent, «The ecology of the mudhif,» in *Eco-Architecture II*, 2008. doi:10.2495/ARC080021

[35] D. Witte, *Contemporary Bamboo Housing in South America - Master Thesis,* University of Washington, 2018.

[36] «ARCHITIZER,» [Online]. Available: https://architizer.com/projects/zeri-pavilion-expo-hannover/.

[37] H. Abdel, «The Arch at Green School / IBUKU,» 30 June 2021. [Online]. Available: https://www.archdaily.com/964059/the-arc-at-green-school-ibuku.

[38] A. Griffiths, «Vo Trong Nghia Architects completes bamboo welcome centre for Grand World Phu Quoc,» 29 March 2022. [Online]. Available: https://www.dezeen.com/2022/03/29/vo-trong-nghia-architects-bamboo-welcome-centre-grand-world-phu-quoc-vietnam-architecture/.

[39] A. Peacock, «Kengo Kuma tops sculptural community centre with swooping bamboo roof,» 18 December 2024. [Online]. Available: https://www.dezeen.com/2024/12/18/bamboo-gate-kengo-kuma-community-facility-japan/.

[40] J. Astbury, «RAW Architecture celebrates bamboo's versatility at home and community centre in Indonesia,» 23 September 2022. [Online]. Available: https://www.dezeen.com/2022/09/23/raw-architecture-bamboo-house-indonesia-piyandeling-artisan/#/.

[41] K. Kusbiantoro, C. Lesmana e I. Gunawan, «Designing folded modular houses as refugee shelters at disaster sites,» *IOP Conference Series: Earth and Environmental Science,* vol. 1361, 2024. doi:10.1088/1755-1315/1361/1/012014

[42] K. N. Dev e A. K. Das, «Design of Bamboo Shelter Kit for Post-disaster Temporary Shelter Response,» in *Design for Tomorrow—Volume 1*, Springer Singapore, 2021, pp. 923-934. https://doi.org/10.1007/978-981-16-0041-8_76

[43] B. Owoo, «Floating Bamboo House offers model for "stable and safe accommodation",» 17 June 2023. [Online]. Available: https://www.dezeen.com/2023/06/17/floating-bamboo-house-hp-architects-vietnam/.

[44] AmberP, «Bamboo Shelter by Esan Rahmani + Mukul Damle,» 20 Semtember 2010. [Online]. Available: https://www.archdaily.com/77334/bamboo-shelter-by-esan-rahmani-mukul-damle.

[45] C. Gauss, M. Kadivar, R. G. Pereira e H. Savastano Jr., «Assessment of dendrocalamus asper (Schult and schult f.) (Poaceae) bamboo treated with tannin-boron preservatives,» *Construction and Building Material,* vol. 282, 2021. https://doi.org/10.1016/j.conbuildmat.2021.122723

[46] Kaminski, Lawrence e Trujillo, «Structural use of bamboo. Part 2: Durability and Preservation,» *The Structural Engineer,* vol. 94, n. 10, pp. 38-43, 2016.

[47] D. Wei, O. Schmidt e W. Liese, «Durability test of bamboo against fungi according to EN standards,» *European Journal of Wood and Wood Product,* vol. 71, pp. 551-556, 2013. doi: 10.1007/s00107-013-0707-2

[48] W. Liese e U. Schmitt, «Development and structure of the terminal layer in bamboo culms,» *Wood Science and Technology,* vol. 40, pp. 4-15, 2006. https://doi.org/10.1007/s00226-005-0046-5

[49] C. Okhio, J. Waning e Y. Mekonnen, «An Experimental Investigation of the Effects of Moisture Content on the Mechanical Properties of Bamboo and Cane,» *Cyber Journals: Multidisciplinary Journals in Science and Technology, Journal of Selected Areas in Bioengineering (JSAB),* 2011.

[50] H. Wang, G. Tian, W. Li, D. Ren, X. Zhang e Y. Yu, «Sensitivity of bamboo fiber longitudinal tensile properties to moisture content variation under the fiber saturation point,» *Wood Science and Technology,* vol. 61, pp. 262-269, 2015. doi:10.1007/s10086-015-1466-y

[51] H. Wang, H. Wang, W. Li, D. Ren and Y. Yu, «Effects of Moisture Content on the Mechanical Properties of Moso Bamboo at the Macroscopic and cellular Levels,» *BioResources,* pp. 5475-5484, 2013. https://doi.org/10.15376/biores.8.4.5475-5484

[52] Y.M. Zhang, Y. L. Yu and W. J. Yu, «“Effect of thermal treatment on the physical and mechanical properties of Phyllostachys pubescen bamboo,» *European Journal of Wood and Wood Product,* vol. 71, n. 1, pp. 61-67, 2012. https://doi.org/10.1007/s00107-012-0643-6

[53] B. Loktongman and R. K. Borah, «Traditional Methods of Post Harvest Bamboo Treatment for Durability Enhancement,» *International Journal of Scientific & Engineering Research,* vol. 8, n. 1, 2017.

[54] abiani, M., Greco, S., Mentrasti, L., Molari, L., Valdrè, G., 2023. Thermal treatment of bamboo with flame: influence on the mechanical characteristics. Advances in Bamboo Science (Online) 2, 100015. https://doi.org/10.1016/j.bamboo.2023.100015

[55] C. Gauss, M. Kadivar, K. A. Harries e H. Savastano Jr., «Chemical modification of Dendrocalamus asper bamboo with citric acid and boron compounds:

Effects on the physical-chemical, mechanical and thermal properties,» *Journal of Cleaner Production,* vol. 279, 2021. https://doi.org/10.1016/j.jclepro.2020.123871

[56] M. Sileo, F. T. Gizzi e N. Masini, *Monitoraggio microclimatico: passato, presente e prospettive future,* 2016.

[57] E. A. Amede, E. K. Hailemariama, L. M. Hailemariam e D. A. Nuramo, «A Review of Codes and Standards for Bamboo Structural Design,» *Advances in Materials Science and EngineeringVolume 2021, Issue 1,* 2021. https://doi.org/10.1155/2021/4788381

[58] «New international standard on bamboo structures,» 2021. [Online]. Available: https://www.inbar.int/iso-22156-2021/.

[59] UNEP, «Global Status Report for Buildings and Construction,» 2024. [Online]. Available: https://www.unep.org/resources/report/global-status-report-buildings-and-construction.

[60] P. Das, C. Korde. P. Sudhakar and S. Satya, «Traditional bamboo houses of North-Eastern Region: A field study of Assam and Mizoram,» *Key Engineering Materials,* vol. 517, pp. 197-202, 2012. doi: 10.4028/www.scientific.net/KEM.517.197

[61] G. Zhou, C. Meng, P. Jiang e Q. Xu, «Review of Carbon Fixation in Bamboo Forests in China,» *The Botanical Review,* vol. 77, n. 3, pp. 262-270, 2011. https://doi.org/10.1007/s12229-011-9082-z

[62] X. Song, G. Zhou, H. Jiang, S. Yu, J. Fu, W. Li, W. Wang, Z. Ma and C. Peng, «Carbon sequestration by Chinese bamboo forests and their ecological benefits: assessment of potential, problems, and future challenges,» *Environmental Reviews,* vol. 19, pp. 418-428, 2011. https://doi.org/10.1139/a11-015

[63] R. Vadalà, N. Cicero, G. Dugo e R. Costa, «Suitability and Eligibility of Phyllostachys pubescens (Moso Bamboo) Afforestation for GHG (Greenhouse Gases)Projects: Case Study in Central Italy,» *Frontiers in environmental science,* n. 10, 2022. https://doi.org/10.3389/fenvs.2022.817177

[64] G. W. Evans, «The built environment and mental health,» *Journal of Urban Health,* 2003. https://doi.org/10.1093/jurban/jtg063

[65] E. N. Untaru, H. Han, A. David e X. Chi, «Biophilic Design and Its Effectiveness in Creating Emotional Well-Being, Green Satisfaction, and Workplace Attachment Among Healthcare Professionals: The Hospice Context,» *HERD: Health Environments Research & Design Journal,* vol. 17, n. 1, 2023. https://doi.org/10.1177/19375867231192087

[66] M. G. Berman e J. J. a. S. Kaplan, «The Cognitive Benefits of Interacting with Nature,» *Psychological Science,* vol. 19, n. 12, pp. 1207-1212, 2008. https://doi.org/10.1111/j.1467-9280.2008.02225.x

[67] A. Basu, J. Duvall e R. Kaplan, «Attention Restoration Theory: Exploring the Role of Soft Fascination and Mental Bandwidth,» *Environment and Behavior,* vol. 51, May 2018. https://doi.org/10.1177/0013916518774400

[68] K. J. Williams, K. E. Lee, T. Hartig, L. D. Sargent, N. S. Williams e K. A. Johnson, «Conceptualising creativity benefits of nature experience: Attention restoration and mind wandering as complementary processes,» *Journal of Environmental Psychology,* vol. 59, pp. 36-45, 2018. https://doi.org/10.1016/j.jenvp.2018.08.005

[69] A. Hassan, Q. B. Chen, T. Jiang, B. Y. Lyu, N. Li, S. Li, Z. Y. Shangguan, Y. T. Li, Z. L. Jun, Q. Luo, X. Y. Chen, Y. Y. Wang, C. C. Zeng, J. Yang e M. S. Tahir, «Psychophysiological Effects of Bamboo Plants on Adults,» *Biomedical and Environmental Sciences,* vol. 30, n. 11, pp. 846-850, 2017. https://doi.org/10.3967/bes2017.114

[70] Y. Wang, H. Qu, T. Bai, Q. Chen, X. Li, Z. Luo, B. Lv e M. Jiang, «Effects of Variations in Color and Organ of Color Expression in Urban Ornamental Bamboo Landscapes on the Physiological and Psychological Responses of College Students,» *International Journal of Environmental Research and Public Health,* vol. 18, n. 3, 2021. https://doi.org/10.3390/ijerph18031151

[71] B. Chengcheng Zeng, S. Deng, Y. Yu, N. Li, W. Lin, D. Li e Q. Chen, «Benefits of a Three-Day Bamboo Forest Therapy Session on the Physiological Responses of University Students,» *International Journal of Environmental Research and Public Health,* vol. 17, n. 9, 2020. https://doi.org/10.3390/ijerph17093238

[72] A. Manunza, G. Giliberto, E. Muroni, O. Mosca, F. Fornara, I. Blečić e M. Lauriola, «"Build It and They Will Stay": Assessing the Social Impact of Self-Build Practices in Urban Regeneration,» *Urban Sciences,* vol. 9, n. 2, 2025. https://doi.org/10.3390/urbansci9020030

[73] D. Zhang e T. Yong, «Green building, pro-environmental behavior and well-being: Evidence from Singapore,» *Cities,* vol. 108, 2021. https://doi.org/10.1016/j.cities.2020.102980

[74] S. Abebe, A. S. Minale e D. Teketay, «Socio-economic importance of the bamboo resources in the Lower Beles River Basin, north-western Ethiopia,» *Environment, Development and Sustainability,* vol. 24, pp. 12162-12181, 2022. https://doi.org/10.1007/s10668-021-01938-4

[75] P. Van Der Lugt, A. Van Der Dobbelsteen e J. Janssen, «An environmental,

economic and practical assessment of bamboo as a building material for supporting structures,» *Construction and Building Materials,* vol. 20, n. 9, pp. 648-656, 2006. https://doi.org/10.1016/j.conbuildmat.2005.02.023

[76] O. J. Adebowale e J. N. Agumba, «Bamboo in sustainable construction:effects on productivity and safety,» *International Journal of Productivity and Performance Management,* vol. 74, n. 11, pp. 1-20, 2025. https://doi.org/10.1108/IJPPM-06-2023-0307

[77] INBAR, «Trade Overview 2017,» Wu Junqi, Charlotte King, 2019.

[78] I. Lewandowski, J. Scurlock, E. Lindvall e M. Christou, «The development and current status of perennial rhizomatous grasses as energy crops in the US and Europe,» *Biomass Bioenergy,* vol. 25, 2003. https://doi.org/10.1016/S0961-9534(03)00030-8

[79] G. Antal, «Giant reed (Arundo donax L.) from ornamental plant to dedicated bioenergy species: review of economic prospects of biomass production and utilization,» *International Journal of Horticultural Science,* vol. 24, 2018. https://doi.org/10.31421/IJHS/24/1-2./1545

[80] A. Bonfante, A. Impagliazzo, N. Fiorentino, G. Langella, M. Mori e M. Fagnano, «Supporting local farming communities and crop production resilience to climate change through giant reed (Arundo donax L.) cultivation: An Italian case study,» *Science of The Total Environment,* 2017. https://doi.org/10.1016/j.scitotenv.2017.05.214

[81] L. Pari, M. D. Curt, J. Sanchez e E. Santangelo, «Economic and energy analysis of different systems for giant reed (Arundo donax L.) harvesting in Italy and Spain,» *Industrial Crops and Products,* vol. 84, 2014. https://doi.org/10.1016/j.indcrop.2016.01.036

[82] J. Vijayalaxmi and H. R. Singha, «Use of Bamboo as a Construction Material in the North-East and Southern Vernacular Settlements of India,» *ISVS e-journal,* vol. 8, n. 4, 2021.

[83] D. Opoku, J. Ayarkwa e K. Agyekum, «Factors Inhibiting the Use of Bamboo in Building Construction in Ghana: Perceptions of Construction Professionals,» *Materials Sciences and Applications,* vol. 7, n. 2, 2016. https://doi.org/10.4236/msa.2016.72008

[84] Z. Mekonnen, A. Worku, T. Yohannes, M. Alebachew, D. Teketay e H. Kassa, «Bamboo Resources in Ethiopia: Their value chain and contribution to livelihoods,» *Ethnobotany Research & Applications,* vol. 12, pp. 511-524, 2014. https://doi.org/10.17348/era.12.0.511-524

[85] Velazquez e Santos, «Anatomical study of the culm of five Philippine bamboos,»

Natural and Applied Science Bulletin, vol. 1, n. 4, pp. 281-296, 1931.

[86] S. Amada, T. Munekata, Y. Nagase, Y. Ichikawa, A. Kirigai e Y. Zhifei, «The Mechanical Structures of Bamboos in Viewpoint of Functionally Graded and Composite Material,» *Journal of Composite Materials,* vol. 30, n. 7, pp. 800-819, 1996. https://doi.org/10.1177/002199839603000703

[87] W. Liese, *The Anatomy of Bamboo Culms,* INBAR technical reports, 1998.

[88] J. Q. Krause, F. d. A. Silva, K. Ghavami, O. d. F. M. Gomes e R. D. Toledo Filho, «On the influence of Dendrocalamus giganteus bamboo microstructure on its mechanical behavior,» *Construction and Building Materials,* n. 127, pp. 199-209, 2016. https://doi.org/10.1016/j.conbuildmat.2016.09.104

[89] V. Fiore, T. Scalici e A. Valenza, «Characterization of a new natural fiber from Arundo donax L. as potential reinforcement of polymer composites,» *Carbohydrate Polymers,* vol. 106, pp. 77-83, 2014. https://doi.org/10.1016/j.carbpol.2014.02.016

[90] J. Chen, L. Zhu, X. Gu, J. Xu, L. Dong e J. Qiu, «Reed microstructure detection by optical coherence tomography, an efficient and non-invasive method,» *Applied Optics,* vol. 62, n. 15, 2004. https://doi.org/10.1364/AO.483991

[91] L. Molari, L. Mentrasti e M. Fabiani, «Mechanical characterization of five species of Italian bamboo,» *Structures,* pp. 59-72, 2020. https://doi.org/10.1016/j.istruc.2019.12.022

[92] D. Grosser e W. Liese, «On the Anatomy of Asian Bamboos, with Special Reference to their Vascular Bundles,» *Wood Science and Technology,* vol. 5, pp. 290-312, 1971. https://doi.org/10.1007/BF00365061

[93] W. Liese e M. Köhl, Bamboo, the Plant and its Uses, Hamburg: Tropical Forestry, 2015.

[94] Parameswaran e Liese, «On the Fine Structure of Bamboo Fibres,» *Wood Science and Technology,* vol. 10, pp. 231-246, 1976. https://doi.org/10.1007/BF00350830

[95] J. C. Roland, B. Vian e D. Reis, «Observations with cytochemistry and ultracryotomy on the fine structure of the expanding walls in actively elongating plant cells,» *Journal of Cell Science,* vol. 19, n. 2, pp. 239-259, 1975. https://doi.org/10.1242/jcs.19.2.239

[96] X. Li, T. F. Shupe, G. Peter, C. Hse e T. Eberhardt, «Chemical changes with maturation of the bamboo species phyllostachys pubescens,» *Journal of Tropical Forest Science,* vol. 19, n. 1, pp. 6-12, 2007. Retrieved from https://www.fs.usda.gov/treesearch/pubs/29071

[97] W. Liese e D. Grosser, «Untersuchungen zur Variabilität der Faserlänge bei

Bambus,» *Holzforschung,* vol. 26, n. 6, pp. 202-211, 1972. https://doi.org/10.1515/hfsg.1972.26.6.202

[98] R. Wahab, M. T. Mustafa, S. Rahman, M. A. Salam, O. Sulaiman, M. Sudin e M. S. M. Rasat, «Relationship between physical, anatomical and strength properties of 3-year-old cultivated tropical bamboo,» *ARPN Journal of Agricultural and Biological Science,* vol. 7, n. 10, pp. 782-791, 2012. https://doi.org/10.5539/jas.v5n8p66

[99] D. Liu, J. Song, D. P. Anderson, P. R. Chang e Y. Hua, «Bamboo fiber and its reinforced composites:structure and properties,» *Cellulose,* vol. 19, p. 1449–1480, 2012. https://doi.org/10.1007/s10570-012-9741-1

[100] Y. Dessalegn e B. Singh, «Effect of analysis on morphology of bamboo fibre: a review,» *International Journal of Engineering Sciences & Research Technology,* vol. 8, n. 3, 2019. https://doi.org/10.5281/zenodo.14211838

[101] W. Liese e U. Schmitt, «Development and structure of the terminal layer in bamboo culms,» *Wood Science and Technology,* vol. 40, pp. 4-15, 2006. https://doi.org/10.1007/s00226-005-0046-5

[102] C. Ngernsaengsaruay, B. Puangsin, N. Leksungnoen, S. Khantayanuwong, P. Chanton, T. Thaepthup, P. Wessapak, R. Meeboonya, P. Yimlamai, K. Wanitpinyo, K. Chitbanyong, T. Andriyas and N. Banjatammanon, «Morphology, Taxonomy, Culm Internode and Leaf Anatomy,and Palynology of the Giant Reed (Arundo donax L.), Poaceae, growing in Thayland,» *Plants (Basel),* vol. 12, n. 9, p. 1850, 2023. https://doi.org/10.3390/plants12091850

[103] F. Dai, Z. Wang, H. Wang, W. Zhang, T. Zhong e G. Tian, «Vascular bundle characteristics and mechanical properties of Dendrocalamus sinicus,» *Construction and Building Materials,* vol. 363, 2023. https://doi.org/10.1016/j.conbuildmat.2022.129858

[104] J. Jiang, «Microstructure features and the prediction of longitudinal elastic modulus of small-diameter-original Bamboo,» *Journal of Reinforced Plastics and Composites (Phyllostachys glauca McClure),* vol. 35, n. 10, p. 824–833, 2016. https://doi.org/10.1177/0731684416630115

[105] M. Seixas, S. Paciornik, D. Cardoso e L. E. Moreira, «Mesostructural Characterization of Phyllostachys aurea bamboo using optical microscopy and digital image processing,» in *International Conference on Non-conventional Materials and Technologies NOCMAT* , 2022.

[106] X. Londoño, G.-C. Camayo, N. M. Riaño e Y. López, «Characterization of the anatomy of Guadua angustifolia (Poaceae: Bambusoideae) culms,» *J. Amer. Bamboo Soc.,* vol. 16, pp. 18-31, 2003.

[107] W. Silva e C. Silva, « LABfit curve fitting software (nonlinear regression and treatment of data program V 7.2.50c Available from world wide web: www.labft.net».

[108] S. Mannan, J.P. Knox and S. Basu «Correlations between axial stiffness and microstructure of a species of bamboo» *Royal Society open science*, vol. 4, 160412, 2017 https://doi.org/10.1098/rsos.160412

[109] F. Wang, Z. Shao e Y. Wu, «Mode II interlaminar fracture properties of Moso bamboo,» *Composites Part B: Engineering,* vol. 44, n. 1, pp. 242-247, 2013. https://doi.org/10.1016/j.compositesb.2012.05.035

[110] P. Dixon e L. Gibson, «The structure and mechanics of Moso bamboo material,» *Journal of the Royal Society Interface,* vol. 11, 2014. https://doi.org/10.1098/rsif.2014.0321

[111] S. Greco, L. Molari e M. Maraldi, «Assessing the mechanical properties of bamboo cultivated in Italy,» in *IC-NOCMAT 2019*, Nairoby, Kenya, 2019.

[112] L. Molari, F. S. Coppolino e J. J. Garcìa, «Arundo donax: A widespread plant with great potential as sustainable structural material,» *Construction and Building Materials,* vol. 268, n. 121143, 2021. https://doi.org/10.1016/j.conbuildmat.2020.121143

[113] L. Molari e J. J. García, «On the radial variation of the transverse mechanical properties of bamboo,» *Journal of Building Engineering,* vol. 33, 2021. https://doi.org/10.1016/j.jobe.2020.101557

[114] S. Greco e L. Molari, «Flexural Behaviour of Five Species of Italian Bamboo,» *Construction Technologies and Architecture. Trans Tech Publications Ltd,* vol. 1, pp. 723-729, January 2022. https://doi.org/10.4028/www.scientific.net/cta.1.723

[115] Z.-P. Shao, C.-H. Fang, S.-X. Huang e G.-L. Tian, «Tensile properties of Moso bamboo (Phyllostachys pubescens) and its components with respect to its iber-reinforced composite structure,» *Wood Science and Technology,* vol. 44, pp. 655-666, 2010. https://doi.org/10.1007/s00226-009-0290-1

[116] Z. Aiping, H. Dongsheng, L. Haitao e S. Yi, «Hybrid approach to determine the mechanical parameters of fibers and matrixes,» *Construction and Building Materials,* vol. 35, pp. 191-196, 2012. https://doi.org/10.1016/j.conbuildmat.2012.03.011

[117] Y. Akinbade e K. Harries, «Is the rule of mixture appropriate for assessing bamboo material properties?,» *Construction and Building Materials,* vol. 267, 2021. https://doi.org/10.1016/j.conbuildmat.2020.120955

[118] F. Nogata e H. Takahashi, «Intelligent functionally graded material: Bamboo,»

Composites Engineering, vol. 5, n. 7, pp. 743-751, 1995. https://doi.org/10.1016/0961-9526(95)00037-N

[119] L. S. Al-Rukaibawi, S. L. Omairey e G. Károlyi, «A numerical anatomy-based modelling of bamboo microstructure,» *Construction and Building Materials,* vol. 308, 2021. https://doi.org/10.1016/j.conbuildmat.2021.125036

[120] E. C. N. Silva, M. C. Walters e G. H. Paulino, «Modeling bamboo as a functionally graded material: lessons for the analysis of affordable materials,» *Journal of Material Science,* vol. 41, pp. 6991-7004, 2006. https://doi.org/10.1007/s10853-006-0232-3

[121] Y. Akinbade, K. Harries, C. V. Flower, I. Nettleship, C. Papadopoulos e S. Platt, «Through-culm wall mechanical behaviour of bamboo,» *Construction and Building Materials,* vol. 216, pp. 485-495, 2019. https://doi.org/10.1016/j.conbuildmat.2019.04.214

[122] Y. Akinbade, K. Harries, C. Flower, I. Nettleship, C. Papadopoulos e S. Platt, «Through-culm wall mechanical behaviour of bamboo,» *Construction and Building Materials,* vol. 216, pp. 485-495, 2019. https://doi.org/10.1016/j.conbuildmat.2019.04.214

[123] M. Chen, L. Ye, G. Wang, X. Ma, Q. Chen, C. Fang, B. Fei e C. Dai, «In-situ investigation of deformation behaviors of moso bamboo cells pertaining to flexural ductility,» *Cellulose,* 2020. https://doi.org/10.1007/s10570-020-03414-0

[124] ISO, *ISO/DIS 22157-1,* 2019.

[125] E. Obataya, P. Kitin e H. Yamauchi, «Bending characteristics of bamboo (Phyllostachys pubescens) with respect to its fiber-foam composite structure,» n. 41, pp. 385-400, June 2007. https://doi.org/10.1007/s00226-007-0127-8

[126] M. Habibi, A. Samaei, B. Gheshlaghi, J. Lu e Y. Lu, «Asymmetric flexural behavior from bamboo's functionally graded hierarchical structure: Underlying mechanisms,» *Acta Biomateralia,* February 2015. https://doi.org/10.1016/j.actbio.2015.01.038

[127] R. Lorenzo, L. Mimendi, H. Li e D. Yang, «Bimodulus bending model for bamboo poles,» *Construction and building materials,* n. 262, 2020. https://doi.org/10.1016/j.conbuildmat.2020.120876

[128] Maulana, Marwanto, Nawawi, Sikmatin, Febrianto e Kim, «Chemical components content of seven Indonesian bamboo species,» *IOP Conference Series. Materials Science and Engineering,* vol. 935, n. 1, 2020.

[129] T.-T. You, J.-Z. Mao, T.-Q. Yuan, J.-L. Wen e F. Xu, «Structural Elucidation of the Lignins from Stems and Foliage of Arundo donax Linn,» *Journal of Agricultural*

and Food Chemistry, vol. 61, n. 22, pp. 5361-5370, 2013. https://doi.org/10.1021/jf401277v

[130] C. Ververis, K. Georghiou, N. Christodoulakis, P. Santas e R. Santas, «Fiber dimensions, lignin and cellulose content of various plant materials and their suitability for paper production,» *Industrial Crops and Products,* vol. 19, n. 3, pp. 245-254, May 2004. https://doi.org/10.1016/j.indcrop.2003.10.006

[131] X.-Q. Wang e H.-Q. Ren, «Surface deterioration of moso bamboo (Phyllostachys pubescens) induced by exposure to artificial sunlight,» *Journal of Wood Science volume,* vol. 55, pp. 47-52, 2009. https://doi.org/10.1007/s10086-008-0994-0

[132] H.-x. Yu, X. Pan, M.-p. Xu, W.-m. Yang, J. Wang and X.-w. Zhuang, «Surface chemical changes analysis of UV-lightirradiated Moso bamboo (Phyllostachys pubescens Mazel),» *Royal Society Open Science,* vol. 5, n. 6, 2018. https://doi.org/10.1098/rsos.180110

[133] X. Wang e H. Ren, «Comparative study of the photo-discoloration of moso bamboo (Phyllostachys pubescens Mazel) and two wood species,» *Applied Surface Science,* vol. 254, n. 21, pp. 7029-7034, 2008. https://doi.org/10.1016/j.apsusc.2008.05.121

[134] D. Trujillo, *ISO 19624:2018: Bamboo structures — Grading of bamboo culms — Basic principles and procedures,* 2018.

[135] E. T. Bahtiar, A. Imanullah, D. Hermawan, N. Nugroho e Abdurachman, «Structural grading of three sympodial bamboo culms (Hitam, Andong, and Tali) subjected to axial compressive load,» *Engineering structures ,* 2019. https://doi.org/10.1016/j.engstruct.2018.12.026

[136] Nurmadina, N. Nugroho e E. T. Bahtiar, «Structural grading of Gigantochloa apus bamboo based on its flexural properties,» *Construction and Building Materials,* vol. 157, pp. 1173-1189, 2017. https://doi.org/10.1016/j.conbuildmat.2017.09.170

[137] J. J. Janssen, Designing and Building with Bamboo, INBAR, 2000.

[138] K. Disén e P. L. Clouston, «Building with bamboo: a review of culm connection technology,» *Journal of Green Building,* vol. 8, n. 4, pp. 83-93, 2013. https://doi.org/10.3992/jgb.8.4.83

[139] K. A. Harries e B. Sharma, «Joints in Bamboo Construction,» in *Nonconventional and Vernacular Construction Materials*, United Kingdom: Elsevier Science & Technology, 2019.

[140] D. Malkowska, D. Trujillo, E. Toumpanaki and J. Norman «Study of screwed bamboo connection loaded parallel to fibre,» *Construction and Building*

Materials, vol. 398, 2023. https://doi.org/10.1016/j.conbuildmat.2023.132532

[141] G. Oka, A. Triwiyono, A. Awaludin e S. Siswosukarto, «Experimental and Theoretical Investigation of Bolted Bamboo Joints without Void Filled Material,» *Applied Mechanics and Materials,* vol. 776, pp. 59-65, 2015. https://doi.org/10.4028/www.scientific.net/AMM.776.59.

[142] R. Moran e J. J. García, «Bamboo joints with steel clamps capable of transmitting moment,» *Construction and Building Materials,* vol. 216, pp. 249-260, 2019. https://doi.org/10.1016/j.conbuildmat.2019.05.025

[143] G. Donini, S. Greco, L. Molari e A. Zanetti, «Structural design of an Italian bamboo house in an Italian regulatory context: Revisiting a small building built in Costa Rica with tropical bamboo,» *Case Studies in Construction Materials,* 2021. https://doi.org/10.1016/j.cscm.2022.e00891

[144] Arch Daily, «From common sight to cultural symbol: the rise and decline of bamboo scaffolding in Hong Kong,» 20 April 2025. [Online]. Available: https://www.archdaily.com/1029052/from-common-sight-to-cultural-symbol-the-rise-and-decline-of-bamboo-scaffolding-in-hong-kong.

[145] P. Stevens, «The scarcity and creativity studio uses bamboo for shade shelter in the galapagos,» 17 January 2017. [Online]. Available: https://www.designboom.com/architecture/the-scarcity-and-creativity-studio-bamboo-shade-shelter-galapagos-playa-man-01-17-2017/.

[146] L. I. B. Commune, «Archello - Energy Efficient Bamboo House,» [Online]. Available: https://archello.com/it/project/energy-efficient-bamboo-house.

[147] H. Oki, 3 Novembre 2015. [Online]. Available: https://www.domusweb.it/it/architettura/2015/11/03/vo_trong_nghia_nama n_retreat_conference_hall.html.

[148] «Canyaviva - Arquitectura Natural,» [Online]. Available: https://canyaviva.org/.

[149] J. C. Wright, Pasos claves de la Construcciòn con caña segùn el Mètodo Canyaviva, 2019.

[150] M. Bertoli, PASSI CHIAVE DELLA COSTRUZIONE IN BAMBU' & ARUNDO DONAX, Arundo Costruzioni Organiche, 2024.

[151] R. Andùjar, M. F. Morell, O. P. Juliàn, B. P. Renngli e J. M. Carreras, «Estudi del comportament mecànic d'arcs de canya Arundo Donax,» *Quaderns d'estructures: Dijous a l'ACE,* n. 46, pp. 38-52, 2013.

[152] «ISO 22156 - Bamboo structures — Bamboo culms — Structural design». 2021.

[153] M. F. García-Aladín, J. F. Correal e J. J. García, «Theoretical and experimental analysis of two-culm bamboo beams,» *Structures and Buildings,* vol. 171, n.

SB4, pp. 316-325, 2018. https://doi.org/10.1680/jstbu.16.00044

[154] H. Zhou, Y. Yan, N. Su, C. Fang, H. Liu, X. Zhang, B. Fei e X. Ma, «Flexural Properties of Multiple Bamboo Beams with Connection Joints,» *Forests,* vol. 13, n. 1851, 2022. https://doi.org/10.3390/f13111851

[155] T. Mouka, E. G. Dimitrakopoulos e R. Lorenzo, «Effect of a longitudinal crack on the flexural performance of bamboo culms,» *Acta Mech,* vol. 233, pp. 3777-3793, 2022. https://doi.org/10.1007/s00707-022-03314-3

[156] A. (. C. d. I. Sísmica), «NSR-10: Reglamento Colombiano de construcción sismo resistente,» *Presidencia de la República, Bogotá DC, Colombia,* 2010.

[157] K. Perolli, COMPORTAMENTO MECCANICO DI BAMBÙ IN FASCI AL VARIARE DELLA GEOMETRIA DELLA SEZIONE: un'analisi sperimentale e numerica - *Master Thesis,* Università degli studi di Bologna, 2024.

[158] L. Á. d. Oliveira, G. L. C. Coura, M. L. PassaiaTonatto, T. H. Panzera, V. Placet e F. Scarpa, «A novel sandwich panel made of prepreg flax skins and bamboo core,» *Composites Part C: Open Access,* vol. 3, n. 100048, 2020. https://doi.org/10.1016/j.jcomc.2020.100048

[159] S. Greco, M. Maraldi e L. Molari, «Grading bamboo through four-point bending tests. A report on six species of Italian bamboo,» *Construction and Building Materials,* vol. 404, n. 133168, 2023. https://doi.org/10.1016/j.conbuildmat.2023.133168

[160] Z. Jiang, H. Wang, G. Tian, X. Liu e Y. Yu, «Sensitivity of several selected mechanical properties of moso bamboo to moisture content change under the fibre saturation point,» *BioResources,* vol. 7, n. 4, pp. 5048-5058, 2012. https://doi.org/10.15376/biores.7.4.5048-5058

[161] A. A. Valls, MEMÒRIA DE CÀLCUL de PROJECTE DE MARQUESINA TEMPORAL – PRIMAVERA SOUND 2017 BARCELONA, Universitat Politecnica de Catalunya, 2017.

[162] H. K. S. Museum, «Curator's Blog - An eco-friendly material - Bamboo,» 2023. [Online]. Available: https://hk.science.museum/en/web/scm/online-explore/cb/20230127_aefmb.html.

[163] S. Greco, Il Bambù Italiano: prove meccaniche e connessioni assiali per prospettive sostenibili (in Italian) - Master Thesis, Bologna: University of Bologna, 2018.

[164] S. Greco, L. Molari, G. Valdrè e J. J. Garcìa, «Multilevel analysis of six species of Phyllostachys bamboo and Arundo donax: preliminary survey on Italian grown stands,» *Wood Science and Technology,* n. 58, pp. 1025-1049, 2024. https://doi.org/10.1007/s00226-024-01547-0

[165] *EN 14081-1 Timber structures - Strength graded structural timber with rectangular cross section,* 2016.

[166] S. Greco, L. Molari, G. Valdrè e J. Garcìa, «Finite element analysis for the prediction of the circumferential bamboo strength,» in *NOCMAT*, 2022.

[167] A. Sghedoni, *Analisi microscopica del comportamento meccanico e igro-meccanico di diverse specie di bambù italiano - Master Thesis,* Università degli Studi di Bologna, 2024.

[168] S. Greco, S. Manzi, L. Molari, A. Saccani, G. Ulian e G. Valdrè, «Photodegradation of Bamboo: A Study on Changes in Mechanical Performances,» *Materials,* vol. 16, n. 1, 2023. https://doi.org/10.3390/ma16010285

Appendix A

From the top to the bottom: a piece from the inner, middle and external part of the section of each species for both part A, and B, on the right. Differences in colour depend from the prevalence of transmission or reflection technique. Enlargement 10X.

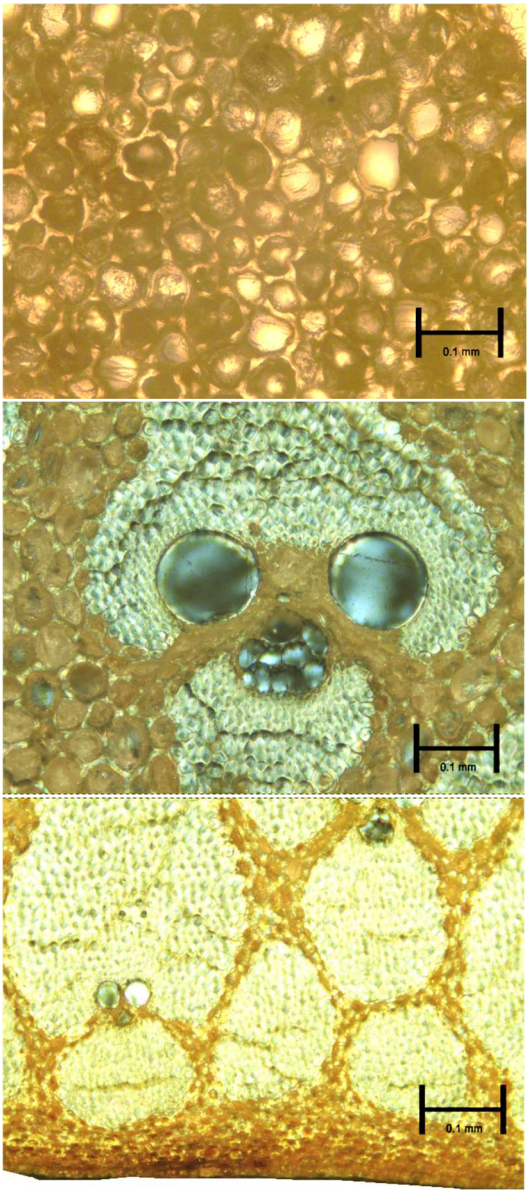

P. viridiglaucescens
Part B

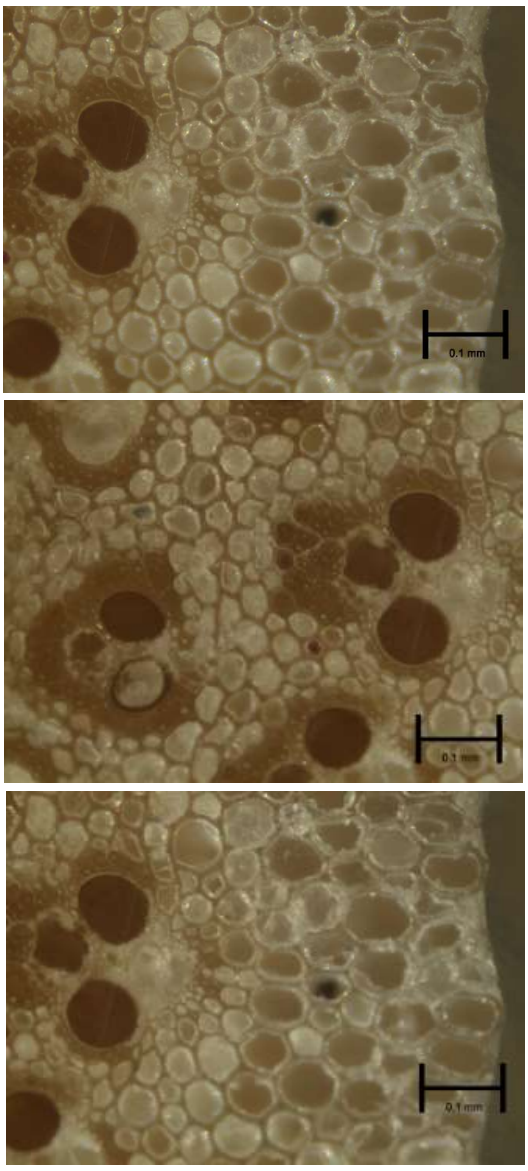

Arundo donax*
Part A

*Unfortunately, pictures of Arundo donax, part A, have been taken vertically and here are so reported for the layout.

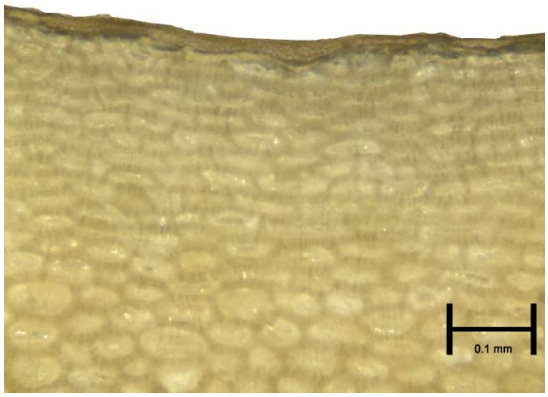

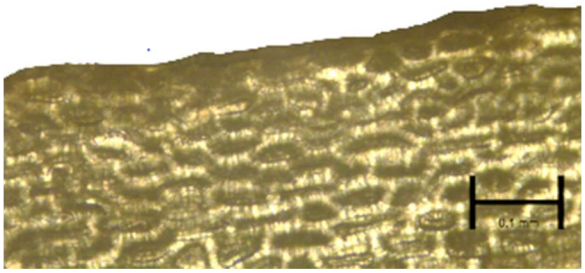

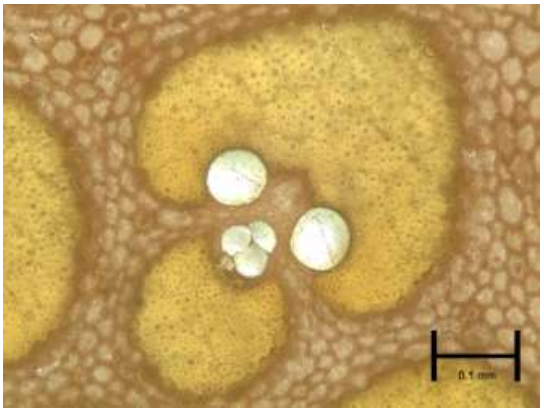

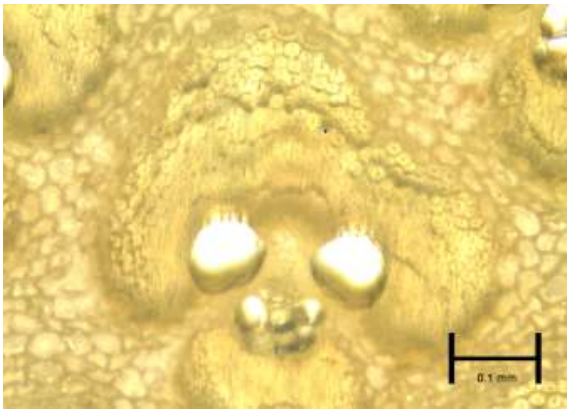

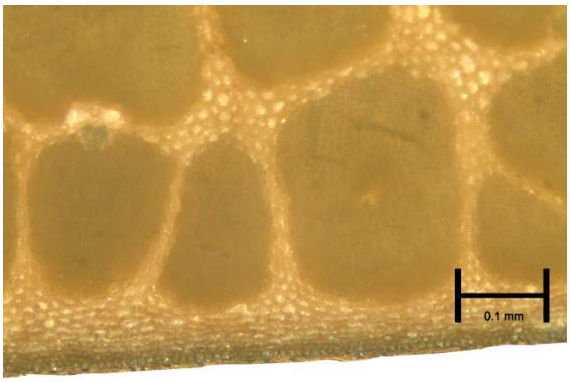

P. edulis
Part A

P. edulis
Part B

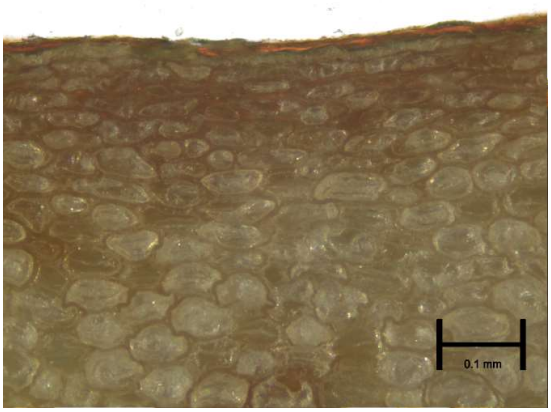

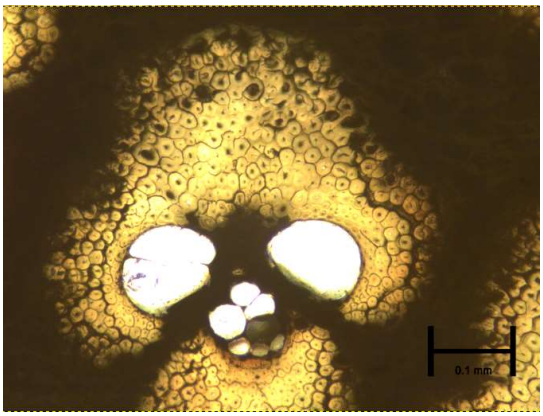

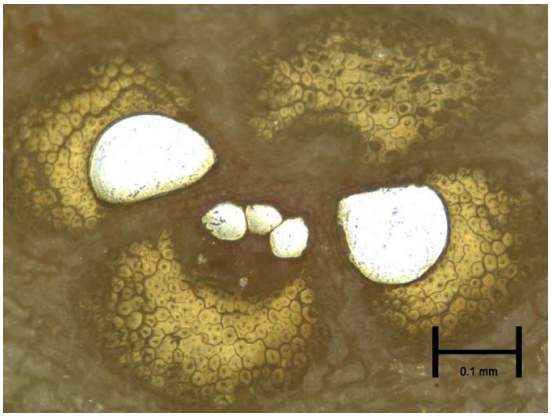

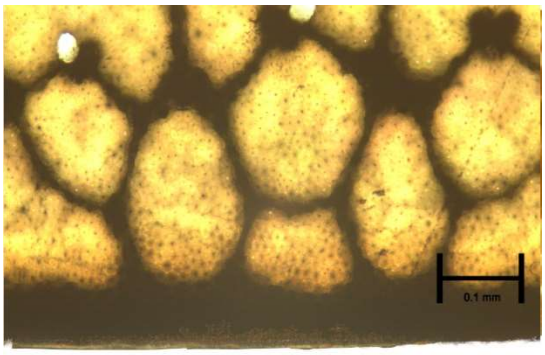

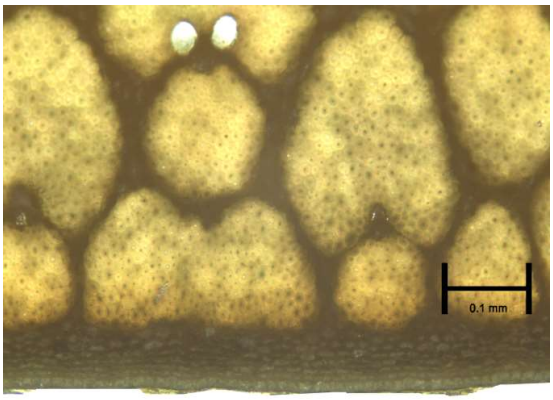

P. bambusoides
Part A

P. bambusoides
Part B

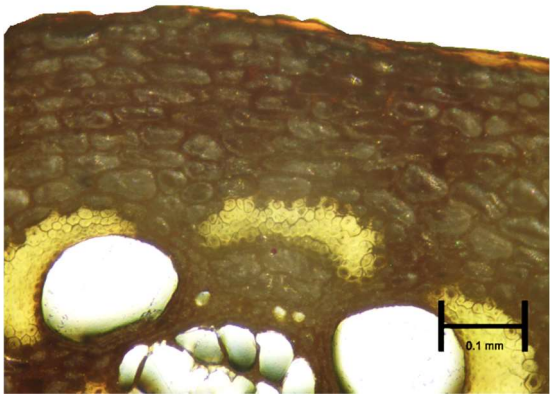

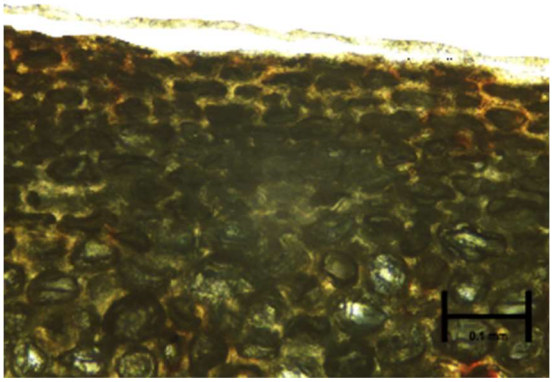

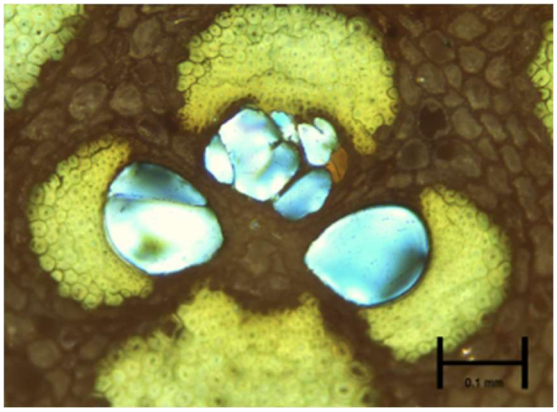

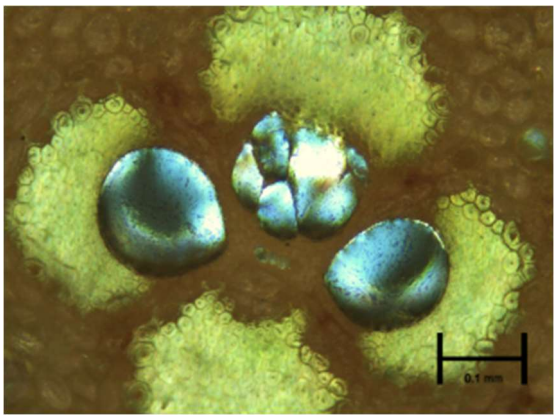

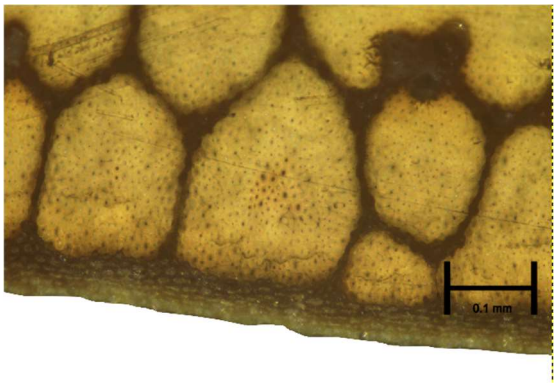

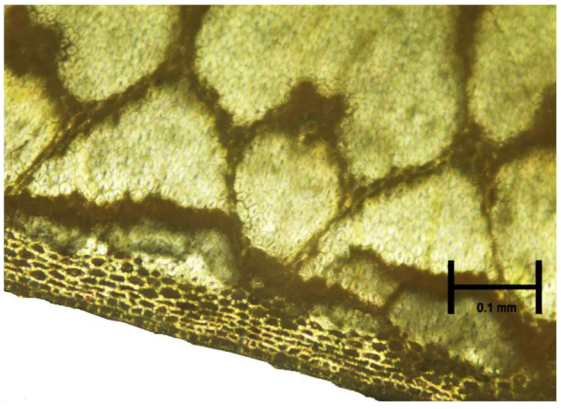

P. iridescens
Part A

P. iridescens
Part B

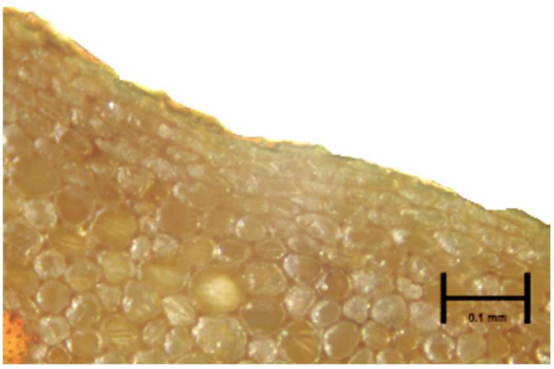

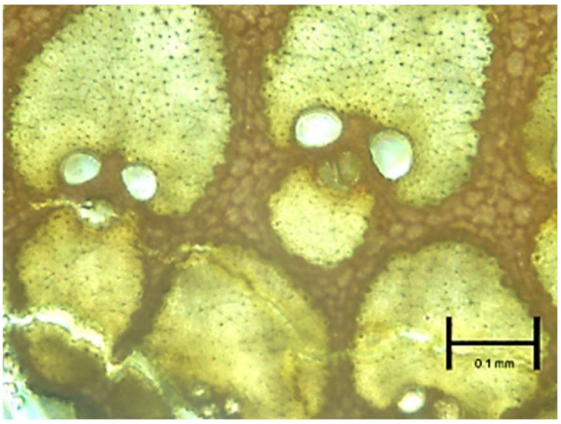

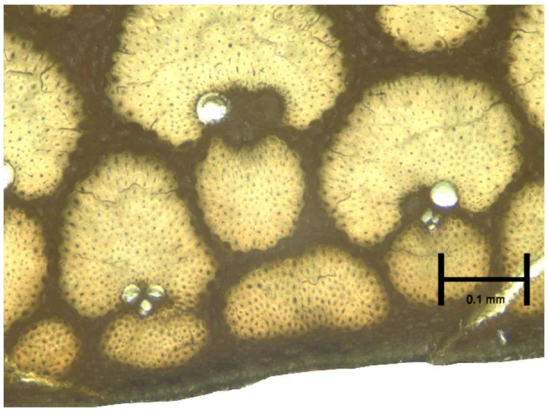

P. violacescens
Part A

P. violacescens
Part B

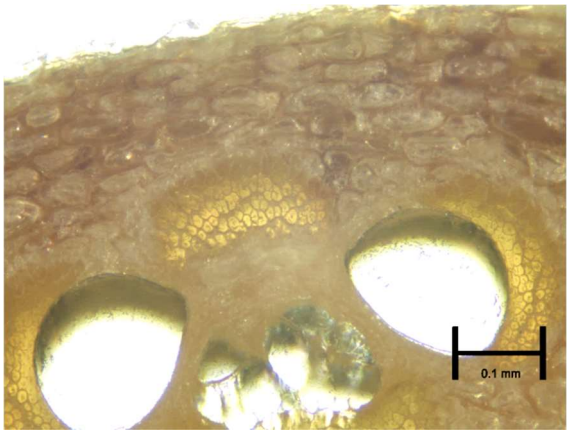

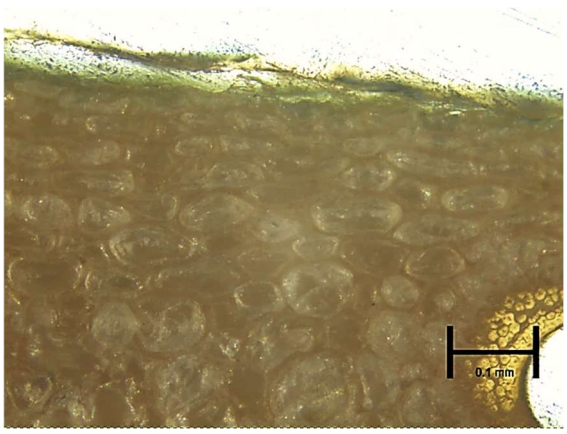

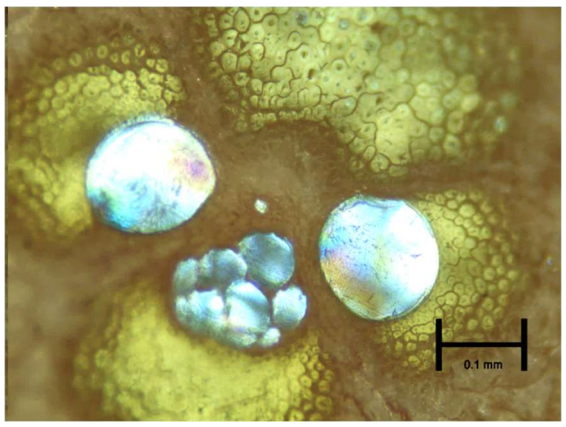

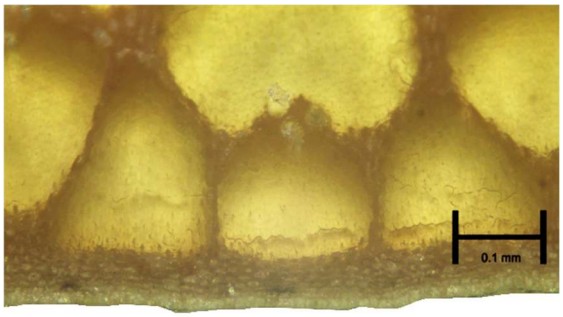

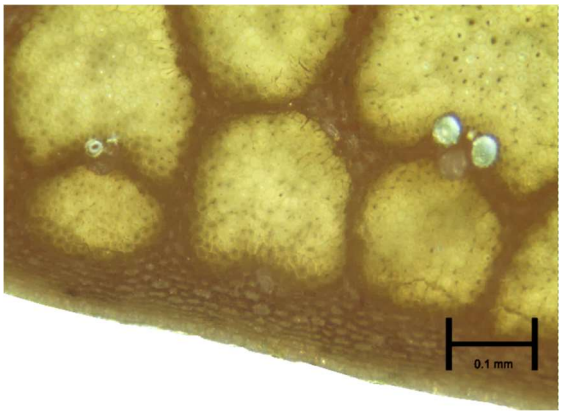

P. vivax
Part A

P. vivax
Part B

Appendix B

Table 31 Fitting functions for components distribution for all the six species. The best fitting, the reduced Chi square and differences with linear and quadratic curves are shown. Data are performed with Labfit Software.

Name of the species		Best fitting $F(x,A,B,C)$	Reduced Chi Square	Parabolic fitting $Ax^2 + Bx$	Reduced Chi Square	Linear fitting $Ax + B$	Reduced Chi Square
P. edulis	A	Asinh(Bx)+ Cx^2 A=0.3773 B=2.379 C=1.194	0.0069	A=0.6371 B=0.0 C=0.0988	0.00790	A=0.6419 B=0.01870	0.0092
	B	Asinh(Bx)+ Cx^2 A=0.3297 B=2.5351 C=-1.1252	0.0117	A=0.6044 B=0.0773 C=0.0	0.01250	A=0.5950 B=-0.0217	0.0151
P. viridi-glaucescens	A			A=0.3030 B=0.3675 C=0.0589	0.01847	A=0.6698 B=0.0074	0.01889
	B	Atan(Bx+C) A=0.7035 B=0.7853 C=-0.3658	0.01346	A=0.2678 B=0.4342 C=0.0373	0.01359	A=0.7011 B=-0.0083	0.01380
P. bambusoides	A	A(exp(Bx)-exp(Cx)) A=0.2105 B=1.251 C=-8.935	0.0081	A=-0.0049 B=0.6699 C=0.0770	0.00910	A=0.6215 B=0.08493	0.0083
	B	Parabolic fitting $Ax^2 + Bx$		A=-0.316 B=0.0 C=0.9879	0.01480	A=0.6732 B=0.05367	0.0153
P. vivax	A	A(exp(Bx)-exp(Cx)) A=0.2678 B=0.9597 C=-5.4551	0.01288	A=-0.4316 B=1.0752 C=0.0	0.01344	A=0.6170 B=0.0919	0.01362
	B	Atan(Bx+C) A=0.7035 B=0.7853 C=0.03658	0.01346	A=0.1392 B=0.5859 C=0.0	0.01359	A=0.7011 B=0.0083	0.01378

P. iridescens	A	$(A+x)/(B+Cx^2)$ A=0.06827 B=1.6500 C=-0.3513	0.00545	A=0.7002 B=0.0876 C=0.0	0.00574	A=0.7540 B=0.0072	0.00582
	B	A(exp(Bx)-exp(Cx)) A=0.08854 B=2.1814 C=34.444	0.01515	A=0.6465 B=0.0 C=0.1019	0.01540	A=0.6401 B=-0.0057	0.01791
P. violacescens	A	A(exp(Bx)-exp(Cx)) A=0.08541 B=2.1346 C=-14.916	0.01464	A=0.4914 B=0.1293 C=0.4914	0.01483	A=0.6188 B=-0.0205	0.01597
	B	Acosh(Bx) A=0.09059 B=2.860	0.01405	A=0.6355 B=0.0 C=0.0617	0.01466	A=0.6151 B=-0.03694	0.01849
Arundo Donax	A	Linear		A=0.0820 B=0.3369 C=-0.022	0.01904	A=0.4177 B=-0.03546	0.01902
	B	$Asinh(Bx)+ Cx^2$ A=-5.2306 B=-0.0570 C=0.00171	0.0178	A=0.2556 B=0.0 C=0.0722	0.01796	A=0.2539 B=0.02998	0.19022

Table 32 Fitting functions for voids distribution for all the six species. The best fitting, the reduced Chi square and differences with quadratic curves are shown. Data are performed with Labfit Software.

Name of the species		Best fitting F(x, A, B, C,)	Reduced Chi Square	Parabolic fitting $Ax^2 + Bx$	Reduced Chi Square
P. edulis	A	Parabolic fitting $Ax^2 + Bx$		A=-0.3231 B=0.3149	0.0028856
	B	Parabolic fitting $Ax^2 + Bx$		A=-0.2481 B=0.2410	0.0036552
P. viridiglaucescens	A	A sin(Bx) A=0.07488 B=3.236	0.0048671	A=-0.3089 B=0.2992	0.0048792
	B	Parabolic fitting $Ax^2 + Bx$		A=-0.3028 B=0.2961	0.0048128
P. bambusoides	A	Ax^2+C A=-0.0598 C=0.06619	0.0027324	A=-0.3221 B=0.2965	0.0028484

	B	Parabolic fitting $Ax^2 + Bx$		A=-0.2898 B=0.2810	0.0048460
P. vivax	A	Parabolic fitting $Ax^2 + Bx$		A=-0.4518 B=0.4155	0.0053336
	B	Parabolic fitting $Ax^2 + Bx$		A=-0.3008 B=0.2916	0.0052646
P. iridescens	A	Parabolic fitting $Ax^2 + Bx$		A=-0.4265 B=0.4149	0.0038107
	B	Costant 0.05066	0.0068086	A=-0.2311 B=0.2471	0.0068771
P. violacescens	A	Parabolic fitting $Ax^2 + Bx$		A=-0.3249 B=0.3301	0.0080319
	B	Ax^2+C A=-0.0481 C=0.08269	0.0064252	A=-0.3759 B=0.3702	0.0066126

Appendix C

Specification of each model used for the FEM analysis of the section 3 is reported for each species. Name, distance from the external surface, calculation of the area occupied by each component, measures of the average vessels and maximum stress recorded for both fibre and matrix are specified.

Table 33 Description of the geometries and maximum stress for each model of the P. edulis species

Name	Normalized distance from the inner surface (mm)	Area %			Average vessel (10^3 mm)		$S_{f,max}$	$S_{m,max}$
		Fibre	Matrix	Voids	$A_{v,avg}$	$D_{v,avg}$		
Edu_1	0-0.1	0.51	99.49	0	-	-	21.78	20.03
Edu_2	0.1-0.2	15.03	78.62	6.35	12.17	124.53	106.36	44.41
Edu_3	0.2-0.3	18.70	74.84	6.46	12.39	125.61	156.65	60.68
Edu_4	0.3-0.4	21.22	71.45	7.32	10.03	113.02	172.11	180.77
Edu_5	0.4-0.5	23.68	67.21	9.11	9.70	111.15	178.97	99.72
Edu_6	0.5-0.6	29.47	63.39	7.14	5.70	85.23	217.02	85.37
Edu_7	0.6-0.7	36.99	54.59	8.43	5.77	85.73	178.76	75.00
Edu_8	0.7-0.8	49.92	46.49	3.59	2.46	55.99	104.32	23.15
Edu_9	0.8-0.9	54.35	41.34	4.31	2.17	52.63	107.57	34.39
Edu_10	0.9-1	61.95	37.31	0.74	1.02	36.00	79.43	26.28

Table 34 Description of the geometries and maximum stress for each model of the P. viridiglaucescens species

Name	Normalized distance from the inner surface (mm)	Area %			Average vessel (10^3 mm)		$S_{f,max}$	$S_{m,max}$
		Fibre	Matrix	Voids	$A_{v,avg}$	$D_{v,avg}$		
Vir_1	0-0.1	8,85	89,45	1,70	34,00	208,06	56.17	52.12
Vir_2	0.1-0.2	12,30	86,95	0,75	15,00	138,20	25.39	13.21
Vir_3	0.2-0.3	17,49	75,26	7,25	36,25	214,84	30.99	58.65
Vir_4	0.3-0.4	19,40	71,90	8,70	58,00	271,75	51.39	40.29
Vir_5	0.4-0.5	34,30	57,05	8,65	57,67	270,97	169.36	89.18
Vir_6	0.5-0.6	32,10	57,95	9,95	33,17	205,50	148.36	24.56
Vir_7	0.6-0.7	46,85	47,95	5,20	20,80	162,74	60.69	10.45
Vir_8	0.7-0.8	53,40	41,55	5,05	16,83	146,40	43.83	15.89
Vir_9	0.8-0.9	63,55	34,80	1,65	6,60	91,67	37.92	15.60
Vir_10	0.9-1	57,90	40,30	1,80	6,00	87,40	48.80	17.75

Table 35 Description of the geometries and maximum stress for each model of the P. vivax species

Name	Normalized distance from the inner surface (mm)	Area %			Average vessel (10^3 mm)		$S_{f,max}$	$S_{m,max}$
		Fibre	Matrix	Voids	$A_{v,avg}$	$D_{v,avg}$		
Viv_1	0-0.1	2,82	97,18	0,00	-	-	35.81	25.12
Viv_2	0.1-0.2	23,86	66,85	9,30	38,20	220,54	138.73	45.69
Viv_3	0.2-0.3	29,60	60,81	9,59	28,14	189,30	467.97	96.91
Viv_4	0.3-0.4	34,40	59,08	6,52	26,80	184,72	313.70	64.62
Viv_5	0.4-0.5	37,83	50,44	11,73	34,43	209,37	231.67	91.62
Viv_6	0.5-0.6	49,49	39,66	10,85	24,78	177,62	175.1	329.27
Viv_7	0.6-0.7	54,09	39,82	6,09	15,63	141,05	140.11	27.36
Viv_8	0.7-0.8	52,19	42,79	5,01	12,88	128,03	142.19	46.52
Viv_9	0.8-0.9	63,34	32,04	4,63	6,79	92,95	265.51	158.53
Viv_10	0.9-1	59,15	40,51	0,34	2,33	54,51	86.84	65.22

Table 36 Description of the geometries and maximum stress for each model of the P. iridescens species

Name	Normalized distance from the inner surface (mm)	Area %			Average vessel (10^3 mm)		$S_{f,max}$	$S_{m,max}$
		Fibre	Matrix	Voids	$A_{v,avg}$	$D_{v,avg}$		
Iri_1	0-0.1	6,34	88,44	5,21	20,00	159,58	116.08	191.54
Iri_2	0.1-0.2	16,16	78,45	5,39	7,75	99,34	140.01	118.99
Iri_3	0.2-0.3	22,07	66,55	11,38	14,56	136,13	156.87	106.17
Iri_4	0.3-0.4	25,69	67,45	6,86	9,88	112,13	145.14	58.64
Iri_5	0.4-0.5	31,94	58,77	9,29	8,23	102,37	137.06	91.58
Iri_6	0.5-0.6	40,31	47,44	12,25	10,85	117,51	230.69	46.70
Iri_7	0.6-0.7	49,96	40,16	9,89	7,60	98,37	191.58	
Iri_8	0.7-0.8	60,16	32,73	7,12	6,31	89,62	156.89	37.37
Iri_9	0.8-0.9	65,16	28,84	5,99	4,06	71,89	121.24	20.99
Iri_10	0.9-1	71,01	27,86	1,13	1,44	42,89	97.60	35.21

Table 37 Description of the geometries and maximum stress of each model for the P. violacescens species

Name	Normalized distance from the inner surface (mm)	Area %			Average vessel (10^3 mm)		$S_{f,max}$	$S_{m,max}$
		Fibre	Matrix	Voids	$A_{v,avg}$	$D_{v,avg}$		
Vio_1	0-0.1	1,70	98,30	0,00	-	-	16.58	11.13
Vio_2	0.1-0.2	18,50	67,60	13,90	92,67	343,49	281.79	30.32
Vio_3	0.2-0.3	10,30	89,70	0,00	-	-	23.08	7.99
Vio_4	0.3-0.4	23,45	69,70	6,85	34,25	208,83	40.62	31.72
Vio_5	0.4-0.5	24,55	69,60	5,85	39,00	222,84	75.56	17.24
Vio_6	0.5-0.6	25,60	65,25	9,15	61,00	278,69	162.32	29.23
Vio_7	0.6-0.7	32,40	58,95	8,65	57,67	270,97	92.75	15.72
Vio_8	0.7-0.8	44,50	46,05	9,45	27,00	185,41	132.16	23.65
Vio_9	0.8-0.9	57,45	37,35	5,20	14,86	137,54	50.93	11.23
Vio_10	0.9-1	55,80	43,10	1,10	5,50	83,68	28.88	10.86